Nasa CR-65221

CONFIDENTIAL

4171-6001-RC000

FINAL REPORT

STUDY OF TRADEOFFS RELATED TO DIRECT INJECTION FROM EARTH INTO TRANSLUNAR ORBIT FOR APOLLO

Prepared for the

NATIONAL AERONAUTICS AND SPACE ADMINISTRATION

MANNED SPACECRAFT CENTER

Under Contract No. NAS 9-3022

8 FEBRUARY 1965

CR 65221

30

CATEGORY

TRW SPACE TECHNOLOGY LABORATORIES

THOMPSON RAMO WOOLDRIDGE INC.

This document contains information affecting the national defense of the United States within the meaning of the espionage laws, 18 U.S.C., Section 793 and 794, the transmission or revelation of which in any manner to an unauthorized person is prohibited by law.

CONFIDENTIAL

[redacted]

C66-3418

4171-6001-RC000
COPY_____ OF_____
TOTAL PAGES 304

FINAL REPORT

STUDY OF TRADEOFFS RELATED TO DIRECT INJECTION FROM EARTH INTO TRANSLUNAR ORBIT FOR APOLLO [redacted]

Prepared for the
NATIONAL AERONAUTICS AND SPACE ADMINISTRATION
MANNED SPACECRAFT CENTER
Under Contract No. NAS 9-3022

8 FEBRUARY 1965

Samuel E. Benesch

S.E. BENESCH
Project Engineer

P. Dergarabedian

P. DERGARABEDIAN
Director
Systems Research and Engineering Laboratory

DOWNGRADE AT 3 YEAR INTERVALS
DECLASSIFY AFTER 12 YEARS
DOD DIR. 5200.10

TRW SPACE TECHNOLOGY LABORATORIES
THOMPSON RAMO WOOLDRIDGE INC.

[redacted]

[redacted]AL [redacted]

ACKNOWLEDGEMENTS

The following STL people have prepared contributions to this report. The support and assistance of many others are acknowledged.

J. A. Bossart
R. D. Dodge, Jr.
J. R. Duffett
R. E. Hartman
F. G. Lewis
P. A. Penzo
C. L. Smith
R. E. Wesel
R. L. Wolpert

The General Electric Apollo Support Department, Daytona Beach, Florida contributed to the numerical evaluations on mission success and crew safety.

The active participation by Mr. Kenneth L. Thomas, NASA/Manned Spacecraft Technical Representative, in this study had a major influence on the significance of the results.

ABSTRACT

18118

The use of direct rather than earth parking orbit injection may yield advantages for manned missions, both lunar and interplanetary. The tradeoffs for Apollo missions were therefore investigated in order to develop methods and techniques for application to manned missions.

The study provides comparison data on the direct and parking orbit injection methods of achieving a translunar orbit for the Apollo mission. These comparison data are of special interest for advanced Apollo missions, such as those involving lunar logistics systems.

The study covered tradeoffs of relative mission success and crew safety for the two injection techniques. Included were considerations of performance, launch windows, launch opportunities, on-time launch probabilities, equipment sequencing and usage, and abort trajectories.

The comparison data resulting from this study indicate that the direct injection method offers increased inflight reliability and increased crew safety, but because of fewer launch opportunities, offers a lower probability of mission success within a given year.

Author

SUMMARY

In June, 1964, Contract No. NAS9-3022 was awarded by NASA-MSC to TRW Space Technology Laboratories for a Study of Tradeoffs Related to Direct Injection from Earth into Translunar Orbit for Apollo. The primary objective of this study was to provide comparison data on the direct and parking orbit methods of achieving a translunar orbit for the Apollo mission. These comparison data were to be in the areas of mission success, crew safety, flight mechanics, performance and on-time launch probability. The study results were to be presented in a manner such that more current assumptions may be introduced to produce more current comparisons.

The General Electric Apollo Support Department (GE/ASD), Daytona Beach, Florida was directed by NASA Hqs. to perform certain tasks in support of this contract. These tasks included the generation of comparative mission success and crew safety probability estimates, based on data supplied by NASA and by STL, using the SOAR III/Cindy I computer reliability model. For this reason, the STL-generated in-flight reliability estimates were limited to the S-IVB stage.

The comparison data generated in this study are separated into two categories: Part I—flight mechanics and performance, and Part II—the probabilistic aspects of mission success and crew safety.

I. Flight Mechanics and Performance

Launch window displays for the direct injection mode were generated for the years 1968, 1969, and 1970. These displays reflect the combined effects of direct injection geometry, booster performance and lunar lighting constraints.

The injection energies required for direct injection were determined for both unrestricted and free return translunar trajectories. The effects of direct injection on the CSM fuel requirements and lunar site availability were determined. The payloads available for direct injection and parking orbit injection were compared utilizing MSC generated data.

The effects of direct injection on earth landing site availability and on the inclination and reentry maneuver angle of the return window were evaluated. Landing window displays were generated and presented with the launch window displays. Mission planning for direct injection can thus be accomplished using a single launch and landing window display for the month of interest.

The characteristics of the pre-abort trajectory for translunar injection powered flight failure were determined. The in-plane abort velocity requirements and corresponding landing areas for proper reentry conditions were generated. The pre-abort and abort flight times associated with in-plane aborts were also determined.

The following conclusions were reached as a result of Part I of this study:

a) With no lighting constraints at the launch site, the Earth parking orbit injection mode offers about ten launch windows per month, or about 120 days per year. In contrast, the direct injection mode offers about 45 launch windows per year. If a daylight launch is required, the number of direct injection launch windows is reduced by approximately one-half, while the number of parking orbit injection launch windows is reduced by about 20 percent.

b) The typical Earth parking orbit launch window is of about 2.5 hours duration, if the launch azimuth is varied through its range of 26 degrees. The typical direct injection window is of about 1.5 hours duration, and is achieved by use of a variable injection flight path angle. The direct injection launch azimuth varies within a narrower range than the parking orbit injection launch azimuth.

c) Regardless of the location of the lunar landing site, the launch period for this site is limited to a three-day interval each month by lunar lighting constraints. Under these conditions,

the earth parking orbit mode offers one opportunity each month, or 12 per year. Unlike the parking orbit mode, the direct injection mode launch opportunities are dependent on the landing site selected. The direct injection mode offers only 5 or 6 opportunities per year with a daylight launch. If the launch lighting constraint is relaxed, the direct injection mode offers from 6 to 9 opportunities per year.

d) Direct injection offers a potential payload increase when only a portion of the available window is utilized. Using the entire 90-minute window results in an allowable payload which is slightly less than that for the nominal parking orbit injection.

II. Mission Success/Crew Safety

The flight sequence changes required for direct injection were determined, and the affected functions, discrete events and equipment were identified. The changes in operating times and duty cycles were estimated for that equipment which would produce the greatest in-flight reliability change as a result of eliminating the parking orbit coast phase. A model was formulated to assess the relative in-flight reliability of the two injection methods. This model, as well as the GE/ASD SOAR III/Cindy I computer reliability model, was exercised utilizing subsystem reliability estimates generated from Douglas Aircraft Company data, MSFC data, GE/ASD data, and historical flight reliability data.

The basic methodology for estimating on-time launch probability was formulated with and without the use of a scheduled or built-in hold in the launch countdown sequence. Estimates of the Saturn V/Apollo on-time launch probability were made based on past study results and available historical data.

Estimates of the comparative mission success and crew safety were made, based on the data and models referred to above.

A summary of the conclusions reached in regard to Part II of this study follows:

a) Without a built-in hold in the countdown, the direct injection mission has a significantly lower probability of on-time launch than the earth parking orbit injection mission.

b) With the judicious use of built-in holds in the countdown, the on-time launch probabilities of the direct injection and earth parking orbit injection missions do not differ appreciably. Furthermore, such advantageous use of built-in holds could be realistically implemented in the Saturn V/Apollo countdown. The estimated improvement in on-time launch probability for the 4.5-hour launch window parking orbit injection mission is insignificant; however, a significant gain can be achieved for the 2.5-hour launch window parking orbit injection mission.

c) It is concluded that the direct injection mission increases the probability of in-flight success by a significant extent, as compared to the earth parking orbit injection mission.

d) It is concluded that the direct injection mission decreases the expected number of crew losses per successful mission.

In summary, direct injection offers a higher in-flight reliability, a comparable on-time launch probability (if a built-in hold is used), fewer launch opportunities per year, and some gain in crew safety. Therefore, it is estimated that direct injection would allow the use of fewer boosters per successful mission, would experience fewer crew losses per successful mission, and would have a lower probability of achieving a successful mission in a given year.

CONTENTS

PART I—FLIGHT MECHANICS

		Page
1.	POWERED FLIGHT SIMULATIONS	I-1
2.	TRAJECTORY AND MISSION ANALYSIS	I-4
2.1	Introduction	I-4
2.2	Direct Ascent Geometry	I-5
2.3	Saturn Performance Characteristics	I-12
2.4	Effects of the Lunar Lighting Constraint	I-31
2.5	Effects of the Free Return Constraint	I-38
2.6	Effects Upon Earth Return Conditions	I-38
2.7	Some Parking Orbit-Direct Ascent Comparisons	I-47
2.8	Mission Planning	I-52
2.9	Launch Window Displays for 1968, 1969, 1970	I-55
2.10	Lunar Site Availability and Performance Gain	I-98
3.	ABORT TRAJECTORY ANALYSIS	I-106
3.1	Introduction	I-106
3.2	Abort Geometry	I-108
3.3	Pre-abort Trajectory Characteristics	I-117
3.4	Aborts to Orbit	I-132
3.5	Minimum Return Time Aborts	I-139
3.6	Returns to Specific Landing Areas	I-164
4.	CONCLUSIONS	I-168

CONTENTS

PART II — MISSION SUCCESS/CREW SAFETY

		Page
1.	INTRODUCTION	II-1
1.1	On-Time Launch Probability	II-1
1.2	Flight Success Probability	II-2
1.3	Mission Success and Crew Safety Probabilities	II-2
1.4	Additional Items	II-3
2.	PROBABILITY OF ON-TIME LAUNCH	II-4
2.1	Prediction of Launch Probability Parameters	II-4
2.1.1	Introduction	II-4
2.1.2	Statistical Similarity of Different Missile Programs	II-5
2.1.3	Booster Holds in Successful Countdowns	II-5
2.1.4	Estimated Saturn Stage S-IC Countdown Performance	II-9
2.1.5	Contribution of Other Saturn V Stages	II-9
2.1.6	Holds Per Count for Saturn V/Apollo Configuration	II-11
2.1.7	Estimated Range of $\bar{h}$	II-11
2.1.8	Probability of a Nonscrub	II-15
2.1.9	Probability of Schedule Slippage	II-17
2.2	On-Time Launch Probability Without Built-In Holds	II-18
2.2.1	Introduction	II-18
2.2.2	Mathematical Model	II-19
2.2.3	Probability Distribution of Excess Countdown Time	II-20
2.2.4	Convolution of Stages and Modules	II-23
2.2.5	Parametric Presentation of Launch Probabilities	II-24
2.2.6	Numerical Calculation of Launch Probability	II-26
2.3	Saturn V/Apollo On-Time Launch Probability With Built-In Holds	II-28
2.3.1	Improvement in Probability of Launch	II-28
2.3.2	Mathematical Model and Convolution Method	II-29
2.3.3	Calculation of Launch Probability With and Without Built-In Hold	II-31
2.3.4	Launch Probability Using Built-In Holds	II-33
2.4	Comparative Summary of Launch Probabilities	II-34
2.4.1	Conditional Probability of Meeting Launch Window	II-34
2.4.2	Two-Day Turn Around for Recommencement of Countdown	II-37

CONTENTS (Continued)

Page

2.4.3 One-Day Turn Around for Recommencement of Countdown II-37
2.4.4 Turn-Around Time in Excess of Two Days for Recommencement of Countdown II-37
2.4.5 Best Estimates of Launch Probabilities II-42
2.4.6 Launch Probability Computer Programs II-42

3. IN-FLIGHT RELIABILITY COMPARISON II-44

3.1 Introduction II-44
3.2 Comparison of Equipment II-44
3.3 Reliability Comparisons II-44
3.4 Summary of In-Flight Reliabilities II-91
3.4.1 Reaction Control System of the S-IVB II-91
3.4.2 S-IVB Reignition II-91
3.4.3 Powered Stage Reliabilities II-93
3.4.4 Relative In-Flight Reliability Model II-93
3.4.5 Unsuccessful Flight and Crew Safety Probabilities II-94
3.5 Areas for Continued Study II-96

4. MISSION SUCCESS AND CREW SAFETY COMPARISONS II-97

4.1 Comparison of Mission Success Probabilities II-97
4.2 Unsuccessful Flight and Crew Safety Probabilities II-100

5. MAJOR RESULTS II-102

5.1 Launch Probability Parameters II-102
5.2 Launch Probability Comparison II-102
5.3 Mathematical Model and Methods for Calculation of Launch Probabilities II-103
5.4 Flight Success Probability Comparison II-104
5.4.1 Relative In-Flight Success Probability II-104
5.4.2 In-Flight Reliability Comparisons II-104
5.4.3 GE/Apollo Support Department's Unsuccessful Mission (Flight) and Crew Safety Probability Estimates II-104

CONTENTS (Continued)

Page

6. CONCLUSIONS II-106

7. RECOMMENDATIONS II-108

REFERENCES II-109

APPENDIX A. LAUNCH PROBABILITY COMPUTER PROGRAMS II-110

TOTAL PAGES 304

ILLUSTRATIONS — PART I

		Page
2-1	Lunar Plane Inclination to Earth Equator 1968, 69, 70	I-6
2-2	Launch Geometry	I-7
2-3	Lunar Trajectory Geometry	I-8
2-4	Parking Orbit In-Plane Geometry	I-9
2-5	Lunar Trajectory True Anomaly	I-10
2-6	Direct Ascent In-Plane Geometry	I-11
2-7	Saturn-V Payload Characteristics January 23, 1968	I-14
2-8	Saturn-V Payload Characteristics January 19, 1968	I-16
2-9	Saturn-V Payload Characteristics January 21, 1968	I-17
2-10	Saturn-V Payload Characteristics January 25, 1968	I-18
2-11	Saturn-V Payload Characteristics January 27, 1968	I-19
2-12	Saturn-V Payload Characteristics January 29, 1968	I-20
2-13	Direct Injection Launch Azimuths January 1968—Month of Near Minimum Lunar Plane Inclination to Earth Equator	I-21
2-14	Direct Injection Launch Azimuth September 1968—Month of Maximum Lunar Plane Inclination to Earth Equator	I-22
2-15	Payload Loss from Launch Azimuth—Direct 72-Hour Lunar Mission	I-24
2-16	Payload Comparison—Free Return Trip Times With 0° Return Inclination to Lunar Plane, 90° Launch Azimuth	I-26
2-17	Energy Requirements January 1968	I-27

ILLUSTRATIONS (Continued)

		Page
2-18	Payload Summary—Direct Ascent Payload Advantage Over Parking Orbit	I-28
2-19	Payload Tradeoff with Flight Time	I-30
2-20	Lunar Lighting Summary - 1968 (Favorable Direct Injection Shaded)	I-32
2-21	Lunar Lighting Summary - 1969 (Favorable Direct Injection Shaded)	I-33
2-22	Lunar Lighting Summary - 1970 (Favorable Direct Injection Shaded)	I-34
2-23	Relationship Between Longitude and Sun Elevation Angle	I-35
2-24	Relationship Between Lunar Site and Sun Elevation Angle	I-35
2-25	Sun Elevation as a Function of Site Location	I-36
2-26	Relationship Between Lunar Phase and the Minimum Lunar Declination	I-37
2-27	Time of Flight Versus Distance of Moon for Free Return Circumlunar Trajectory and for Lines of Constant Return Inclinations With the Moon's Plane	I-39
2-28	Time of Flight Versus Distance of Moon for Free Return Circumlunar Trajectory and for Lines of Constant Return Inclinations With the Moon's Plane	I-40
2-29	Time of Flight Versus Distance of Moon for Free Return Circumlunar Trajectory and for Lines of Constant Return Inclinations With the Moon's Plane	I-41
2-30	Return Window Display for Several Landing Site Latitudes	I-42
2-31	Landing Window Display for Return to Hawaii	I-44
2-32	Landing Azimuth Geometry	I-45
2-33	Landing Window Display for Return to Hawaii	I-45

ILLUSTRATIONS (Continued)

		Page
2-34	Return Flight Time as a Function of Departure and Touchdown Times	I-46
2-35	Earth Lighting Conditions Upon Landing	I-48
2-36	Launch and Landing Window Comparisons Direct Ascent (Shaded) and Parking Orbit	I-49
2-37	Direct Injection Launch Opportunities with Favorable Lunar Lighting	I-51
2-38	Apollo Direct Injection Mission Planning Display	I-53
2-39	Direct Injection Launch Window December 1967 - January 1968	I-56
2-40	Direct Injection Launch Window January 1968	I-57
2-41	Direct Injection Launch Window February 1968	I-58
2-42	Direct Injection Launch Window March 1968	I-59
2-43	Direct Injection Launch Window April 1968	I-60
2-44	Direct Injection Launch Window May 1968	I-61
2-45	Direct Injection Launch Window June 1968	I-62
2-46	Direct Injection Launch Window July 1968	I-63
2-47	Direct Injection Launch Window July - August 1968	I-64
2-48	Direct Injection Launch Window August-September 1968	I-65
2-49	Direct Injection Launch Window September - October 1968	I-66
2-50	Direct Injection Launch Window October 1968	I-67
2-51	Direct Injection Launch Window November 1968	I-68
2-52	Direct Injection Launch Window December 1968	I-69
2-53	Direct Injection Launch Window January 1969	I-70
2-54	Direct Injection Launch Window February 1969	I-71

ILLUSTRATIONS (Continued)

		Page
2-55	Direct Injection Launch Window March 1969	I-72
2-56	Direct Injection Launch Window April 1969	I-73
2-57	Direct Injection Launch Window April - May 1969	I-74
2-58	Direct Injection Launch Window May - June 1969	I-75
2-59	Direct Injection Launch Window June - July 1969	I-76
2-60	Direct Injection Launch Window July 1969	I-77
2-61	Direct Injection Launch Window August 1969	I-78
2-62	Direct Injection Launch Window September 1969	I-79
2-63	Direct Injection Launch Window October 1969	I-80
2-64	Direct Injection Launch Window November 1969	I-81
2-65	Direct Injection Launch Window December 1969	I-82
2-66	Direct Injection Launch Window January 1970	I-82
2-67	Direct Injection Launch Window January - February 1970	I-84
2-68	Direct Injection Launch Window February - March 1970	I-85
2-69	Direct Injection Launch Window March - April 1970	I-86
2-70	Direct Injection Launch Window April 1970	I-87
2-71	Direct Injection Launch Window May 1970	I-88
2-72	Direct Injection Launch Window June 1970	I-89
2-73	Direct Injection Launch Window July 1970	I-90
2-74	Direct Injection Launch Window August 1970	I-91
2-75	Direct Injection Launch Window September 1970	I-92
2-76	Direct Injection Launch Window October 1970	I-93

ILLUSTRATIONS (Continued)

		Page
2-77	Direct Injection Launch Window October - November 1970	I-94
2-78	Direct Injection Launch Window November - December 1970	I-95
2-79	Direct Injection Launch Window December 1970	I-96
2-80	Parking Orbit Apollo Mission - 1 Day Surface Stay 86, 600 Pound Saturn Payload 2. 25° Continuous LEM Plane Change Constraint.	I-99
2-81	Direct Ascent Apollo Mission - 1 Day Surface Stay 88, 250 Pound Saturn Payload - 60 Minute Launch Window 2. 25° LEM Continuous Plane Change Constraint	I-100
2-82	Direct Ascent Apollo Mission - 1 Day Surface Stay 89, 700 Pound Saturn Payload - 30 Minute Launch Window 2. 25° LEM Continuous Plane Change Constraint.	I-101
2-83	LEM Weight Comparison for the Apollo Mission.	I-102
2-84	LEM Weight Contours for Translunar Trajectory Launched on July 23, 1969	I-103
3-1	Abort Point Geometry for Planar Aborts	I-110
3-2	Out-Of-Plane Abort Geometry	I-111
3-3	Schematic of Possible Abort Conic Flight Path Angles and Velocities	I-113
3-4	Permissible Vector Additions of the Abort Velocity Impulse ΔV_{ABORT} to the Pre-Abort Velocity Vector $\overline{V}_n$	I-115
3-5	Comparative Example of Planar Abort Velocity Solutions from Analytic Abort Trajectory Program . . .	I-116
3-6	Launch Azimuth as a Function of the Injection Angle, β_I for a Direct Ascent Launch on 23 January 1968 with a 72 Hour Flight Time	I-120

ILLUSTRATIONS (Continued)

		Page
3-7	Orbit Elements as a Function of S-IVB Translunar Injection Burn Time-To-Go for a Special Earth Model	I-121
3-8	Orbit Elements that are Functions of Injection Angle β_I Only for a Spherical Earth Model	I-121
3-9	Radius of Apogee for Pre-Abort Trajectories as a Function of S-IVB Burn Time-To-Go for All Nominal Injection Angles 80° to 88°	I-122
3-10	Cutoff Velocity, $V_{c.o.}$ as a Function of S-IVB Translunar Injection Burn Time-To-Go	I-123
3-11	Cutoff Angle, $\beta_{c.o.}$ as a Function of S-IVB Translunar Injection Burn Time-To-Go	I-124
3-12	Diagrammatic Variation in Altitude and Flight Path Angle for a Typical Direct Ascent Powered Flight Trajectory	I-125
3-13	Effect of Nominal Injection Angle, β_I on the Variation in Cutoff Altitude as a Function of S-IVB Burn Time-To-Go	I-125
3-14	Effect of Nominal Injection Angle, β_I on the Variation of Cutoff Azimuth as a Function of S-IVB Burn Time-To-Go	I-126
3-15	Effect of Variation in S-IVB Burn Time-To-Go on the Pre-Abort Trajectory Radius as a Function of Coast Time Beyond Premature Cutoff	I-127
3-16	Effect of Nominal Injection Angle, β_I on the Pre-Abort Trajectory Radius as a Function of Coast Time Beyond Premature Cutoff	I-128
3-17	Variation of Pre-Abort Velocity With Radius for Various S-IVB Burn Time-To-Go	I-129
3-18	Pre-Abort Velocity Contour Indicating the Effect of Nominal Injection Angle, β_I	I-130

ILLUSTRATIONS (Continued)

		Page
3-19	Diagrammatic Representation of Pre-Abort Trajectories Resulting from S-IVB Thrust Termination with Various Burn Times-To-Go	I-131
3-20	Variation in Flight Path Angle Along an Elliptical Earth Orbit	I-133
3-21	Short Time History of $\beta_{c.o.}$ for Particular Pre-Abort Trajectories Between 300 (sec) and 360 (sec) S-IVB Burn Time-To-Go	I-135
3-22	Short Time History of Cutoff Altitude, $h_{c.o.}$, for Particular Pre-Abort Trajectories Between 300 (sec) and 360 (sec) S-IVB Burn Times-To-Go	I-136
3-23	Altitude of Closest Earth Passage as a Function of S-IVB Burn Time-To-Go for a Range of Nominal Angles of Injection	I-137
3-24	Equivalent Impulsive Velocity Increment for a 24 Hour Life Time Earth Orbit Resulting from an Abort to Orbit 28 Seconds After a Premature Cutoff of the S-IVB	I-140
3-25	Apogee and Perigee Altitudes for a 24 Hour Life Time Earth Orbit Resulting from an Abort to Orbit 28 Seconds After a Premature Cutoff of the S-IVB	I-141
3-26	Total Return Time from Premature Cutoff to Landing as a Function of Coast Time Prior to the Abort Initiation for a Variation in Abort Velocity Increment at 15 and 60 Seconds Burn Time-To-Go	I-145
3-27	Total Return Time from Premature Cutoff to Landing as a Function of Coast Time Between Cutoff and Abort Initiation for a Variation in Abort Velocity Increment at 180 and 300 (Sec) Burn Time-To-Go	I-146
3-28	Limits of Total Return Time Variation for Burn Times-To-Go Between 0 and 180 Seconds; Planar Survival Aborts	I-147
3-29	Limits of Total Return Time Variation for Burn Times-To-Go Between 180 and 300 (Sec); Planar Survival Aborts	I-148

ILLUSTRATIONS (Continued)

		Page
3-30	Abort Solution Contour Indicating Types of Abort Trajectories Obtained as a Function of Burn Time-To-Go and Coast Time from Cutoff; V_{ABORT} = 1925 Fps	I-151
3-31	Abort Solution Contour Indicating Types of Abort Trajectories Obtained as a Function of Burn Time-To-Go and Coast Time from Cutoff; V_{ABORT} = 5000 Fps	I-152
3-32	Abort Solution Contour Indication Types of Abort Trajectories Obtained as a Function of Burn Time-To-Go and Coast Time from Cutoff V_{ABORT} = 10,000 Fps	I-153
3-33	Limits of Inertial Re-entry Velocity Variation for Minimum Time Aborts	I-154
3-34	Landing Site Loci for Various Launch Azimuths as a Function of Burn Time-To-Go at Cutoff	I-158
3-35	Landing Site Loci as a Function of Abort Velocity Impulse and Burn Time-To-Go at Cutoff	I-159
3-36	Abort Point and Landing Site Latitude Variation as Function of Abort True Anomaly	I-160
3-37	Longitude of Landing Site as a Function of Total Return Time from Cutoff to Landing for a Variation in S-IVB Burn Time-To-Go	I-161
3-38	Longitude of Landing Site as a Function of Total Return Time from Cutoff to Landing for a Variation in S-IVB Burn Time-To-Go	I-162
3-39	Longitude of Landing Site as a Function of Total Return Time from Cutoff to Landing for a Variation in S-IVB Burn Time-To-Go	I-163
3-40	Some Values of Abort Velocity Impulse Required for Various Plane Changes to Specified Landing Sites	I-167

ILLUSTRATIONS—PART II

		Page
2-1	Atlas D Holds Versus Time	II-12
2-2	Titan II Holds Versus Time	II-13
2-3	Probability of Launch (P_H) as a Function of Launch Window Length	II-25
2-4	Probability of Launch (P_L) as a Function of Window Length for Various Built-In Holds	II-32
2-5	Probability of Launch (P_L) as a Function of Window Length for the Range of Values Estimated for $\bar{h}$ With and Without Built-In Holds	II-36
3-1	Histogram of Time of Failures in the Agena ACS System	II-94a

Tables—Part I

		Page
1-1	Direct Injection and Parking Orbit Payloads	I-2
3-1	Possible Posigrade Aborts	I-112
3-2	Summary of NASA/MSC Powered Flight Data	I-118
3-3	Orbital Elements of Low Altitude Pre-Abort Trajectories Resulting From Thrust Terminations ≈ 300 Seconds Burn-Time-To-Go	I-134
3-4	Summary of Abort Trajectory Type as Indicated by the Post Abort Velocity Direction Relative to the Earth	I-150
3-5	Some Representative Values of the Abort Reentry Velocities	I-155
3-6	Aborts to Specified Landing Areas	I-166

Tables—Part II

2-1	Comparison of the Countdown Performance During the "R and D" Development of Boosters at ETR	II-6
2-2	Comparison of the Countdown Performance During the "R and D" Development of Boosters at ETR (Excluding R and D Data)	II-6
2-3	Saturn I Booster Development Countdown Record	II-8
2-4	Atlas Hold Recurrence	II-10
2-5	Estimated Range of $\overline{h}$	II-14
2-6	Conditional Probability of Meeting Launch Window if Countdown Begins and is Not Scrubbed for Technical Reasons	II-35
2-7	Probability of Launch During Three Day Firing Period (Excludes Consideration of Sea States)* Two-Day Turn-Around	II-38
2-8	Probability of Launch During Three Day Firing Period (Includes Consideration of Sea States)* Two-Day Turn-Around	II-39

Tables —Part II (Continued)

		Page
2-9	Probability of Launch During Three-Day Firing Period (Excludes Consideration of Sea States)* One-Day Turn-Around	II-40
2-10	Probability of Launch During Three-Day Firing Period (Includes Consideration of Sea States)* One-Day Turn-Around	II-41
2-11	Comparison of Best Estimates of Launch Probabilities	II-43
3-1	Equipment Operating Time	II-45
3-2	Comparison of DAC S-IVB Reliability Estimates for Earth Parking Orbit Versus Direct Injection	II-48
3-3	MSFC Criticality Ranking Summary	II-50
3-4	General Electric/Daytona SOAR III/Cindy I Component Reliability Summary	II-57
3-5	Relevant Flight Test Failure Data	II-83
3-6	Reasons for Failures	II-84
3-7	Agena Attitude Control Failures	II-86
3-8	Summary Table	II-88
4-1	Probability of Mission Success During Specified Firing Period	II-101

1. POWERED FLIGHT SIMULATIONS

The generation of representative powered flight profiles is the starting point in the development of the flight mechanics and abort analyses. This was performed by NASA/MSC for the parking orbit and direct injection trajectory modes. The energy reference chosen corresponds to a 72-hour translunar flight launch on January 23, 1968, and due east from Cape Kennedy. No attempt is made here to list the trajectory assumptions or to describe the method of analysis (see Reference 1). Only that information pertinent to the comparison between the parking orbit injection and direct injection is presented.

Specifically, one parking orbit and six direct injection powered flight trajectories were generated, utilizing a two-dimensional, nonrotating spherical earth program with a calculus of variations approach. This approach included determining the optimum propellant distribution among the Saturn V stages for a fixed liftoff thrust-to-weight ratio. The vehicles flown were identical in every respect except that 6074 pounds of third stage propellants and gases were lost in the parking orbit injection mode due to nonpropulsive weight expenditures. These weights were assumed to be consumable in the direct mode; their breakdown follows:

a)	Fuel vented in orbit (~4 revolutions)	4000
b)	Auxiliary boiloff	572
c)	Second ullage	392
d)	Second chilldown	398
e)	Attitude control	127
f)	Thrust buildup propellants	485
g)	Thrust decay propellants	100
	Total	6074 lb

The propellants in a) and b) are lost in the parking orbit; the remaining weight losses (1502 pounds) may then be attributed to restart.

The direct injection trajectories were generated to achieve translunar injection flight path angles of 80, 82, 84, 84.4, 86 and 88 degrees.* The payloads attainable with these burnout angles are presented in Table 1-1. The last value included is the payload for the parking orbit which has the characteristics described above.

Table 1-1. Direct Injection and Parking Orbit Payloads

Burnout Flight Path Angle (deg)	Payload (lb)
80.00	91,250
82.00	93,200
84.00	94,500
84.40	94,500
86.00	94,000
88.00	91,925
83.29	90,750

All of these powered flight simulations reach translunar burnout with essentially the same energy, i.e., that required to achieve a 72-hour translunar flight to the moon on January 23, 1968. In order to apply this data to other energy levels, it is necessary to assume a specific energy/payload ratio. This is computed by observing that 10.5 pounds of fuel is consumed at the end of translunar burn for each foot per second gained. Assuming a negligible potential energy gain, and a direct tradeoff of propellant with payload, this converts to a ratio of 2920 lb-sec^2/km^2, which is the value used in this analysis. This ratio applies to the parking orbit as well as the direct injection mode.

The effects of the parking orbit coast on payload can be determined by the rocket equation and the weight information of Reference 1. This equation, for the parking orbit discussed here, yields a tradeoff ratio of approximately 0.465 pound of injected payload to pounds of propellant lost

*Measured from the vertical.

in the coast phase. Applying the losses in a) and b) above yields a payload loss of 2130 pounds. This implies that the parking orbit payload for zero coast would yield 92,880 pounds which, for the energy level achieved, would be the maximum available with the parking orbit mode.

2. TRAJECTORY AND MISSION ANALYSIS

2.1 INTRODUCTION

The purpose of this section is to determine, first, the launch opportunities available in the three-year period of 1968 to 1970, if the direct ascent* trajectory mode for the Apollo mission is chosen. Then these launch opportunities are compared with those of the parking orbit mode to determine the relative merits of each. The comparison is made on the basis of number and length of launch opportunities available, relative translunar payload capabilities, and the lunar landing site accessibility. In all cases, every attempt is made to provide parametric displays which convey not only the implications of direct ascent but also present clear comparisons with the parking orbit mode.

The launch window results from the combined effects of many variables—the most prominent of which are direct ascent geometry, booster performance, and lunar lighting. These are treated separately in the next three sections. To a lesser and more subtle extent the window may be influenced by the free return trip time and inclination, and earth lighting at launch. These are treated in later sections. Some direct comparisons between parking orbit and direct ascent are made in Section 2.7. Section 2.8 presents an integrated method of tying many parameters together. Section 2.9 presents each of the 41 direct ascent launch opportunities which occur during the three-year period under study. Due to the lunar lighting constraint, approximately half of the 41 opportunities are eliminated. If lighting at earth during launch provides a rigid constraint, the number of opportunities is further reduced.

---

* "Direct ascent" is equivalent to "direct injection" and applies to the single burn launch to the moon.

2.2 DIRECT ASCENT GEOMETRY

Direct ascent windows occur for about eight consecutive days each lunar month. It requires about 27.3 days for the moon to circle the earth and complete a sidereal lunar month. During this period, the moon's declination varies between limits which are equal to the inclination of the lunar plane to the earth equator. Figure 2-1 shows the lunar inclination for the 1968 to 1970 time period under study. Thus for example, in October 1968 the inclination is 28.68 degrees and the range of declination will be within ±28.68 degrees. It is during the moon's passage through the negative declination range that direct ascent trajectories are possible. Therefore, direct ascent is possible every sidereal lunar month. However, the lunar lighting conditions are in phase with the synodic month which is two days longer. For this reason, direct ascent opportunities may be out of phase with proper lunar lighting which, as will be shown, rules out many months of the year. This section will, however, explain only geometrical characteristics of direct ascent launch.

The mechanics of direct ascent are easily explained if first some basic concepts regarding lunar trajectories are reviewed and then applied to the "special case" of direct ascent. Considerable detail is included for the reader with no direct ascent experience.

In defining lunar launch windows, two primary geometry considerations are involved—launch azimuth A_L and total in-plane angle from lift-off to lunar intercept Φ. These are depicted in Figure 2-2, from which it can be seen that A_L and Φ depend upon earth-moon geometry considerations that involve the time of day (position of the launch site θ_L) and the time of month (declination of the moon δ). Generally speaking, trajectories can be launched to the moon any time of day or any day of the month. However, to do this would require a launch azimuth range from 0 to 180 degrees and the utilization of parking orbits. Because of range safety constraints that are placed upon the firing azimuth from AMR, launch using parking orbits may be performed every day but only during that time of day when the required azimuth falls within the acceptable range, which occurs twice each day. With the further restriction of direct ascent launch, trajectories can only be flown during those days in the month when the coast angle is near zero, i.e., when the moon is near minimum declination.

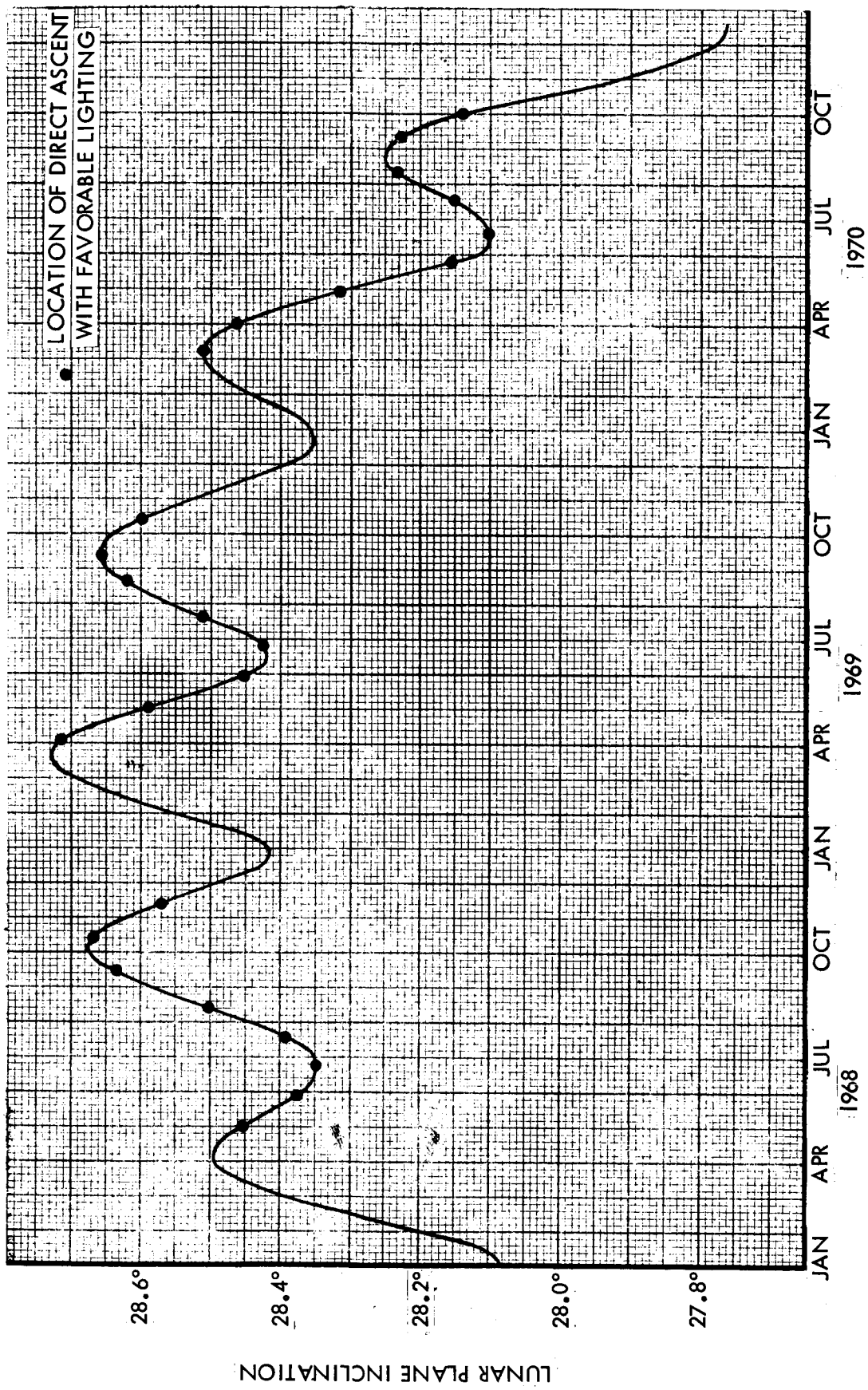

Figure 2-1. Lunar Plane Inclination to Earth Equator 1968, 69, 70

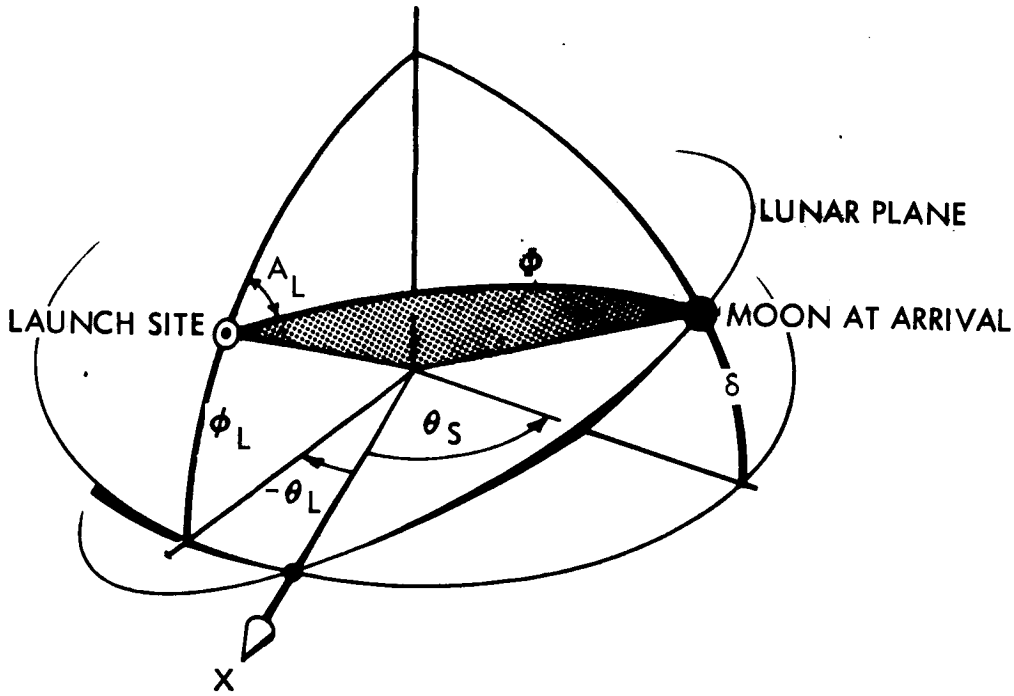

Figure 2-2. Launch Geometry

Thus, direct ascent windows occur only once each day and only during certain days each month. These fundamentals are demonstrated in Figure 2-3. Here the interdependency of liftoff time, total in-plane angle, and launch azimuth are shown for a complete lunar cycle of lunar declination δ and right ascension θ_s. The normalized liftoff times are referenced to the ascending node represented by the x-axis in Figure 2-2. For any lunar position, the interval of window between AMR azimuth constraints can be read by differencing the beginning and final liftoff times while moving left to right on the constant declination line. The pattern of changing Φ's and A_L's is apparent through each window. For example, if the moon is at maximum declination (+27.4 degrees) the Pacific injection window opens with a 72-degree launch azimuth at 68 minutes and closes with a 108-degree azimuth at 346 minutes. The total window length is 278 minutes. The total in-plane angle Φ varies from about 63 degrees initially to approximately 5 degrees when the window closes. Similarly the Atlantic injection window (sometimes referred to as short coast window) opens at 371 minutes and closes at 649 minutes, again a 278-minute length. The Φ values through the second window are approximately 356 to 297 degrees.

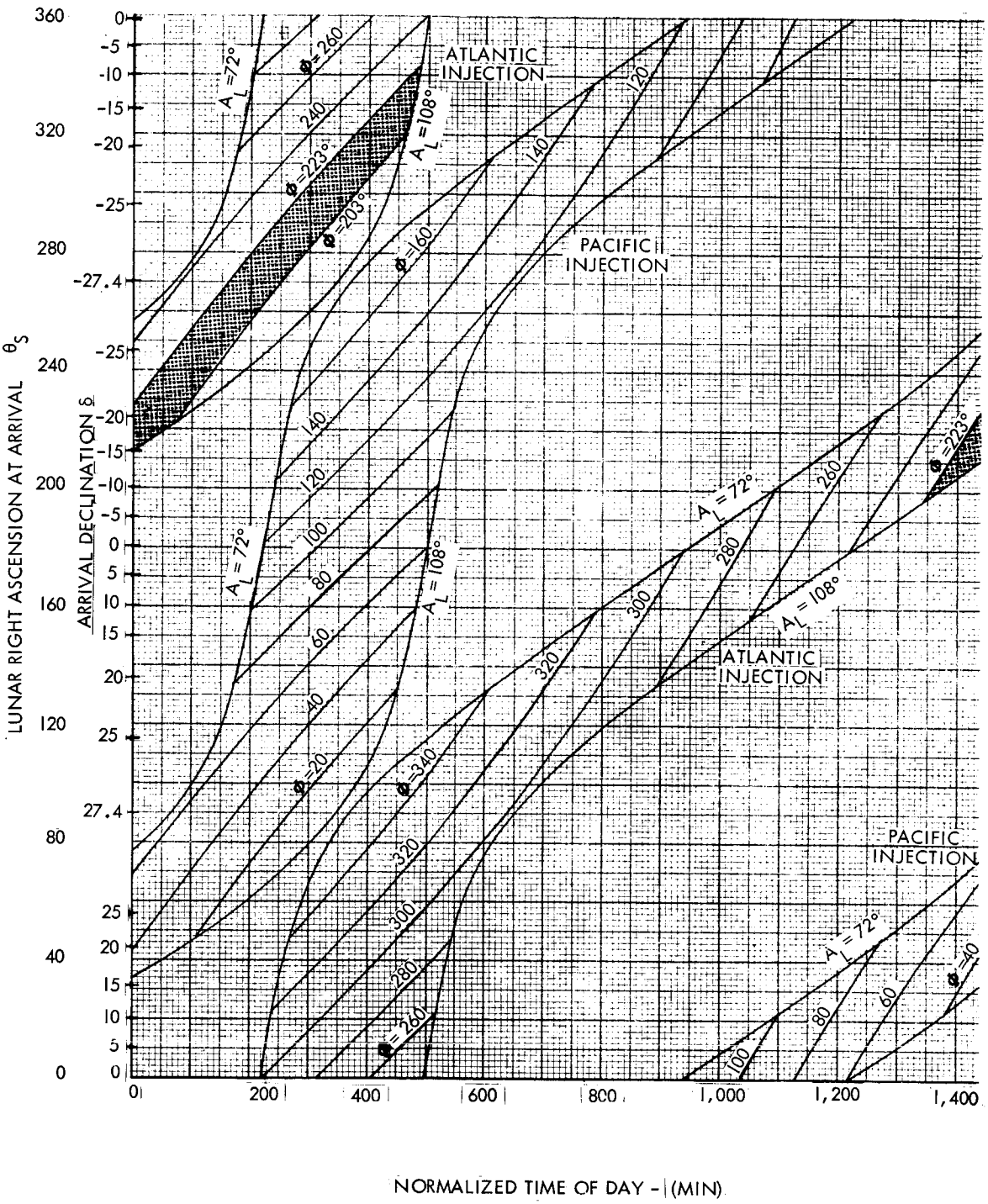

Figure 2-3. Lunar Trajectory Geometry

The significance of the Φ value and its bearing upon launch operations for parking orbit or direct ascent shall now be established. For the parking orbit mode, Figure 2-4 shows the components of the in-plane total angle Φ for a typical parking orbit case. This angle Φ can be expressed by the summation

$$\Phi = \theta_{PF} + \theta_C - \eta_o + \eta_T$$

where

θ_{PF} = The downrange powered flight arc which is approximately 52 degrees ±0.5 degree for the Saturn V.

θ_C = The coast angle which, for parking orbits, is varied so that the in-plane geometry conforms to the required total angle Φ. For example, assume θ_C is 142 degrees.

η_o = The true anomaly of the transfer ellipse at injection. To a very close approximation, $\eta_o \cong 2\gamma$ where γ is the injection flight path angle. For S-V launch from a parking orbit γ is a constant 5.6 degrees, and therefore, η_o is 11.2 degrees. Whereas θ_C is varied to adjust the total in-plane angle in a parking orbit, η_o (or γ) is varied in the direct ascent case.

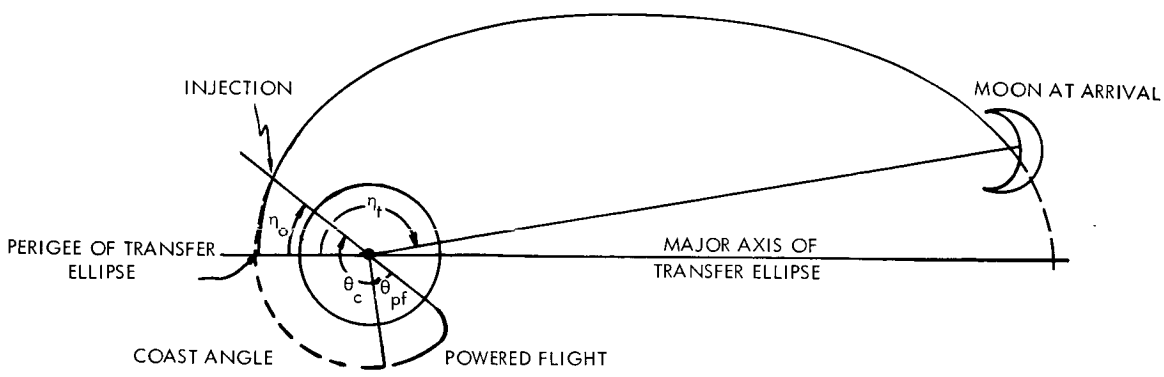

Figure 2-4. Parking Orbit In-Plane Geometry

η_T = The true anomaly in the transfer ellipse at lunar intercept. It is a function of the lunar distance (which is essentially fixed on a given day) and the trip time. The latter, as described in Figure 2-5, does not alter η_T significantly. For example, a value of 173 degrees, corresponding to a 72-hour trip time and minimum lunar distance is used.

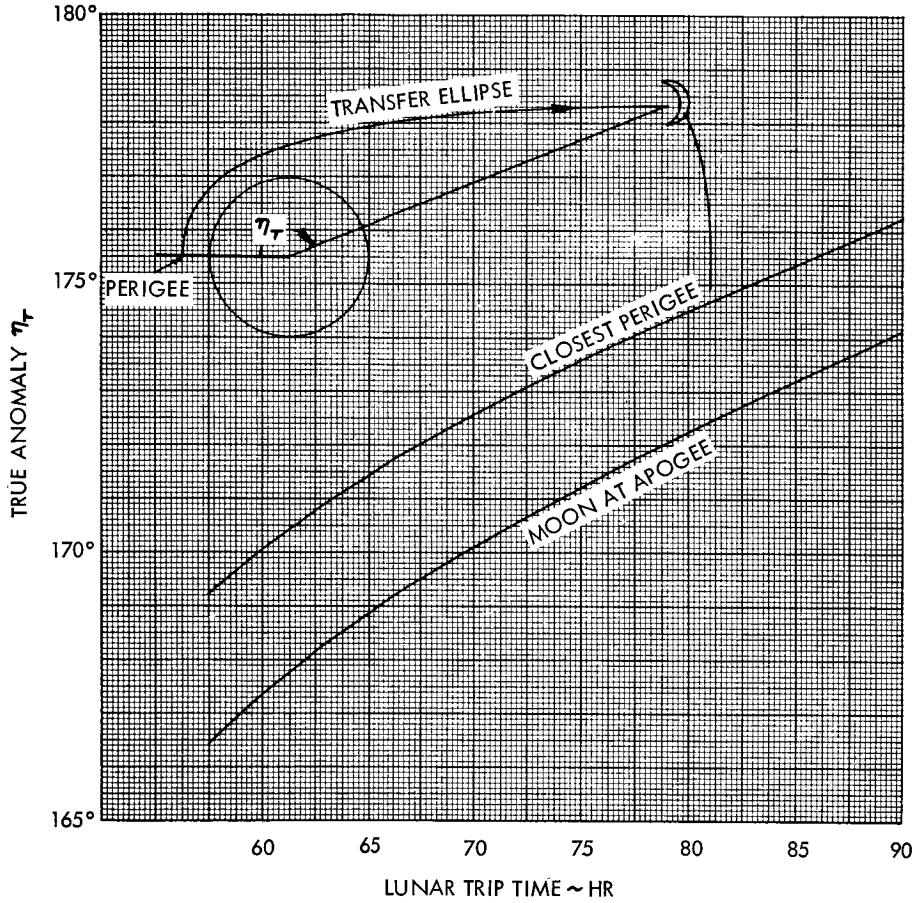

Figure 2-5. Lunar Trajectory True Anomaly

Summing up the example values

$$\Phi = 52^\circ + 142^\circ - 11^\circ + 173^\circ$$

$$= 356^\circ$$

This happens to be the Φ value which opened the Atlantic injection window in the example in Figure 2-3. Returning again then to that example, it was observed that Φ decreased through the window from 356 to 297 degrees. Considering parking orbits, the only variable in the Φ equation is θ_C and thus it must also decrease through the window in one to one correspondence with Φ. Thus, if launch were made at 108 degrees A_L at the end of the window, Φ is 297 degrees and θ_C must be 83 degrees. The lines of constant Φ may be labeled as constant coast lines if desired.

For the direct ascent mode, the coast angle θ_C is zero so that it must be excluded from the Φ equation, or

$$\Phi = \theta_{PF} - \eta_o + \eta_T$$

These components are described in Figure 2-6.

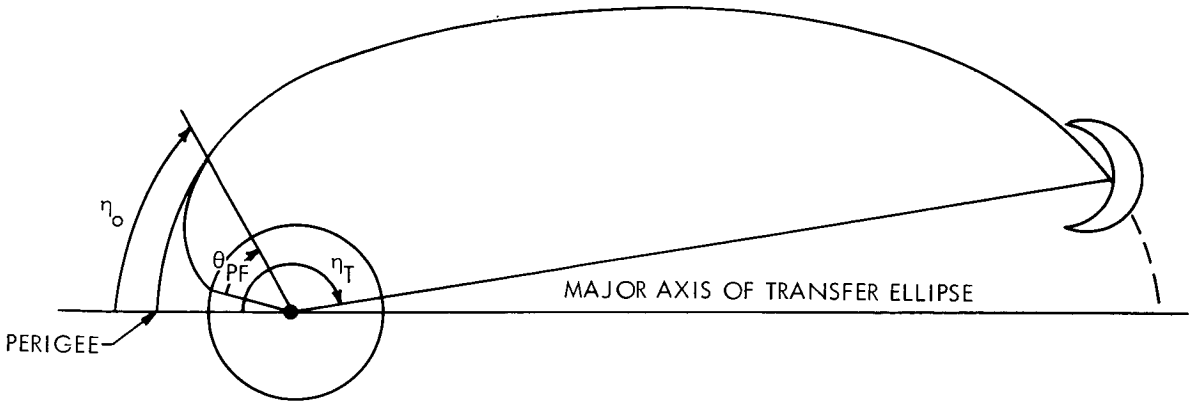

Figure 2-6. Direct Ascent In-Plane Geometry

Again θ_{PF} and η_T are essentially constant. Thus, if Φ is to be varied in order to generate a window, the flexibility must exist in η_o. Since it is more meaningful to think in terms of γ rather than η_o, the substitution $\eta_o = 2\gamma$ is made yielding

$$\Phi = \theta_{PF} - 2\gamma + \eta_T$$

It will be shown in the performance section that the range of γ without sacrifice in direct ascent payload relative to parking orbit payload, is about 1 to 11 degrees. Thus, direct ascent constraints determined by the corresponding limits in Φ, using the previously established values for θ_{PF} and η_T are

$$\Phi_{max} = 52^\circ - 2(1^\circ) + 173^\circ$$

$$= 223^\circ$$

$$\Phi_{min} = 52^\circ - 2(11^\circ) + 173^\circ$$

$$= 203^\circ$$

The resulting window is shown shaded in Figure 2-3. It can be seen that launch is possible only for lunar declinations lower than -9 degrees. However, for a 60-minute minimum window, launch must be confined to declinations below -16 degrees. It is interesting to note that since Φ decreases as one progresses through the daily window, γ is increasing and the trajectory must be "lofted" more and more.

2.3 SATURN PERFORMANCE CHARACTERISTICS

The performance characteristics of direct ascent and parking orbit missions are compared in this section. The influence of payload affecting factors such as injection flight path angle, launch azimuth, flight time and launch date is discussed.

Payload information was generated for a 72-hour translunar trajectory launched on 23 January 1968. This data was supplied by NASA/MSC Houston for injection flight path angles of 2, 4, 5.6, 6, 8, and 10 degrees.* Results were expanded to other flight times and dates in the following manner: first an energy to payload conversion factor ($\Delta W/\Delta E$) value of 2920 lb-sec^2/km^2, was established by processing vehicle performance information from the Houston data near the end of burn. Then the 23 January free-flight trajectories with a 72-hour flight time were run on

*Measured from the horizontal

the STL direct ascent program to establish a reference energy level. The energies were then obtained for other flight times and launch days in the January* window and converted to payload data.

Figure 2-7 is a display of injection payload for the 23 January launch day. The 72-hour flight time curve is identical to that supplied in the Houston document.(1) The other curves were obtained by differencing the energy levels computed by the STL direct ascent lunar trajectory program (referenced to the 72-hour flight time) and multiplying by the $(\Delta W/\Delta E)$ adjustment factor.

Thus, for a given γ

$$W_{new} = W_{ref} + (E_{ref} - E_{new}) \frac{\Delta W}{\Delta E}$$

where

W = Total payload in pounds

E = The energy of the lunar trajectory transfer ellipse

new = Denotes condition of the changed trajectory

ref = Denotes the 72-hour 23 January reference data

$\frac{\Delta W}{\Delta E}$ = The conversion factor for converting energy to payload. The value used is 2920 lb-sec^2/km^2.

Several significant items are shown by Figure 2-7. The direct ascent payload drops below parking orbit payload outside the γ range of 1 to 11 degrees. This is the source for the γ values used in the

*The January 1968 window is used to evaluate performance characteristics since that is the month for which data was received. However, it is not a good mission window since, as will be pointed out later, the lunar lighting is not favorable at that time.

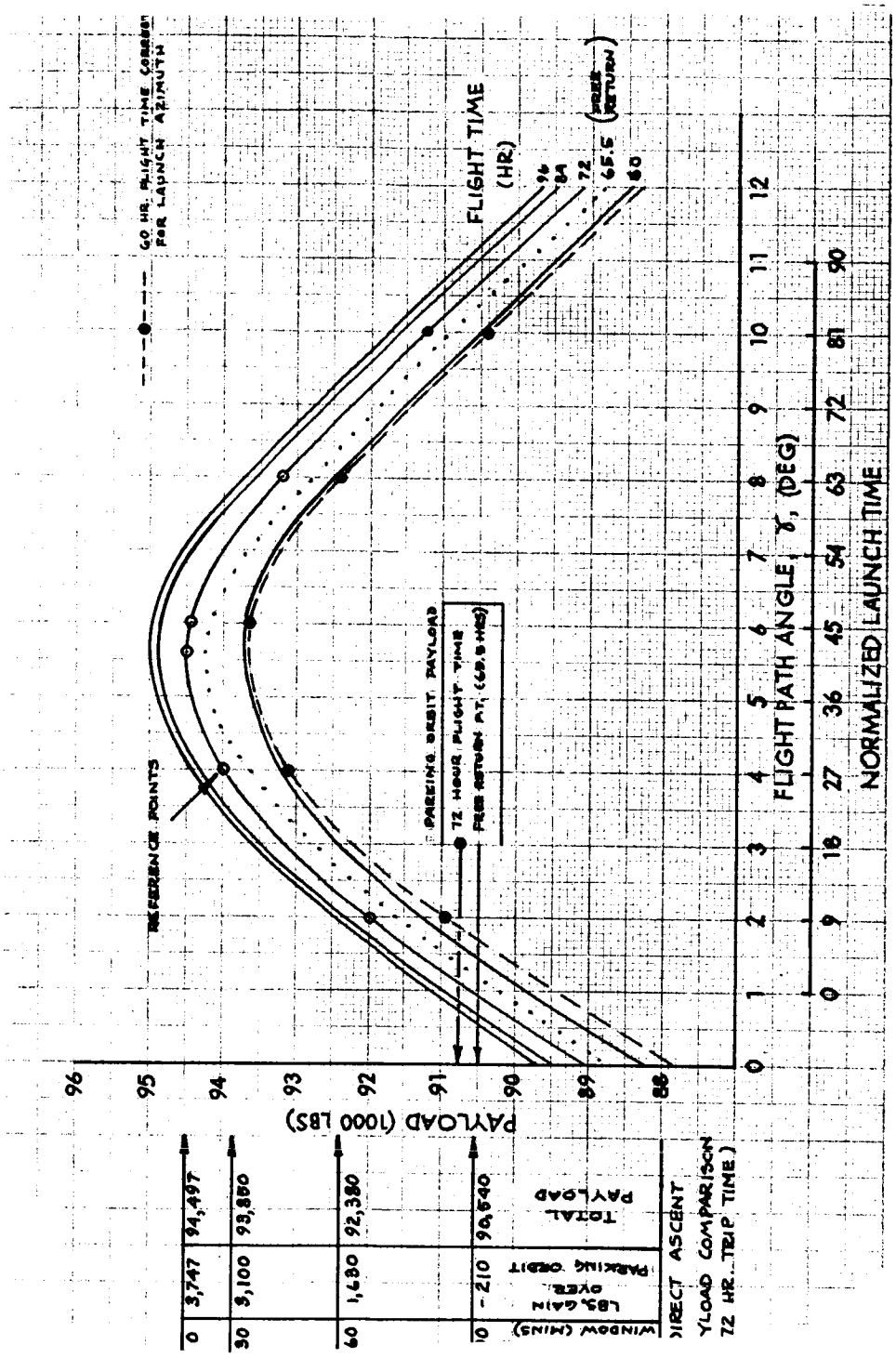

Figure 2-7. Saturn-V Payload Characteristics
January 23, 1968

geometrical definition of the direct ascent launch window in the previous section. It is apparent that if a payload higher than the parking orbit capability (90,750 lb)* is desired, the range of γ is decreased and the length of the daily window must likewise diminish. Payloads corresponding to 30-, 60- and 90-minute launch windows are indicated by marks at the upper left. A 30-minute window, for example, provides a 93,850-pound payload and utilizes flight path angles from 3.8 to 7.2 degrees.

The parking orbit payload data, which is used for comparison, was generated in the same manner as the direct ascent information and was also supplied by NASA/MSC. Figure 2-7 shows the 90,750-pound parking orbit reference payload as well as the parking orbit payload resulting from a free return trajectory. Launch from parking orbit is always at a 5.6-degree injection flight path angle.

The resulting payload calculation for direct ascent and parking orbit with several flight times (including free return flight times) are presented for the January window in Figures 2-8 through 2-12. It is noticed that the displays change only slightly from day to day. These changes are due to the lunar distance effect. It is pointed out that Figures 2-7 through 2-12 are all for a 90-degree launch azimuth. Some remarks regarding the effect of this factor upon performance degradation will now be discussed.

The daily trend in launch azimuth through the typical January direct ascent window (which, as shown in Figure 2-1, happens to be near the minimum lunar inclination within the stated three year period) is described in Figure 2-13. The vertical date lines which are superimposed upon this figure pinpoint the unique azimuth and launch time on each day. The shape of this curve depends upon the lunar plane inclination. For comparison, the figure is repeated in Figure 2-14 for September 1968, i.e., the direct

*In generating this parking orbit payload, MSFC has assumed that 6074 pounds of fuel has been lost due to boil-off during three revolutions in the parking orbit and engine restart.

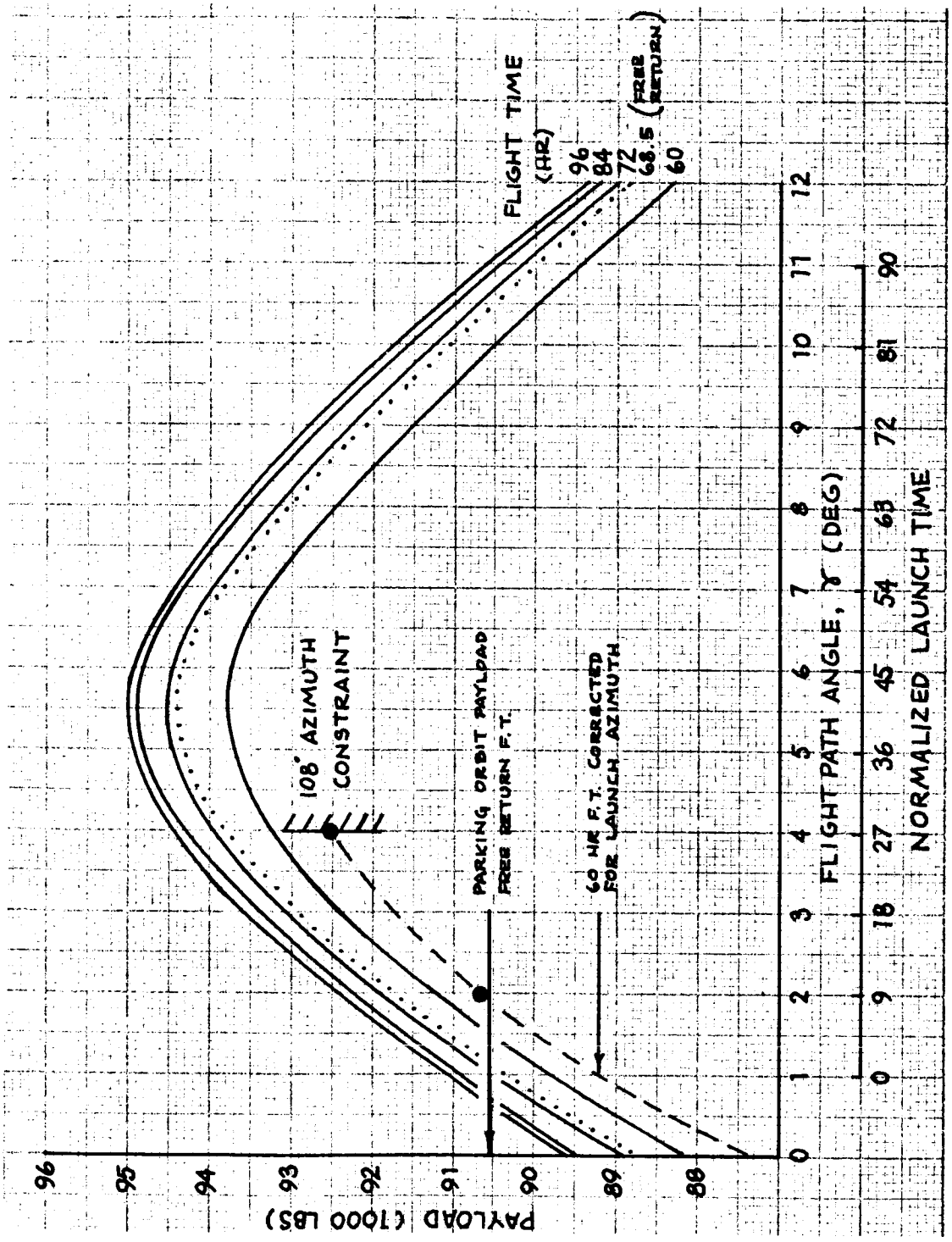

Figure 2-8. Saturn-V Payload Characteristics
January 19, 1968

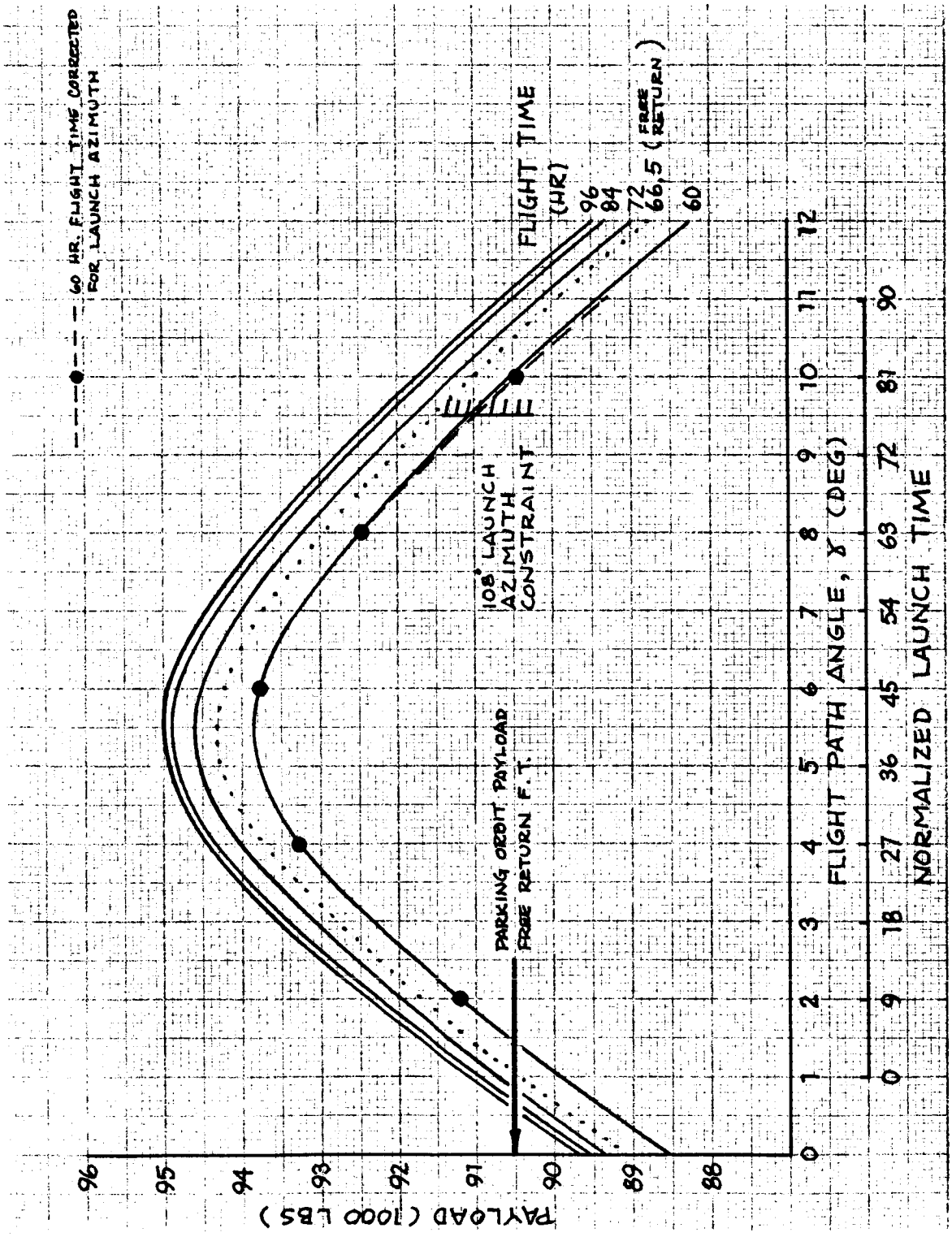

Figure 2-9. Saturn-V Payload Characteristics
January 21, 1968

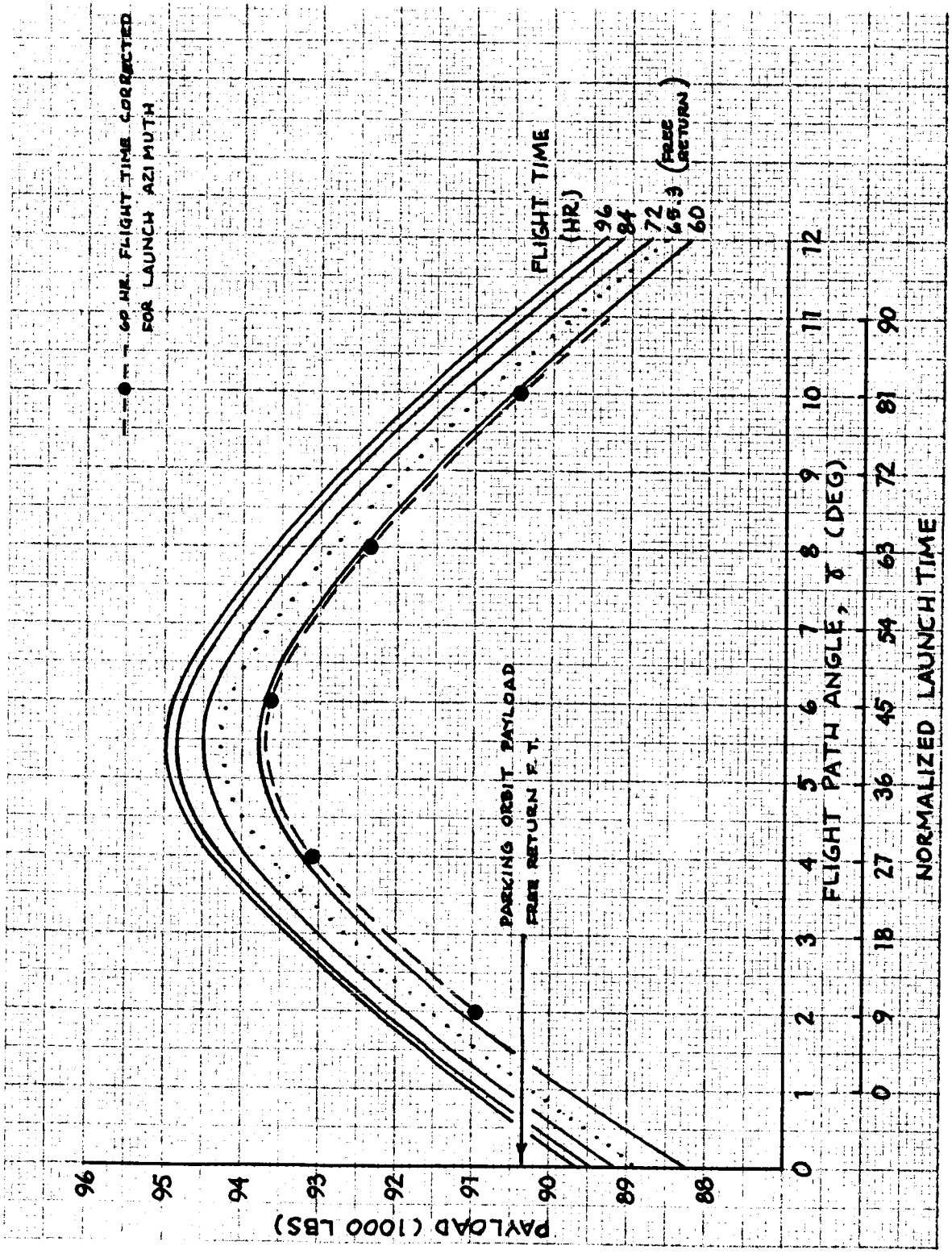

Figure 2-10. Saturn-V Payload Characteristics
January 25, 1968

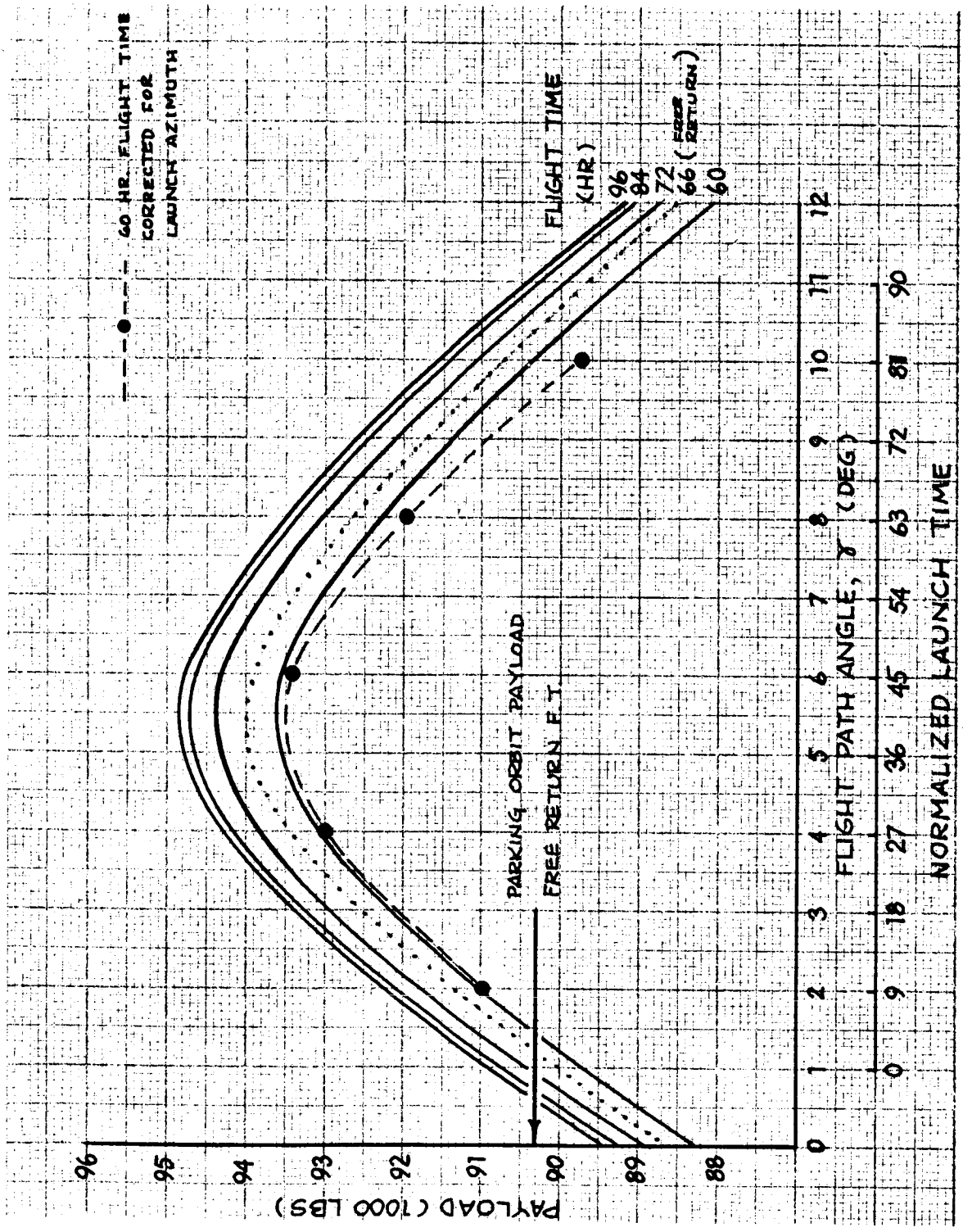

Figure 2-11. Saturn-V Payload Characteristics
January 27, 1968

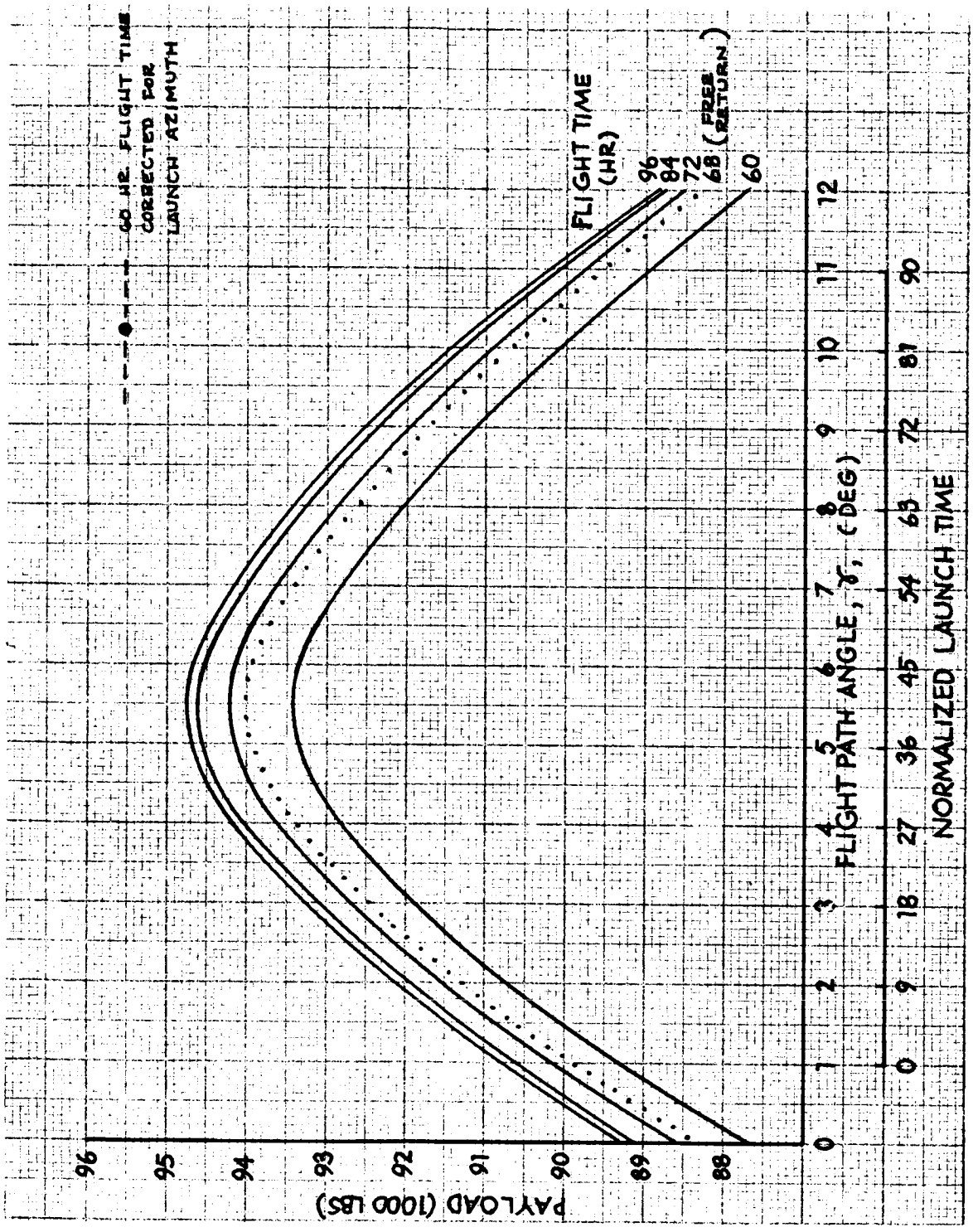

Figure 2-12. Saturn-V Payload Characteristics
January 29, 1968

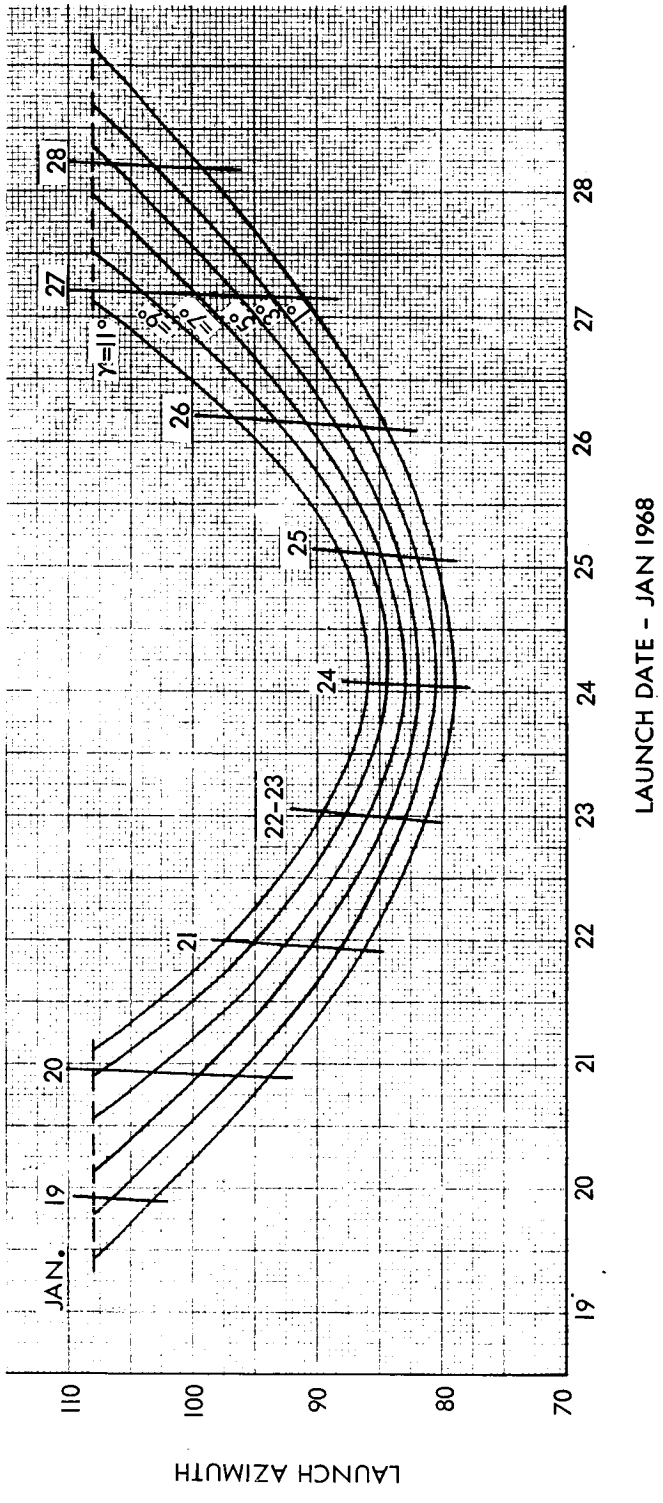

Figure 2-13. Direct Injection Launch Azimuths, January 1968—Month of Near Minimum Lunar Plane Inclination to Earth Equator

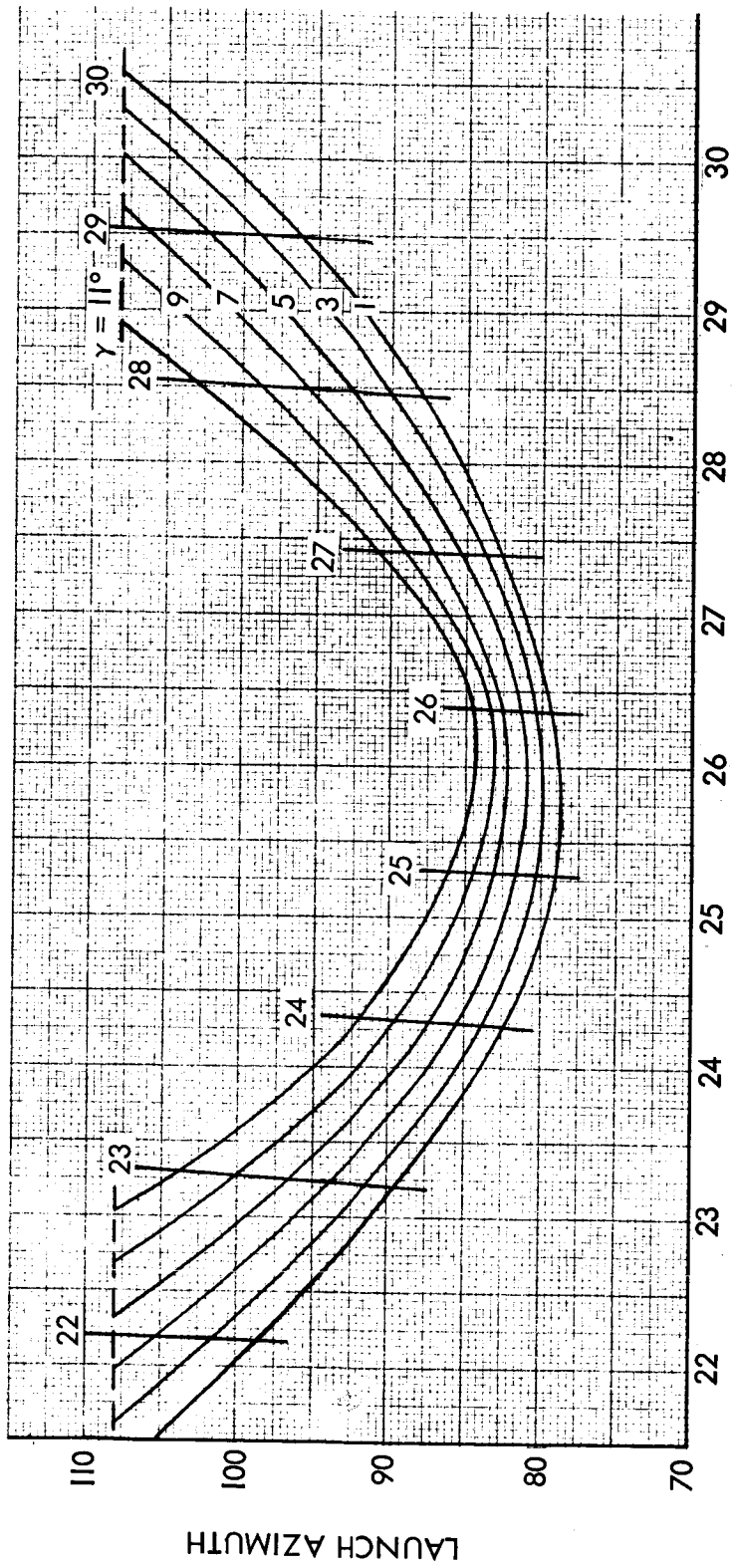

Figure 2-14. Direct Injection Launch Azimuth.September 1968—Month of Maximum Lunar Plane Inclination to Earth Equator

ascent month of maximum lunar inclination.* Comparison of the two curves indicates a basic resemblance, that is, a high (90 to 180 degree) range at the beginning and end of windows and a lower (80 to 90 degree) range through the middle days. This similarity exists through all direct ascent windows.

Figure 2-15 shows the Saturn V payload loss due to launches at other than 90-degree azimuths. Using data from Figures 2-13 and 2-15, the azimuth effects have been computed and are shown with black symbols for the 60-hour trajectories in Figures 2-7 to 2-12. These figures show that azimuth effect causes a loss in total payload. While shown only for the 60-hour flight time, the effect is similar (although not identical) for all flight times. The losses are greater for launch dates near the end of the window where launch azimuths in the 108-degree range are encountered.

In evaluating Figures 2-7 through 2-12, two gross considerations should be kept in mind. One, a comparison is being made between the two modes and thus payload differences are of interest. Two, a general analysis of direct ascent is being made and thus actual values are desirable. In the latter case the launch azimuth corrected data is the applicable information. However, when making comparisons, it is desirable to fix azimuth. Thus, since the parking orbit payloads used in Figures 2-7 through 2-12 are for a 90-degree launch azimuth, the corresponding data for direct ascent is applied. This brings up a question—is it realistic to hold azimuth constant while comparing the two launch modes especially in lieu of the differing launch azimuth patterns through the window? Possibly a better way of stating the problem is, does either launch mode gain a payload advantage through the azimuth philosophy applied? The answer, being very dependent upon the method of comparison, is approached in the following manner. Because of shipposition constraints, Apollo mission

*It is noted that lunar plane inclinations sometimes exceed the September 1968 value during the three-year period, as evidenced in Figure 2-1; however, a mission window does not exist at any of these times.

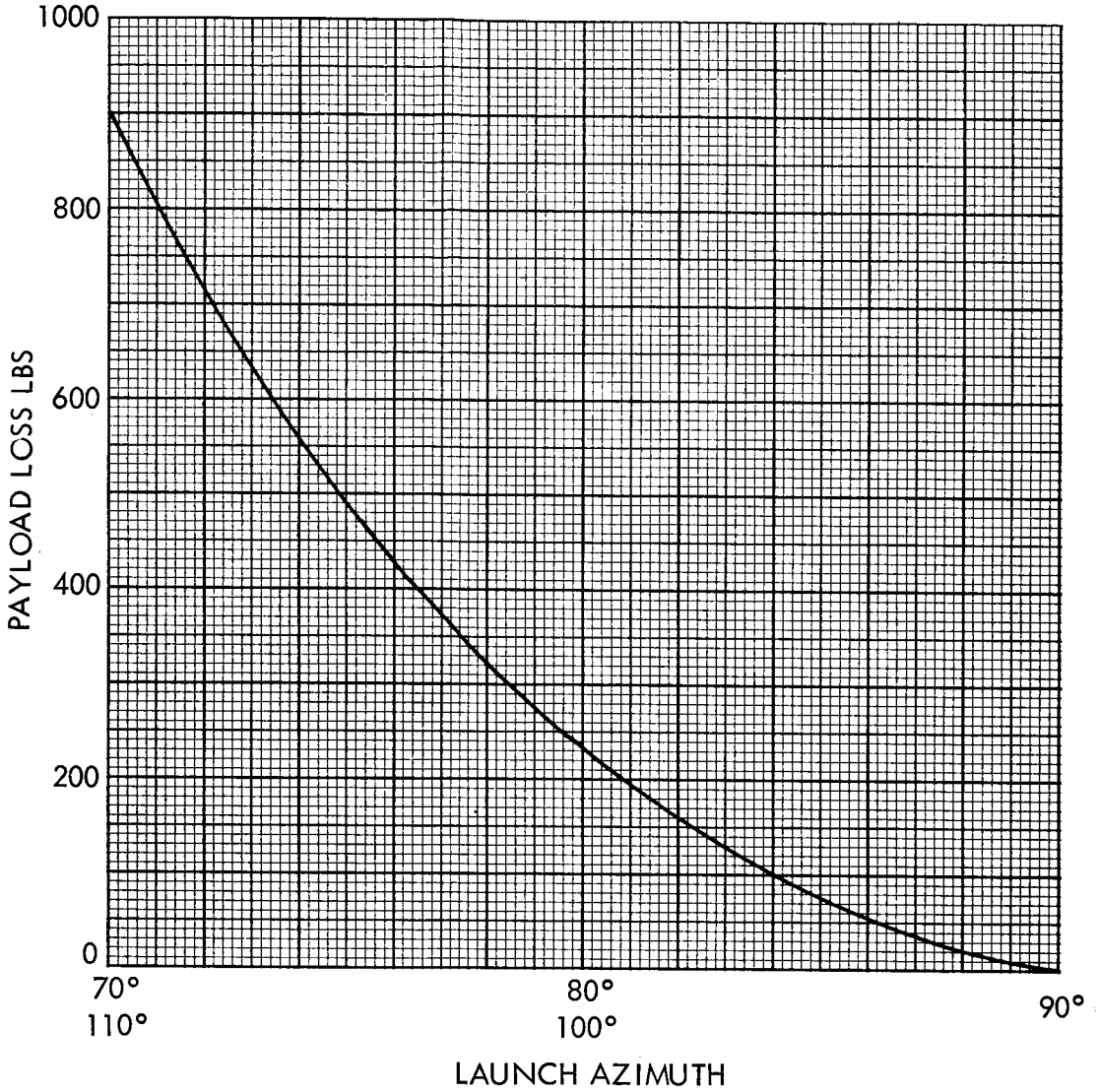

Figure 2-15. Payload Loss from Launch Azimuth—
Direct 72-hour Lunar Mission

launch azimuth is confined to 26 consecutive degrees anywhere within the 72 to 108 degrees. For minimum loss due to azimuth, the range should be 77 to 103 degrees—13 degrees on either side of 90 degrees. Thus, from Figure 2-15, a maximum loss of 370 pounds is the result of launching at 77 or 103 degrees. Regarding direct ascent, Figure 2-13 shows a launch azimuth of 108 degrees on some days (early and late in the window) or 715 pounds loss compared with a 90-degree launch azimuth. This

results in an advantage of 345 pounds to parking orbit. However, a similar analysis in the middle days when the direct ascent launch azimuth is closer to 90 degrees shows a 100-pound advantage for direct ascent. The conclusion is thus made that, while launch azimuth can be considered in specific situations, it is not a factor to be weighed in gross payload comparisons. This is particularly true since the parking orbit mode requires launch azimuths other than 90 degrees as well as the direct ascent mode. It has therefore been decided to ignore the azimuth effects and compare the two trajectory modes based on flight times corresponding to the free return trajectory.

Figure 2-16 shows the resulting comparison made on the basis of direct ascent launch window size. It is the result of processing the data in Figures 2-7 through 2-12. From these figures, it is clear that the smaller the acceptable window, the greater the injection payload. It is significant that if a 90-minute minimum window is demanded, there is a slight payload disadvantage to direct ascent of about 210 pounds. The payloads for each mode are equal for a direct ascent launch window size of 87 minutes.

It is of interest to make two additional points concerning Figure 2-16. First, the sloping lines are nearly parallel. This is because two of the three contributors to day-to-day differences in injected payload weight (i.e., flight time and lunar distance) are common to both modes.

The second item of interest is the explanation of the gradual decrease in payload with advancing launch date. Consider Figure 2-17 which is a plot of the lunar transfer ellipse energy as a function of the time (in days) from perigee of the moon at arrival for the January 1968 window. Actually being reflected here is the effect of lunar distance at arrival. The energy for constant flight time is seen to have a negative dip which bottoms out at the moon's perigee. With a decrease in energy, larger payloads are possible. Thus, the payloads of both direct ascent and parking orbit would reflect this with gains in payload for decreased lunar distances. The dotted line in this figure is the energy locus of free return trajectories in this January window. It is the result of combined day-to-day changing of both

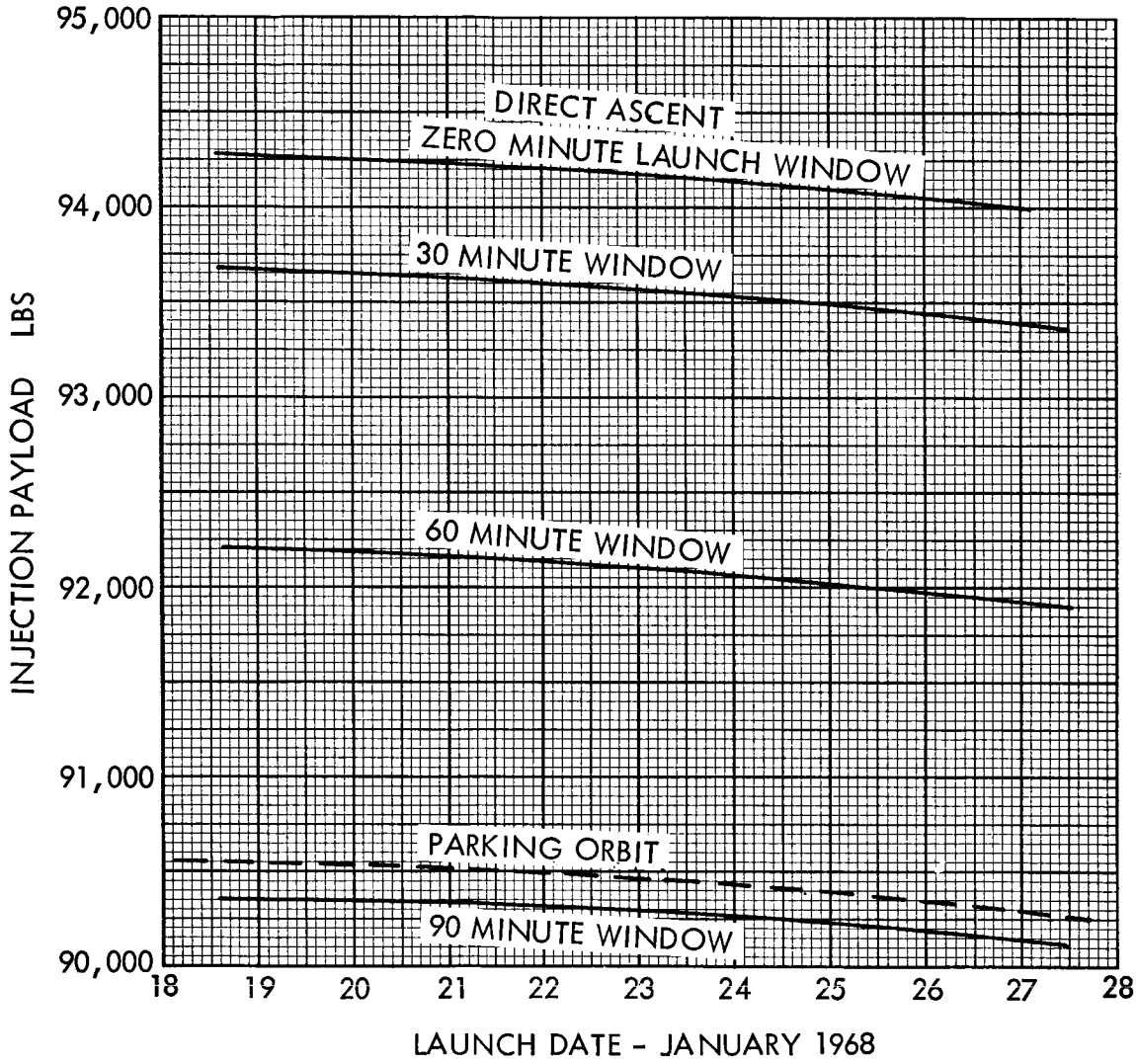

Figure 2-16. Payload Comparison—Free Return Trip Times with 0° Return Inclination to Lunar Plane, 90° Launch Azimuth

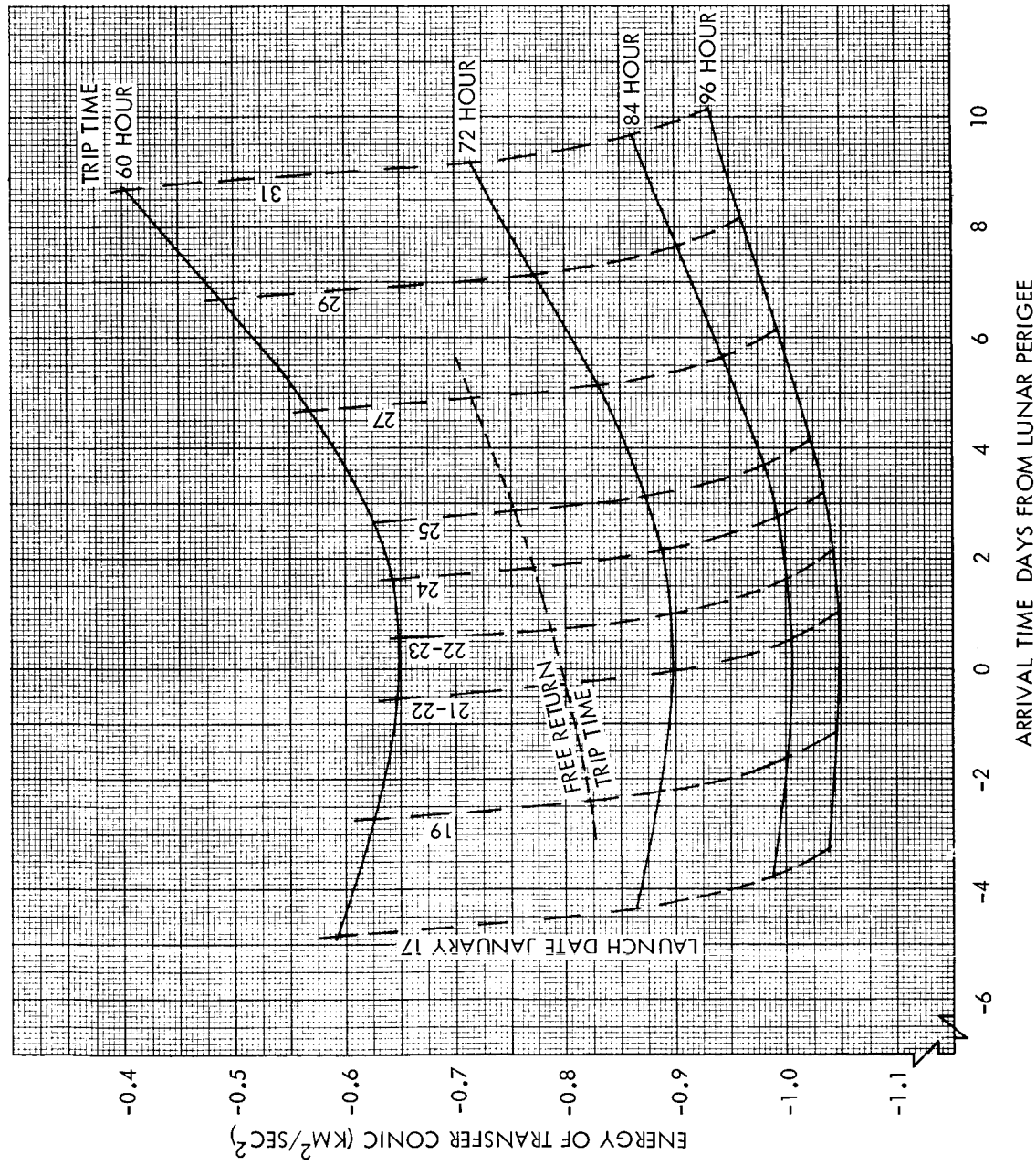

Figure 2-17. Energy Requirements in January 1968

lunar distance and free return flight time. The required energy increases with date through the January window, and thus the payload in Figure 2-16 decreases accordingly.

The feature of near parallel lines in Figure 2-16 makes it possible to construct a simple yet extremely significant crossplot comparing direct ascent and parking orbit payloads. This is the payload summary curve presented in Figure 2-18. It is a somewhat universal display and a few points shall be emphasized:

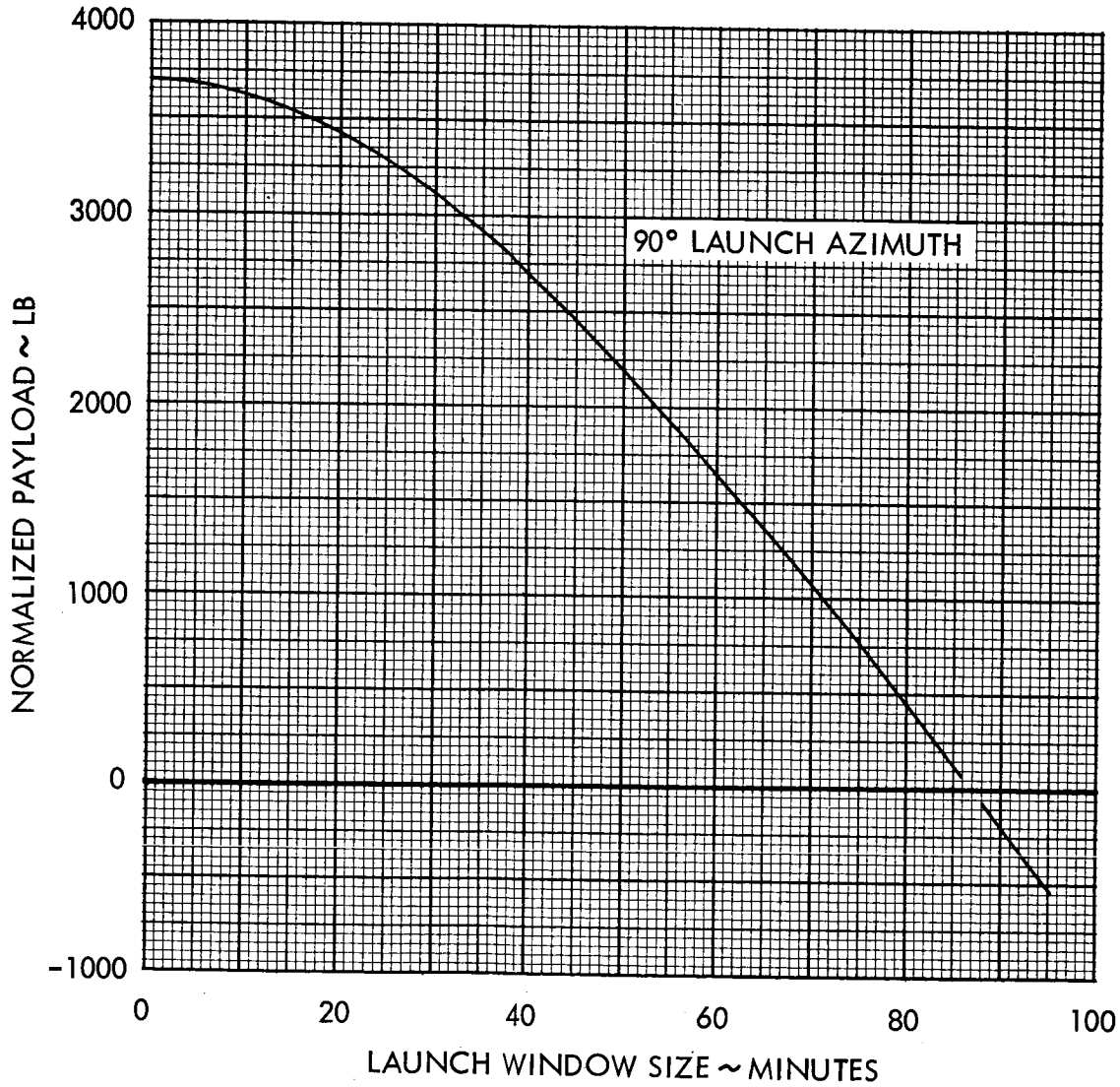

Figure 2-18. Payload Summary—Direct Ascent Payload Advantage Over Parking Orbit

a) The comparison is independent of flight time and lunar distance since these are common to both. Thus, the payload differences shown apply for all launch windows exclusive of date.

b) The effect of launch azimuth upon the comparison, being small, can be exempted on a "lost in the noise" basis.

c) The tradeoff between payload and launch window size is nearly linear between 30 and 90 minutes and is about 54 lb/min. A 10-minute window size attains the nearly maximum payload gain of 3700 pounds.

Figure 2-18, therefore, represents the rather esthetic reduction of direct ascent payload gain to a function solely of launch window size. From the figure the fact is clear that windows less than 90 minutes must be tolerated if a gain in injected weight is to be realized.

Comparisons between parking orbit and direct ascent payloads have been made on the basis of the free return flight time. It is repeated that as far as comparisons are concerned, it does not matter what flight times are used since the differences will be the same. It is interesting, however, to note the effect of flight time upon payload since free return lunar transfer trajectories tend to have fairly rapid flight times (58 to 75 hours for the direct ascent mode) and can be costly from the payload standpoint. Figure 2-19 shows the payload gain, referenced to the 58-hour flight time, that is realized through longer flight times. The benefits gained in increasing the flight time apply to the parking orbit mode as well as direct ascent.

There is one significant difference in direct ascent as compared to parking orbit if the free return constraint applies. This is concerned with the fact that the free return flight times are shorter for the moon near perigee, which results in higher required energies or lower payloads. For the three-year period considered, the moon's distance is near its minimum value for the direct ascent windows. The mean free return flight time, as shown in Figure 2-19 is about 64 hours for direct ascent. The parking orbit mode, on the other hand, has the option of launch when the moon is near its apogee where the flight times are longer, and as high as 80 hours. The mean free return flight time in this case will be about 70 hours. The average gain in payload for the parking orbit mode, as shown in Figure 2-19, will be about 350 pounds.

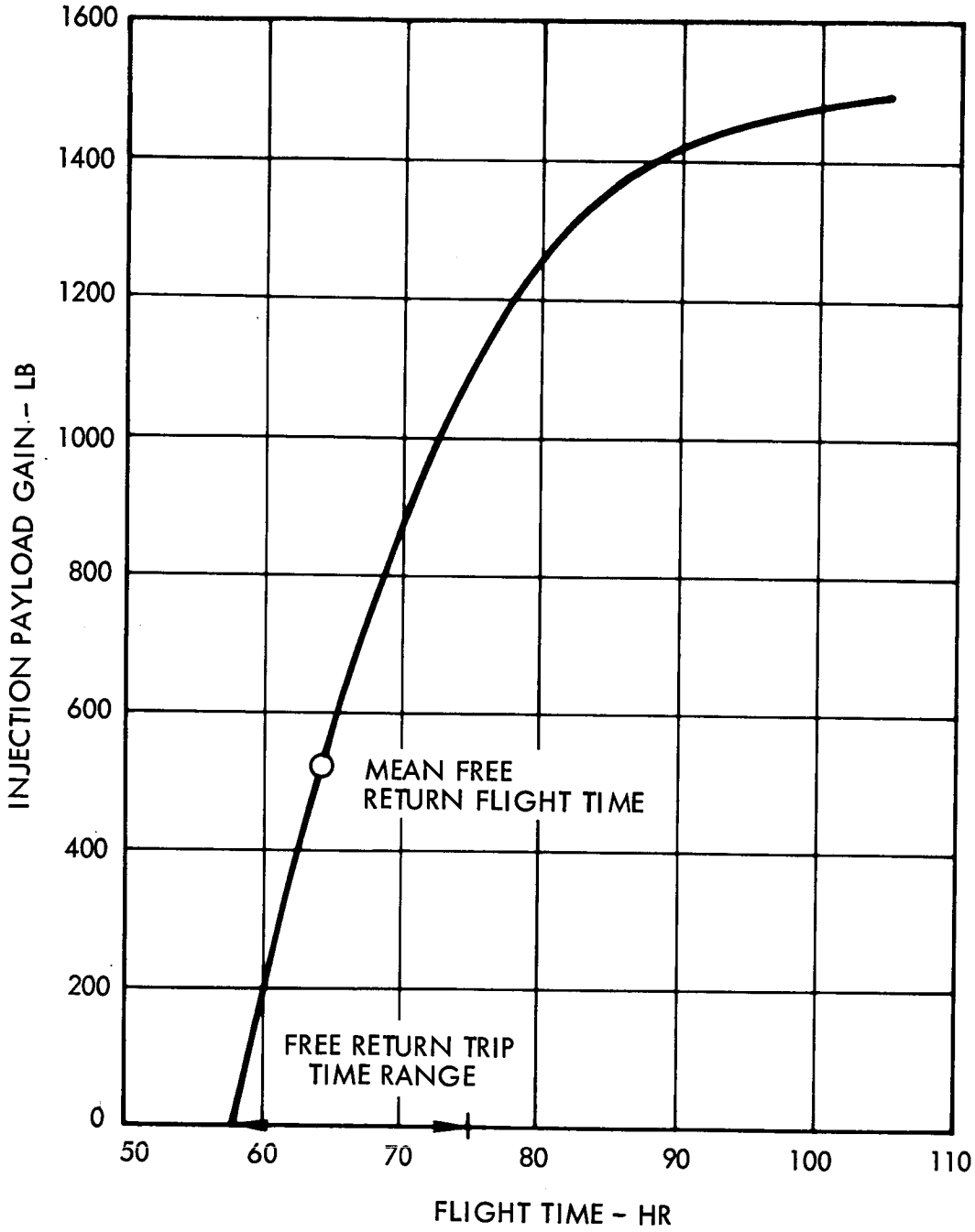

Figure 2-19. Payload Tradeoff with Flight Time

2.4 EFFECTS OF THE LUNAR LIGHTING CONSTRAINT

The lighting constraint at the moon upon landing requires that the site be in direct sunlight with the angle of incidence between 15 and 45 degrees above the horizon. That is, the sun must be behind the astronaut as he views the landing site during translation and touchdown. The range of lunar landing sites selected for this study is confined to ±45 degrees selenographic longitude and ±10 degrees latitude.

Figures 2-20 to 2-22 show the time history for the 3-year period of the combined lighting and site location constraints. Within the boxes in the displays the lighting is favorable for the landing sites being considered. Before discussing these figures in detail, it is instructive to analyze the relation between site location and the sun's position.

The assumption made in generating these displays is that the lunar site lies in the sun plane (ecliptic) and thus there is a one-for-one tradeoff between longitude of the sun from the site and the sun elevation at the site. This coplanar case is shown in Figure 2-23 and is assumed to be correct for sites on the lunar equator.* In this figure, e is the sun's elevation measured from the eastern horizon and λ is the sun's eastward longitude relative to the site being considered. For sites off of the lunar equator, Figure 2-24 is helpful. Here, the sun's zenith is located at the center of the circle and has a longitude λ with respect to the site indicated. The sun's zenith angle α completes the right spherical triangle shown, where μ is the site latitude. The relation for the sun's elevation is given by

$$e = 90^{\circ} - \cos^{-1} (\cos \mu \cos \lambda)$$

Sun elevation angle versus relative sun longitude is plotted for constant landing site latitudes in Figure 2-25. The amount of error in the coplanarity assumption is indicated by the separation of the various latitude lines from the 0 degree latitude case. For the assumed bounds on latitude

*In reality, the ecliptic is inclined only 1.5 degrees with the moon's equator.

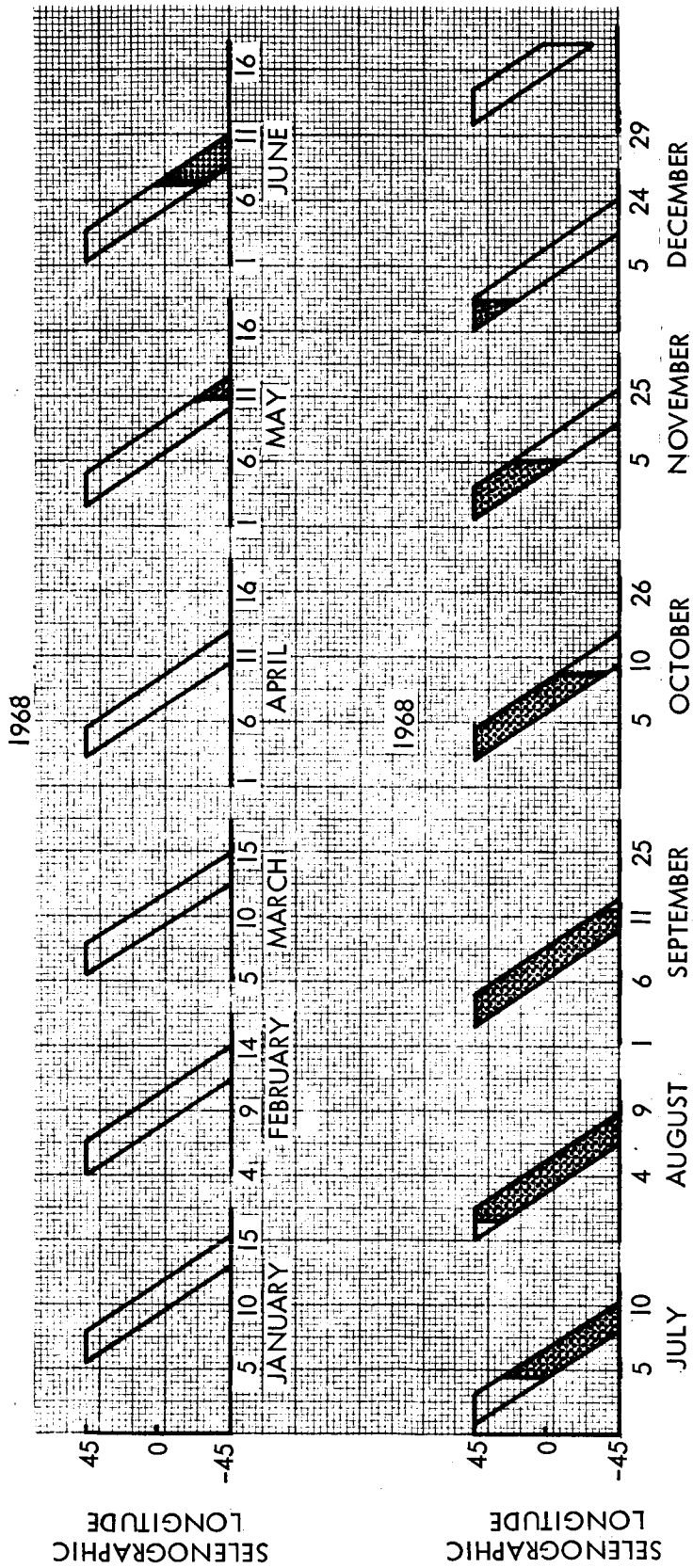

Figure 2-20. Lunar Lighting Summary - 1968 (Favorable Direct Injection Shaded)

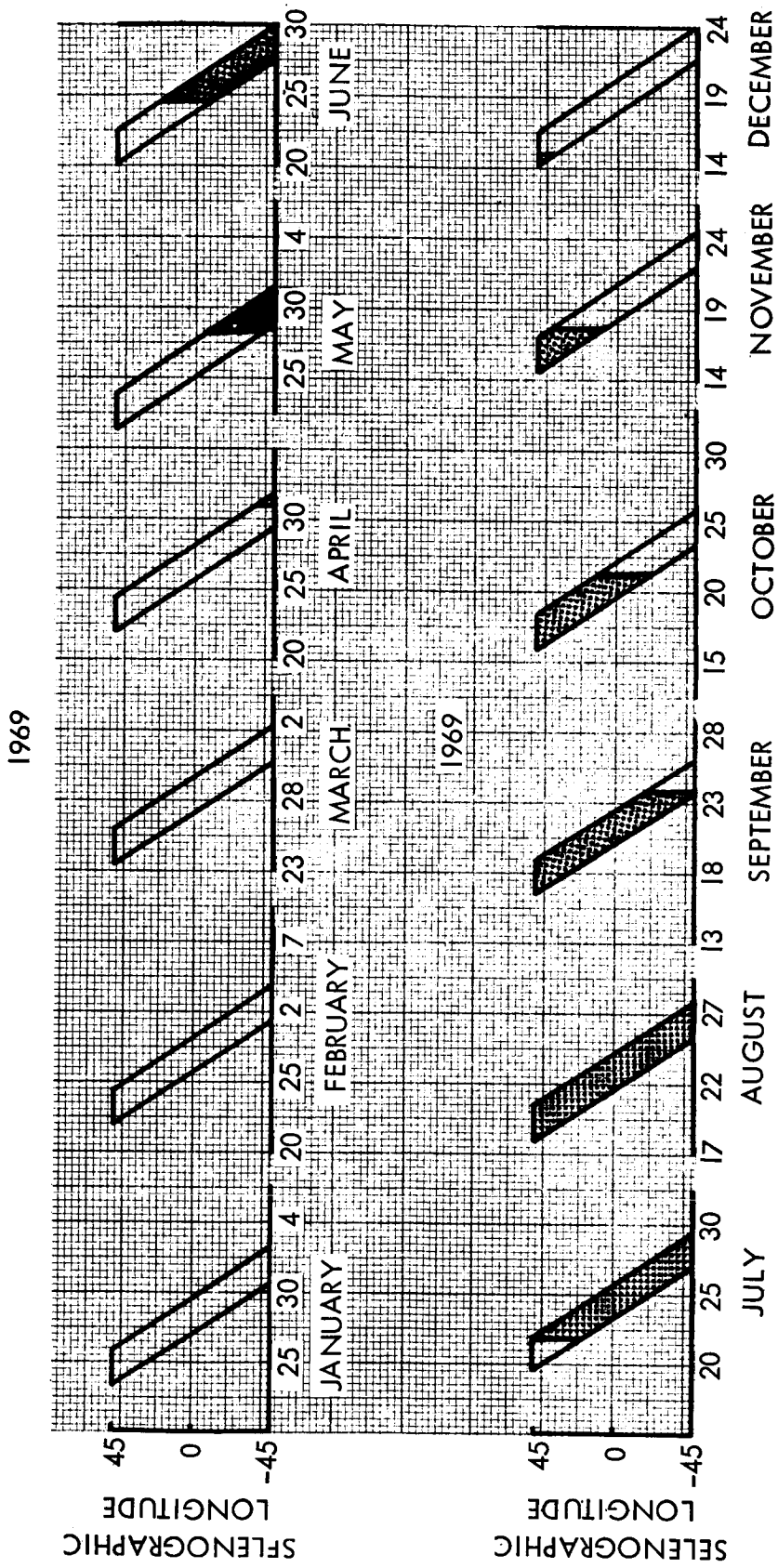

Figure 2-21. Lunar Lighting Summary - 1969 (Favorable Direct Injection Shaded)

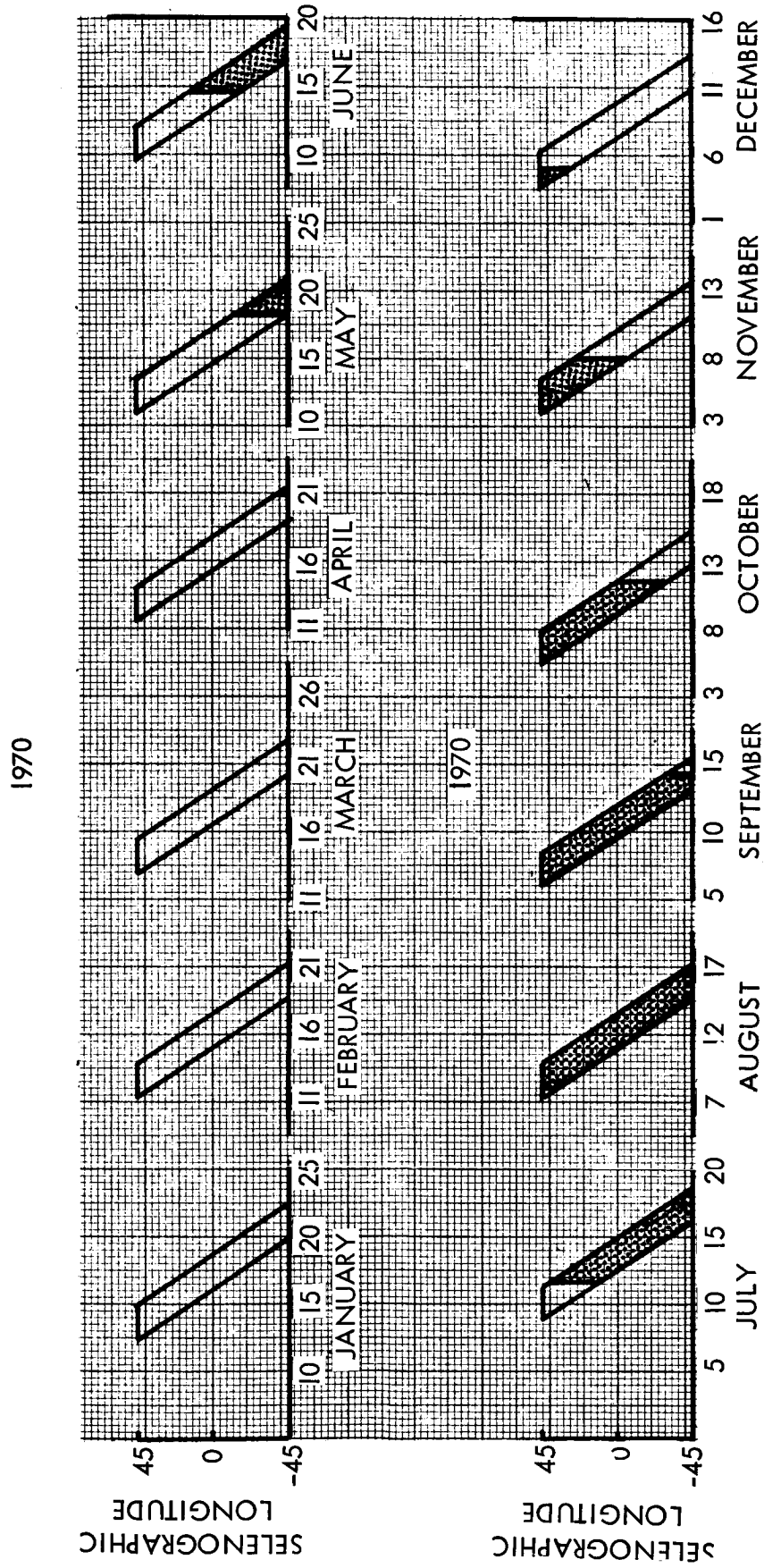

Figure 2-22. Lunar Lighting Summary - 1970 (Favorable Direct Injection Shaded)

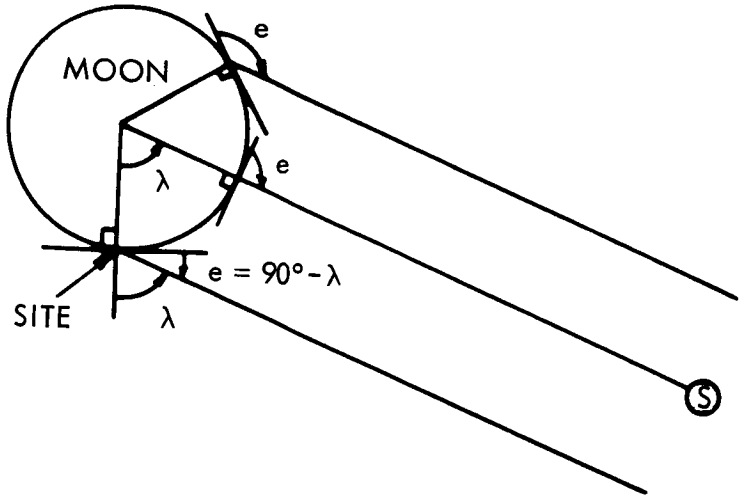

Figure 2-24. Relationship Between Lunar Site and Sun Elevation Angle

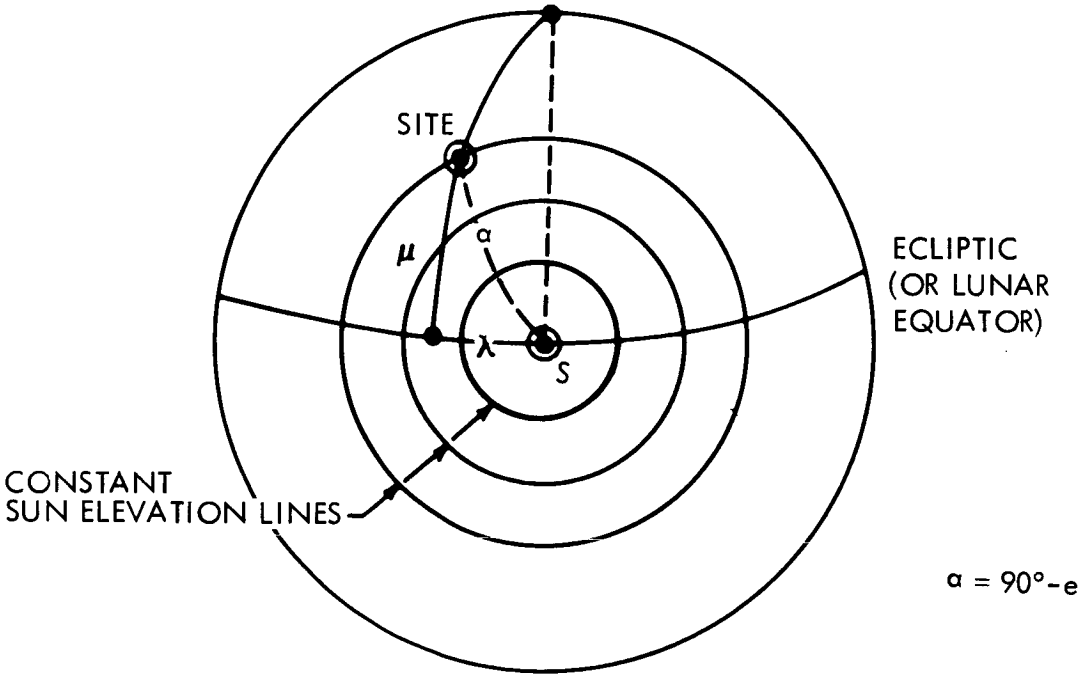

Figure 2-24. Relationship Between Lunar Site and Sun Elevation Angle

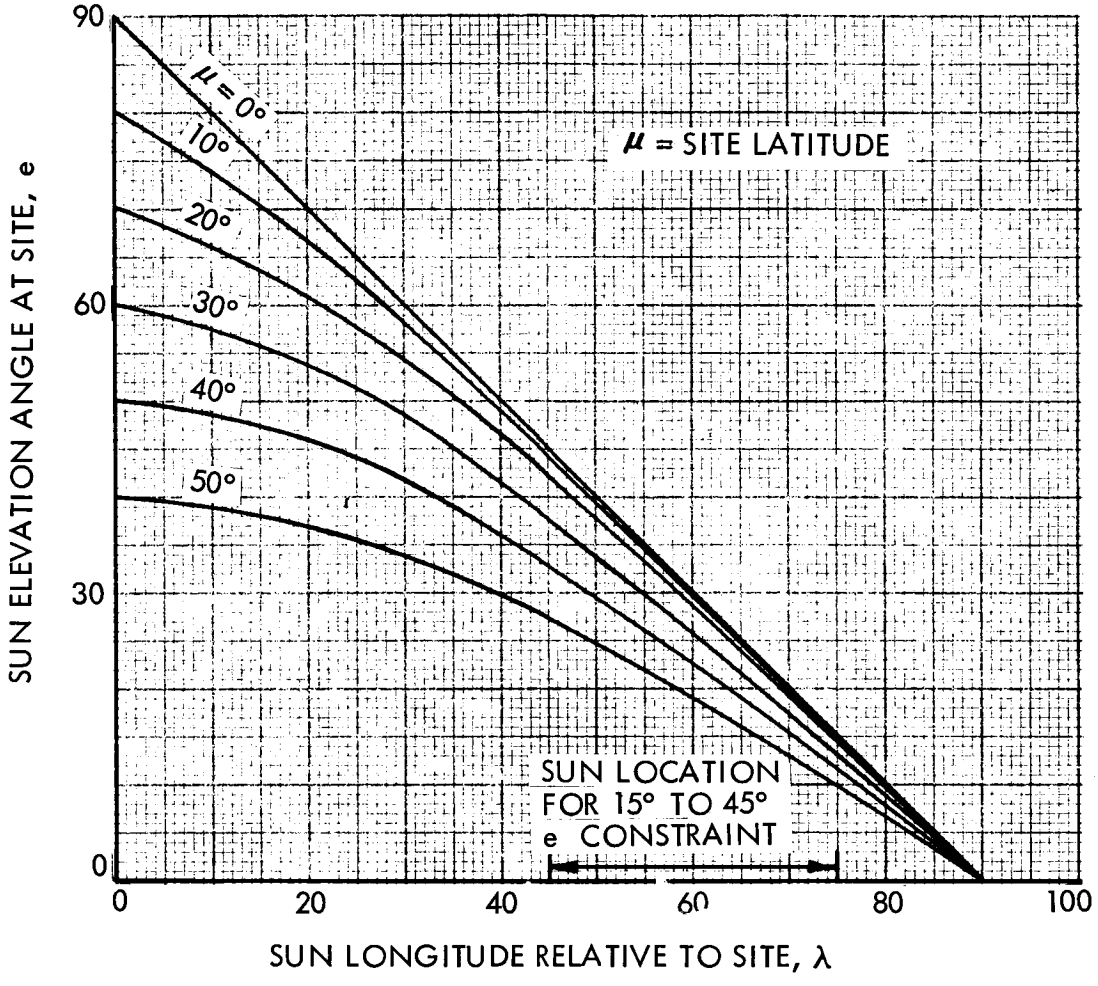

Figure 2-25. Sun Elevation as a Function of Site Location

and longitude, maximum deviations occur for the ±45 degree sun longitudes at the ±10 degree latitudes. Whereas the assumption indicates a 45-degree sun elevation angle, the actual value is almost 44 degrees. Thus, the displays in Figures 2-20 to 2-22 are accurate to within 1 degree of sun elevation. The shaded areas on these figures show the arrival dates for which direct ascent trajectories are geometrically possible. In these areas then both lighting and geometry constraints are satisfied within the defined lunar landing region. The phase difference between the geometrical and lighting constraints is apparent in these displays. This phasing, explained in Figure 2-26, is due to the fact that the moon's declination occurs every sidereal month whereas lighting repeats every synodic month, the difference of which is about two days. In the figure, the moon is shown at minimum declination (middle of direct ascent window) on two successive sidereal months. The position of the terminator with respect to the earth-moon line is seen to differ on successive passes by the amount of earth rotation around the sun (about 27 degrees).

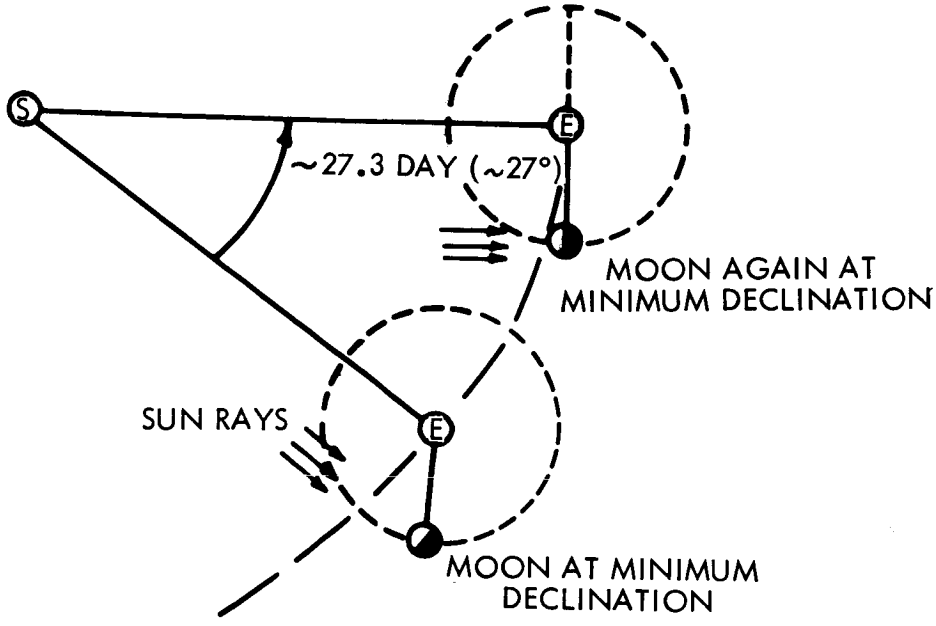

Figure 2-26. Relationship Between Lunar Phase and the Minimum Lunar Declination

2.5 EFFECTS OF THE FREE RETURN CONSTRAINT

Trajectories which pass around the moon and return to near earth space without the aid of any major correction to the path are called free return lunar trajectories. The outbound time of flight is a function primarily of the inclination to the lunar plane, the distance of the moon at arrival, whether its distance is increasing or decreasing, the major axis of the moon's orbit and the return inclination.

Figures 2-27 to 2-29 display the outbound trip time for free return trajectories. The faster free return trajectories occur when the moon is at closest approach to the earth. Unfortunately, the direct ascent windows are nearly coincident with the times of lunar closest approach. Thus, direct ascent free return flight times are always fairly rapid and, as explained in Section 2.3, result in a payload disadvantage compared to parking orbit. Over the three-year period the translunar free return flight times for direct ascent range from a minimum of 58 to a maximum of 73 hours.

2.6 EFFECTS UPON EARTH RETURN CONDITIONS

Landing windows shall first be discussed generally and then with emphasis upon the direct ascent problem. Several return landing windows for departure from the moon during January and early February 1969 are shown in Figure 2-30. The specific landing sites shown are Hawaii, Samoa and an equatorial site (shown dashed) located between them. The windows are bounded by constraints upon η_r, the re-entry maneuver angle (20 to 83 degrees) and a 40-degree maximum inclination to the earth equator. The length of the landing windows is read by projecting vertically between the window limits. Depending upon the declination of the moon at departure, landing may be made at Hawaii and/or Samoa. A landing can always be achieved at an equatorial site although at times, like January 16 and 30, it bottlenecks down to a minimum of 75 minutes.

The window for the Hawaii landing site (positive latitude) is centered by the date of minimum lunar declination. Similarly, the Samoa site, having a negative latitude, is centered by the date of maximum lunar declination. The degree of overlap between the two windows is a function of their latitudes. Sites located further from the equator would overlap less or not at all.

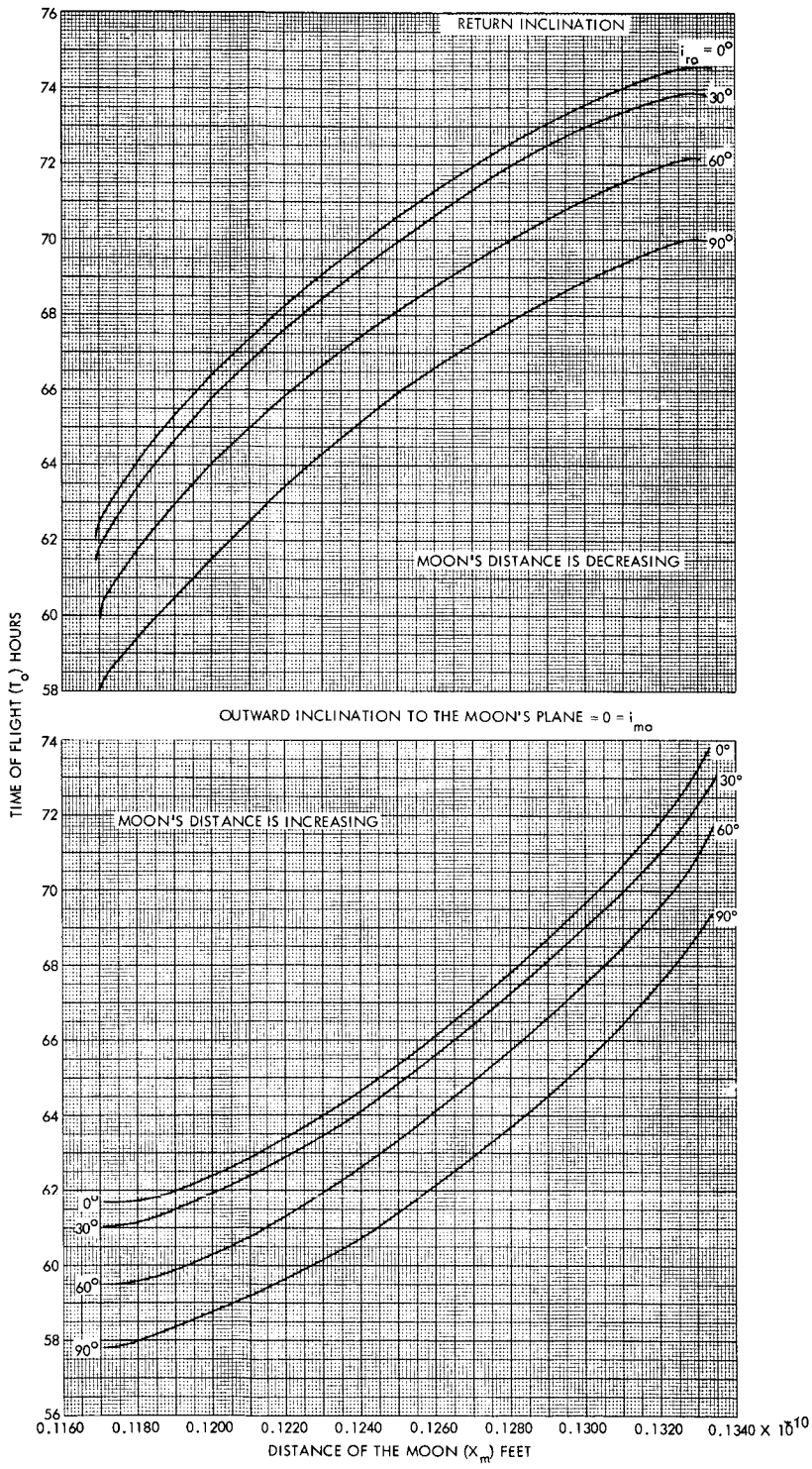

Figure 2-27. Time of Flight versus Distance of Moon for Free Return Circumlunar Trajectory and for Lines of Constant Return Inclinations with the Moon's Plane

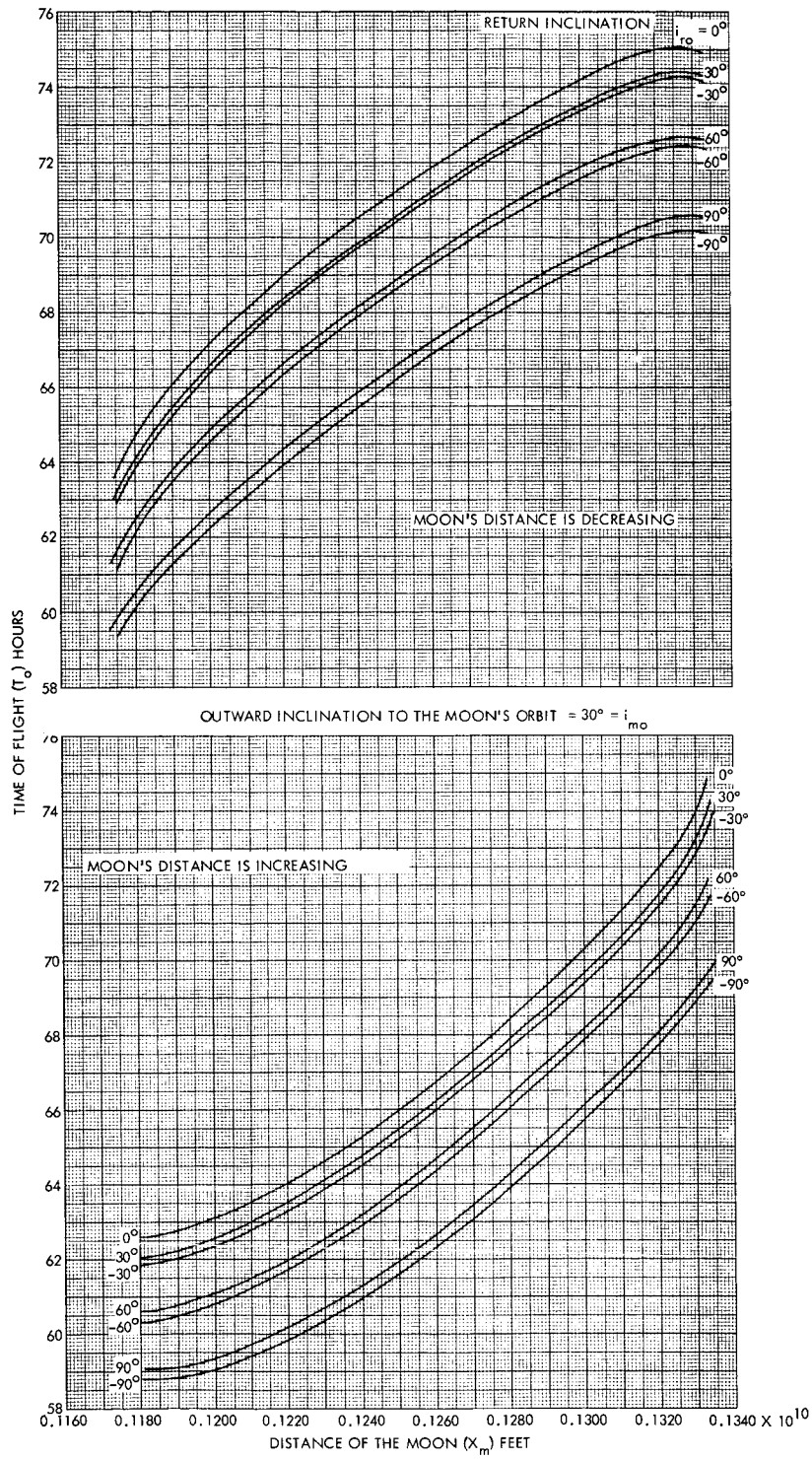

Figure 2-28. Time of Flight versus Distance of Moon for Free Return Circumlunar Trajectory and for Lines of Constant Return Inclinations with the Moon's Plane

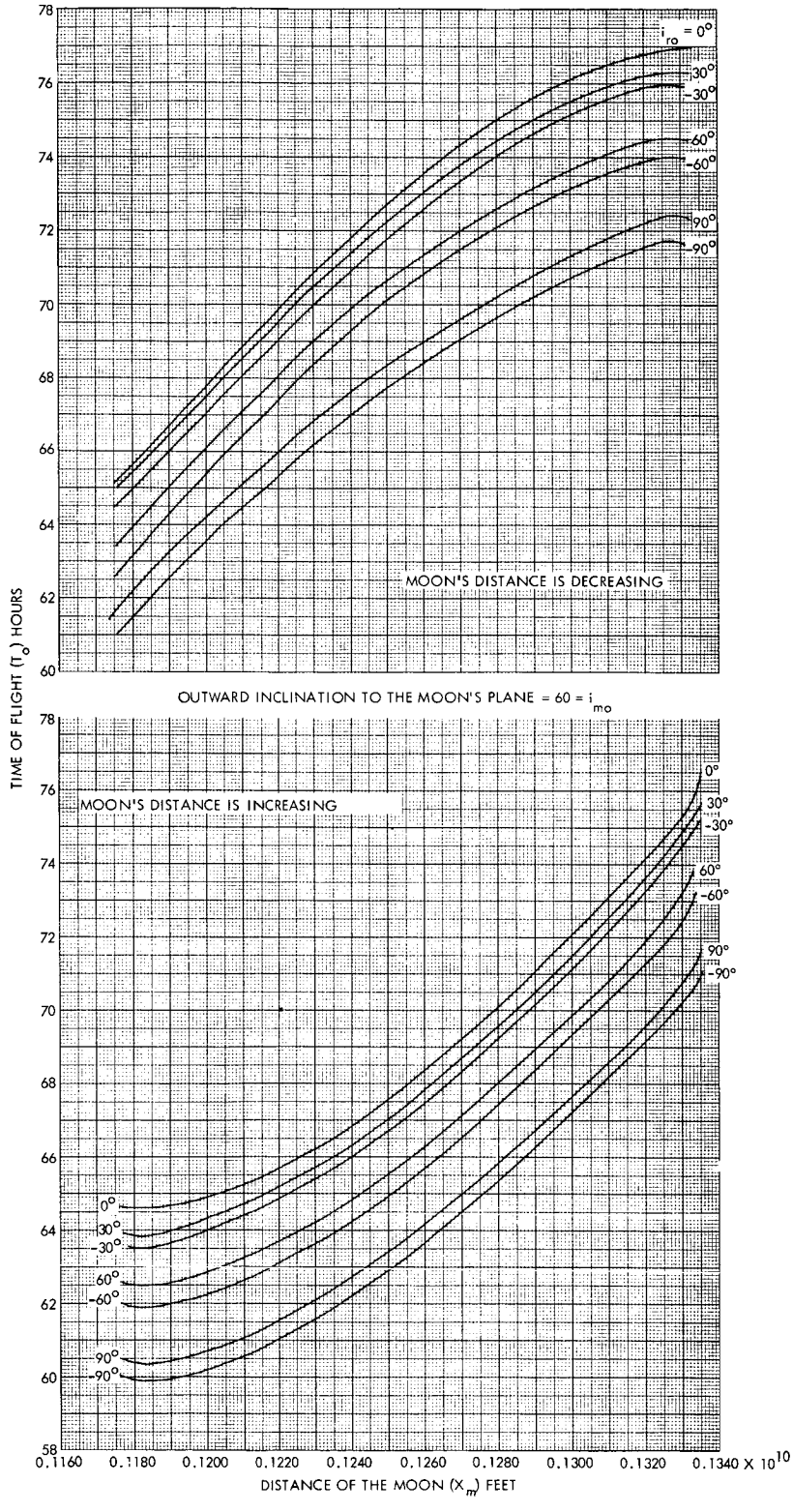

2-29. Time of Flight versus Distance of Moon for Free Return Circumlunar Trajectory and for Lines of Constant Return Inclinations with the Moon's Plane

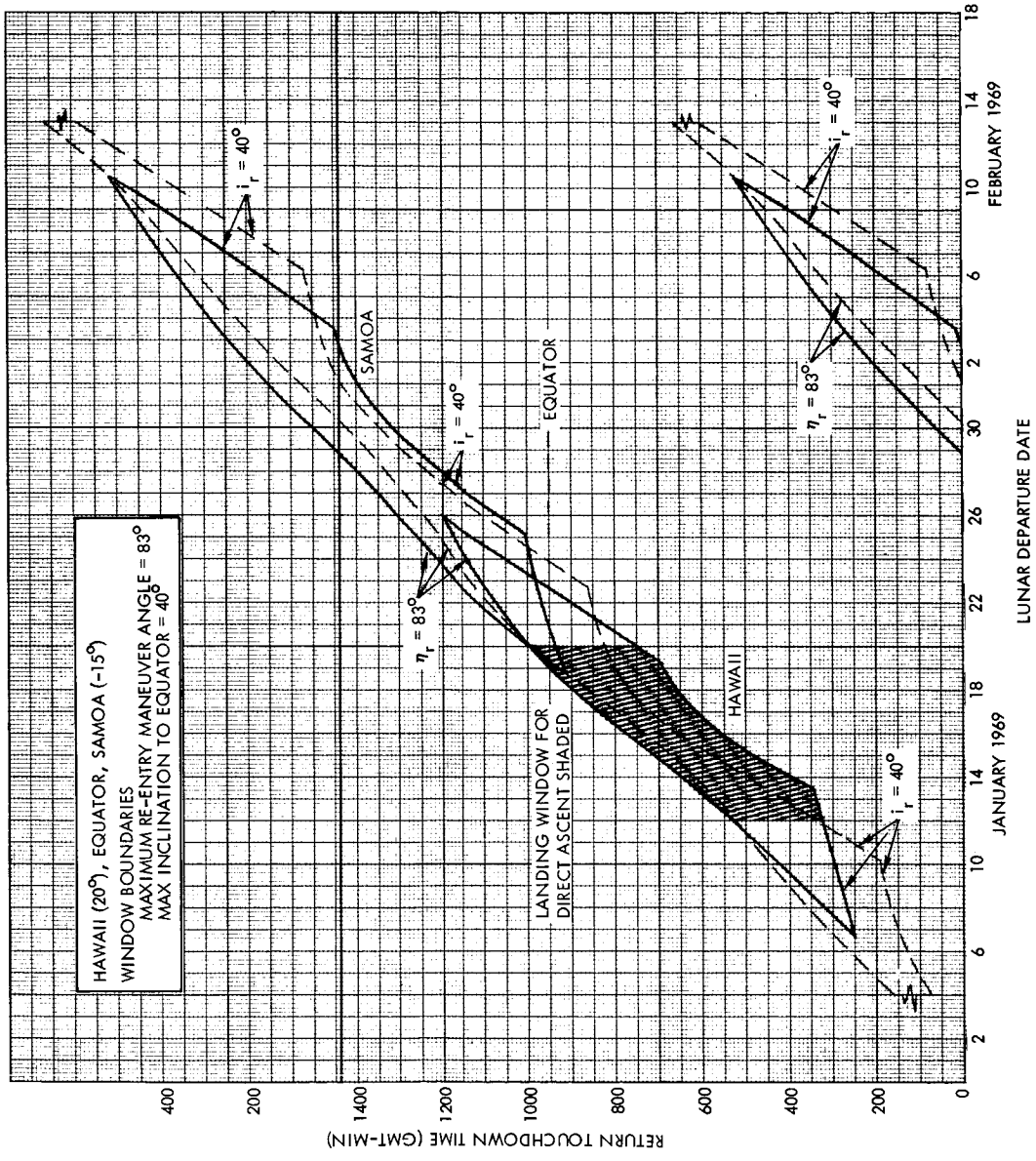

Figure 2-30. Return Window Display for Several Landing Site Latitudes

The landing window "drops" each month by about 200 minutes in touchdown time. The shape, however, varies almost imperceptably from month to month. Thus, characteristics described during any one month apply generally to all months.

It was explained in Section 2.2 that, for reasonable (60 minute) direct ascent launch windows, lunar arrival must occur when the moon's declination is below about -16 degrees. In Figure 2-30, this occurs from January 12 through January 20. Thus, the direct ascent landing windows consist of a specific portion of the total window available to parking orbits. A Samoa landing site would be of little use to a direct ascent mission.

Further descriptions of the landing window are portrayed in the next three displays. In Figure 2-31, the pattern of re-entry maneuver angle (solid lines) and return inclination and landing azimuth (dashed lines) is described for the January 1967 window. The definitions of these two parameters are shown in Figure 2-32. The majority of the trajectories land at azimuths greater than 90 degrees and with inclinations around 25 degrees to the equator. Figure 2-33 is a similar display with lines of constant inclination to the lunar plane overlayed. The shaded portion indicates return above the lunar plane. Most return trajectories are seen to be inclined less than 20 degrees to the lunar plane and divided about 50-50 between above and below orientations.

Figure 2-34 is included for rapid conversion to return trip time knowing the touchdown time and the interval of departure day. This is useful when working with figures like 2-31 and 2-33 and also with the mission planning displays discussed in Section 2.8. As an example, consider departure on January 5.2* in Figure 2-31 and an 83-degree reentry maneuver angle. Read 600 minutes touchdown time on the vertical scale. Now in Figure 2-34 read the return trip time which corresponds to 600 minutes and 0.2. The value is 77.2 hours. Also multiples of 24 hours are solutions, for example, 53.2 and 101.2.

*The fractional date indicates the day plus its fraction.

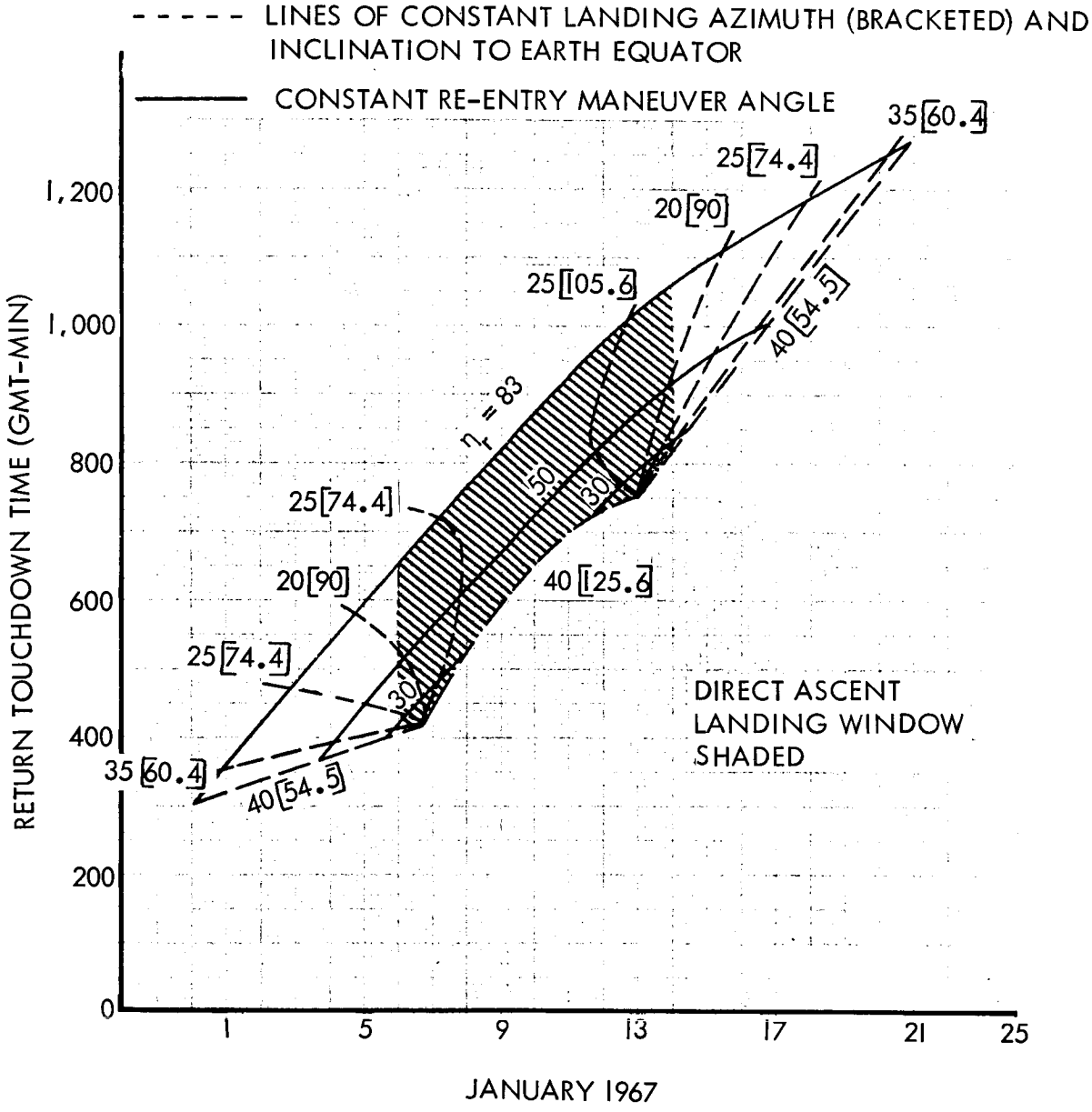

Figure 2-31. Landing Window Display for Return to Hawaii

LANDING GEOMETRY

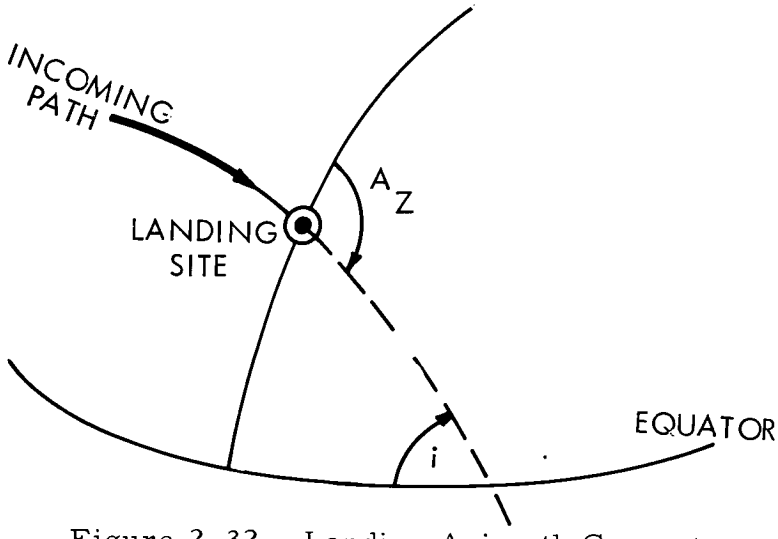

Figure 2-32. Landing Azimuth Geometry

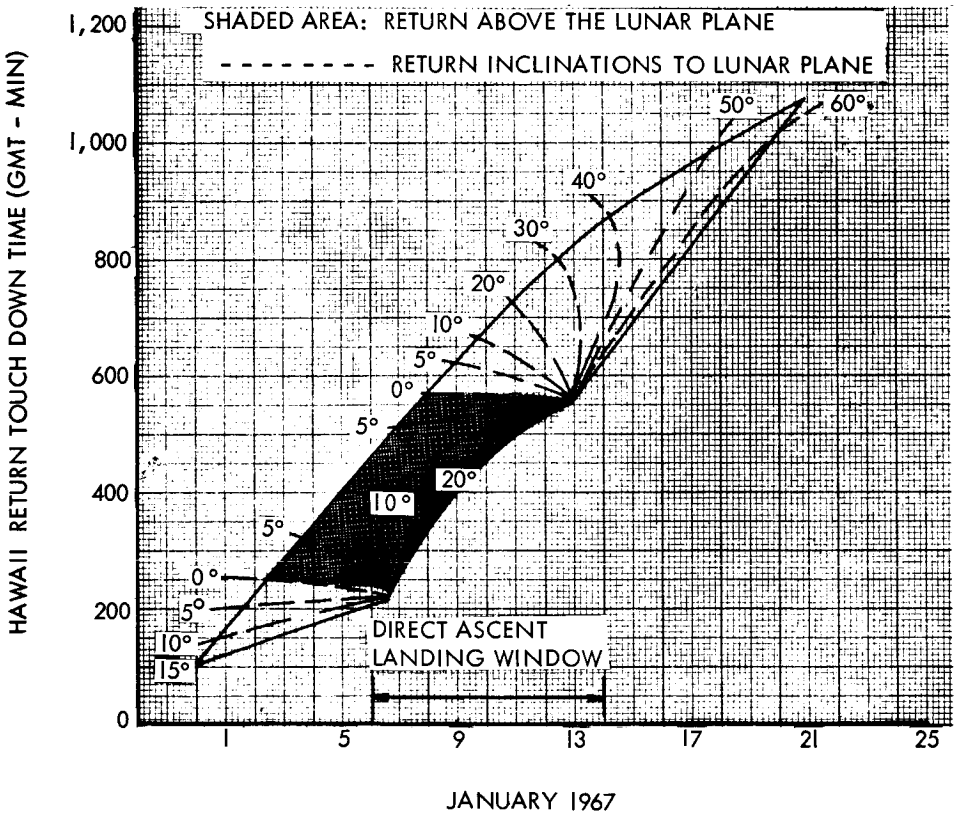

Figure 2-33. Landing Window Display for Return to Hawaii

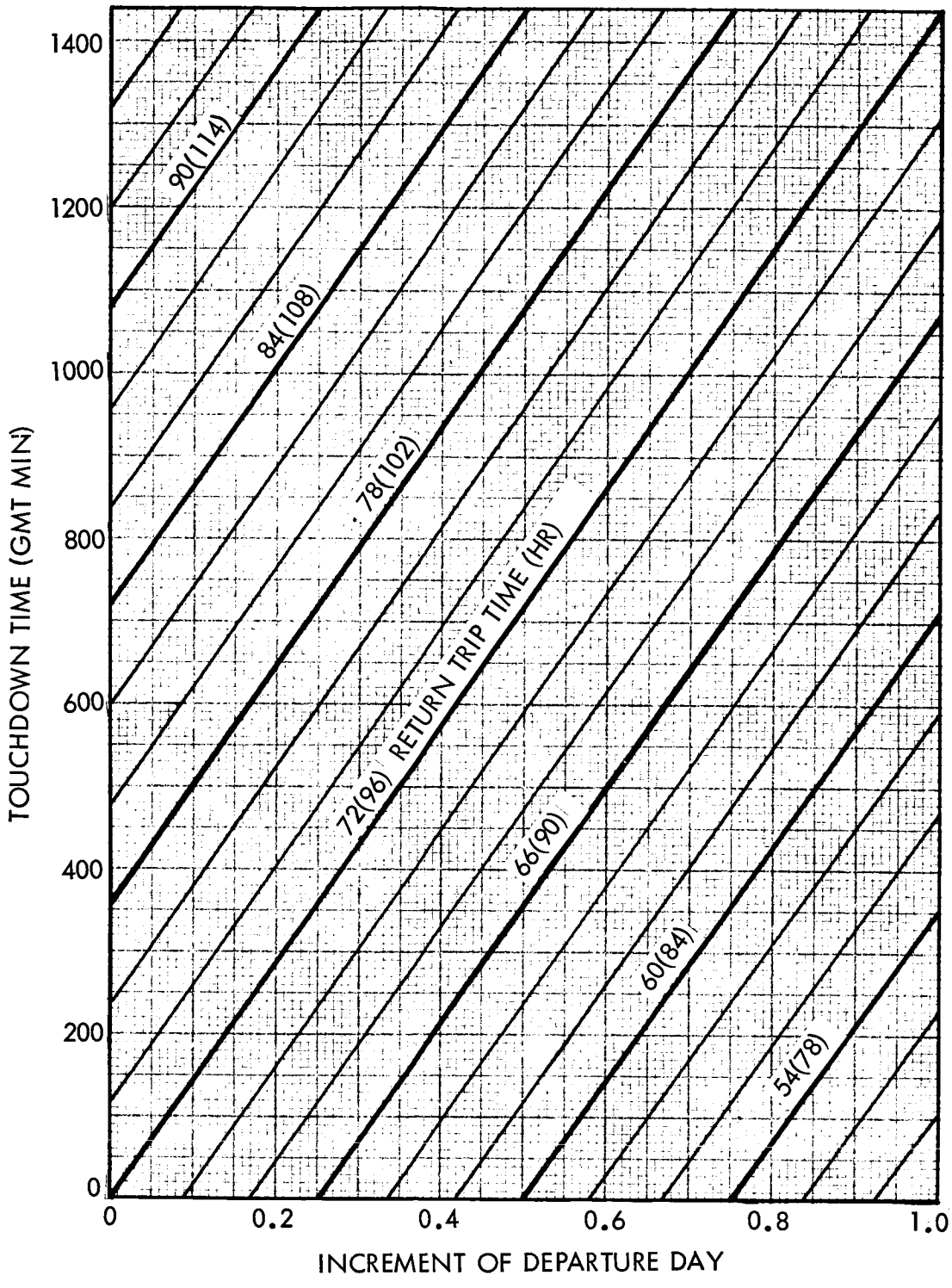

Figure 2-34. Return Flight Time as a Function of Departure and Touchdown Times

A further topic of interest in discussing return windows is the earth lighting at touchdown. The interesting conclusion is that daylight exists under almost all return circumstances, which is true for both parking orbit and direct ascent missions. The explanation for this is illustrated in Figure 2-35. Here the positions of the earth, sun and moon are shown for the extreme ranges of combined site location and sun elevation constraint. These positions are referenced to the earth-moon line. Assuming a 3-day return trip time, the new sun positions are shown relative to the earth. The resulting in-plane geometry shows that any return which requires landing between 18°W and 42°E will always land in daylight. Considering then that the values for return central angle will be $160^{\circ} + (20^{\circ}$ to $83^{\circ})^{*} = 180^{\circ}$ to 243°, or always between 0° and 63°E, the great majority of landings will be in sunshine.

2.7 SOME PARKING ORBIT-DIRECT ASCENT COMPARISONS

Figure 2-36 is a combined description for a typical month of launch and landing windows for both direct ascent and parking orbit. The left portion of the display describes the launch operations. Landing displays are on the right.

The Atlantic and Pacific injection (long and short coast) parking orbit launch windows for a 72- to 108-degree azimuth range are apparent for each day during the 25 May through 22 June period shown. The portion of this period during which direct ascent launches can be made is shaded inside the "knee" of the Atlantic injection window.

The arrival time line in the left figure (shown dashed) enables the launch operation to be tied to lunar arrival and subsequent departure and earth landing operation. This is achieved by projecting vertically from the launch date and flight time scale on the abcissa to the arrival time line and then horizontally to the arrival time scale on the right. Adding the amount of lunar stay time to the arrival time gives the departure time.

---

*Reentry maneuver angle η_r is confined to these limits.

SUN POSITION AT MOON
AT LATEST POSSIBLE ARRIVAL
45° SUN ELEVATION
AT -45° LONGITUDE SITE

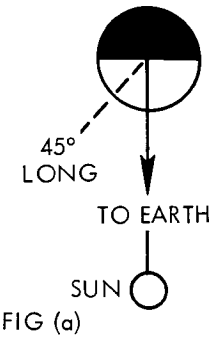

FIG (a)

SUN POSITION AT MOON
AT EARLIEST POSSIBLE ARRIVAL
15° SUN ELEVATION
AT +45° LONGITUDE SITE

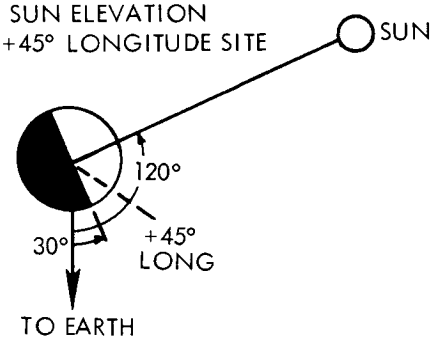

FIG (b)

SUN POSITION AT EARTH
AT LATEST POSSIBLE ARRIVAL

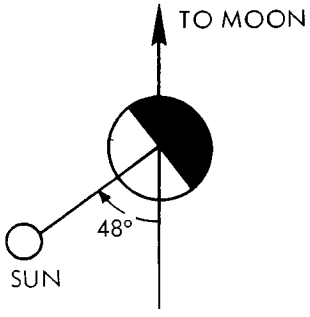

FIG (c)

SUN POSITION AT EARTH 4 DAYS
AFTER EARLIEST ARRIVAL
(1 DAY LUNAR STAY + 3 DAY
RETURN FLIGHT TIME)

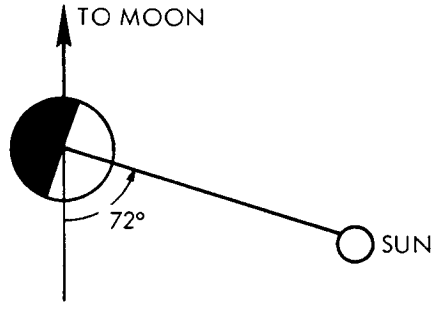

FIG (d)

RANGE OF LONGITUDES
ALWAYS IN SUNLIGHT
AT TOUCHDOWN

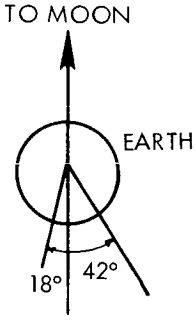

FIG (e)

LANDING LONGITUDE RANGE
AT EARTH

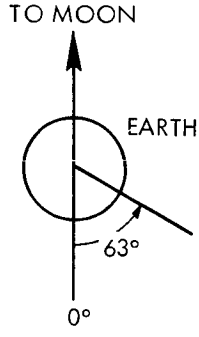

FIG (f)

Figure 2-35. Earth Lighting Conditions Upon Landing

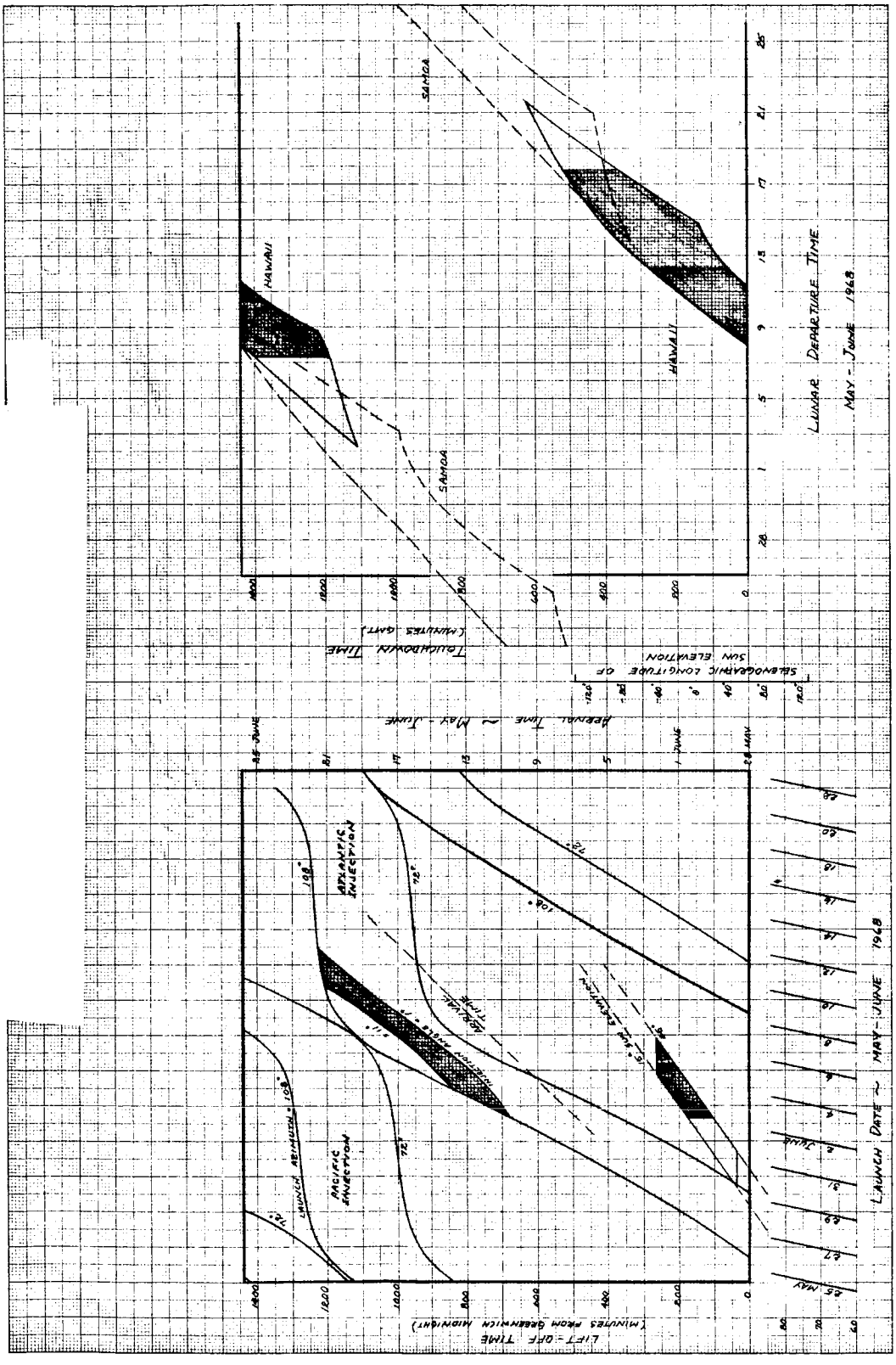

Figure 2-36. Launch and Landing Window Comparisons Between Direct Ascent (Shaded) and Parking Orbit

This time is then used in the return window. The direct ascent landing window is shaded. The limits on initial and final departure time, not considering lunar lighting, are obtained by determining both the initial and final direct ascent opportunities and projecting to arrival time. These limiting times are represented by the tips of the shaded direct ascent window. Projecting down from them to the arrival time line and horizontally to the arrival time ordinate yields the bounds on arrival time at the moon. In this case, the arrival times are June 7.3 and June 16.8. The first possible departure time is obtained at the moon if zero stay time is assumed after the initial arrival. Thus, initial departure occurs on June 7.3. Final departure on June 17.8 is obtained by adding a 24-hour stay time to the June 16.8 final arrival date.

The direct ascent window limits described thus far have neglected the very important lunar lighting constraint. Once this is considered, any portion or all of the direct ascent launch (and hence landing) windows may be eliminated. Considering lunar lighting in the case just covered, the initial arrival time is still June 7.3 but the final arrival date cuts off the launch window at June 11.3 and hence, the landing window at June 12.3. A three-year summary of direct ascent windows with favorable lighting is shown in Figure 2-37. The launch window data in Section 2.9 was processed to gather this information. The minimum window is assumed to be 30 minutes and a trajectory range of 60 to 80 hours is used. The figure shows the number of days in each monthly window; the dotted portion of each bar indicates the number of days that month in which launch from AMR must be made in darkness. Since launch from a parking orbit can be made for about 10 days every month, the yearly total for this mode is around 120 days. Thus, the ratio of direct ascent to parking orbit launch days is about 1:3. Comparison of lighting at earth landing is not a problem since almost all landings (both direct ascent and parking orbit) are in daylight.

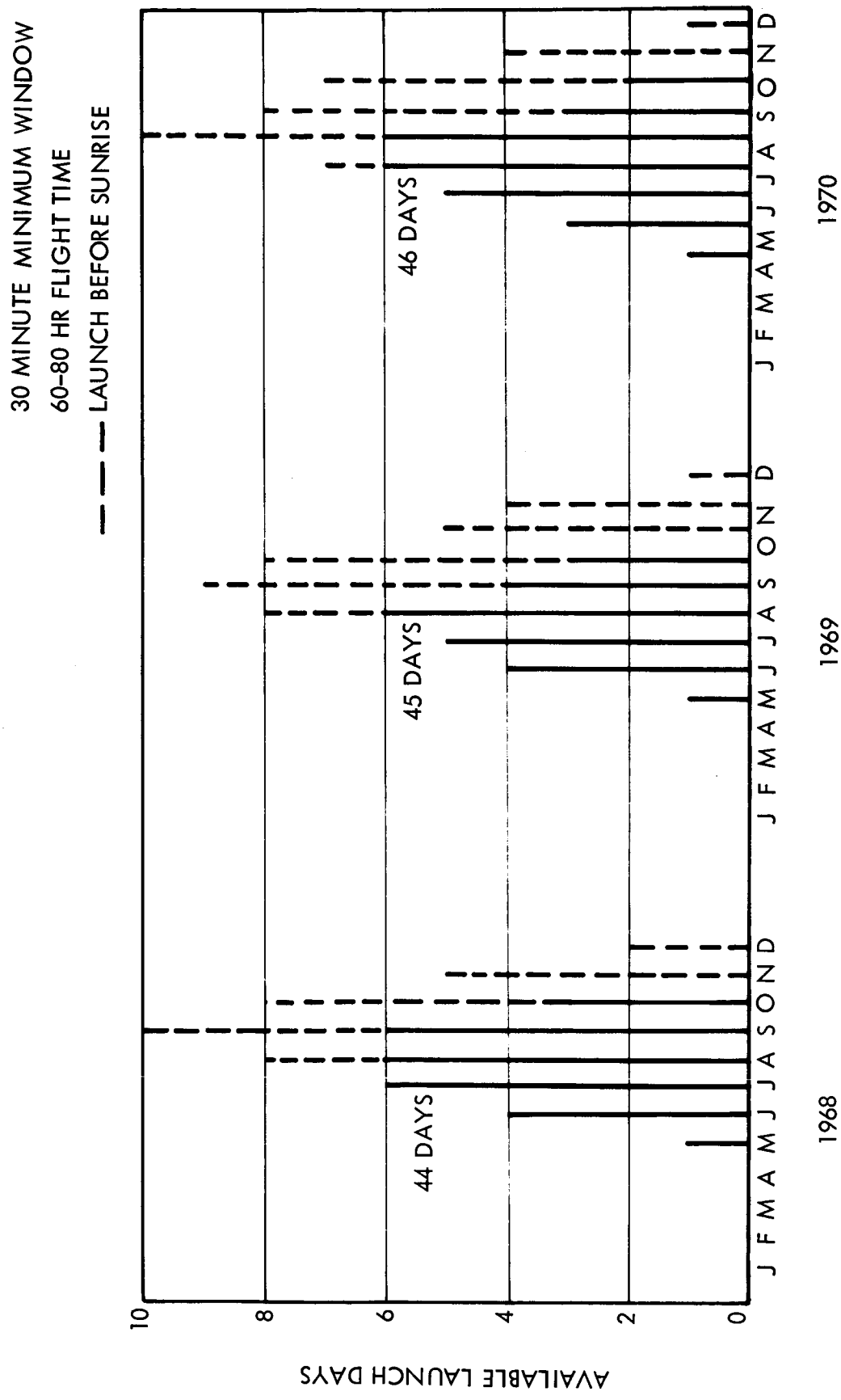

Figure 2-37. Direct Injection Launch Opportunities with Favorable Lunar Lighting

2.8 MISSION PLANNING

Figure 2-38 is identical with Figure 2-36 except that the areas of interest are shown expanded and with more detail. This type of display provides information concerning most of the mission constraints so that a fairly complete mission analysis can be performed for any given month.

As an example, consider the case where the selected landing site has a -30° longitude. What are the direct ascent launch days in June 1968 satisfying all constraints including a free return trajectory inclined 60 degrees to the lunar plane? It is assumed that a flight path angle range from 1 to 11 degrees is available, therefore:

1) June 5 is the first possible date and the outward flight time for the free return trajectory of interest is 64 hours. This locates the abcissa point.

2) Projecting vertically from the June 5, 64-hour flight time point to the dashed arrival time line and reading across horizontally shows a June 8.2 arrival time.

3) Continuing the vertical projection from the abcissa, the sun elevation angle that corresponds to -30 degrees longitude (located on right hand scale) is 15 degrees.

4) Again continuing vertically, the launch window is seen to open at about 711 minutes GMT and close at 780 minutes for about 69 minutes of window. Initial launch occurs about 81 minutes after daylight as shown by the sunrise tick located at 630 minutes GMT. The injection flight path angles and launch azimuth tradeoffs may be interpolated through the window.

   A longer trip time on June 5 would have resulted in a later arrival time, higher elevation angle (for the same site) and a bigger launch window.

5) With the June 8.2 arrival time derived in step two, assume a one-day lunar stay to obtain a departure time of June 9.2.

6) For departure on June 9.2, landing can be made at Hawaii any time between 1256 minutes—through GMT midnight—to 76 minutes GMT for a total landing window of 260 minutes.

7) A specific touchdown time within the landing window is established by the reentry and landing conditions desired at earth. Lines of constant reentry maneuver angle η_r (central arc) from reentry to touchdown) are shown as solid lines. The

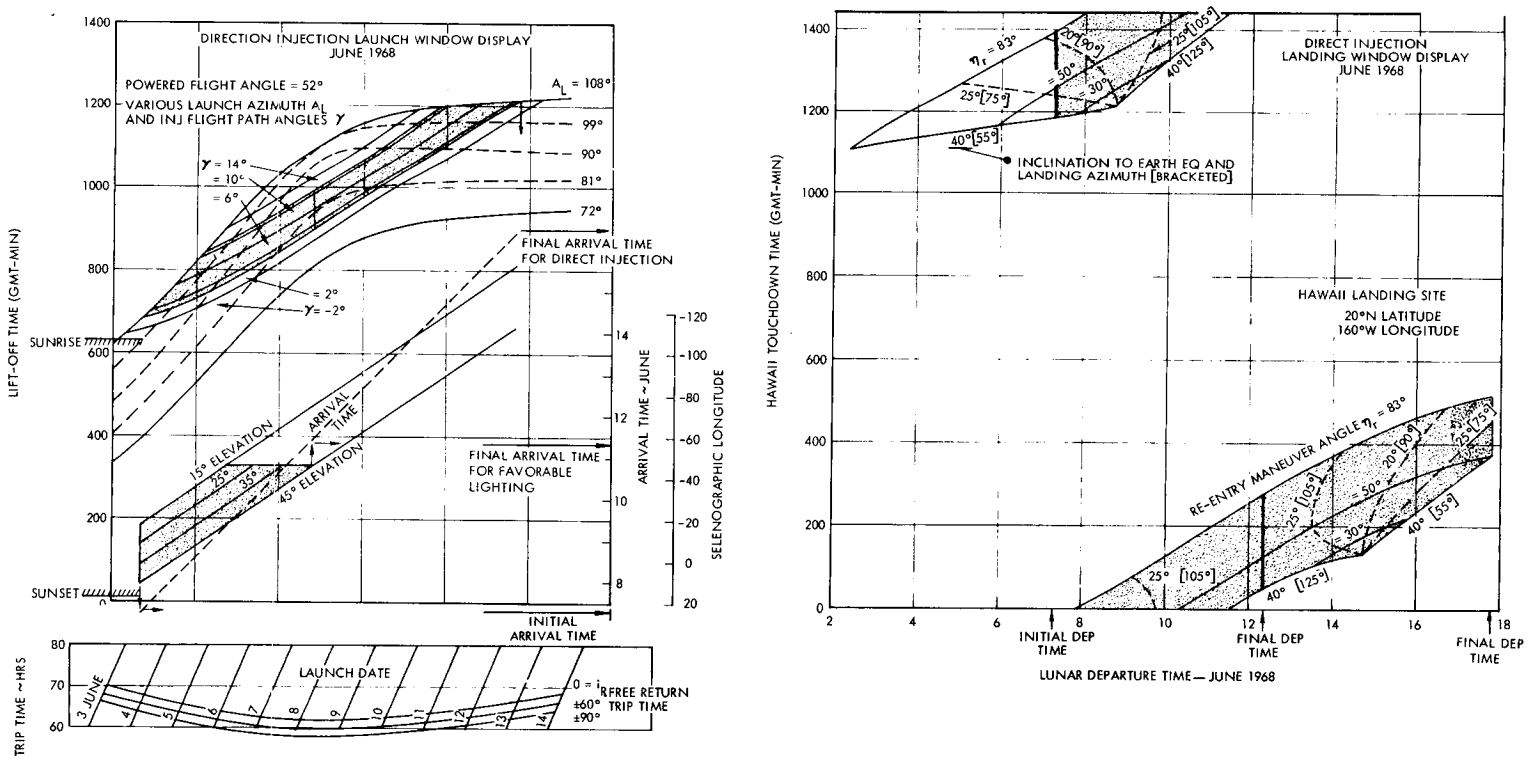

Figure 2-38. Apollo Direct Injection Mission Planning Display

limits on η_r are 20 to 83 degrees. Lines which represent both constant inclination to the earth equator and constant incoming azimuth at the landing site are shown as dashed lines within the window. The limiting value on this variable is 40 degrees maximum inclination to the earth equator.

Now to complete the example, consider that the desired reentry maneuver angle is 30 degrees. Then the touchdown time is 1280 minutes GMT, the inclination to the earth equator is 25 degrees and the incoming landing azimuth at the site is 105 degrees.

8) Using the .2 from the June 9.2, departure time and the 1280 minutes GMT touchdown time in Figure 2-34, the transearth flight time may be read as 89 hours (or 24 hour multiples thereof). Thus other possible flight times are 65 hours and 113 hours.

It can be seen in the figure that the last possible launch opportunity in June is a 67.5 hour flight time on June 8. Although direct ascent is geometrically possible until June 13, the lighting constraints within the defined landing area of ±45 degrees longitude cannot be satisfied for the later days. The June 8 launch point with the 67.5-hour trip time is thus used to define the termination of the window. Projecting to the arrival date shows a final arrival time of June 11.3. Thus, assuming a one-day stay period, the final departure time is June 12.3.

The June window opens on June 4 with a 65-hour trip time. At this time it becomes geometrically possible to launch although a finite launch window does not exist. The prevailing lighting conditions are also favorable. We have thus seen that the window in June 1968 is limited at the beginning by a geometrical constraint and is terminated a few days later by the lunar lighting constraint applied to the ±45 degree longitude lunar landing site locations. The "mission window" then is the lower shaded block defined by elevation angle and site location. It was shown in Figures 2-20 to 2-22 that this shaded area changes from month to month. The next section contains launch window displays like the left hand portion of Figure 2-38 for each of the 41 direct ascent launch windows in 1968, 1969, and 1970. Considerable discussion is repeated so that the section may be somewhat self-contained. On each display the arrival time line is

shown to allow transition to the landing window. The landing windows themselves are not included here since they are in a previous report[2] for years 1967, 1968, and 1969; thus, combining the two analyses will provide the necessary information.

2.9 LAUNCH WINDOW DISPLAYS FOR 1968, 1969, 1970

Figures 2-39 to 2-79 present direct injection launch window possibilities for the three years 1968, 1969, and 1970. These windows, which are generated by permitting variations in the translunar injection flight path angle, are superimposed upon lines of constant launch azimuths ranging from 72 to 108 degrees. The powered flight booster range of 52 degrees has been chosen to correspond with the characteristics of the Saturn V. The length of the direct ascent window is proportional to the flight path angle variation available from Saturn V. It has been shown in Section 2.3 that, for payloads equal to the parking orbit mode, a variation of γ from 1 to 11 degrees is available. As shown in the first figure, for January 1968 the direct ascent launch period will extend about eight days per lunar month with a launch window of approximately 90 minutes per day. A smaller range of γ will reduce the number of minutes available each day (approximately 10 minutes per degree of γ) while holding the number of days available per month nearly constant.

To account for variations in flight time, a slanted flight time scale is provided to determine the correct window. For any one day, that point is chosen on the slanted scale which corresponds to a desired flight time. Then this point is projected vertically upwards to points on the window. If the window intersects two consecutive days near midnight, then the latter part of the window is found by skipping one full day and reading values from the lower portion of the curve.

Also superimposed upon these direct ascent windows is the free return trip time for several return inclinations i_r to the lunar plane. However, free return times are only included for those months when lunar lighting is favorable.

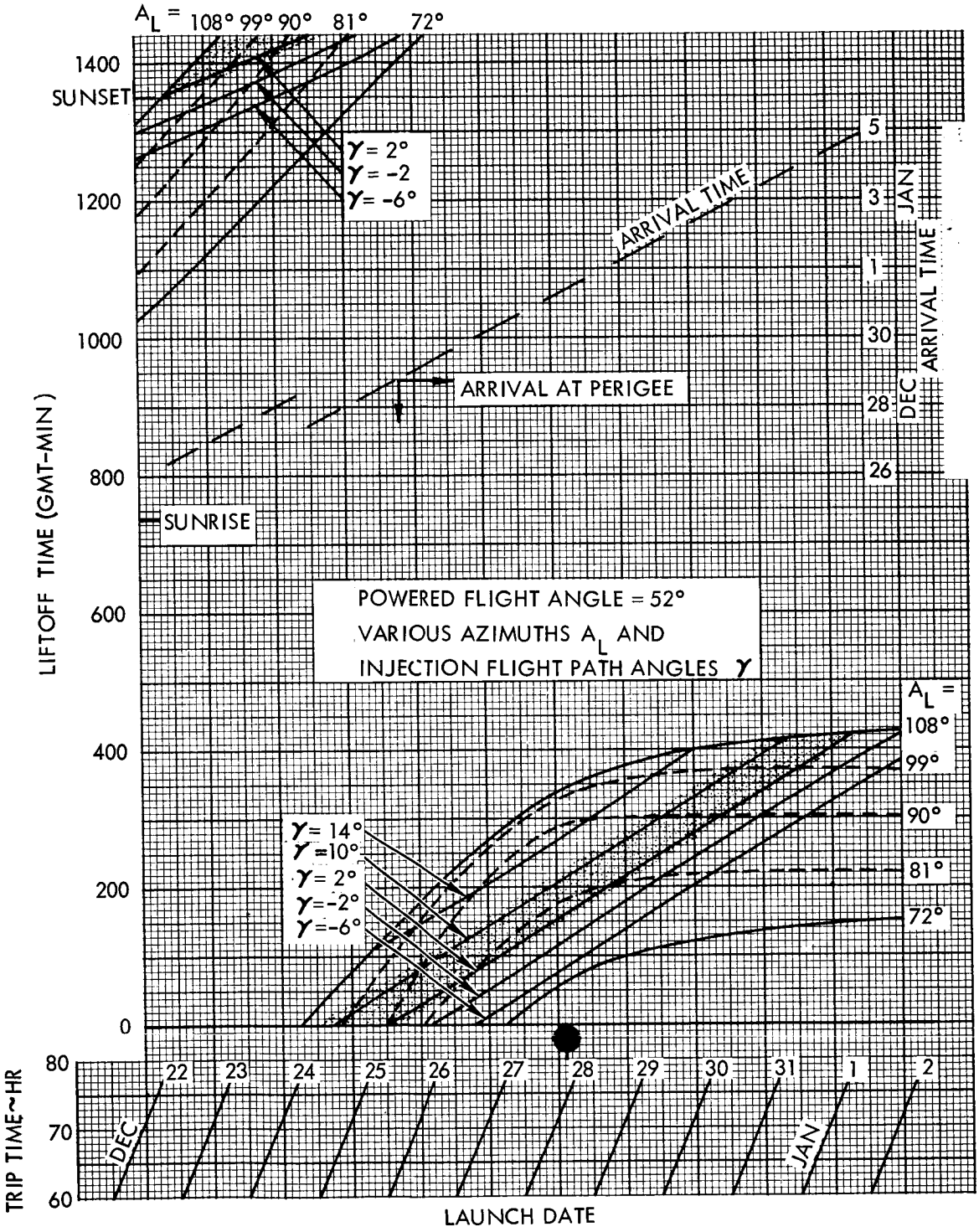

Figure 2-39. Direct Injection Launch Window
December 1967 - January 1968

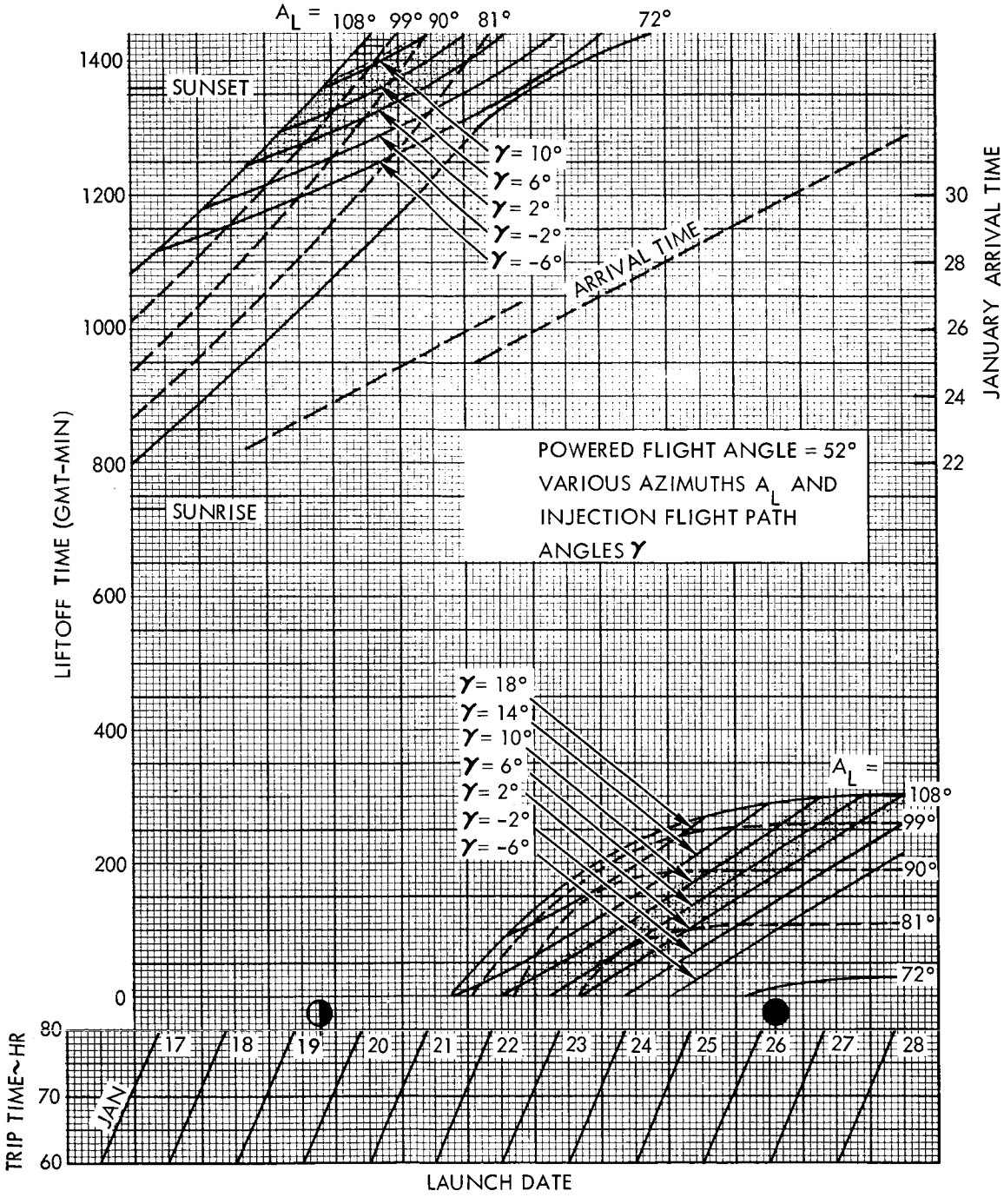

Figure 2-40. Direct Injection Launch Window
January 1968

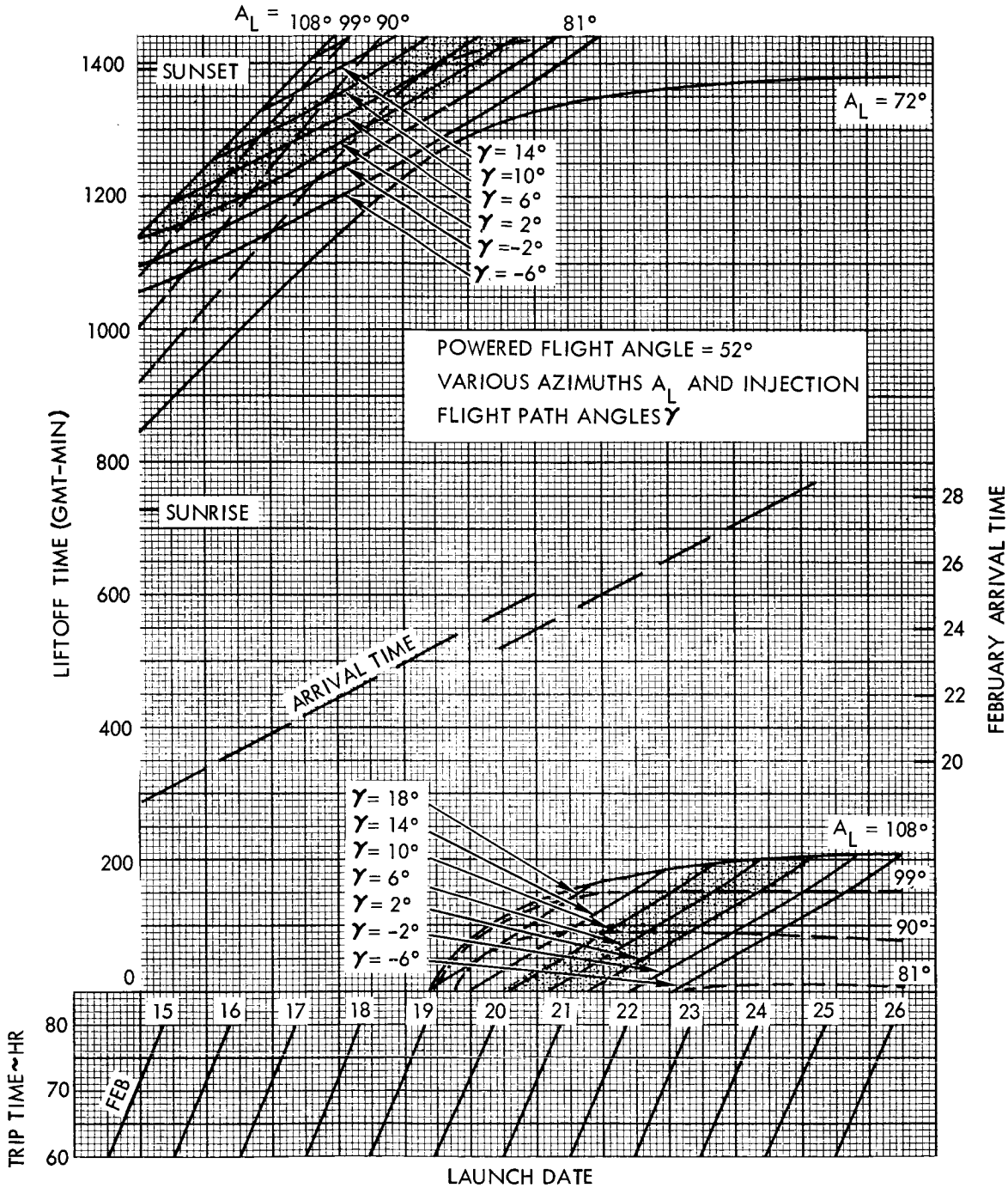

Figure 2-41. Direct Injection Launch Window
February 1968

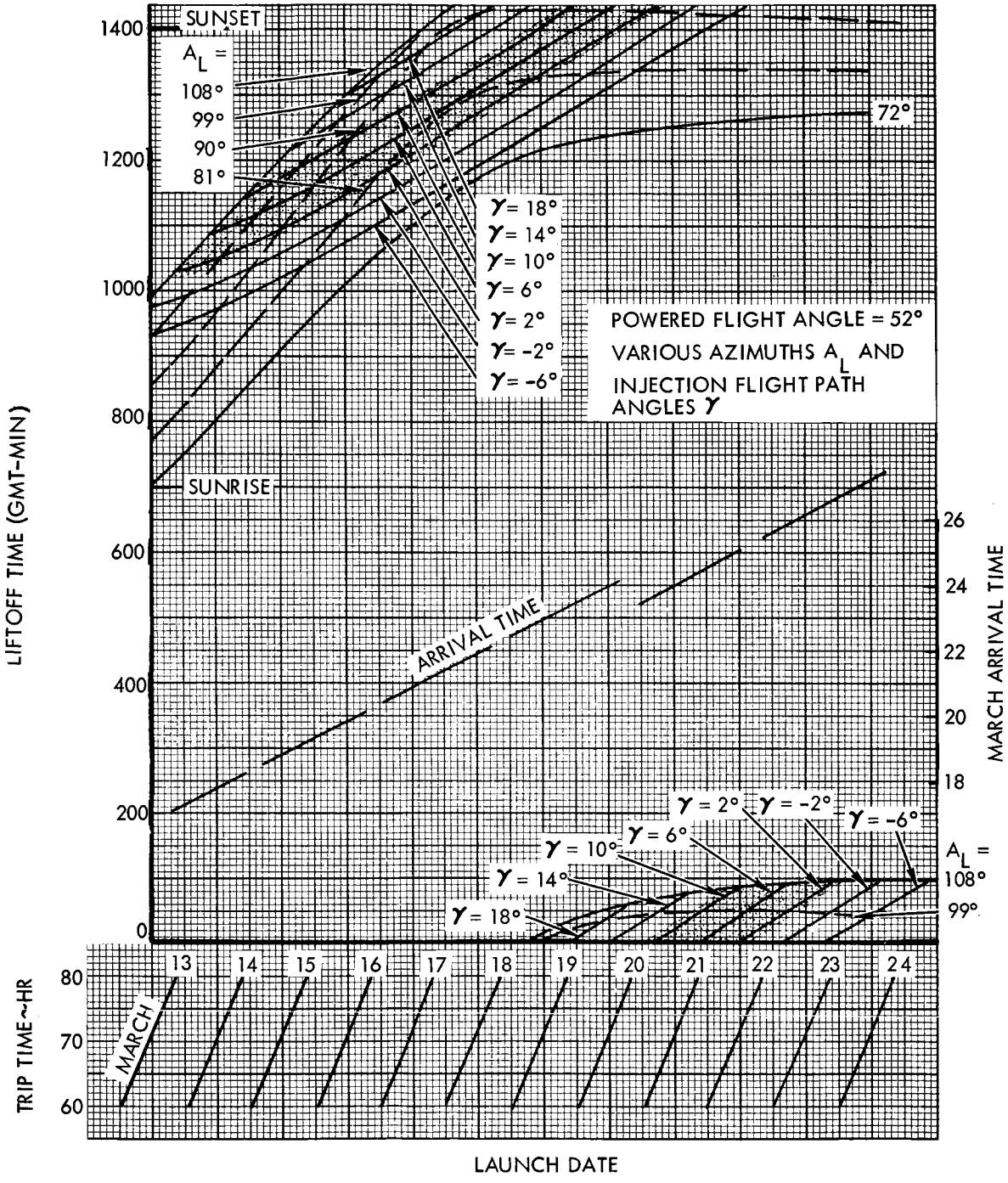

Figure 2-42. Direct Injection Launch Window
March 1968

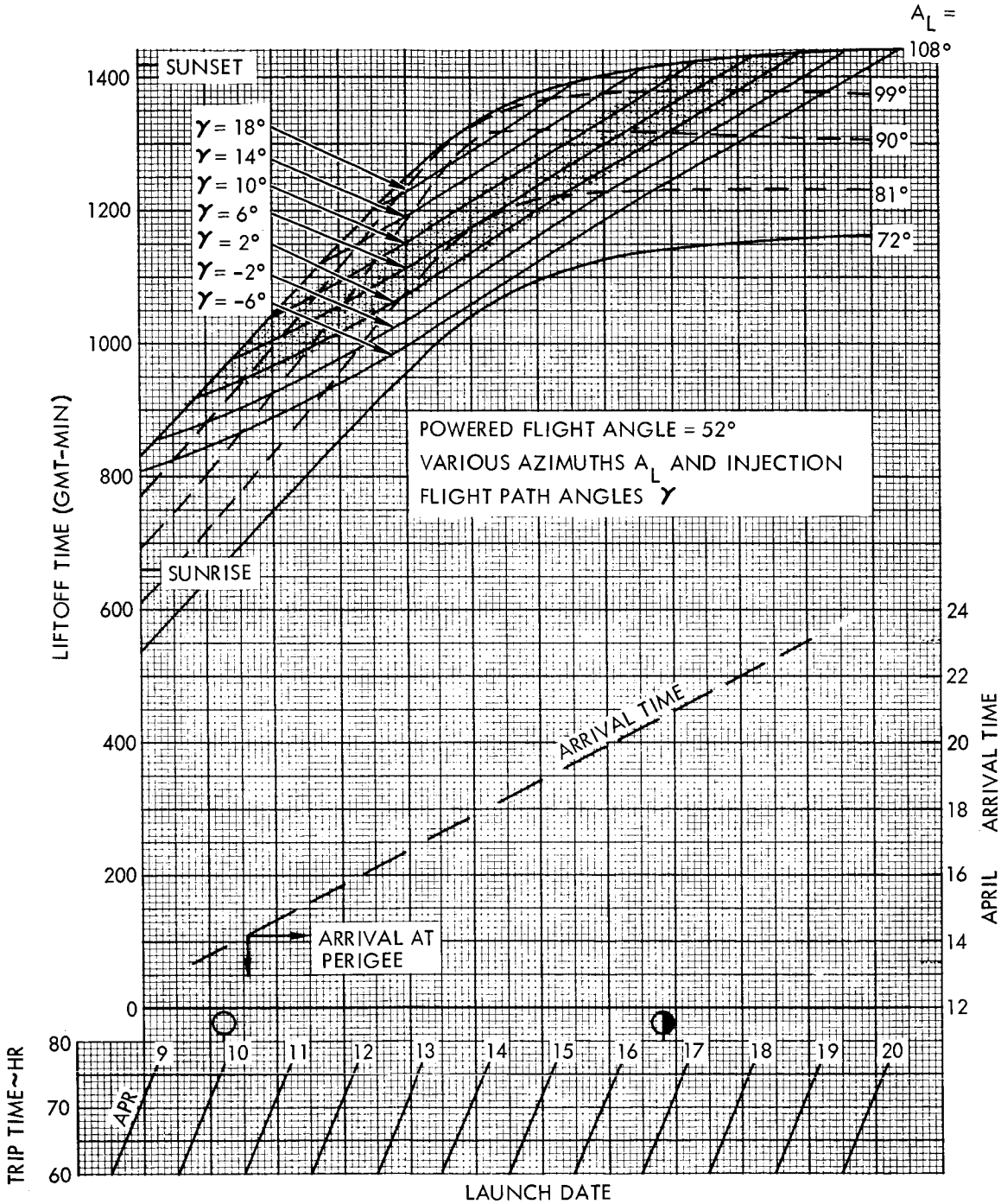

Figure 2-43. Direct Injection Launch Window
April 1968

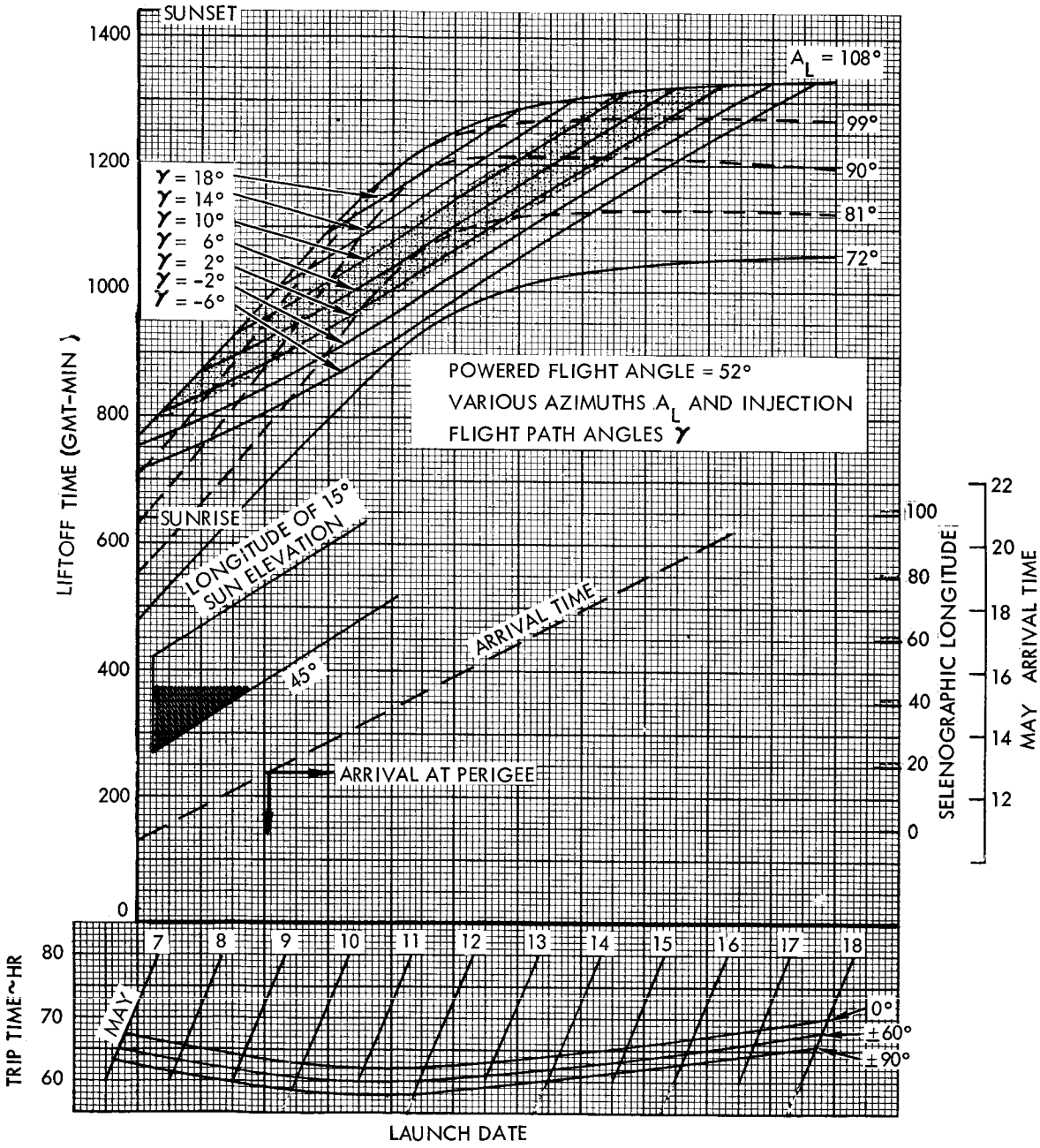

Figure 2-44. Direct Injection Launch Window
May 1968

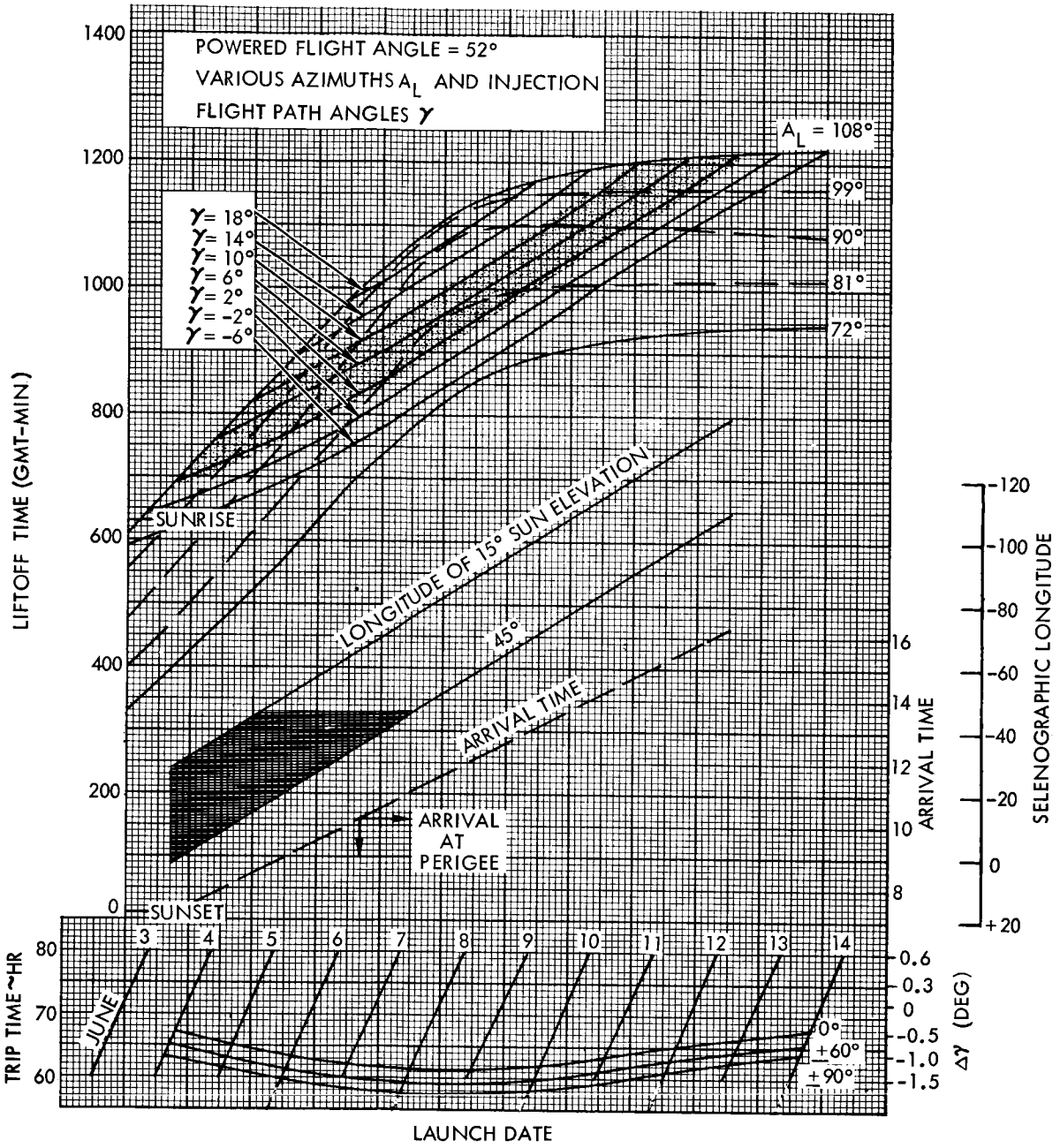

Figure 2-45. Direct Injection Launch Window
June 1968

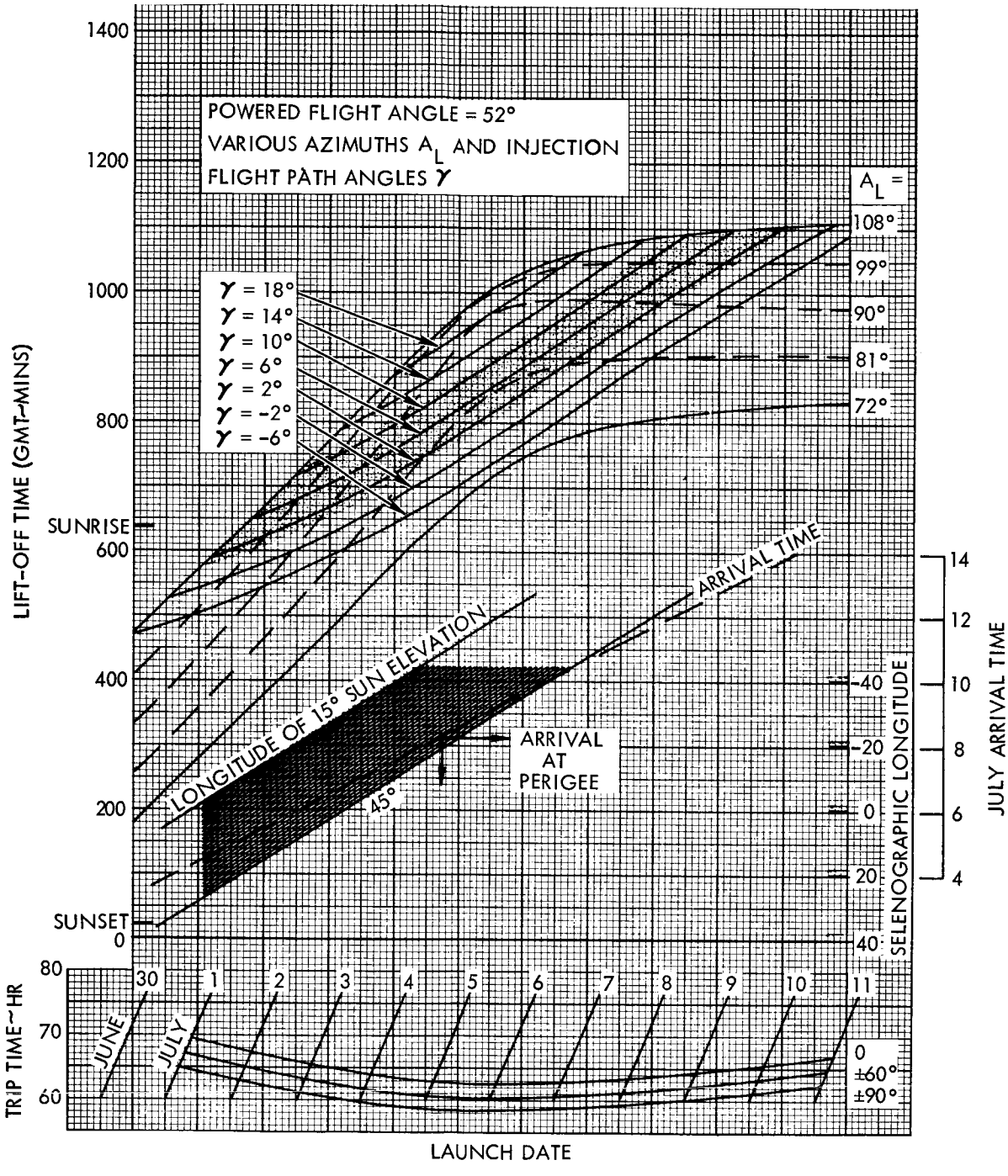

Figure 2-46. Direct Injection Launch Window July 1968

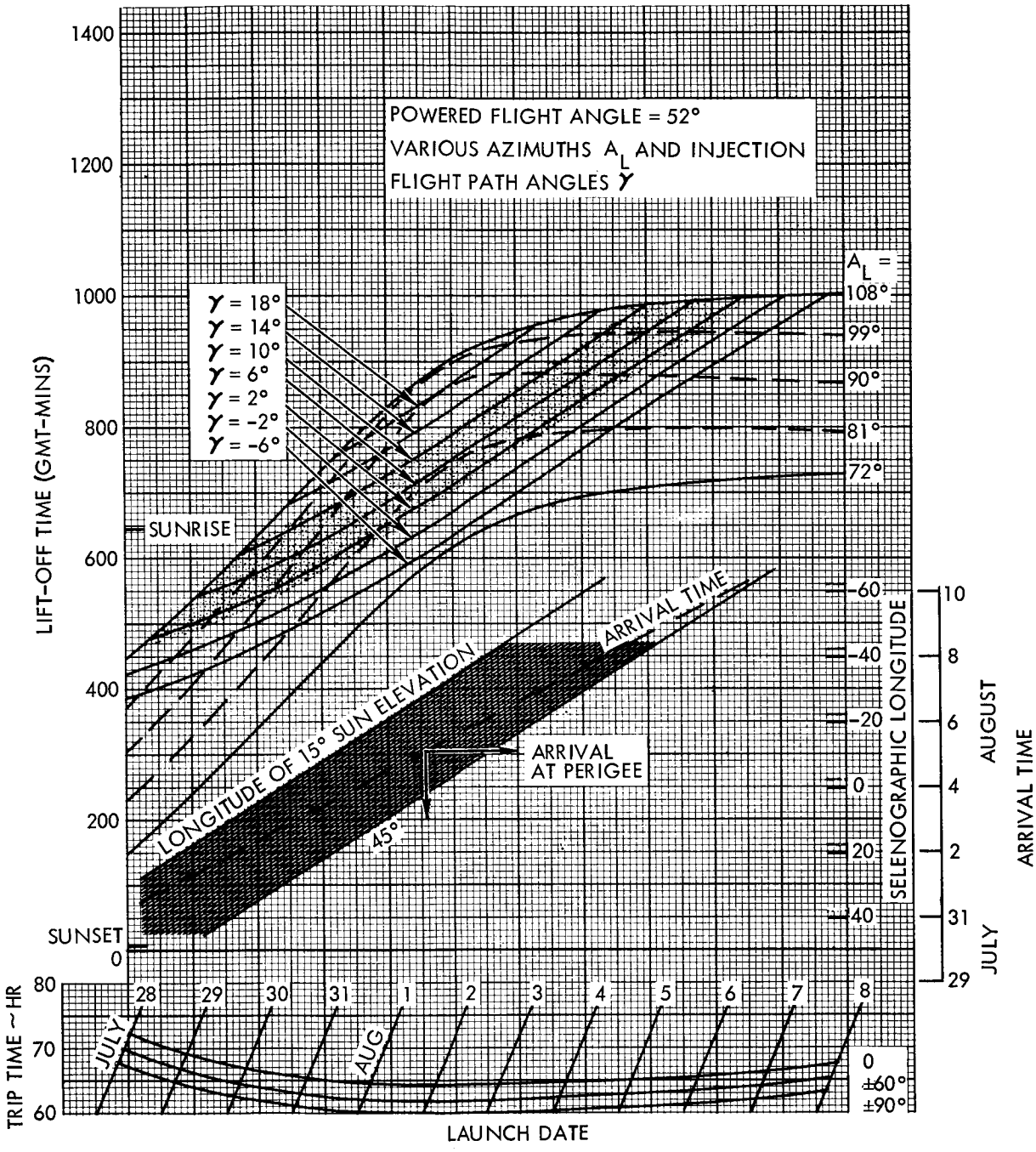

Figure 2-47. Direct Injection Launch Window
July-August 1968

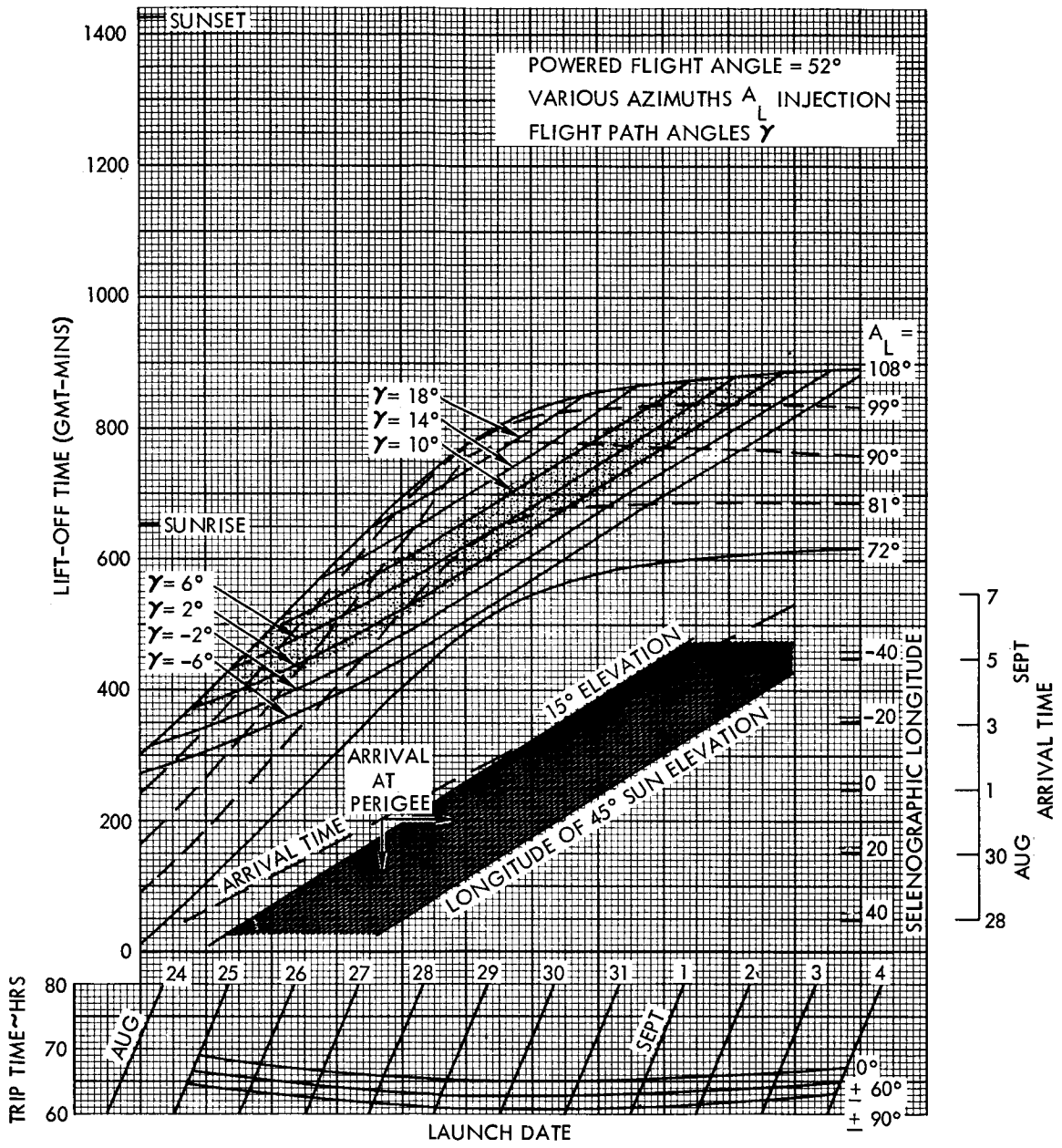

Figure 2-48. Direct Injection Launch Window August-September 1968

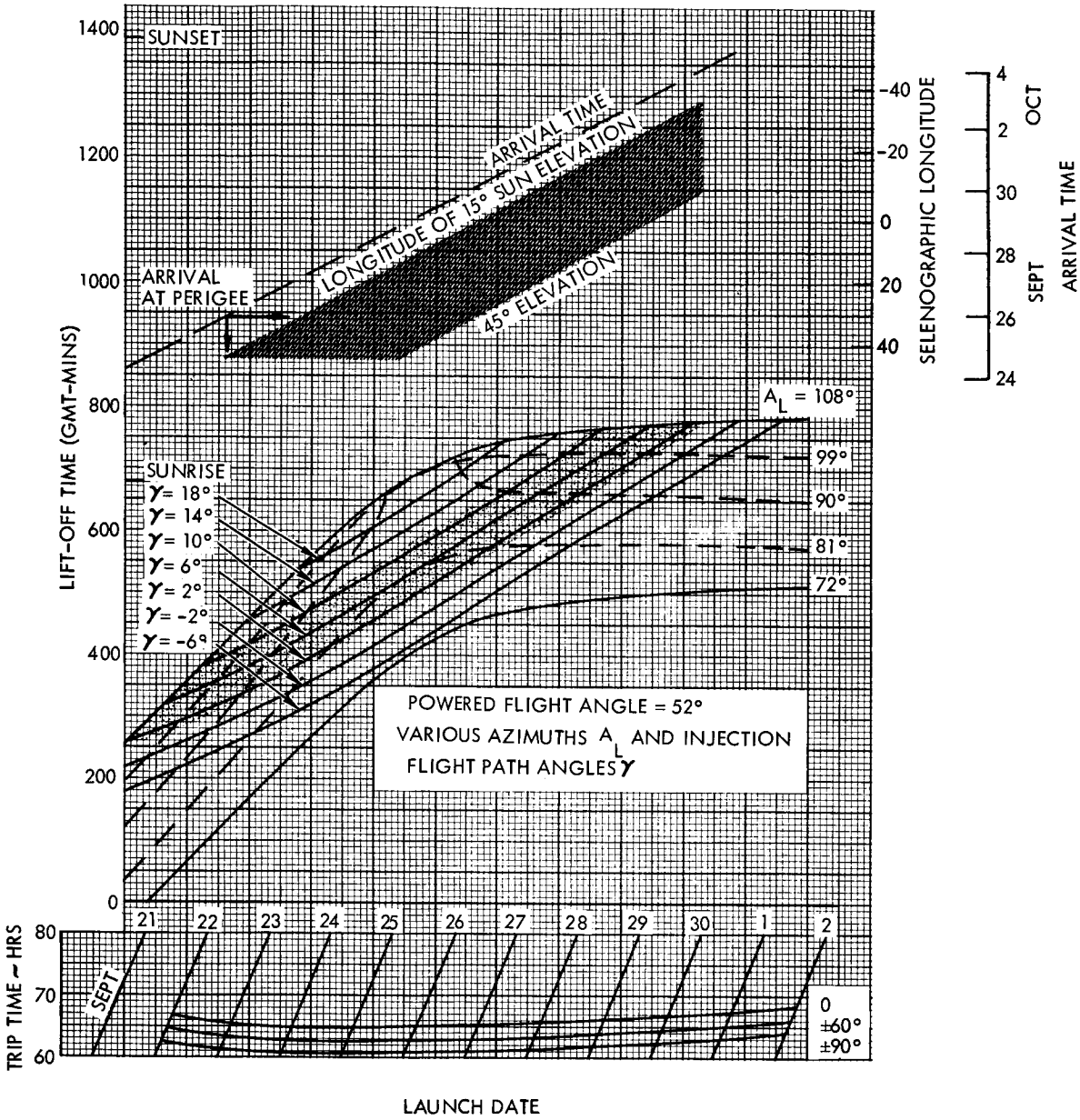

Figure 2-49. Direct Injection Launch Window September-October 1968

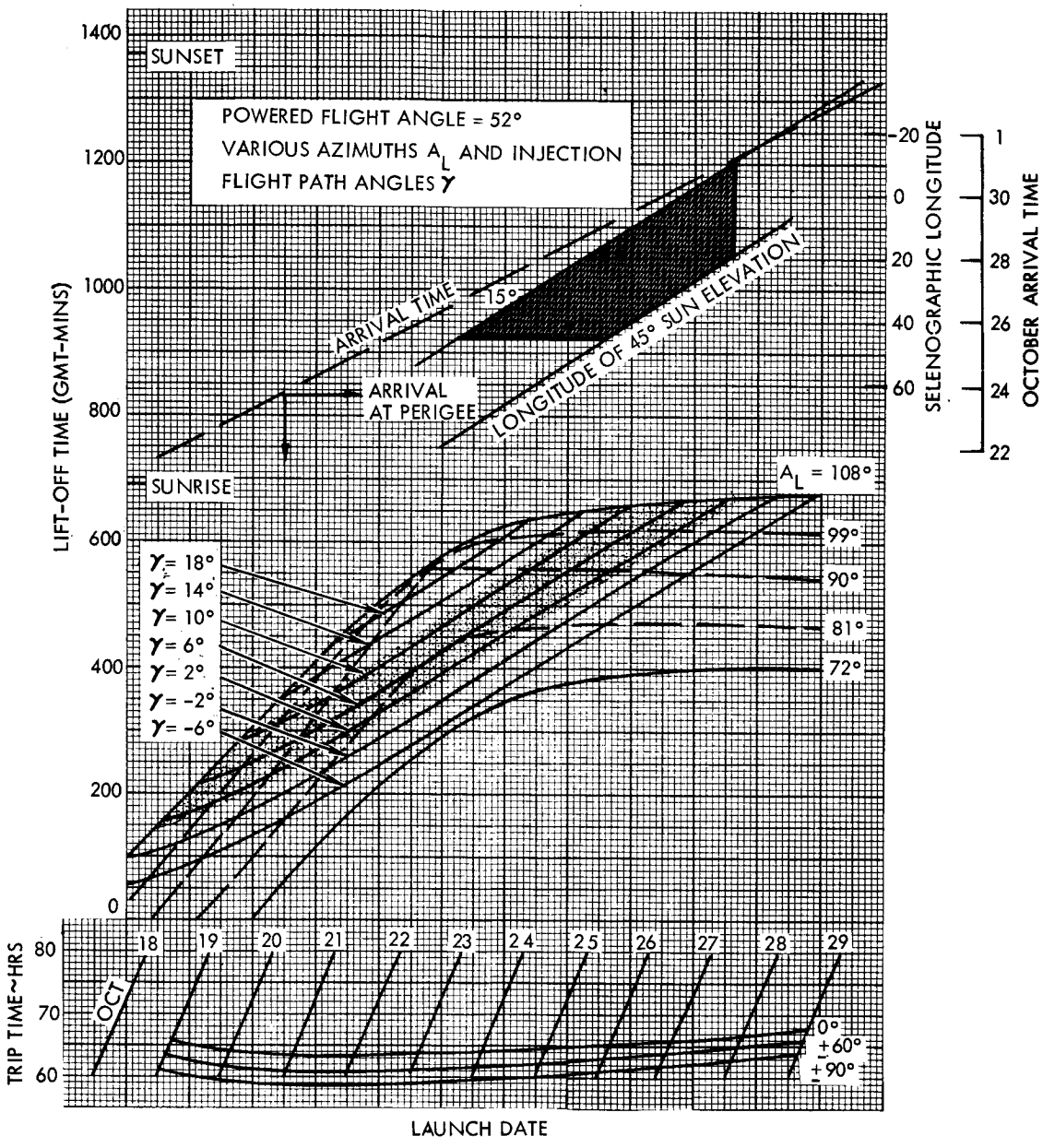

Figure 2-50. Direct Injection Launch Window October 1968

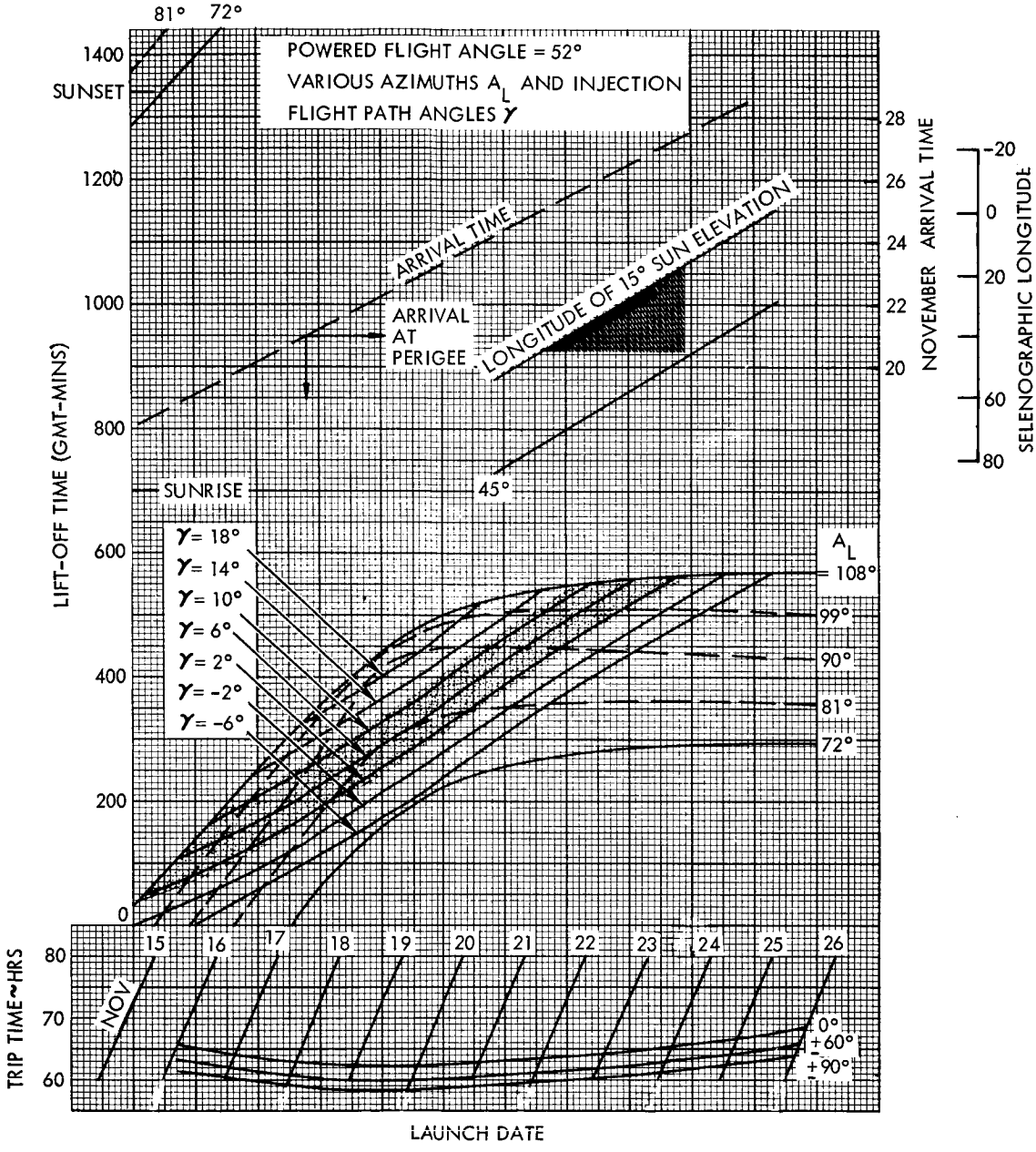

Figure 2-51. Direct Injection Launch Window November 1968

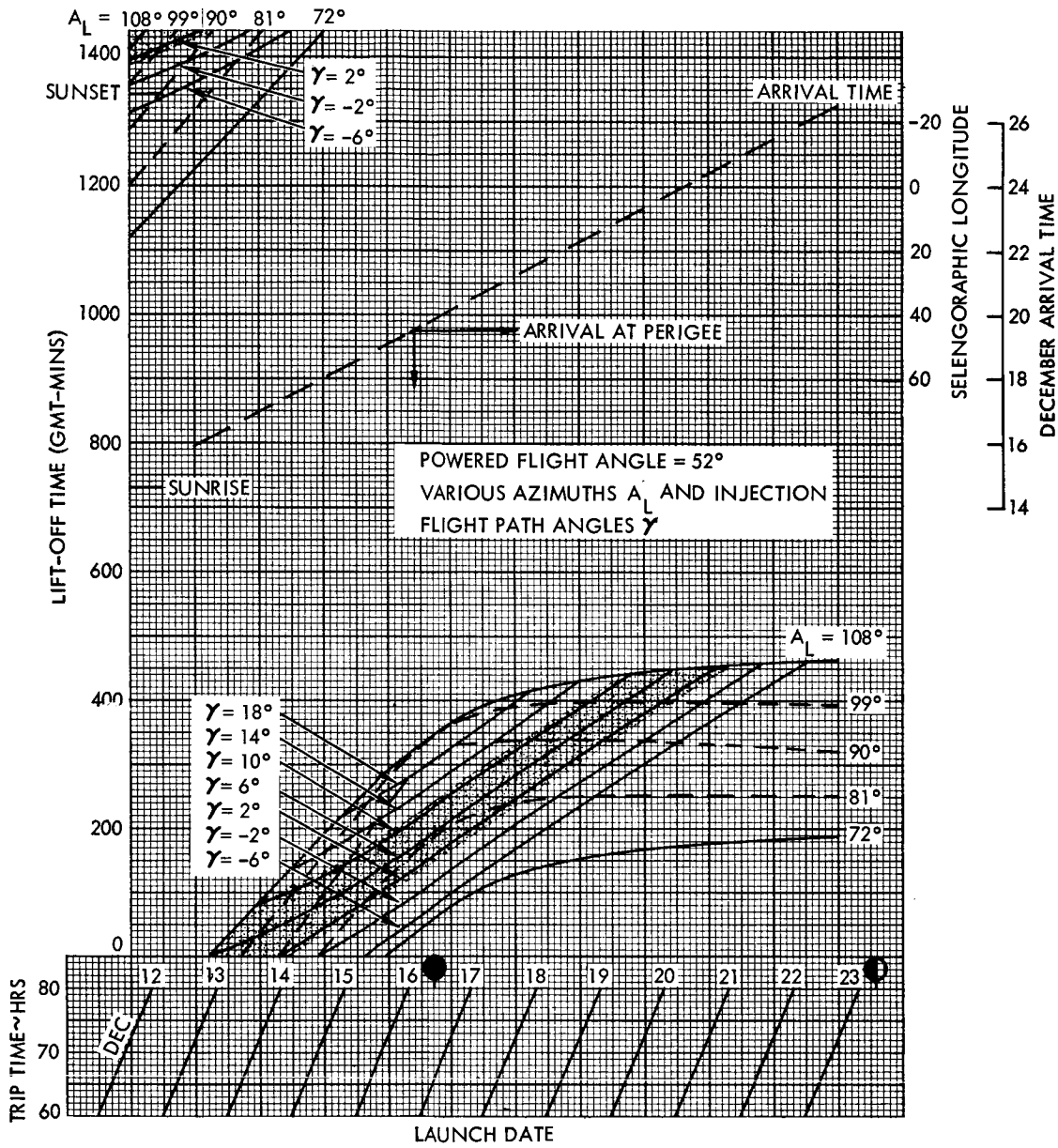

Figure 2-52. Direct Injection Launch Window December 1968

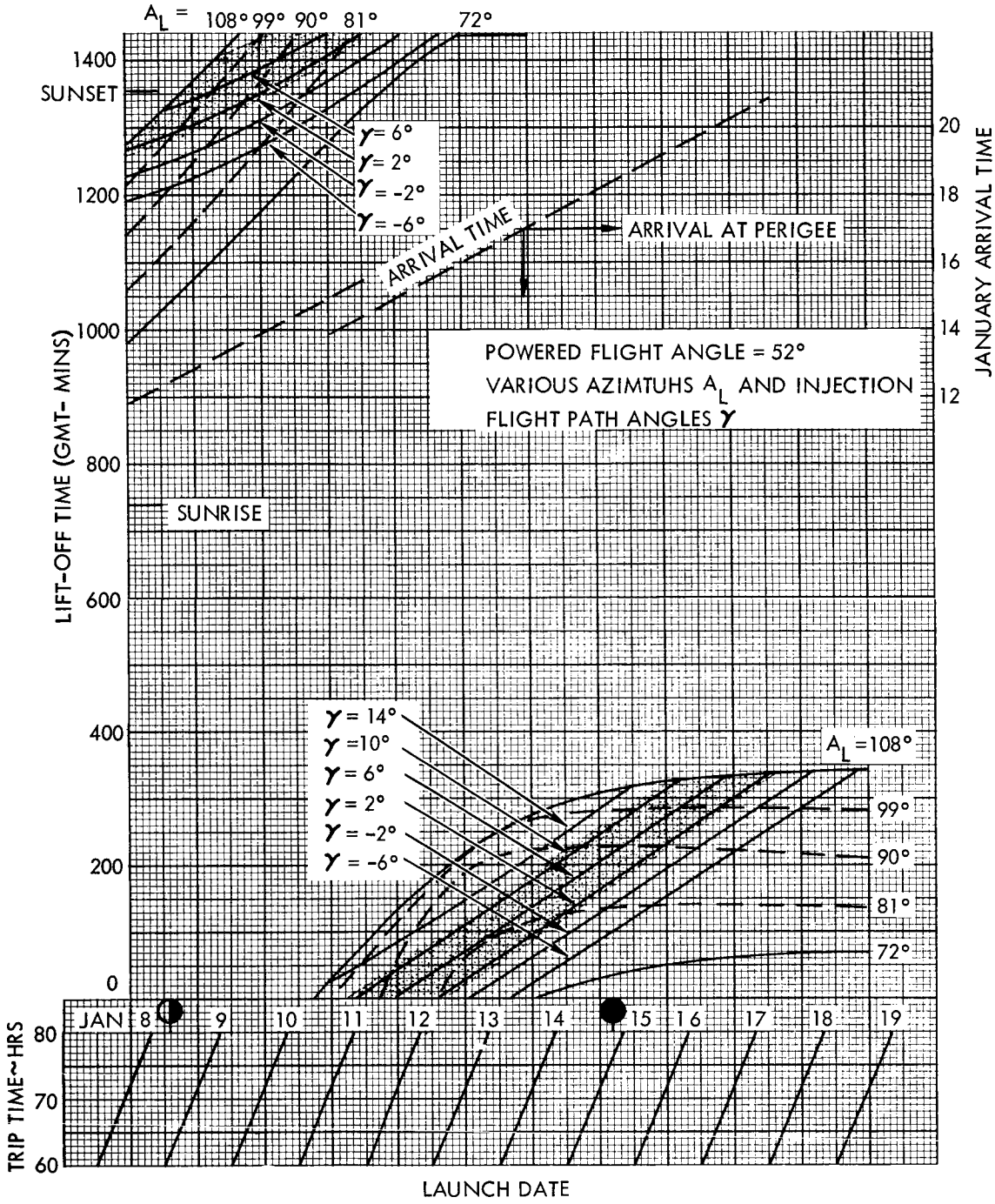

Figure 2-53. Direct Injection Launch Window
January 1969

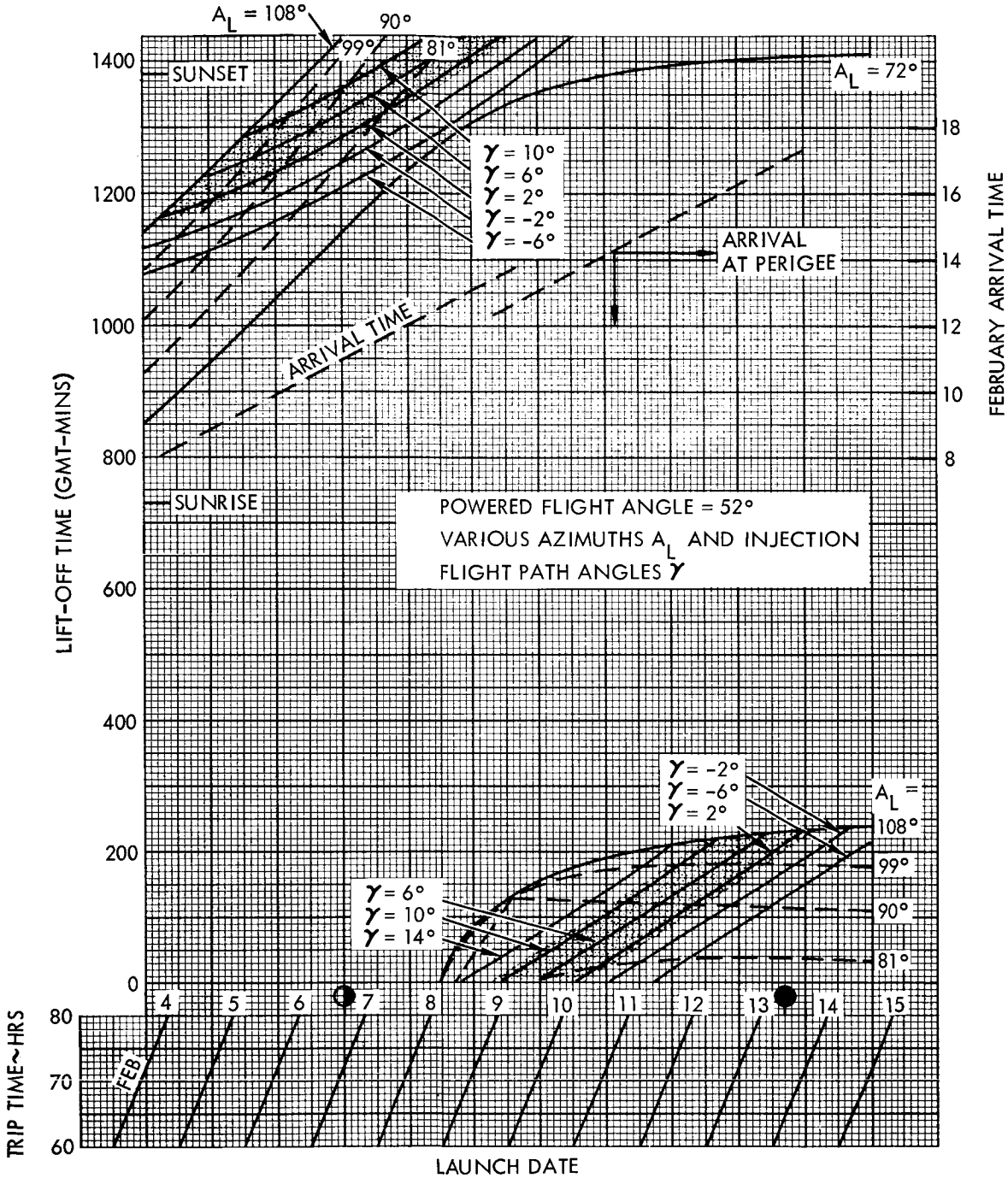

Figure 2-54. Direct Injection Launch Window February 1969

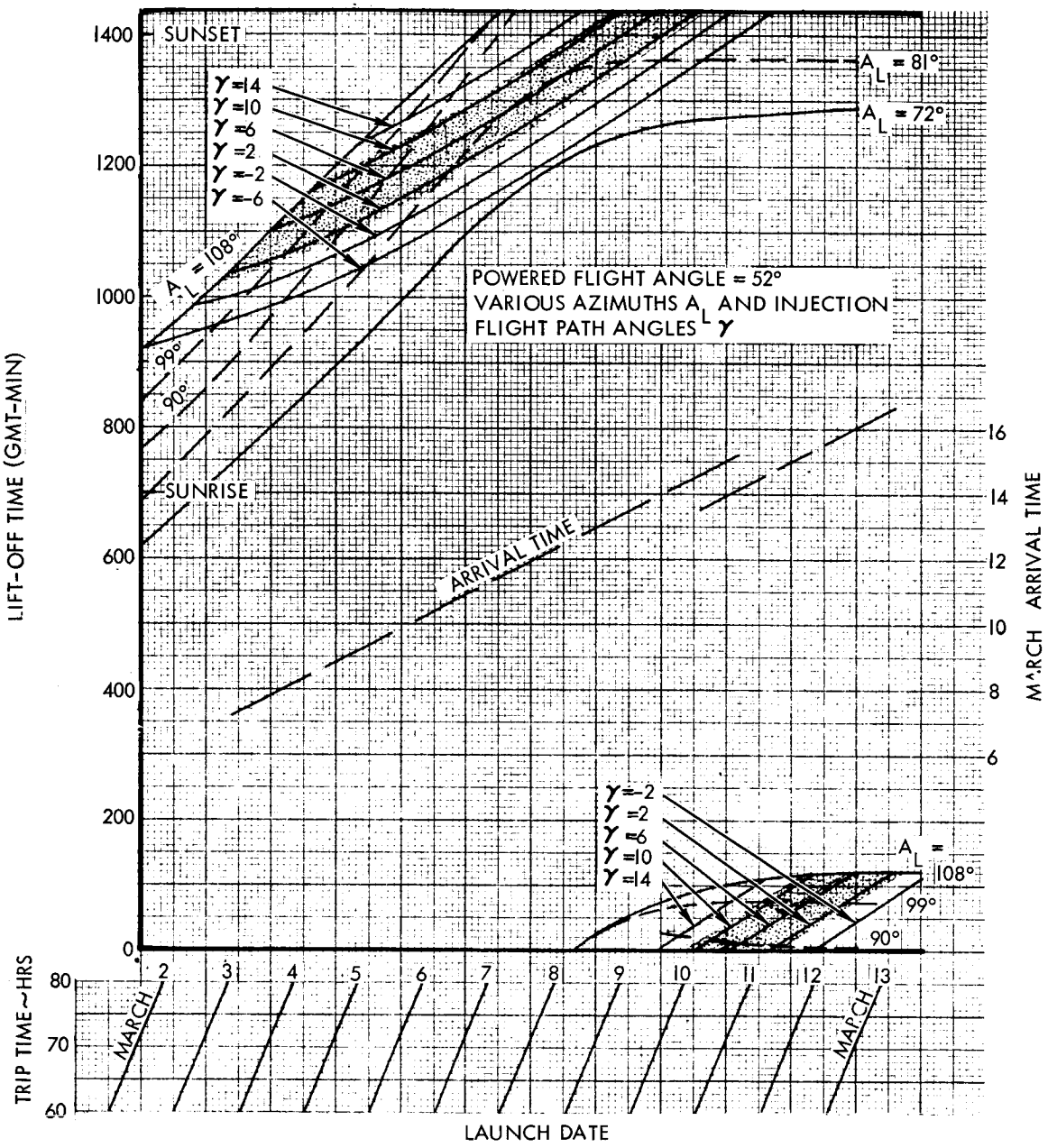

Figure 2-55. Direct Injection Launch Window
March 1969

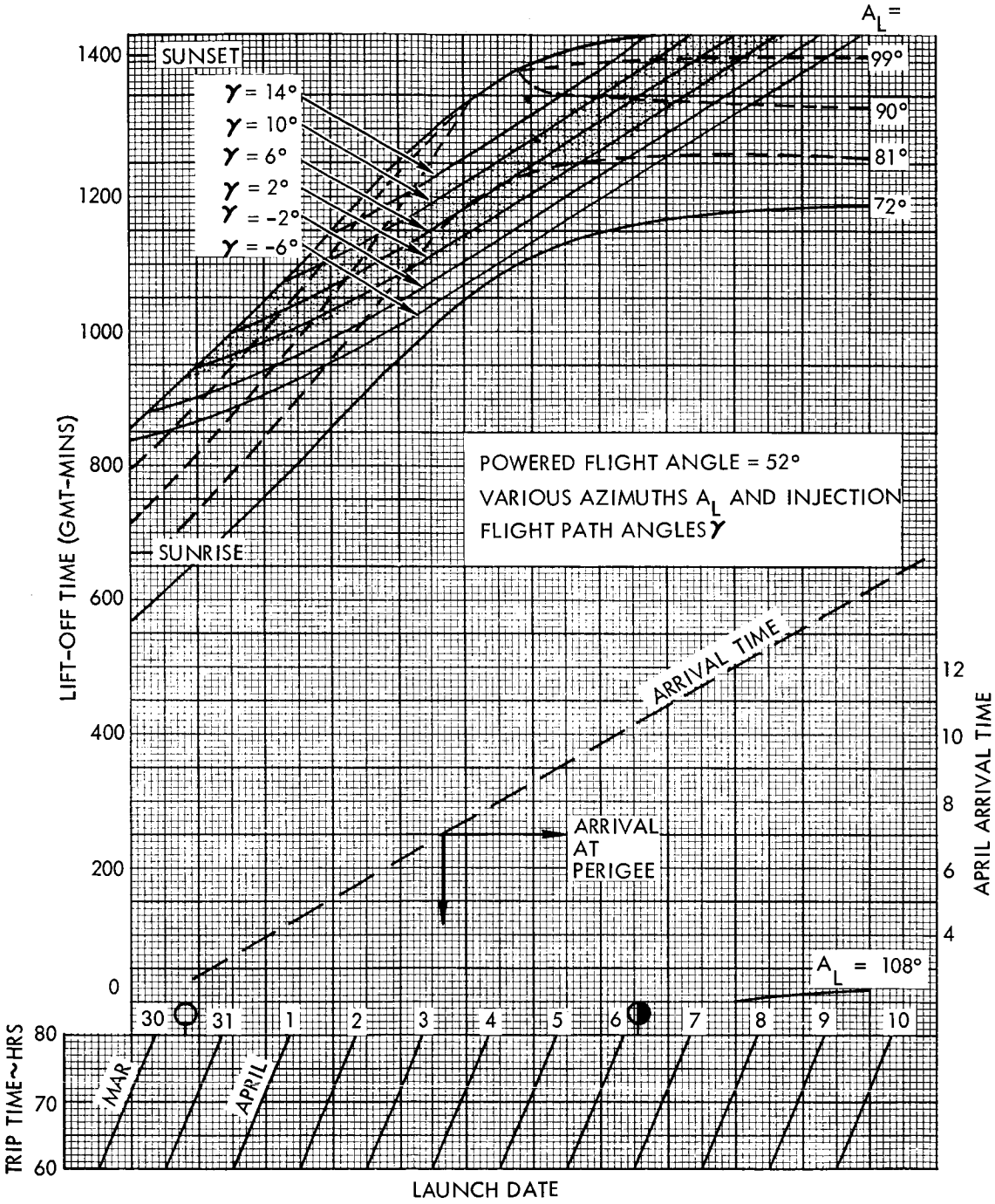

Figure 2-56. Direct Injection Launch Window April 1969

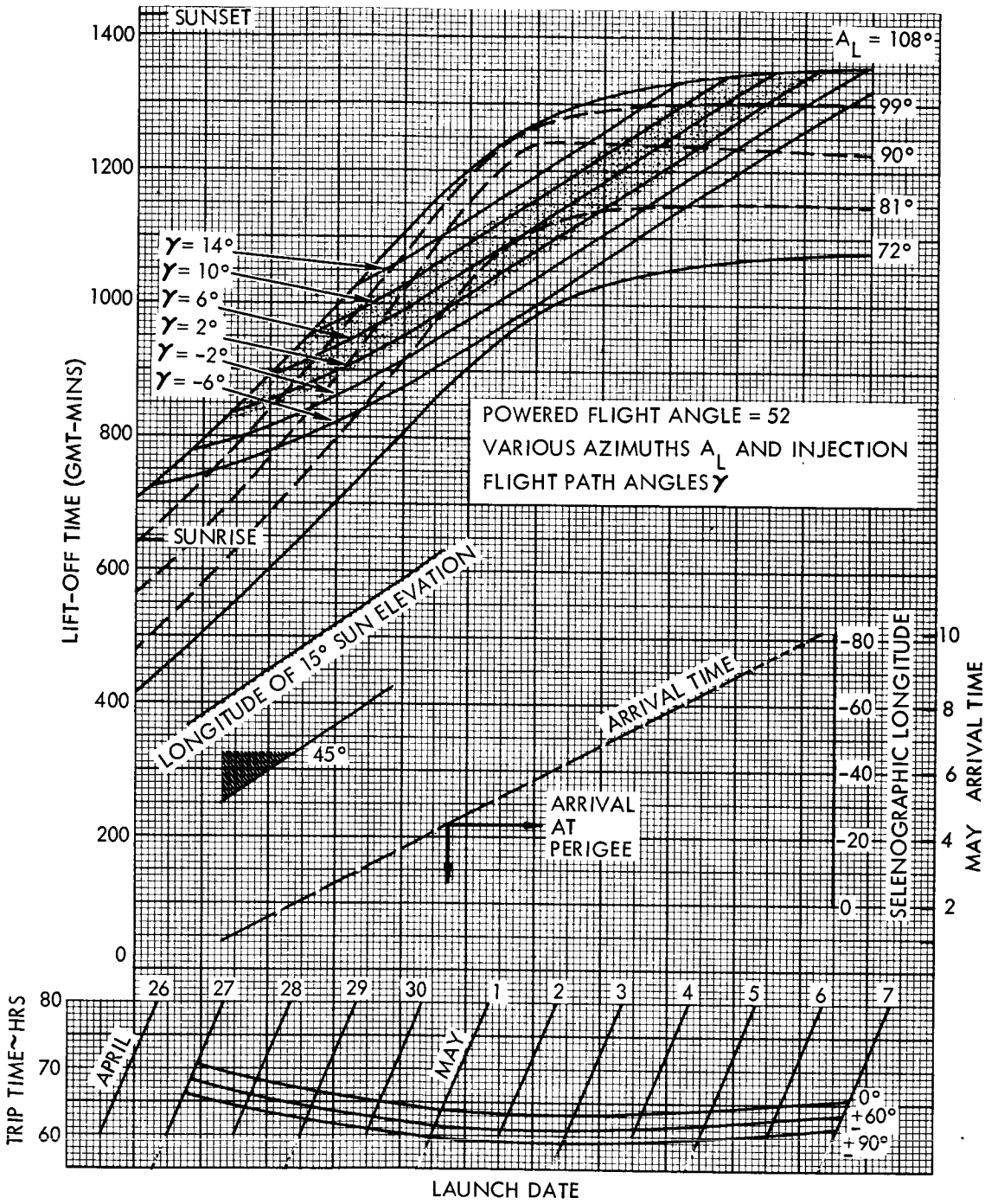

Figure 2-57. Direct Injection Launch Window April-May 1969

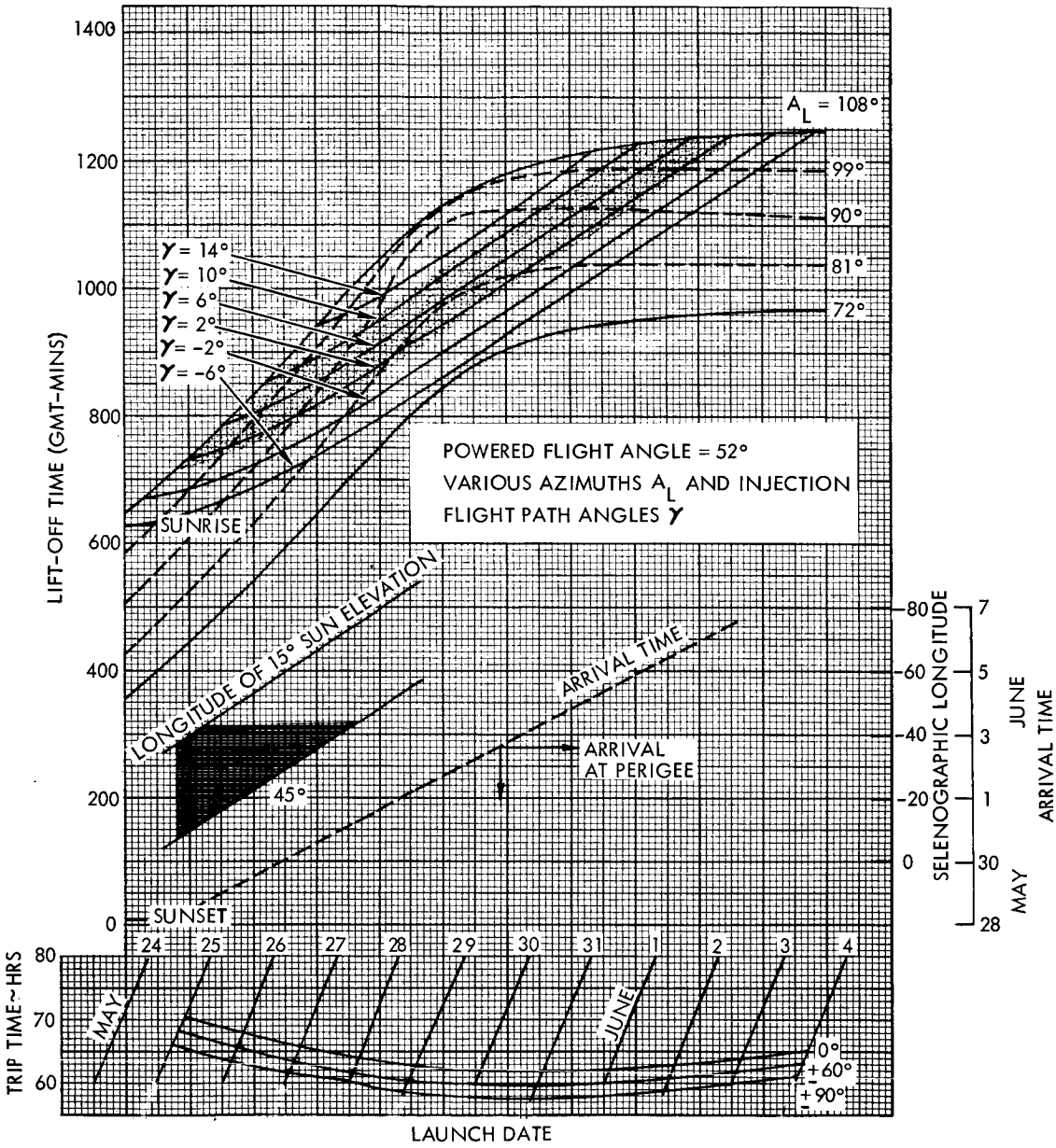

Figure 2-58. Direct Injection Launch Window May-June 1969

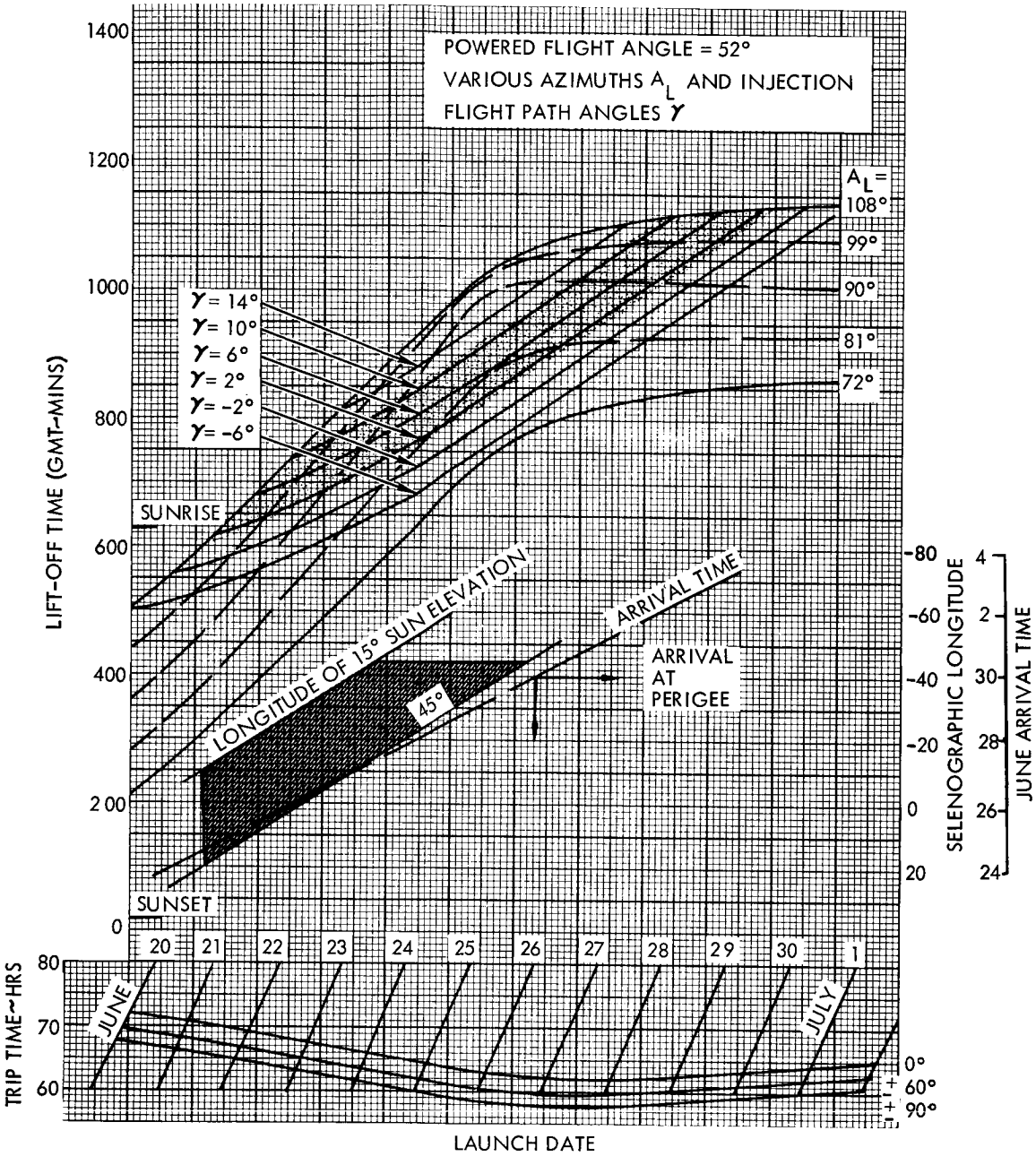

Figure 2-59. Direct Injection Launch Window June-July 1969

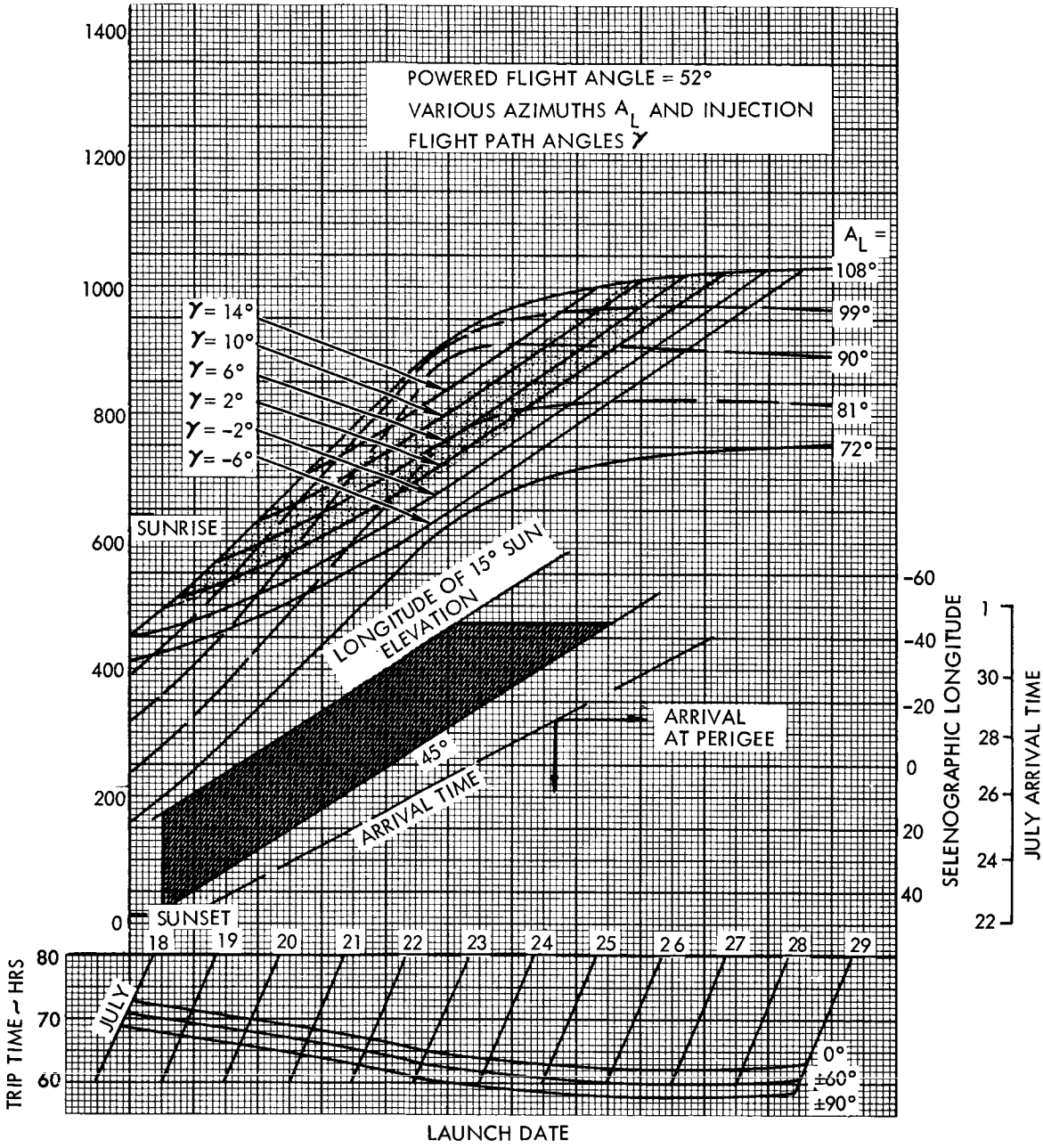

Figure 2-60. Direct Injection Launch Window
July 1969

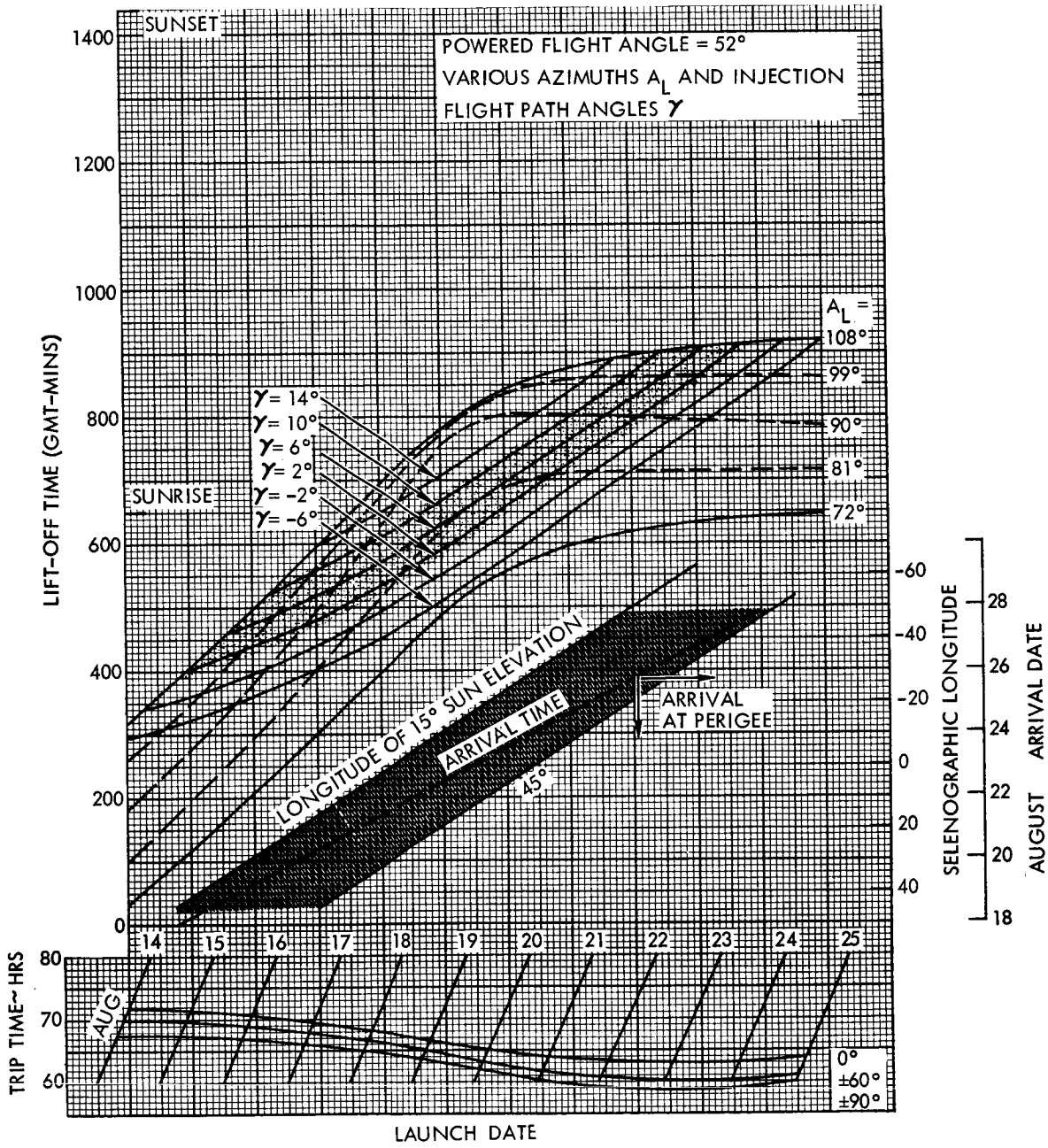

Figure 2-61. Direct Injection Launch Window
August 1969

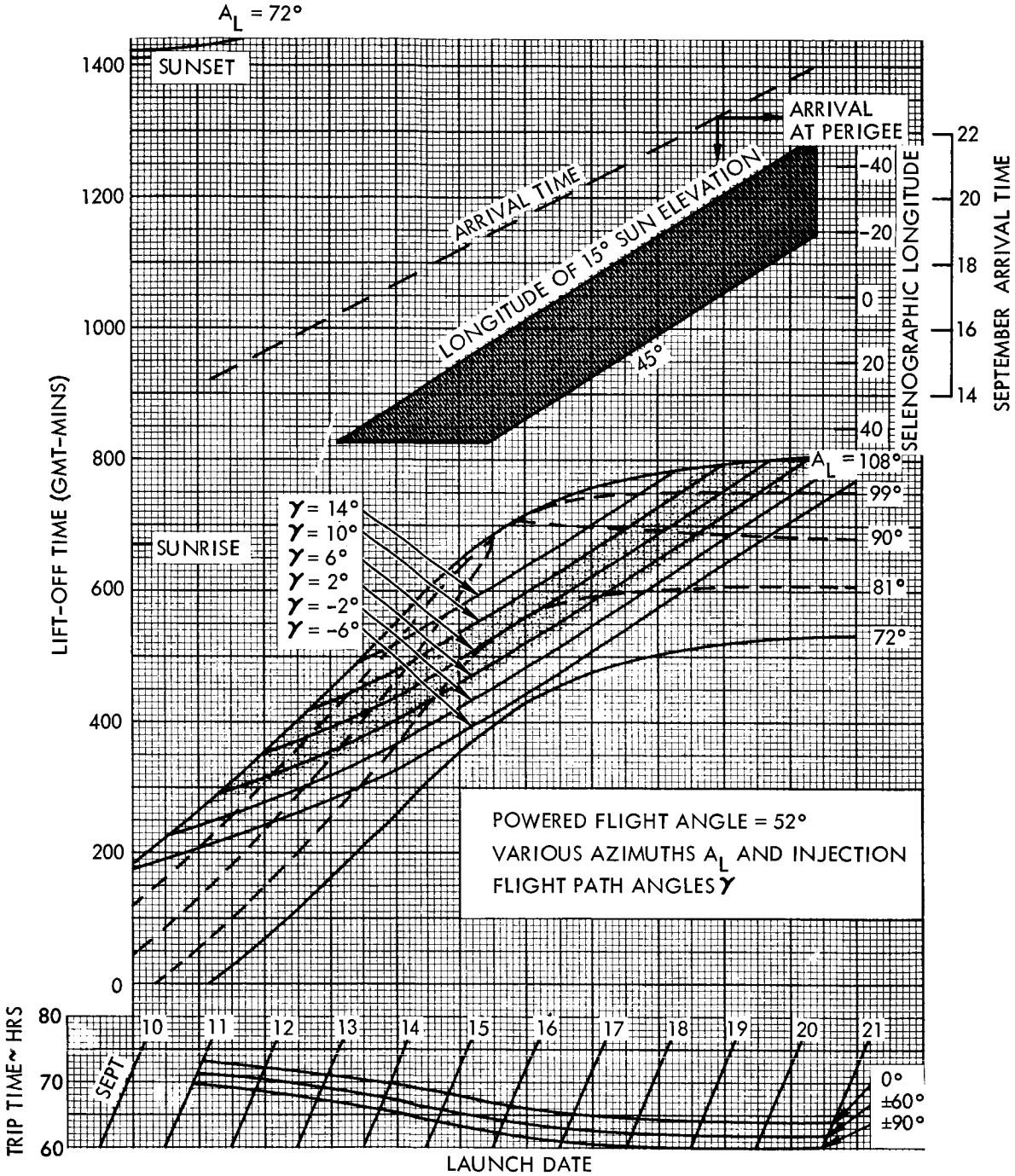

Figure 2-62. Direct Injection Launch Window September 1969

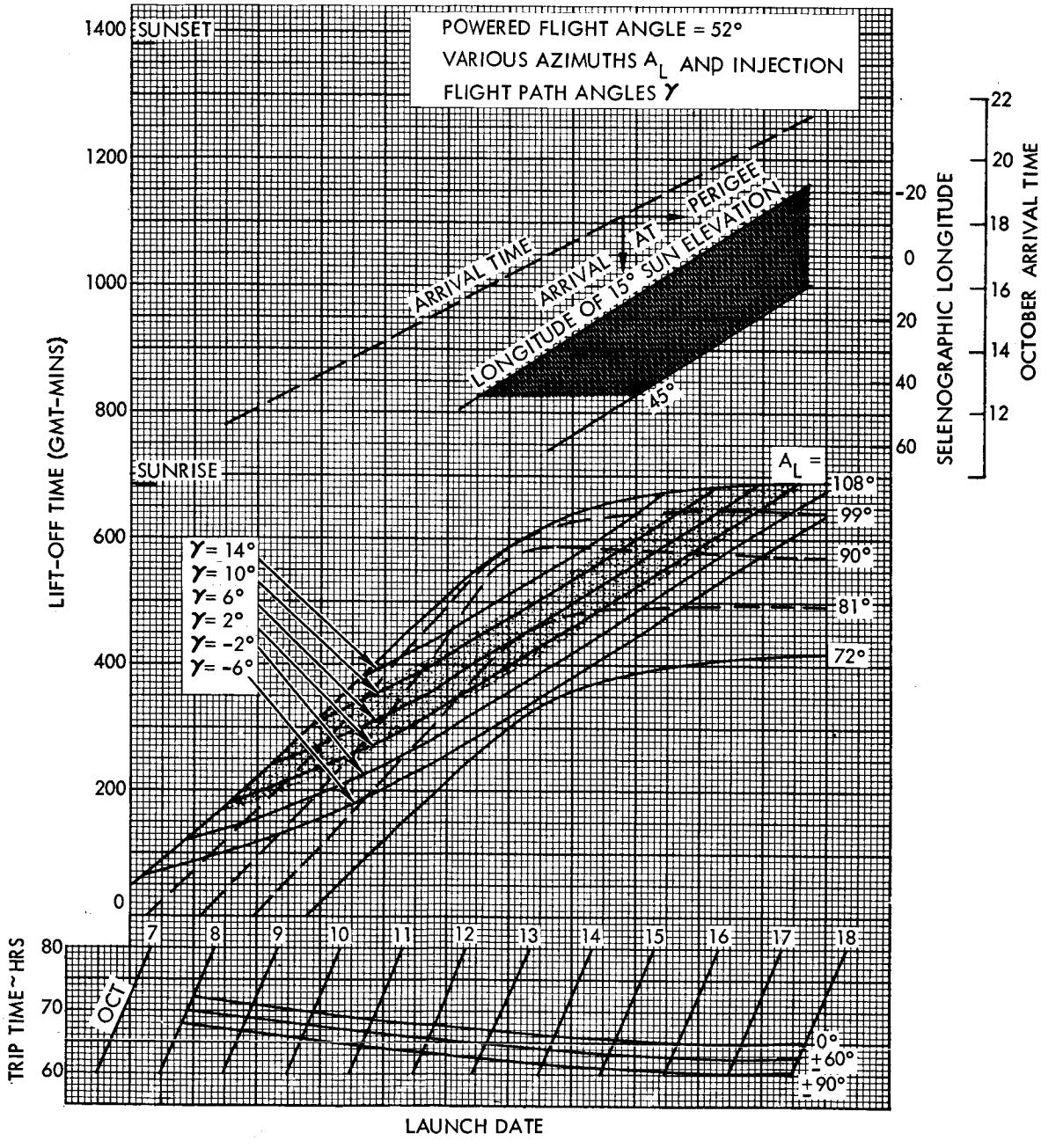

Figure 2-63. Direct Injection Launch Window October 1969

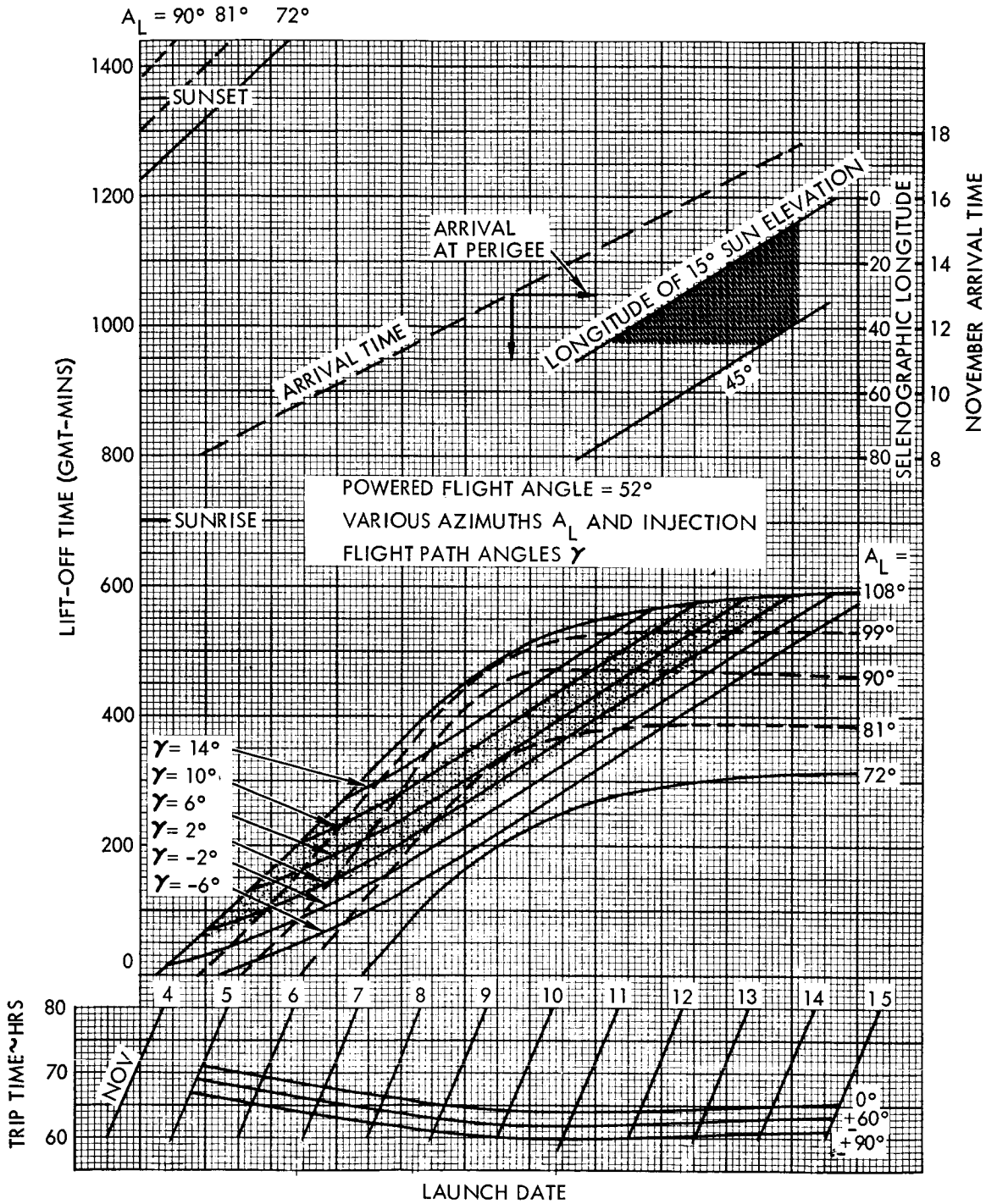

Figure 2-64. Direct Injection Launch Window November 1969

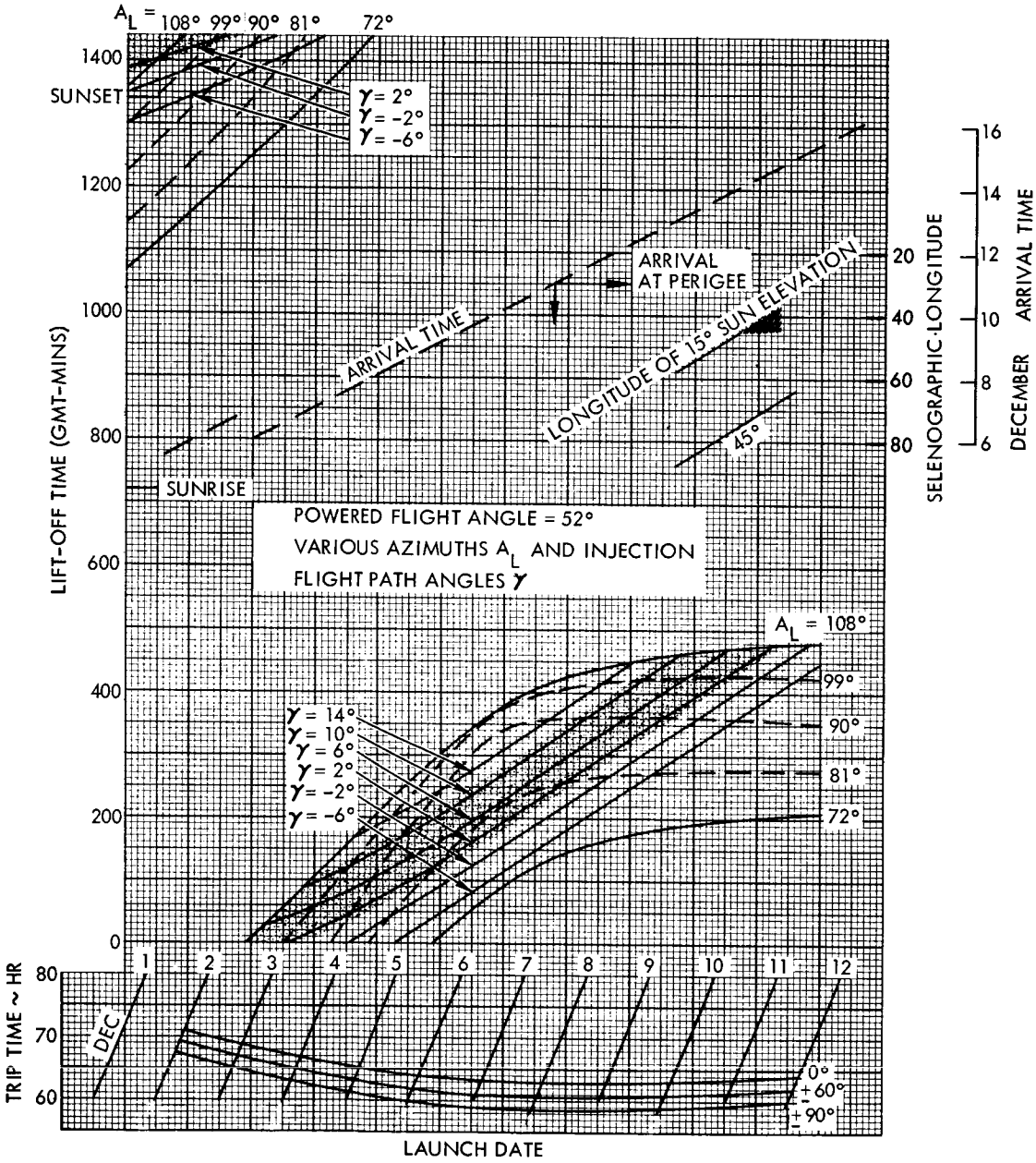

Figure 2-65. Direct Injection Launch Window December 1969

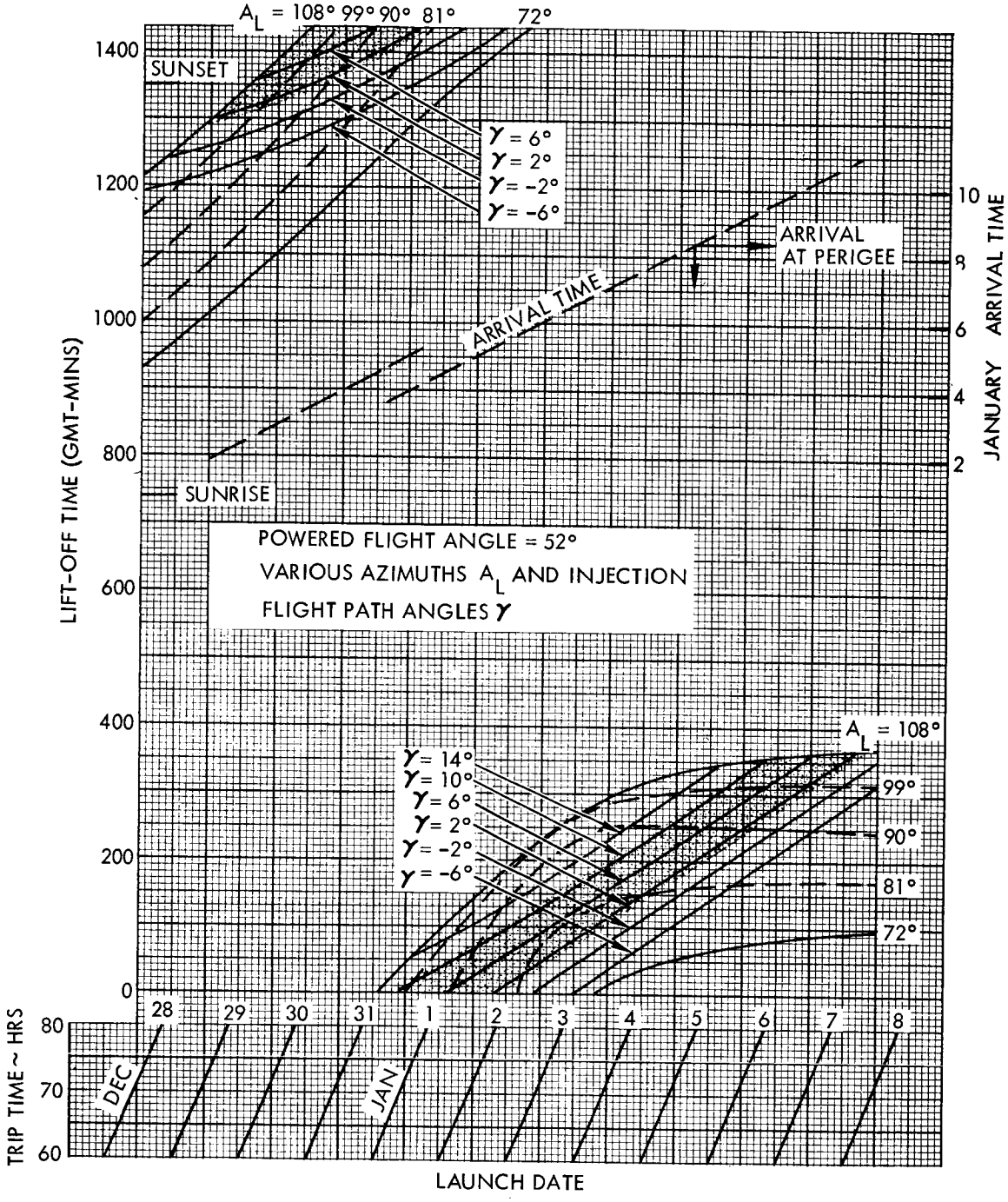

Figure 2-66. Direct Injection Launch Window January 1970

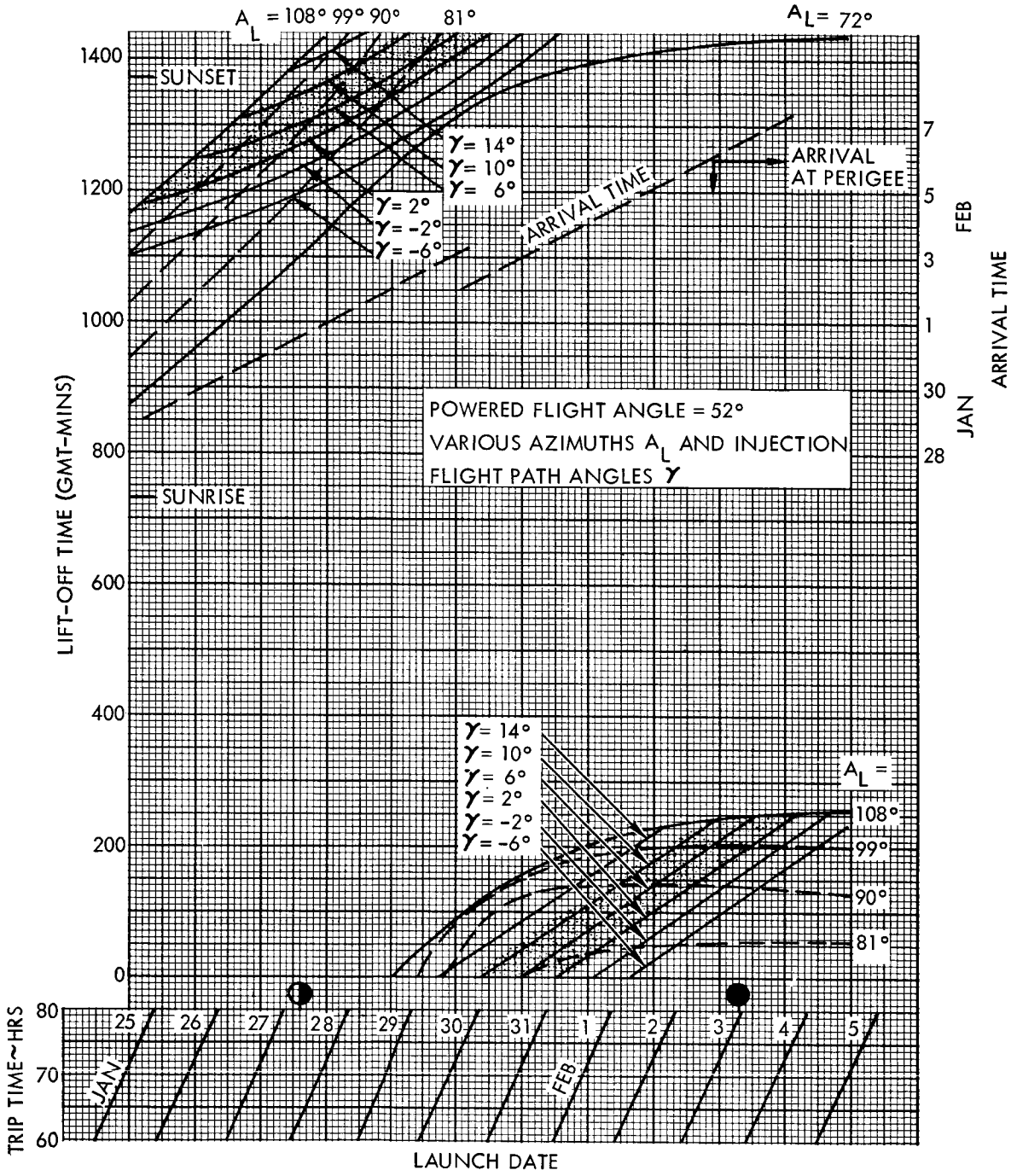

Figure 2-67. Direct Injection Launch Window
January-February 1970

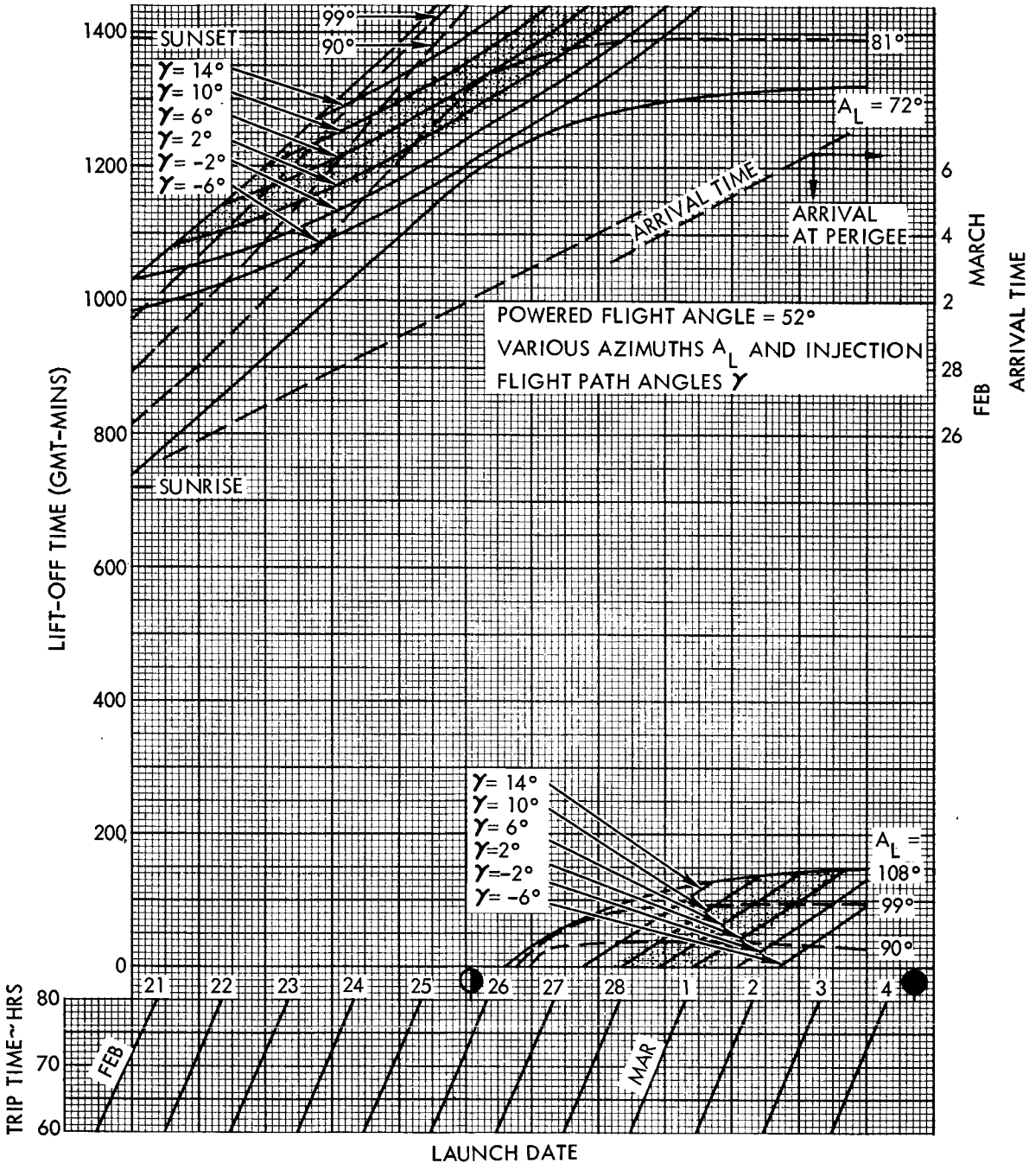

Figure 2-68. Direct Injection Launch Window February-March 1970

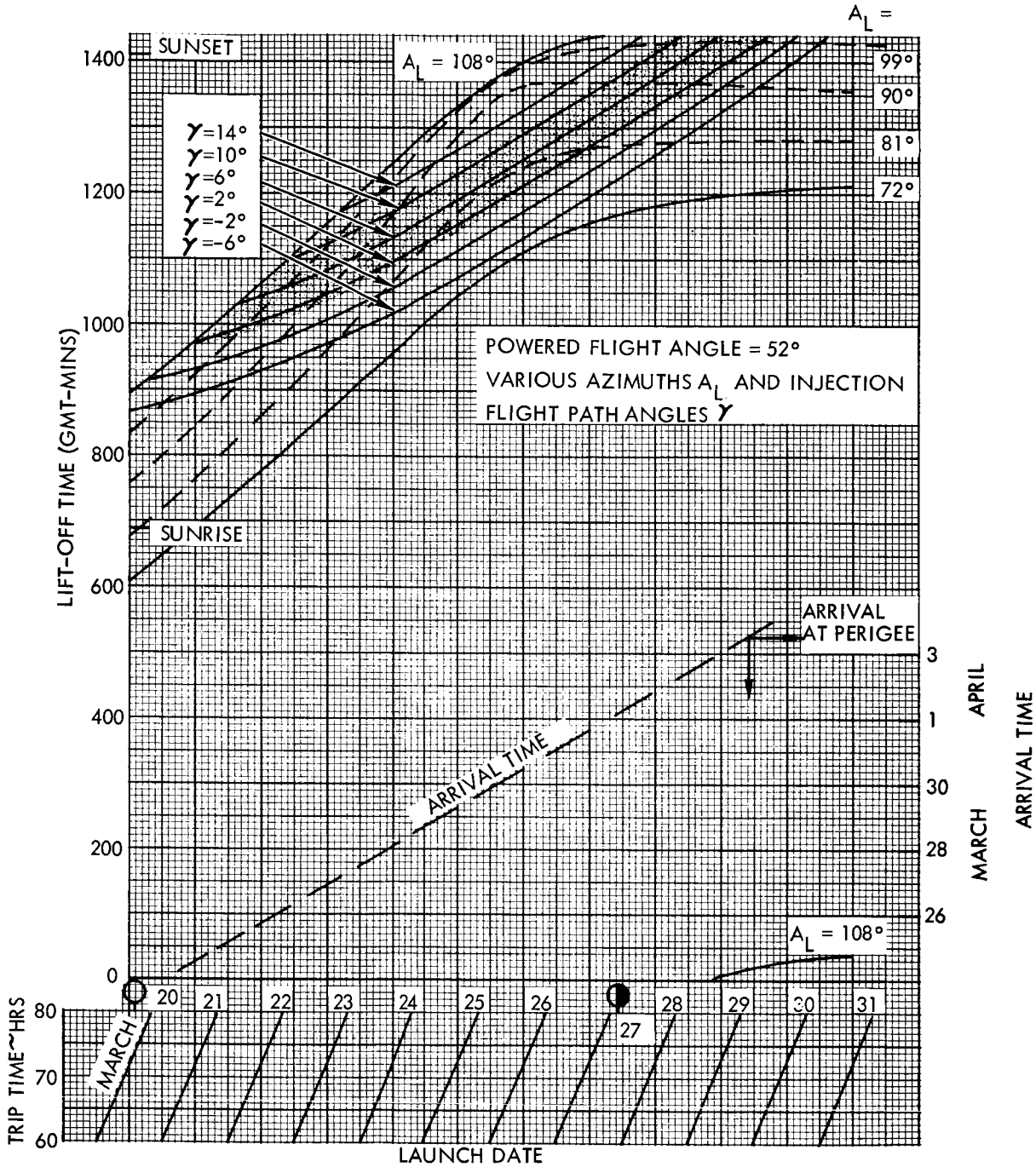

Figure 2-69. Direct Injection Launch Window March-April 1970

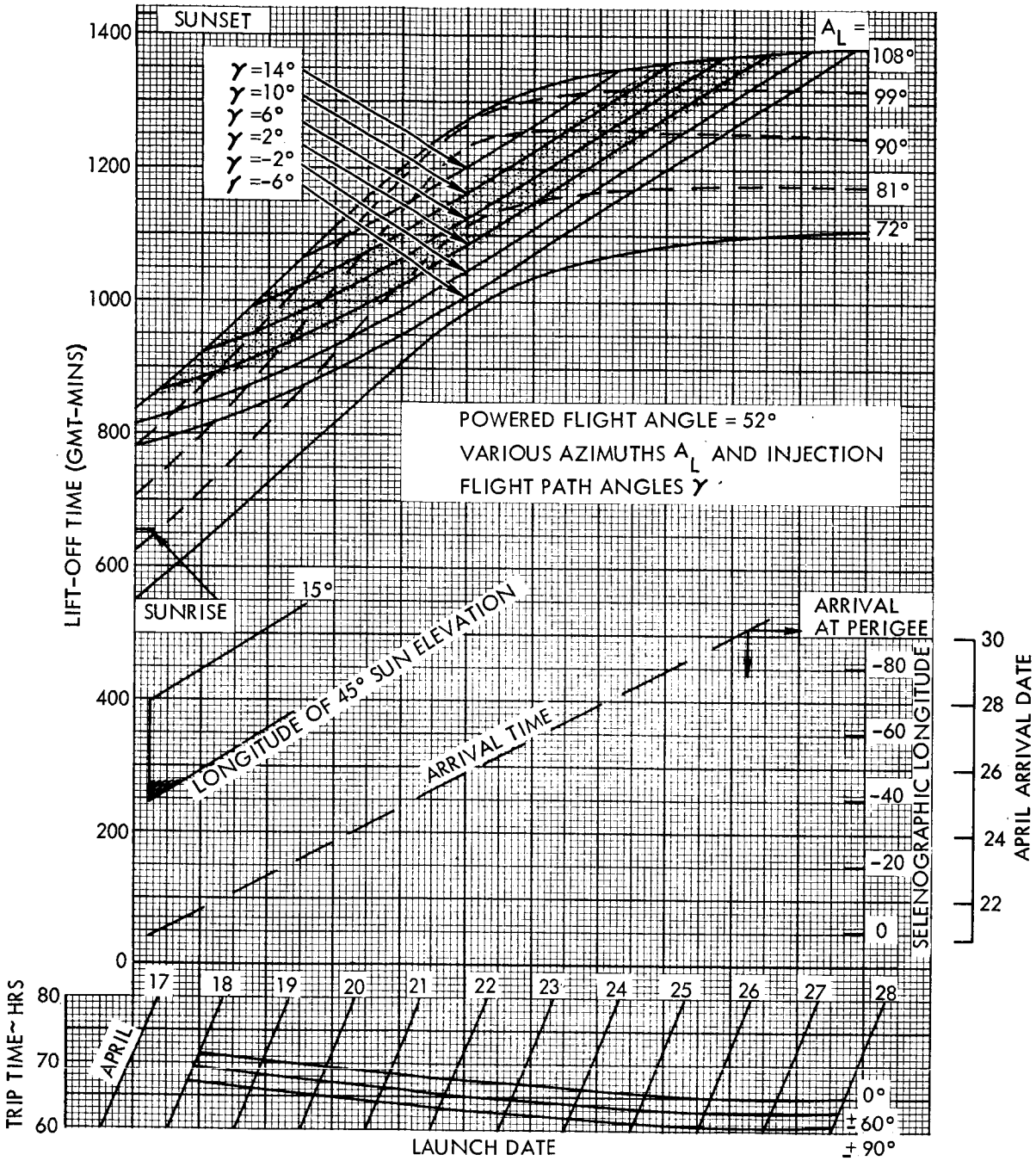

Figure 2-70. Direct Injection Launch Window
April 1970

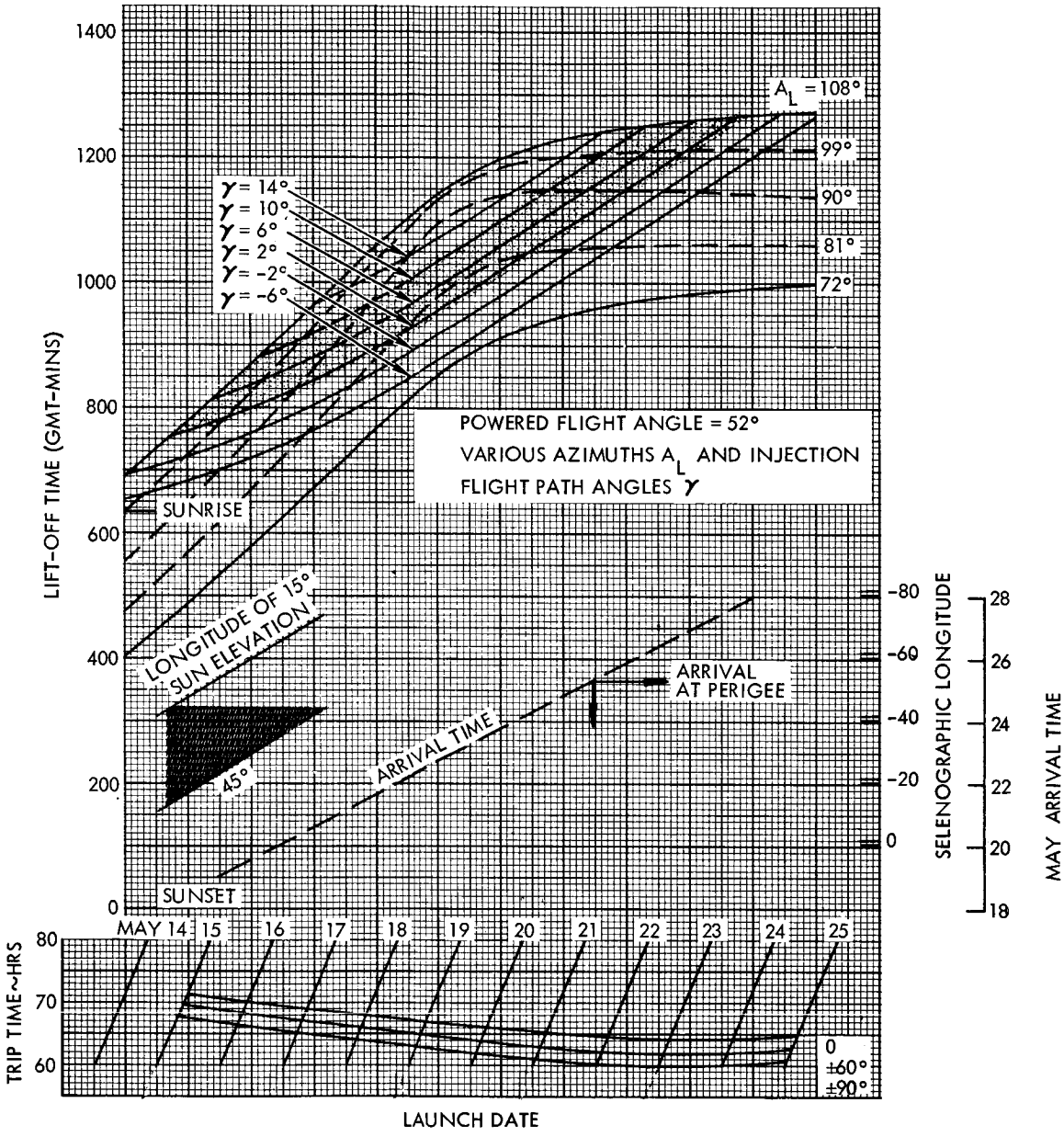

Figure 2-71. Direct Injection Launch Window
May 1970

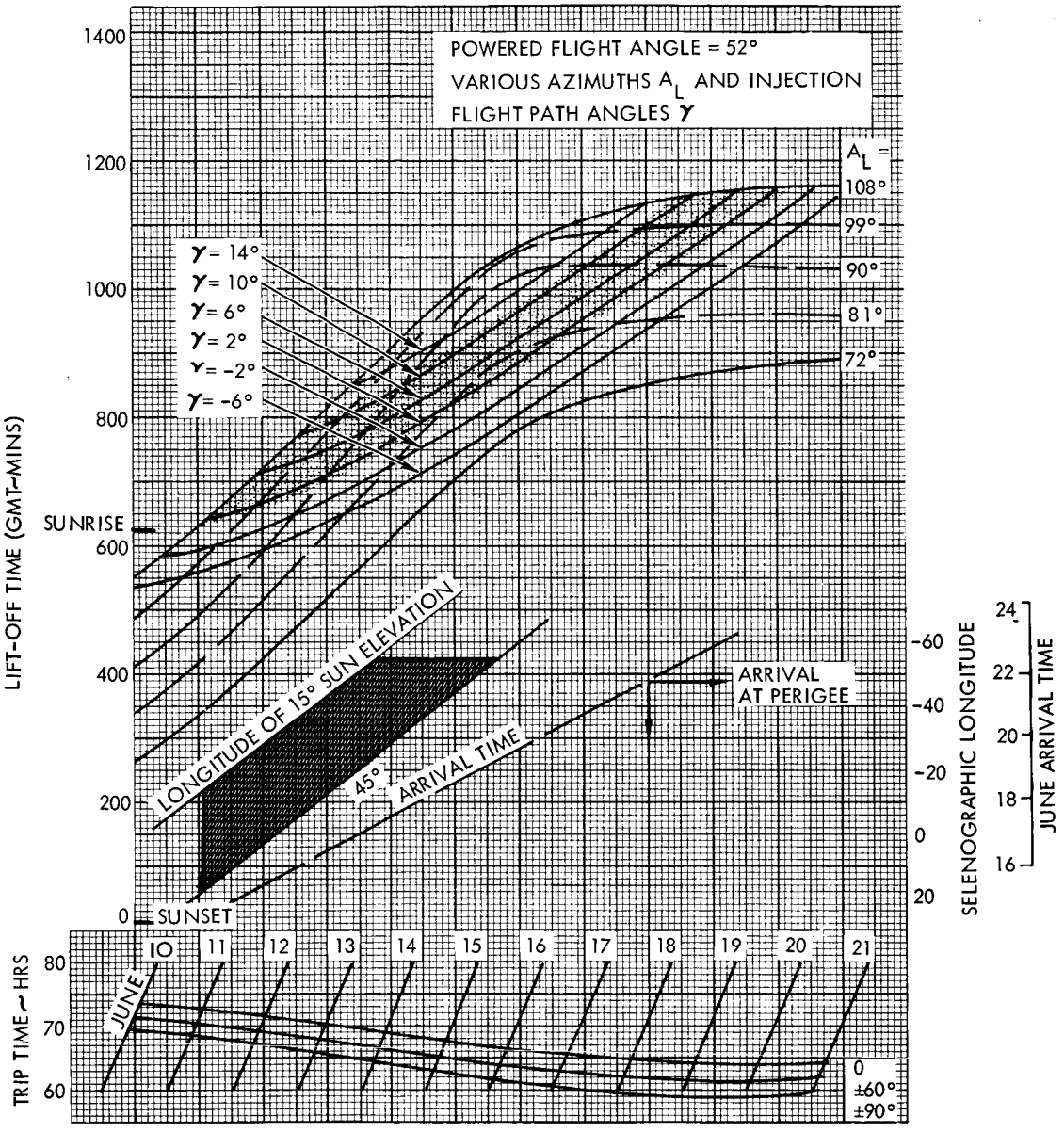

Figure 2-72. Direct Injection Launch Window June 1970

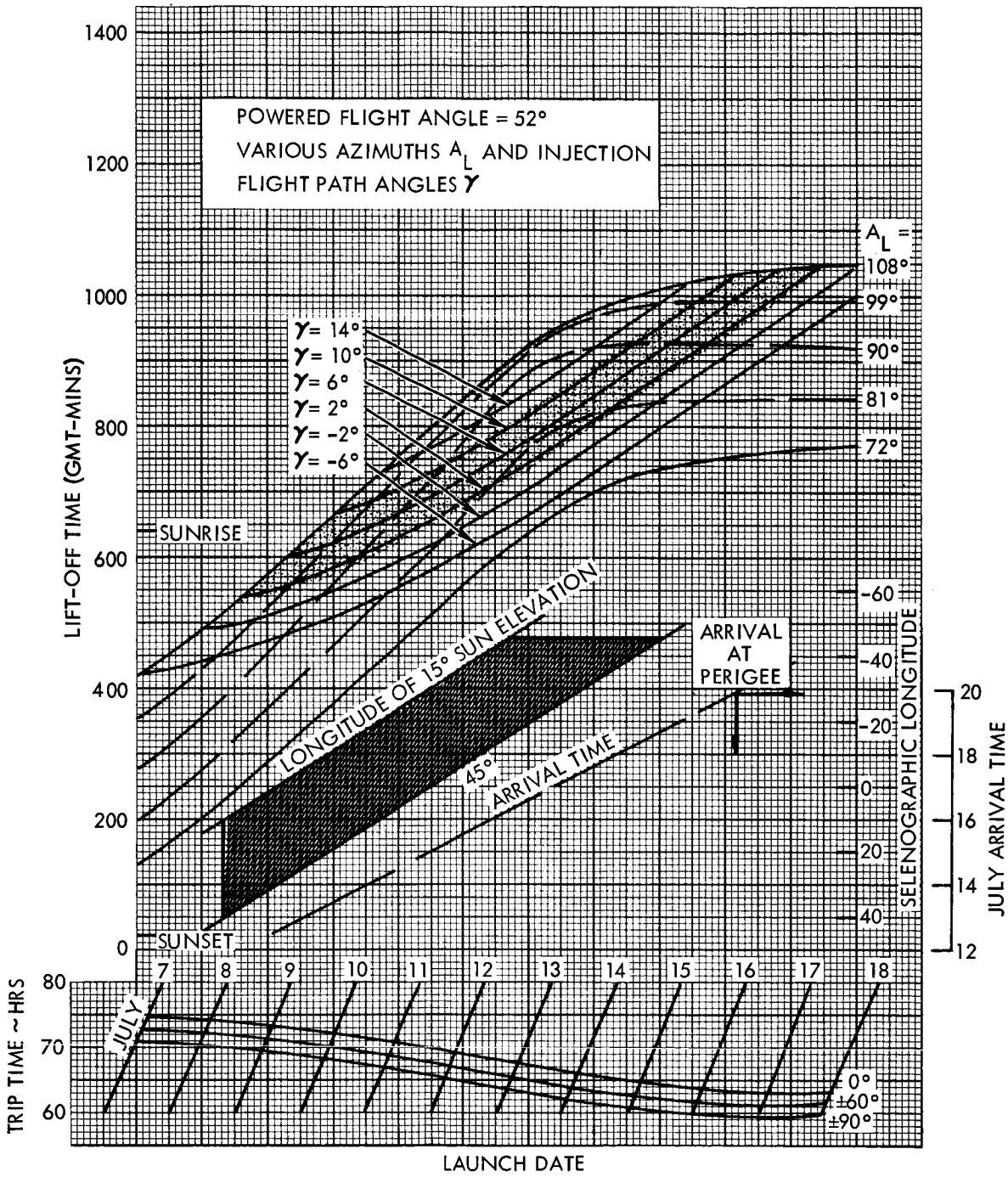

Figure 2-73. Direct Injection Launch Window
July 1970

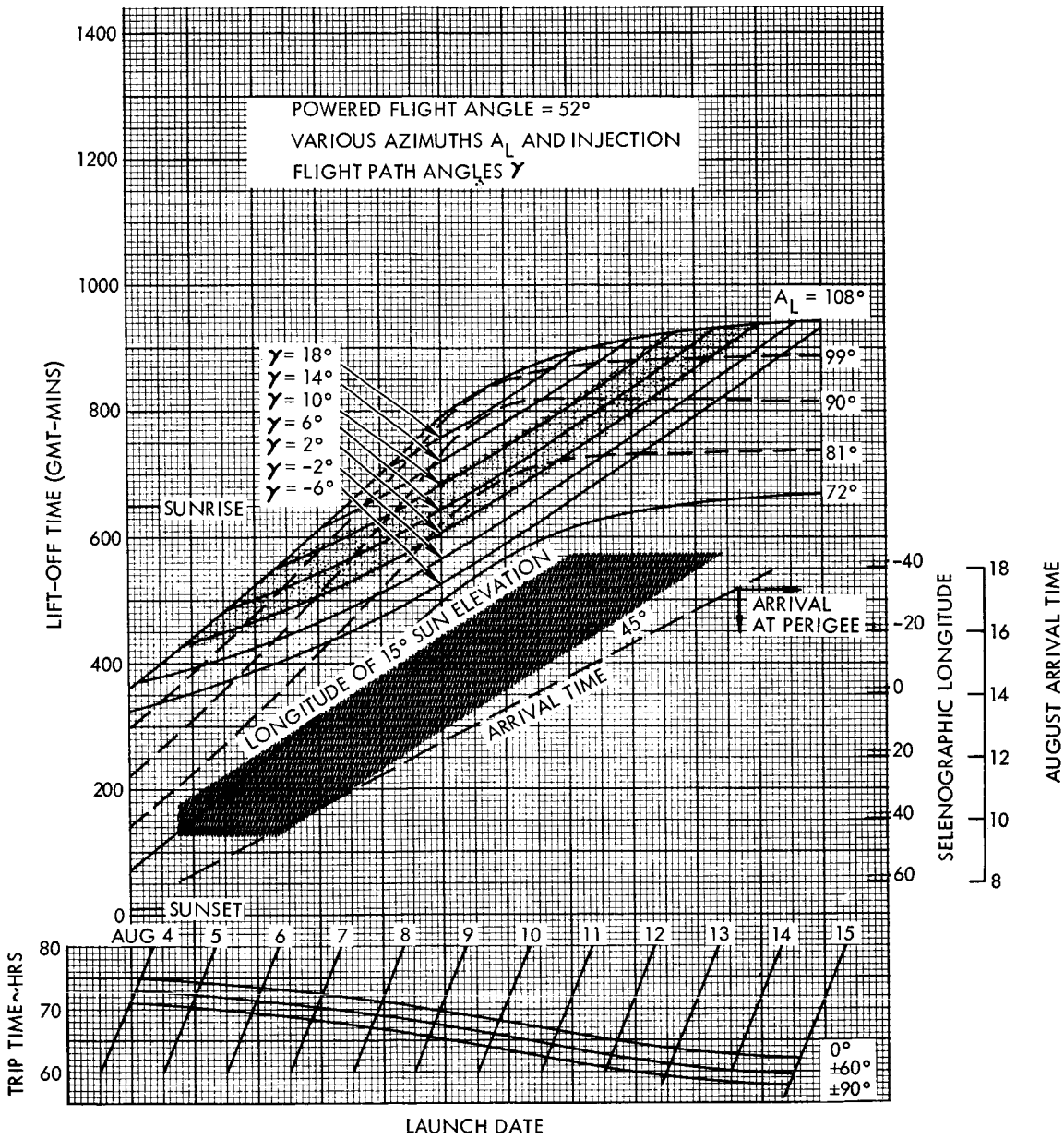

Figure 2-74. Direct Injection Launch Window August 1970

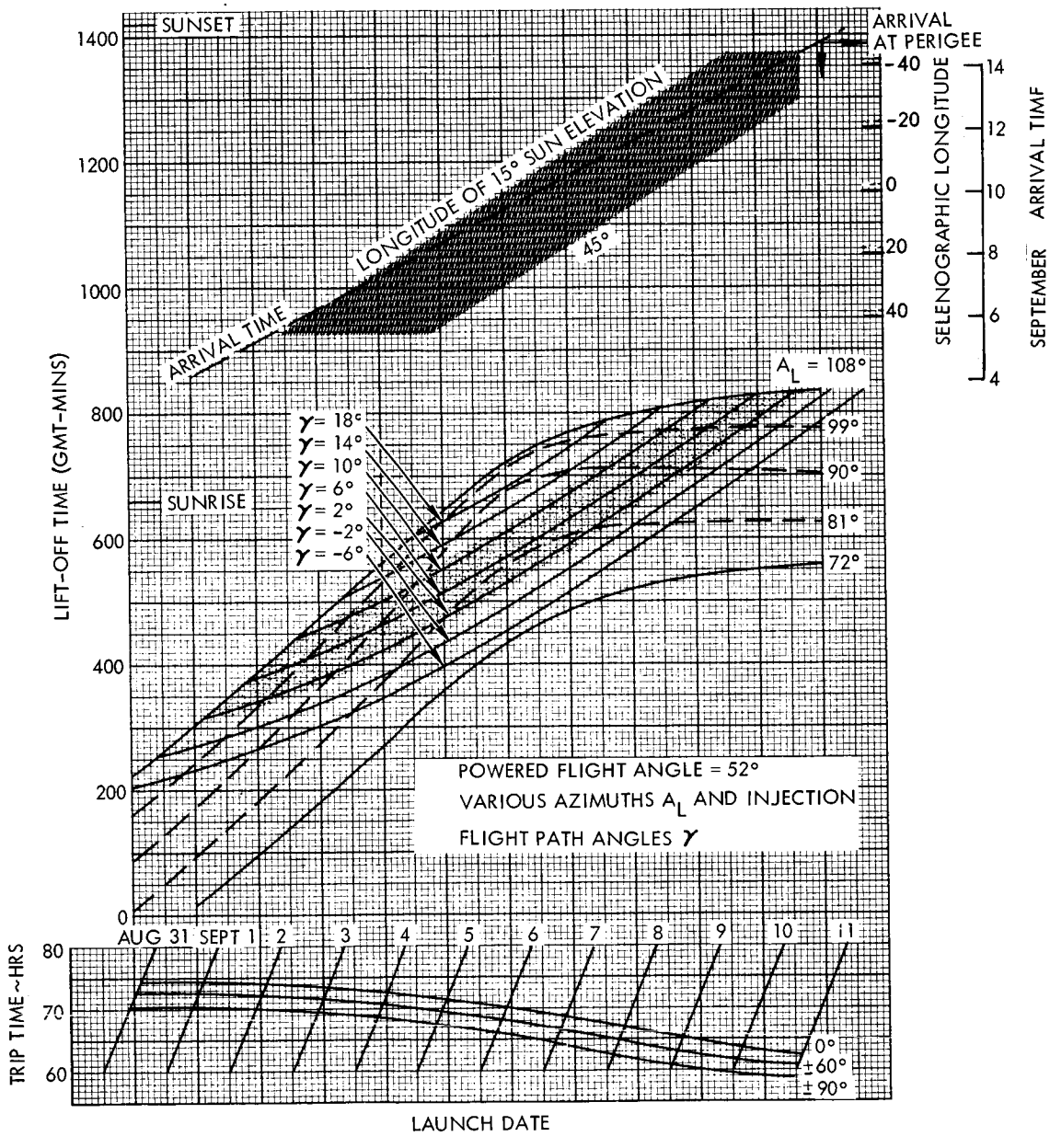

Figure 2-75. Direct Injection Launch Window September 1970

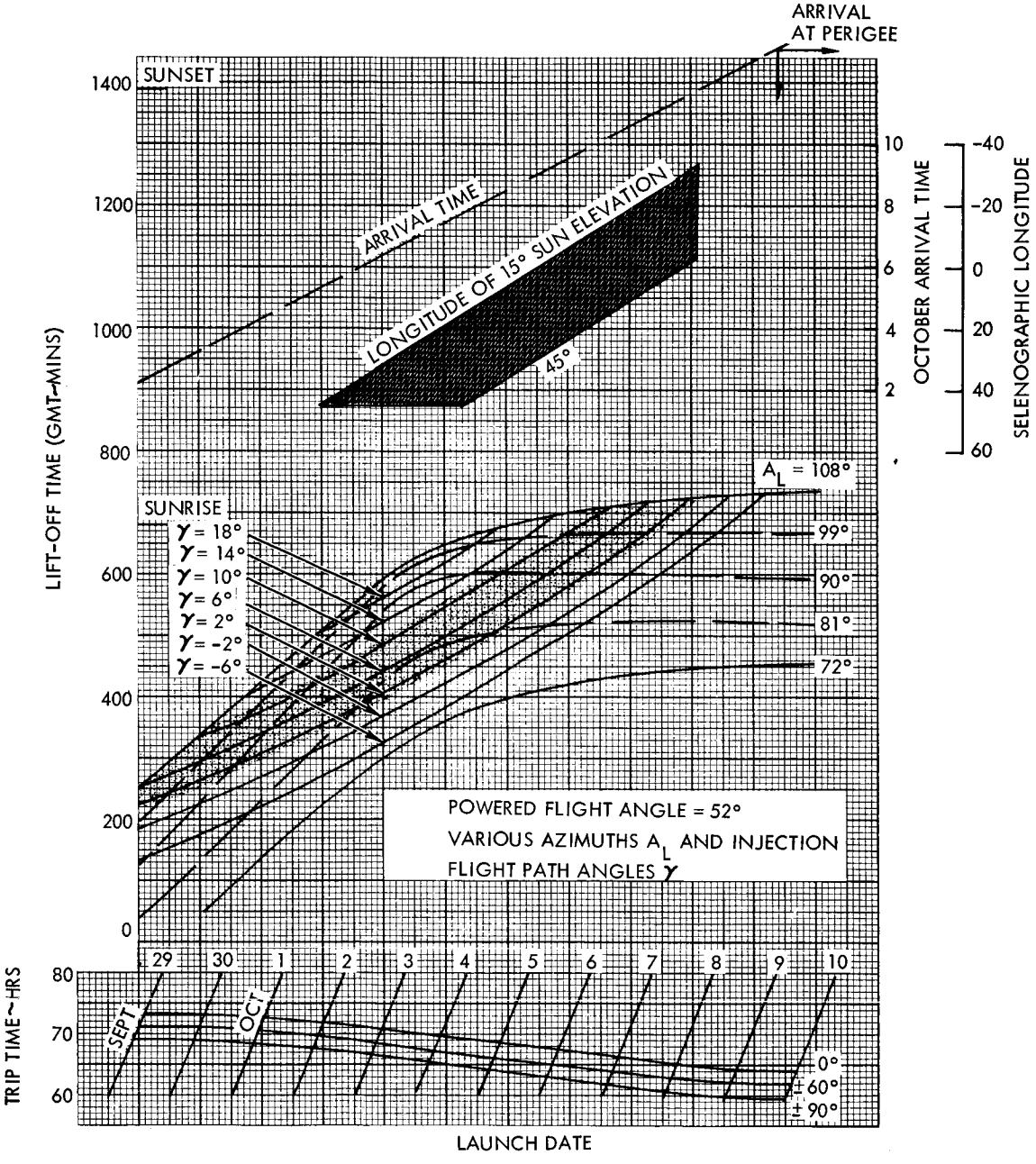

Figure 2-76. Direct Injection Launch Window October 1970

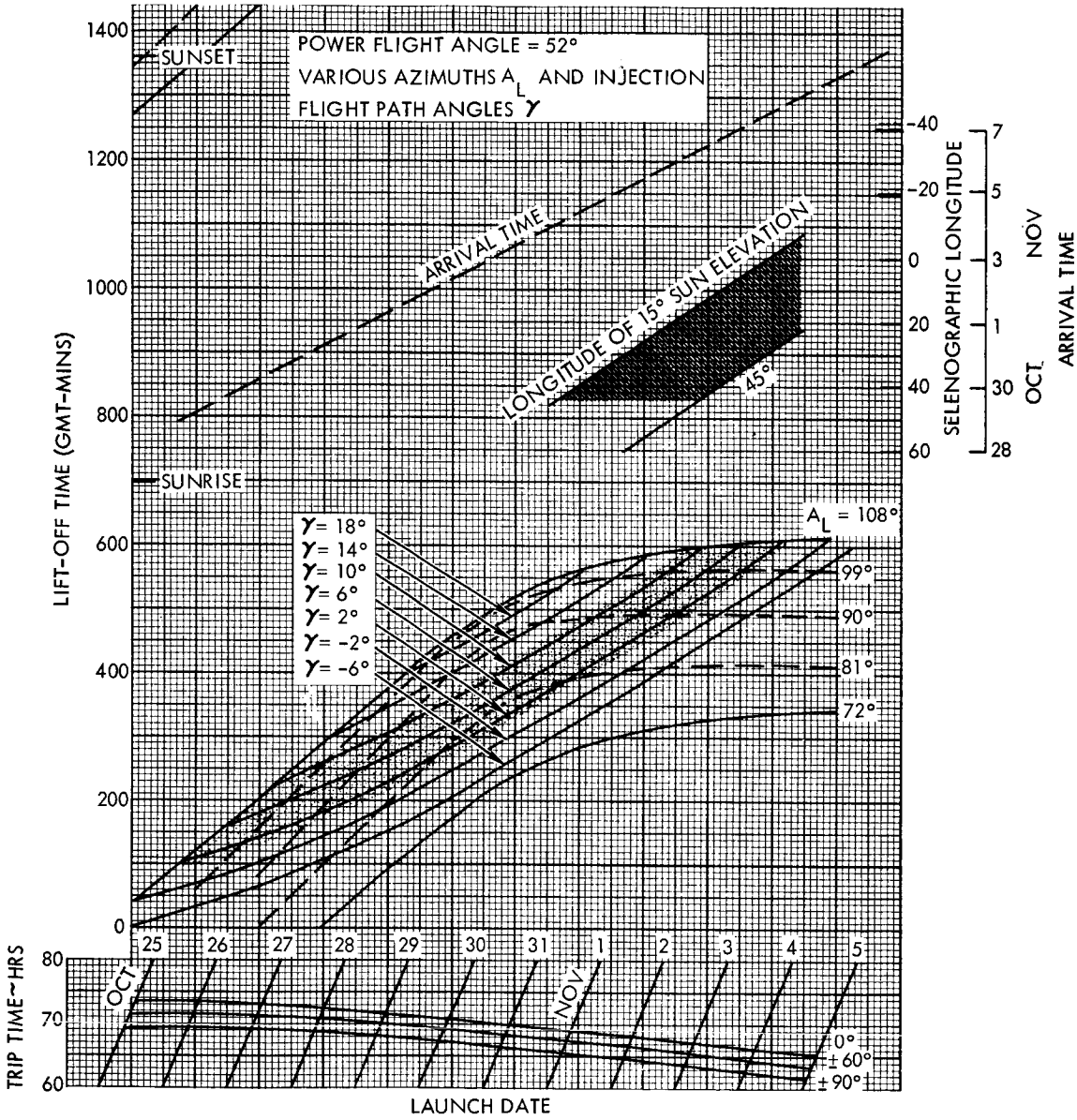

Figure 2-77. Direct Injection Launch Window October-November 1970

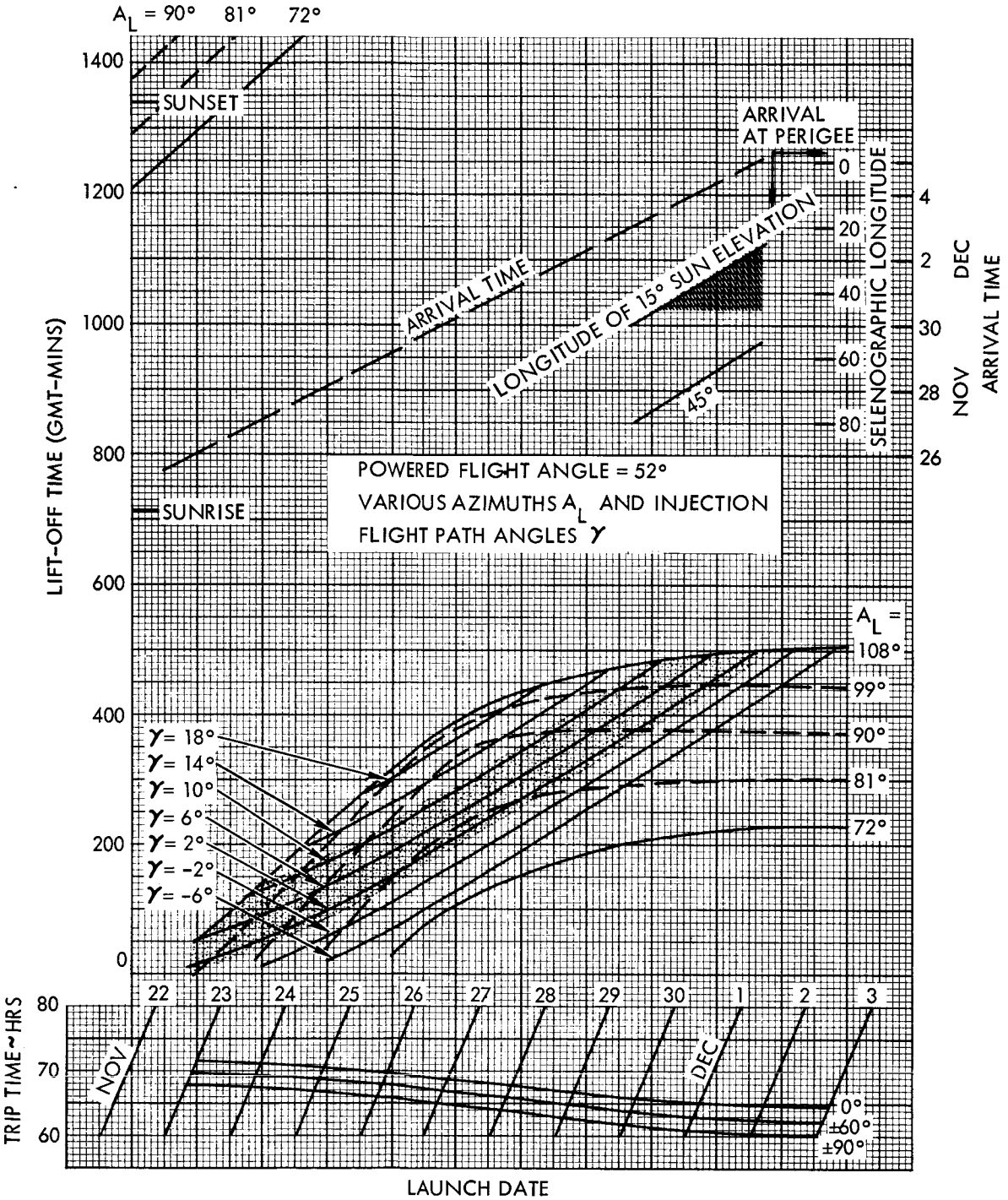

Figure 2-78. Direct Injection Launch Window
November-December 1970

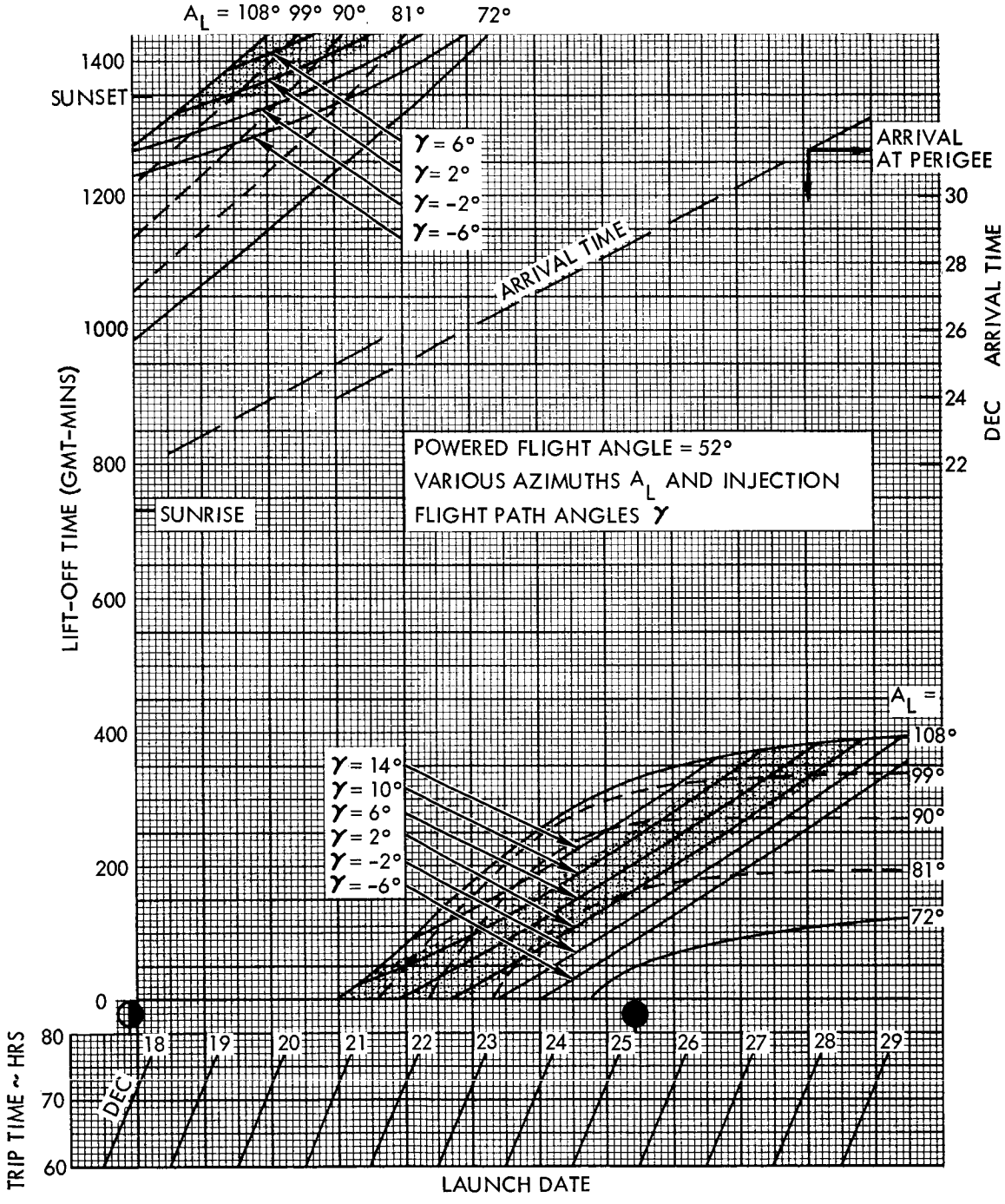

Figure 2-79. Direct Injection Launch Window December 1970

The months with good lighting are indicated by shaded blocks identical to those in Figures 2-20 to 2-22 and 2-38. Now however, the sun elevation at various sites is tied to the launch date and the flight time. This elevation may be read by projecting vertically to the selenographic site longitude of interest, which is found on the scale to the right.

In addition, all windows have an "arrival time" line which links arrival time at the moon to the launch date and flight time. Again, this feature is used by projecting vertically from the launch date-trip time combination on the abcissa to the arrival time line and then horizontally to the arrival time (date) scale on the right.

As an example of the application of these tools, consider launch on 4 July 1968* with a 64-hour outward flight time. (It is noticed that this is the flight time for a zero degree i_r free return trajectory.)

a) Assuming a γ range of 2 to 10 degrees, the window opens at 705 minutes GMT and closes at 778 for 73 minutes total launch time

b) The available landing sites within the 15 to 45 degree sun elevation constraint are -5 to 35 degrees

c) The arrival time at the moon is July 7.2 or July 7 and 5 hour GMT

d) Earth launch is in daylight

e) The launch azimuth range is about 85 to 95 degrees.

In addition to the above, a minor correction for the constant γ curves must be made for flight times other than 72 hours. This is due to the small variation of η_T with trip time as indicated by Figure 2-5. Specifically, an increment $\Delta\gamma$ must be added to the values shown on these curves to account for the variation in this angle. The corrections are given as follows:

Trip Time (hr)	60	64	68	72	76	80
$\Delta\gamma$ (deg)	-1.5	-1.0	-0.5	0	0.3	0.6

*Figure 2-46

These corrections are not shown on the figures and thus the injection flight path angles for very long (96 hour) or short (60 hour) flight times may be off by as much as 1.5 degrees. This correction can usually be ignored for general analysis. However, there is a convenient method of introducing the parameter into the launch window displays if desired. This is shown for the June 1968 window. The $\Delta\gamma$ scale at the right represents the corrections from the above table and applies to the trip times in the left hand scale. For the previous example, a 64 hour outbound trajectory was used. Thus, the γ correction is -1.0 degree and the γ values of 1 to 11 degrees read on the display are actually 0 to 10 degrees when adjusted. The correct window for 1 to 11 γ then is indicated by the 2 to 12 degrees uncorrected γ.

2.10 LUNAR SITE AVAILABILITY AND PERFORMANCE GAIN

The increased Saturn payload capability from the direct ascent injection mode instead of injection out of a parking orbit can be translated into increased LEM weight at the moon. This section describes the effect of the increased Saturn payload on LEM weight and lunar landing site availability. Comparative LEM weight contours are presented for various liftoff and continuous plane change constraints and various Saturn payload weights. Rule of thumb Saturn-to-LEM payload trade factors are also presented.

The LEM weight contours in Figures 2-80 through 2-83 are based on the following assumptions:

a) Twenty-four hour surface stay time

b) Velocity requirements correspond to a launch on 25 July 1969, two days prior to maximum negative lunar declination

c) Total midcourse velocity reserve of 1185 feet per second (370 fps outgoing and 815 fps return)

d) A CSM dry weight of 21,200 pounds

e) A LEM continuous plane change constraint of 2.25 degrees

f) A 60-hour outbound and 76-hour return trip time.

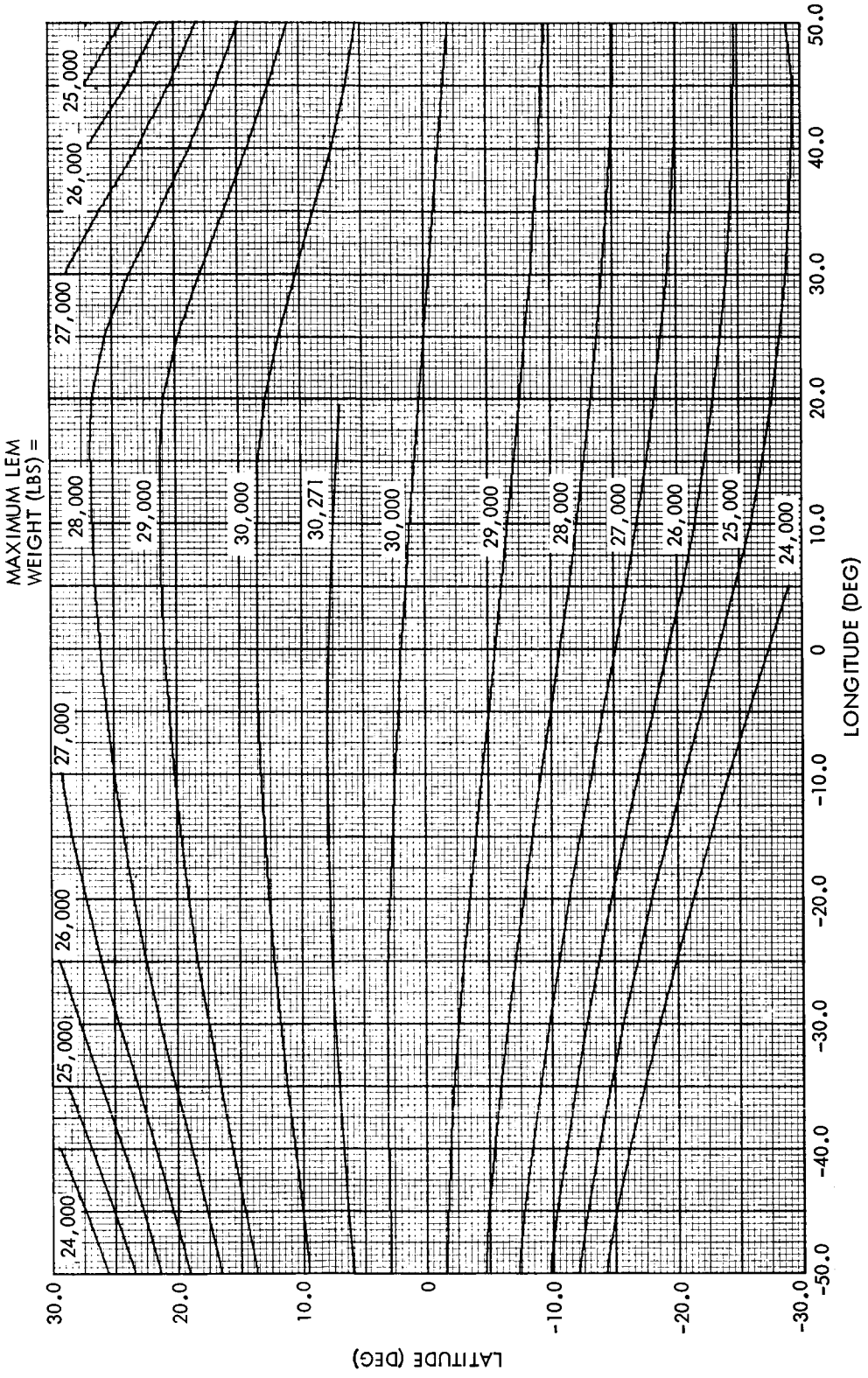

Figure 2-80. Parking Orbit Apollo Mission - 1 Day Surface Stay 86,600-lb Saturn Payload 2.25° Continuous LEM Plane Change Constraint

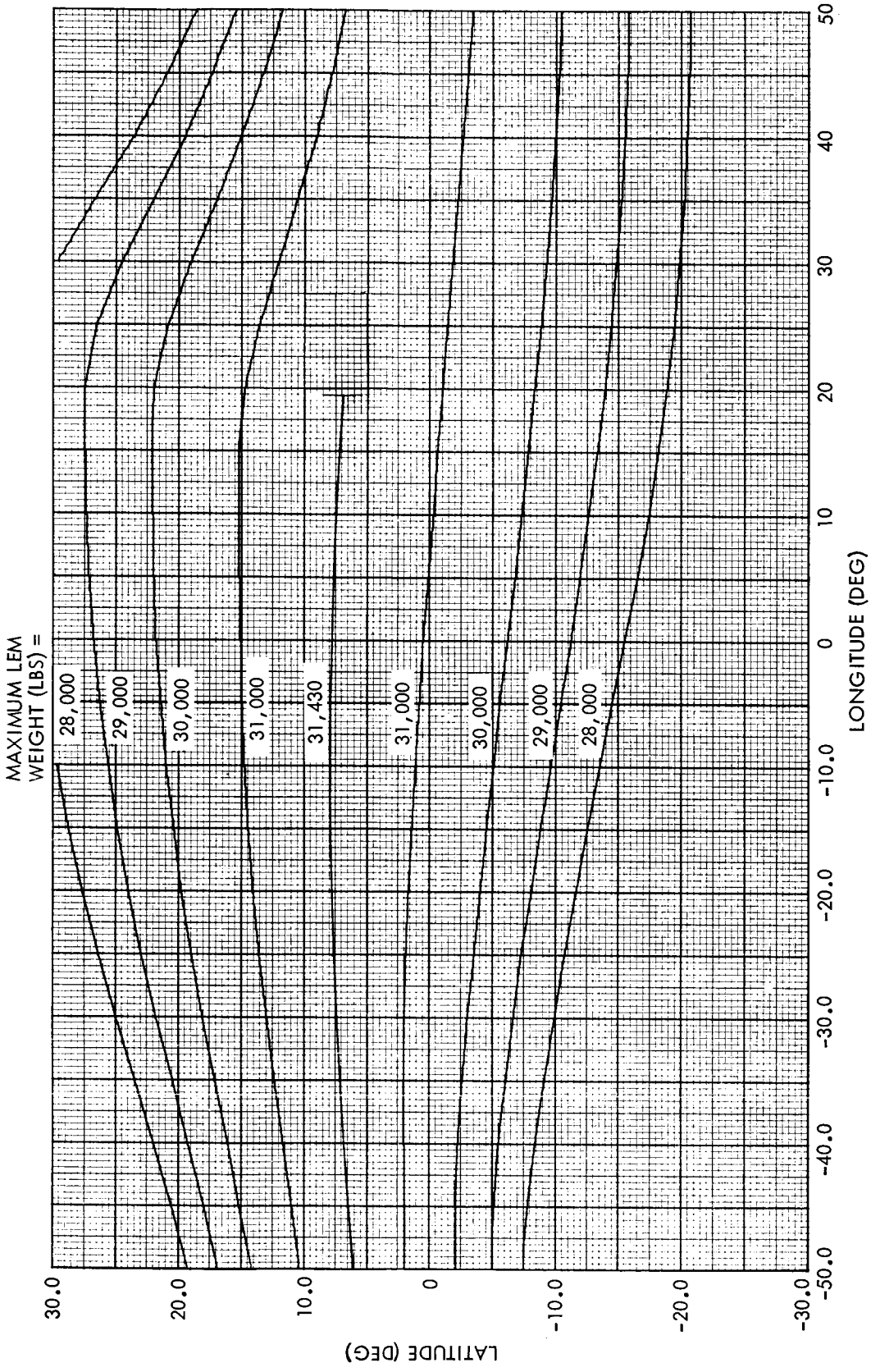

Figure 2-81. Direct Ascent Apollo Mission - 1 Day Surface Stay 88,250-lb Saturn Payload 60 Minute Launch Window 2.25° LEM Continuous Plane Change Constraint

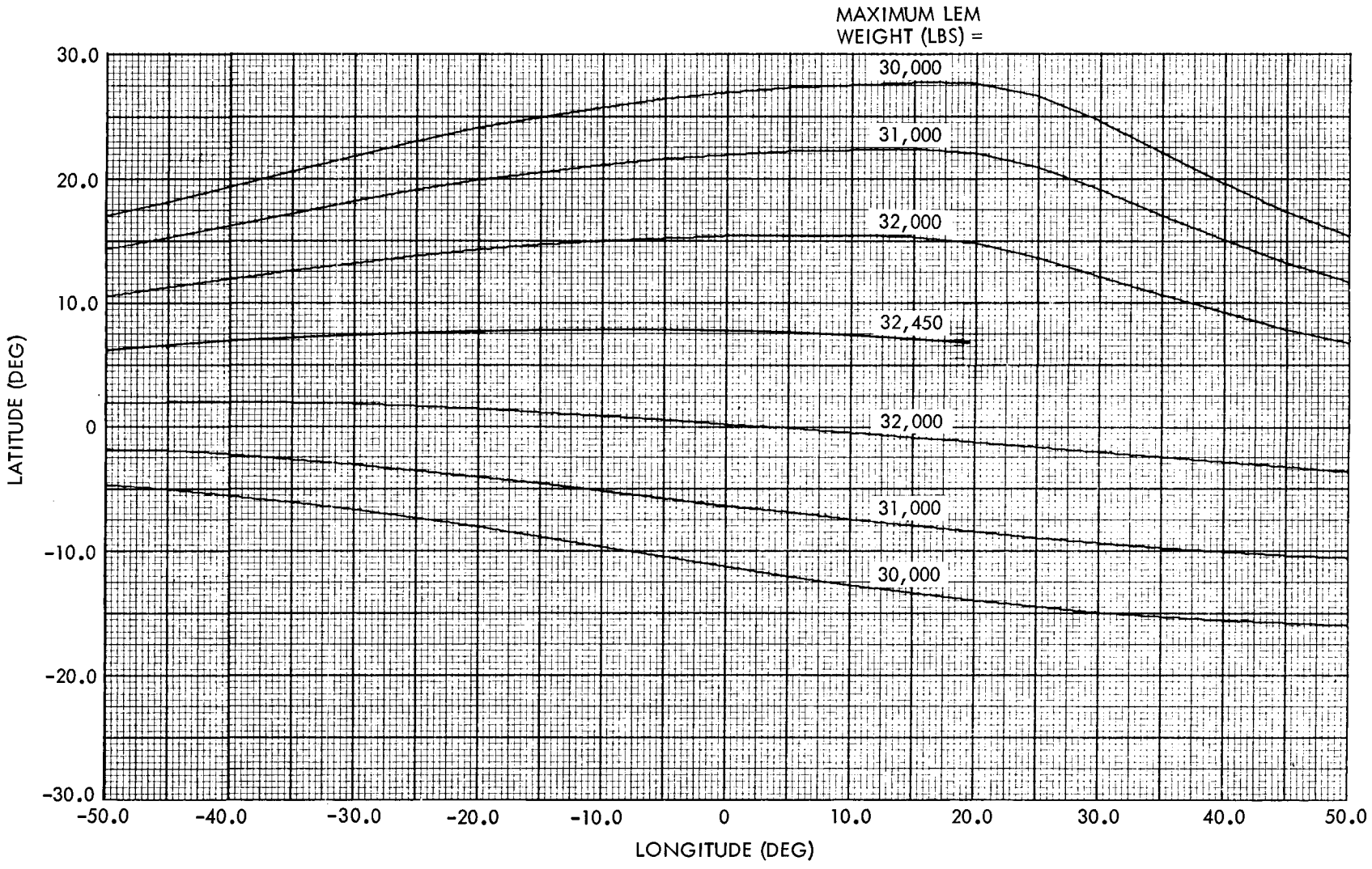

Figure 2-82. Direct Ascent Apollo Mission - 1 Day Surface Stay
89,700 Pound Saturn Payload - 30 Minute Launch Window
2.25° LEM Continuous Plane Change Constraint

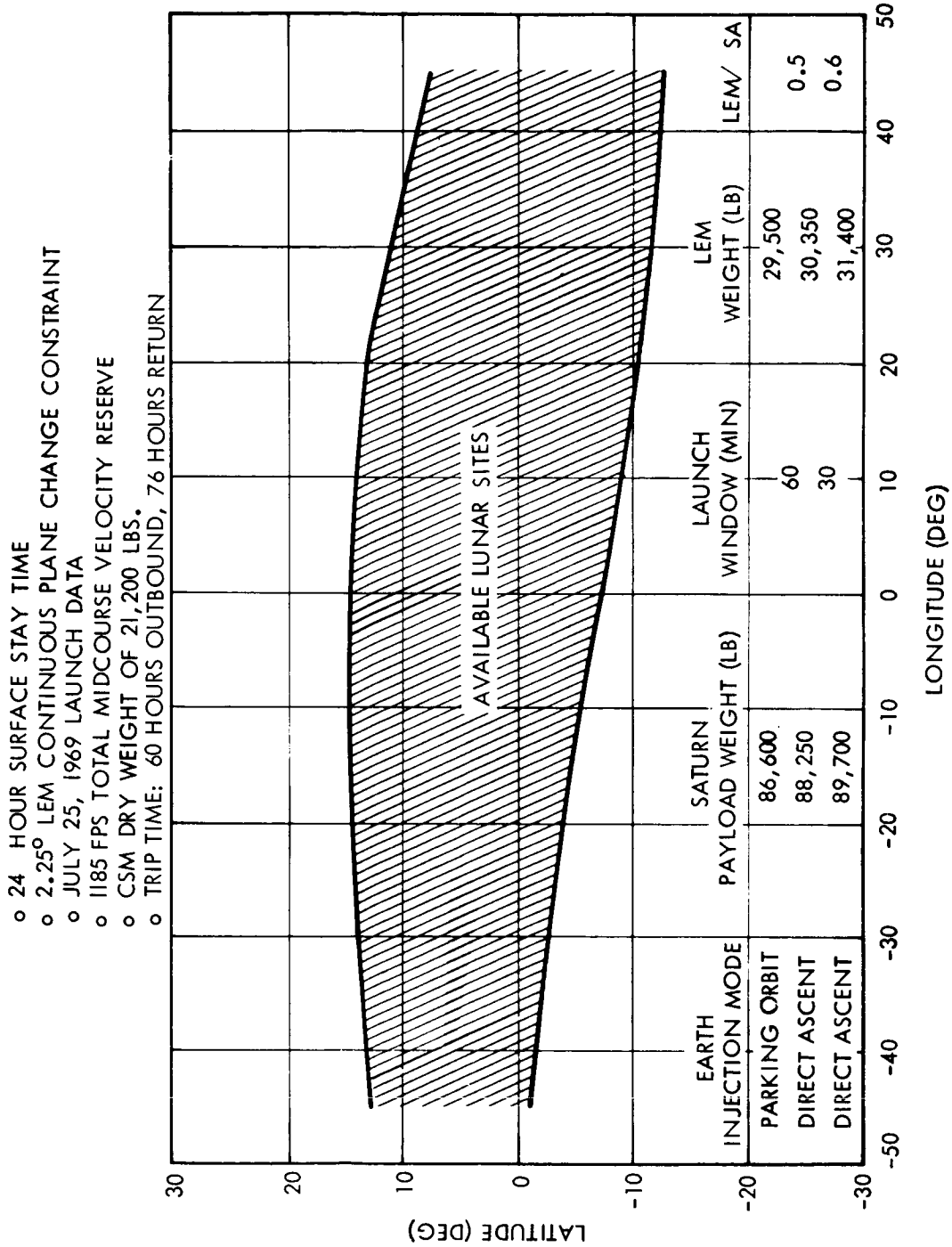

Figure 2-83. LEM Weight Comparison for the Apollo Mission

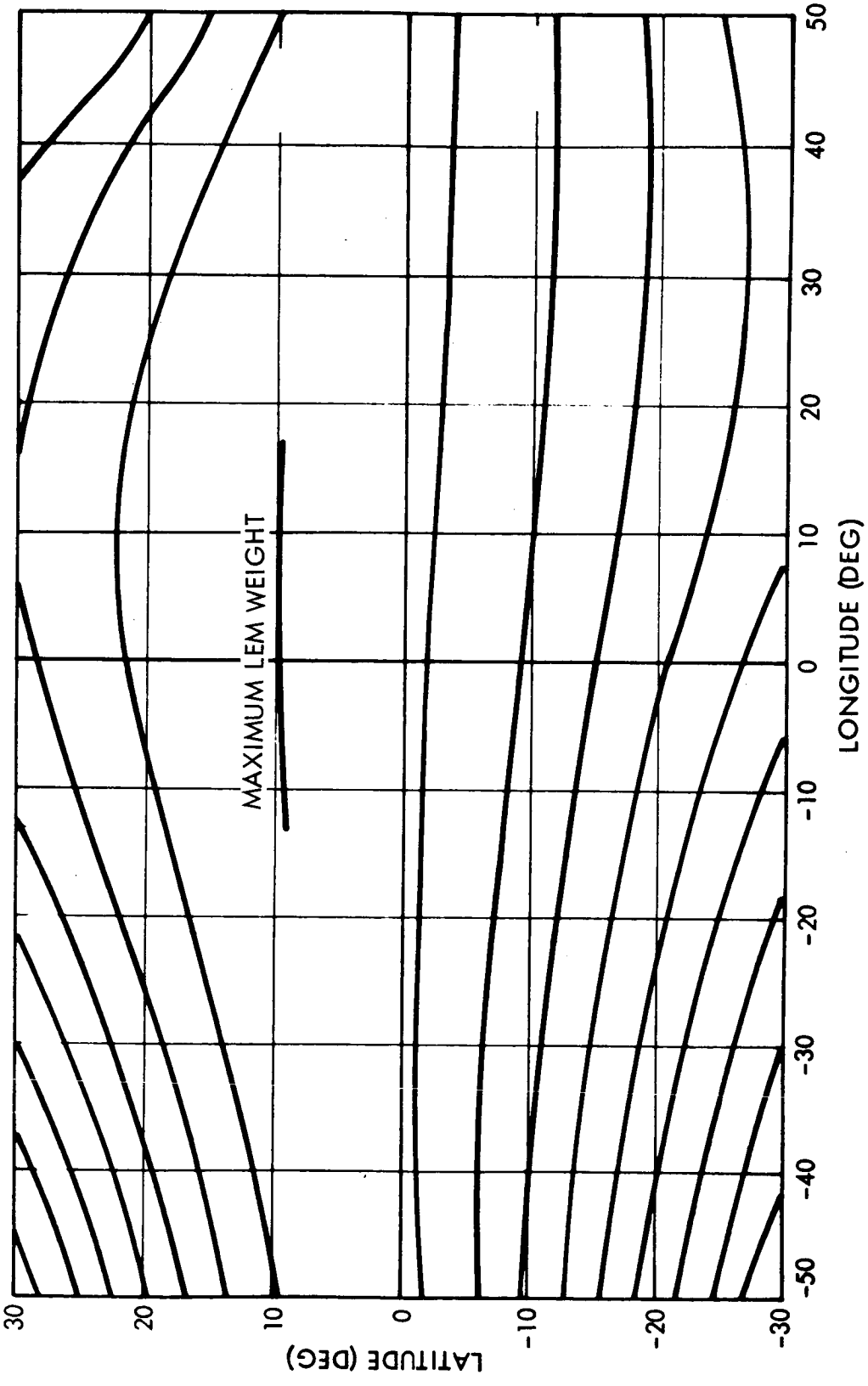

Figure 2-84. LEM Weight Contours for Translunar Trajectory Launched on July 23, 1969

The nominal Saturn payload weight for the parking orbit injection is 86,600 pounds. The resultant LEM weight contours for this injection mode are presented in Figure 2-80. Figures 2-81 and 2-82 present the LEM weight contours for the direct ascent mode with a launch window of 60 minutes, 88,250 pound Saturn payload and 30 minutes, 89,700 pound Saturn payload, respectively. As can be seen by comparing the figures, the location and shape of the contours are almost identical; only the values associated with the curves vary. All of the contours are centered about the 8 degree lunar latitude contour which represents the maximum LEM weight.

Figure 2-83 is a comparative summary curve based on Figures 2-80, 2-81, and 2-82. The cross-hatched portion of the figure represents the region of available lunar sites for the LEM weights shown. For the 60-minute direct ascent launch window, the Saturn payload is 1650 pounds larger than for the parking orbit injection mode. Of this, 850 pounds can be directly applied to increase the LEM weight, or approximately 52 percent. The corresponding numbers for the 30-minute launch window are 3100 pounds, 1900 pounds, and 61 percent. This information is summarized in Figure 2-83. A general rule of thumb which may be stated at this point is that for any given lunar site one-half the Saturn payload increase due to direct ascent may be translated into LEM weight. It should be noted at this point that the LEM weight increase is not divided into descent and ascent portions of the LEM. The determination of this information would require more detailed study beyond the scope of this report.

Although specific lunar site availability has already been discussed, nothing has been mentioned about what happens to the lunar site availability in general when direct ascent is used instead of the parking orbit injection mode. Figure 2-84, for the moon at maximum negative declination, shows the location of the LEM weight contours as being centered about the 0° longitude, 10° latitude point. This northerly location, in general, holds for all direct ascent trajectories, whereas the LEM weight contours for the parking orbit injection mode will vary in their centering between $\pm 10^{\circ}$ latitude, 0° longitude. The result of this is that if southerly lunar latitudes are desired when the moon is at its maximum negative declination a payload

penalty from the increased LEM weight due to the increased Satury payload must be incurred for the direct ascent injection mode of approximately 90 pounds per degree of lunar latitude. This penalty may be reduced somewhat by launching on another date when the moon is not at its maximum negative declination.

By using the direct ascent mode of injection for the Apollo mission, the LEM weight may be increased by approximately one-half the Saturn payload weight increase for northerly lunar landing sites (over 10° lunar latitude). For lunar sites more southerly than this a LEM weight penalty of approximately 90 pounds per degree of lunar latitude will be incurred from the LEM weight increase of one-half the Saturn payload weight increase.

3. ABORT TRAJECTORY ANALYSIS

3.1 INTRODUCTION

It is vital that a comparison between the parking orbit and direct ascent trajectory modes for the Apollo mission include an analysis of their relative capabilities for successful abort. In this regard, one of the major tasks to be performed for each mode is the examination of return opportunities should mission termination be necessary. An improvement in the overall probability of mission success may well be gained at the expense of abort success whereby a mission failure could result in a highly probable crew loss.

Abort contingencies are influenced by the number and duration of the different phases of the mission and by attendant demands on the vehicle's component systems. Conceivably, the optimal ascent path may be one which minimizes system demands by requiring the fewest "changes of state" in system operations. On the other hand, this path may require inordinate demands when going to an abort mode. Such questions are indicative of those that must be resolved in a comparative analysis.

Any comprehensive discussion of the relative advantages of the two ascent modes under consideration must follow an examination of the differences in their abort trajectories. It is then possible to determine, from these differences, relative merits for success within the range of system performance capability.

The following sections undertake the task of defining abort trajectories for the direct ascent launch and of establishing a quantitative basis for comparison. The analysis performed here does not attempt to evaluate system limitations on the problem, nor does it resolve the question of merit between the two ascent modes. It does define the abort problem within limits consistent with the scope of the contract for trajectory analysis and does attempt to uncover those areas requiring further study.

The general study of abort problems is an extensive one not only because of the multiphased character of the lunar mission, but because mission continuance depends on a vast probability network associated with the random failure of each component system and subsystem. Each failure or

sequence of failures causing mission termination will generally dictate a different set of initial state conditions for the abort mode. Thus, depending on the consequences of the malfunction and the state condition at the time of abort, the resulting return trajectory will be directed toward accomplishment of certain primary objectives. For example, it may be necessary to return in the shortest elapsed time after failure or to return using a minimum of fuel; or perhaps more than one impulse must be considered. It may be desirable, where possible, to effect a return to a predetermined landing site. The capability for fulfilling any one or all of these objectives is imposed on each phase of the mission. While a complete study of the abort problem must be accomplished, it will not be necessary for the purposes of a trajectory mode comparison. It is possible to confine the problem to an examination of only that phase of the mission in which the greatest departure in mission trajectory characteristics exists. However, even with this restriction it is necessary to limit the set of circumstances from which to postulate the initial abort conditions, and to restrict the primary objectives of the abort trajectories.

Examining the geometry and trajectory characteristics of corresponding mission phases, it is clear that the primary differences occur after orbital speeds are reached and prior to translunar injection. During liftoff and prior to reaching circular orbit velocity, both ascent modes exhibit close similarity in available abort opportunities and, to a large degree, simularity in the trajectory characteristics of resulting aborts. In addition, once lunar injection has been reached both ascent modes are again quite similar in abort capabilities. The major difference here is that the trajectory will be in a different phase relationship with any given location on the earth. The direct ascent injection will always occur in the same general area whereas the parking orbit injection may occur anywhere within a large area over either the Atlantic or Pacific Oceans. This becomes important when it is necessary to consider aborts to specific landing areas. All subsequent mission and abort phases near the moon's region are identical. In general, it can be expected that very different free-flight and abort trajectories will exist for the region preceding translunar injection, therefore

the present analysis is specifically directed toward defining the direct ascent aborts during the injection phase and in making comparisons where parking orbit data is available.

In view of the above discussion, the following set of ground rules are established.

a) The abort situation is caused by a premature termination in the S-IVB thrust during the translunar injection phase prior to nominal burnout. Time of thrust termination varies from 0 to 6 minutes prior to nominal burnout.

b) Only single velocity impulse aborts are considered.

c) Possible aborts occur during the interval of time between S-IVB engine cutoff and the apogee of the resulting coast ellipse.

d) Possible aborts are restricted to lie in the plane of the coast ellipse, except when it is desirable to land at a specific site.

e) Reentry conditions are characterized by a flight path angle of 96.4 degrees at an altitude of 400,000 feet

3.2 ABORT GEOMETRY

As a condition of this study only that portion of the pre-abort trajectories* lying outside the moon's sphere of influence are considered. The only gravitational attraction is that of the earth, approximated by an inverse square force field. Within this region the free-flight portions of all pre-abort and abort trajectories are conic sections. All abort trajectories generated herein are contrived to enter the earth's atmosphere at a single inertial flight path angle, β_r, of 96.4 degrees from the local vertical and at a common reentry altitude of 400,000 feet. The feasibility of this choice of reentry angle for all values of abort reentry velocity between

*A "pre-abort" trajectory is the free-flight trajectory occurring immediately after S-IVB engine cutoff and prior to the abort injection. This may also be referred to as the coast trajectory.

26,000 and 40,000 fps was examined in conjunction with other studies and found to be valid. Such a choice is entirely satisfactory from a dynamical standpoint, representing a median value between the skip and the maximum deceleration boundaries for reentry maneuver angles from 20 to 83 degrees. It was also determined that a variation in this nominal value of ±1 degree has very little effect on reentry position and on the abort trajectory configuration produced, particularly for abort initiated at the greater distances.

Examining the geometry for an abort point along the outbound pre-abort trajectory, Figure 3-1 indicates four single impulse abort paths that are possible. The solid lines indicate abort conics in the posigrade sense, one directed away from the earth and requiring passage of an apogee point, the other directed toward the earth. The dashed portions of the same conic represent the mirror image solution in the retrograde sense. All four solutions are in the plane of the pre-abort trajectory and have the same post-abort velocity as well as the same return inclination with the earth's equator. The abort velocity increment, ΔV_{ABORT}, however, is generally different, unless the abort occurs at apogee as shown in Figure 3-1.

For each of the posigrade solutions (ignoring for the present the retrograde returns), two abort possibilities exist for a given arbitrary inclination. Figure 3-2(a) indicates this phenomenon. One plane contains an abort directed toward the earth's equator and is characterized by abort azimuths of less than 90 degrees. The other plane contains an abort directed away from the equator which has an abort azimuth greater than 90 degrees. Therefore, any abort trajectory of specified inclination different from the pre-abort trajectory has two possible trajectory planes, each of which contains aborts of the apogee passage or the direct descent type. Table 3-1 summarizes the possible posigrade aborts.

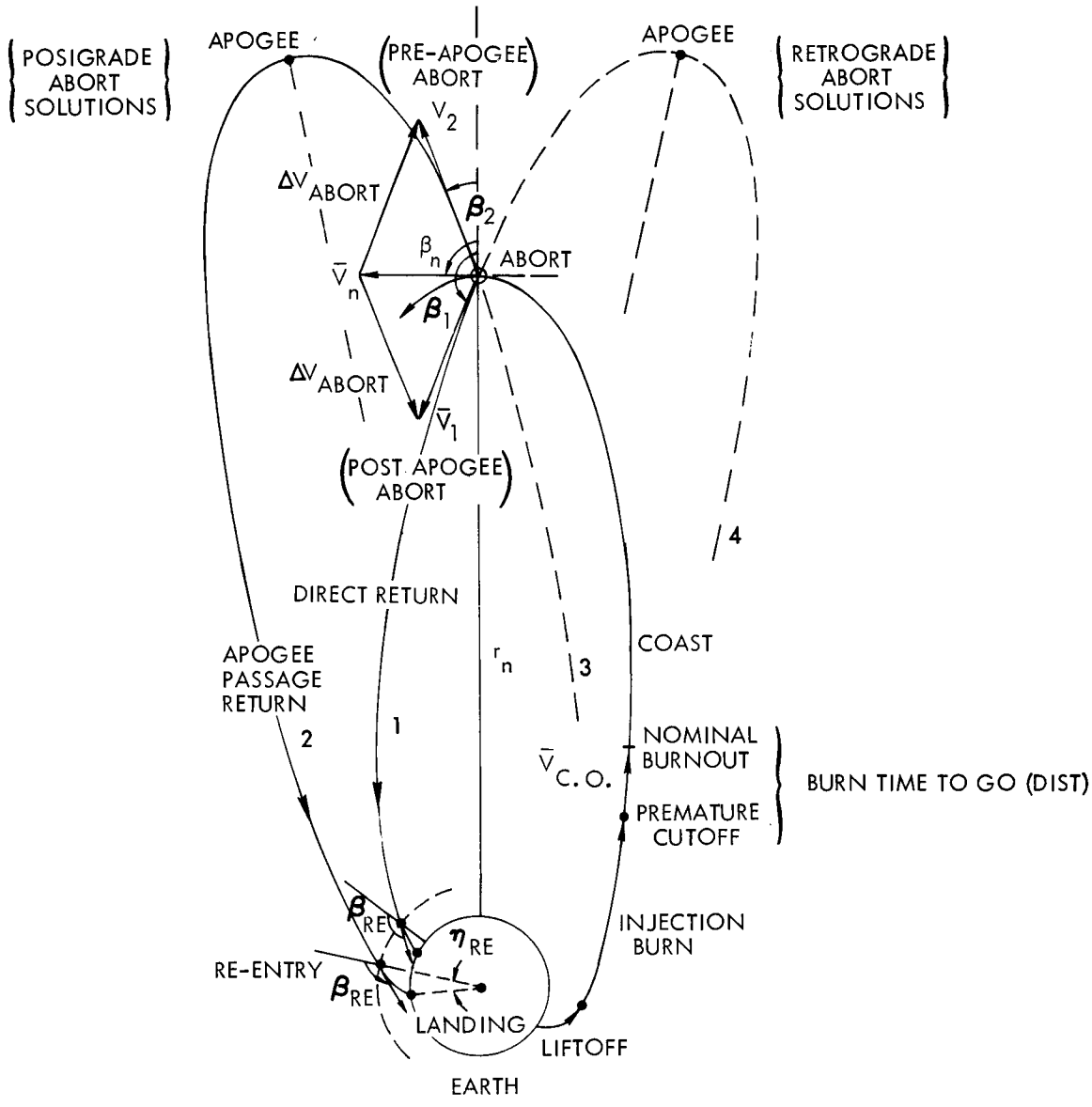

Figure 3-1. Abort Point Geometry for Planar Aborts

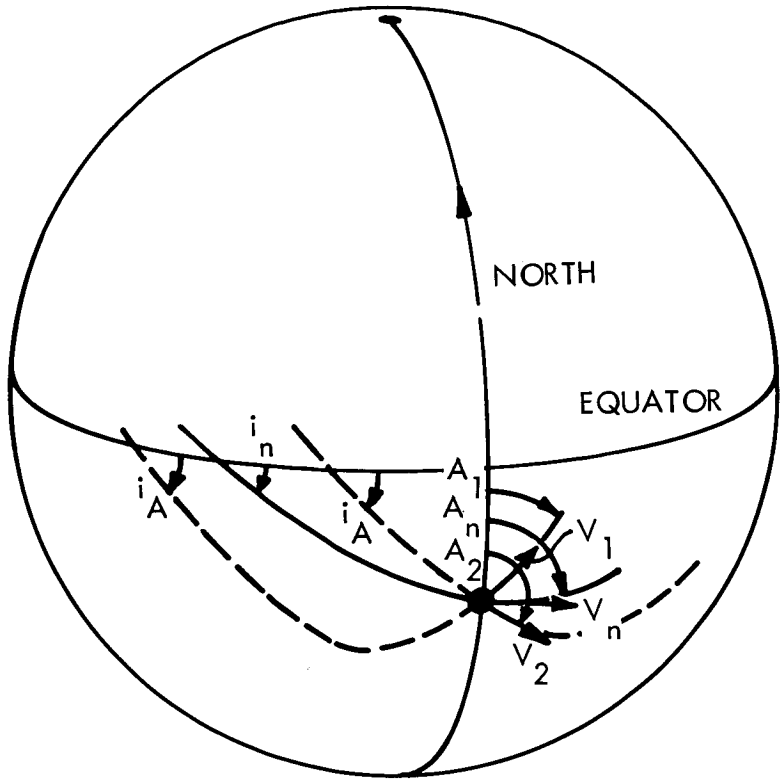

(a) For Arbitrary Inclinations

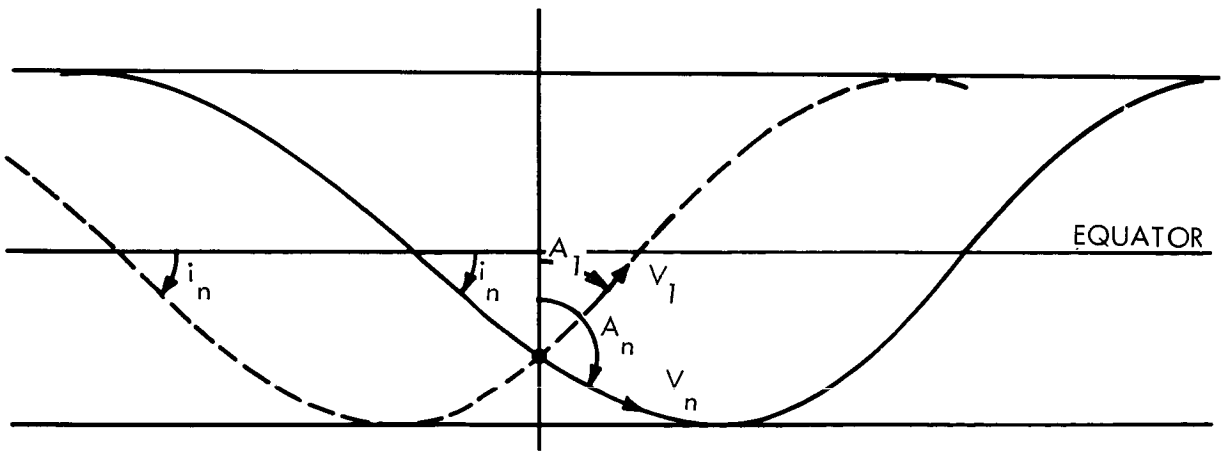

(b) For Inclination Equal to That of the Pre-Abort Trajectory

Figure 3-2. Out-of-Plane Abort Geometry

Table 3-1. Possible Posigrade Aborts

Type of Abort			Abort Velocity Direction
In-Plane	Apogee Passage		In-Plane, Away from Earth
	Direct Descent		In-Plane, Toward the Earth
Fixed Inclination	Toward Equator	Apogee Passage	Toward Equator, Away from Earth
		Direct Descent	Toward Equator, Toward Earth
	Away from Equator	Apogee Passage	Away from Equator, Away from Earth
		Direct Descent	Away from Equator, Toward Earth

It should be noted that for a return inclination equal to that of the pre-abort trajectory, one abort possibility will exist in-plane and one out-of-plane [Figure 3-2(b)]. If, in addition, the spacecraft is at a maximum or minimum declination in the pre-abort trajectory (A_n = 90 degrees), no out-of-plane aborts will exist without a change in inclination.

Upon closer considerations of Figure 3-1, it is evident that the post-abort* velocity vectors are contained within a cone of central angle 2β generated by rotating the velocity vector about the radius vector, r. If the magnitude of the post-abort velocity is plotted as a function of β, as in Figure 3-3, it is evident that it has the smallest magnitude at β = 90 degrees corresponding to the apogee point of the resultant abort conic. That this 90-degree point is an apogee and not a perigee point is evident from the fact that each abort trajectory must satisfy reentry conditions for the shorter radius of 400,000 feet. In addition, if the abort is initiated at the apogee of the pre-abort trajectory, the required ΔV_{ABORT} will also have the smallest magnitude.

*Post-abort refers to the characteristics after the application of the abort velocity increment, ΔV_{ABORT}.

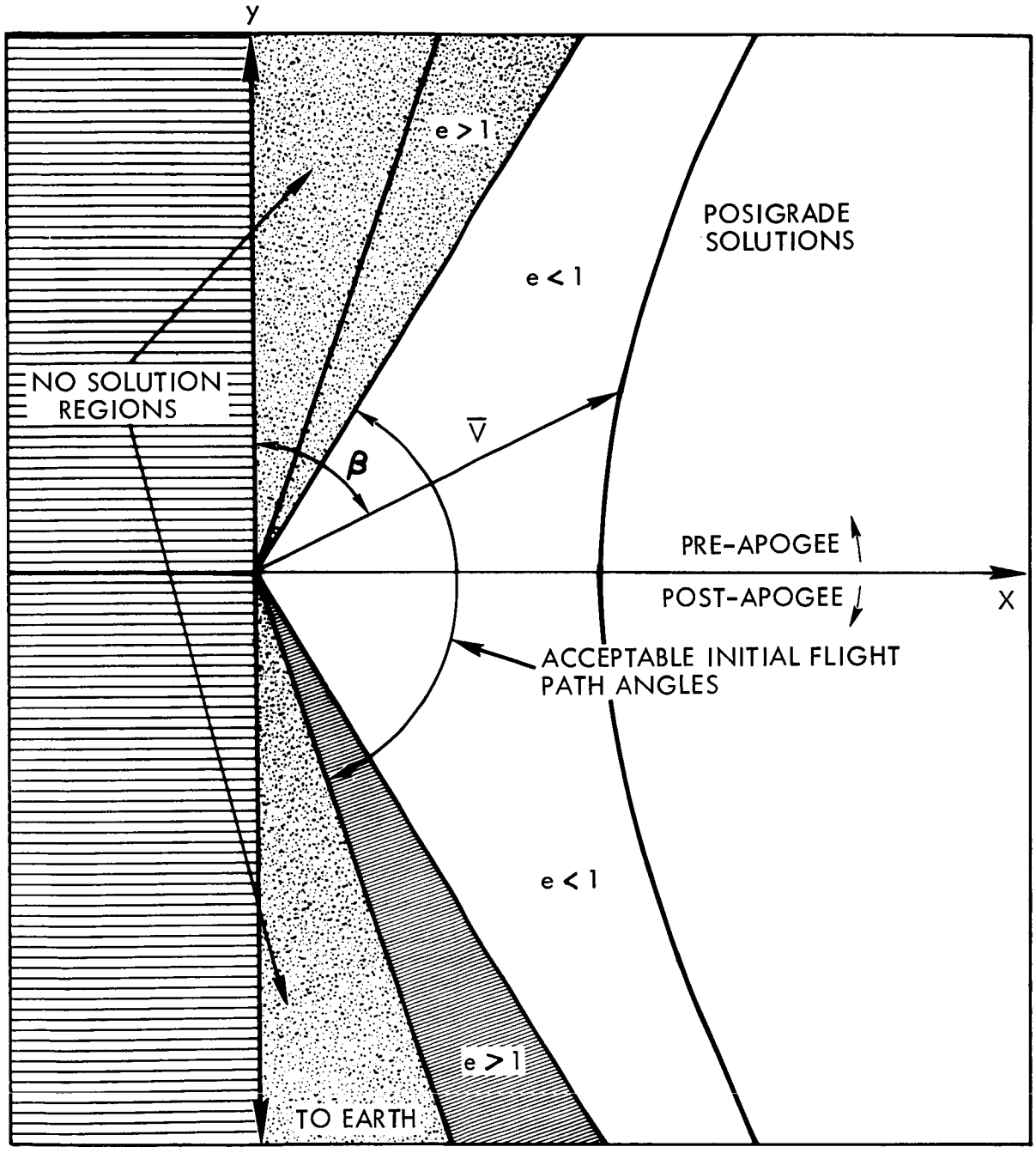

Figure 3-3. Schematic of Possible Abort Conic Flight Path Angles and Velocities

Figure 3-3 indicates that as β departs the 90-degree point, the post-abort velocity increases until the conic becomes hyperbolic (eccentricity, $e > 1.0$). In this region, aborts heading away from the earth will not return and only those heading toward the earth admit an acceptable solution. Finally, a value of β is reached where those aborts heading towards the earth fail to yield satisfactory trajectories. The foregoing restrictions on the post-abort flight path angle are imposed primarily by the conditions of a fixed reentry angle. There are, however, further restrictions in the actual determination of abort trajectories. These are imposed by physical considerations derived from the particular pre-abort trajectory, the abort velocity impulse available and specific return objectives, such as landing at a given site.

In regard to the number of possible solutions for any given magnitude of the abort velocity impulse, reference is made to Figure 3-4. Here, the locus of the post-abort velocity vector, $\overline{V}$, that will produce return trajectories meeting the required reentry conditions is shown as a dashed line, which is similar in shape to the hyperbola of Figure 3-3, as are the corresponding restricted regions. For the in-plane cases, the abort velocity increment, ΔV_{ABORT}, is added to the pre-abort velocity vector, $\overline{V}_n$, in various directions within the circle. The intersection of this circle with the hyperbolic locus of solutions represents the points at which the given ΔV_{ABORT} produces the required abort trajectory. Figure 3-4 again indicates that, in general, there will be two solutions. The magnitude and directions of the pre-abort $\overline{V}_n$ and ΔV_{ABORT} vectors may occur in such a manner as to yield either two solutions away from the earth (apogee passage) or two solutions toward the earth (direct descent), or one of each type. In fact, there may be as many as four solutions from the intersection of the circle and the hyperbola; however, this has not been observed in the course of the abort analysis. Also, should the condition be reached where the ΔV_{ABORT} circle becomes tangent to a segment of the hyperbola, only one analytic solution will actually exist. However in this situation, small variations of the ΔV_{ABORT} direction may admit other solutions within the allowed computational tolerance as shown in Figure 3-5.

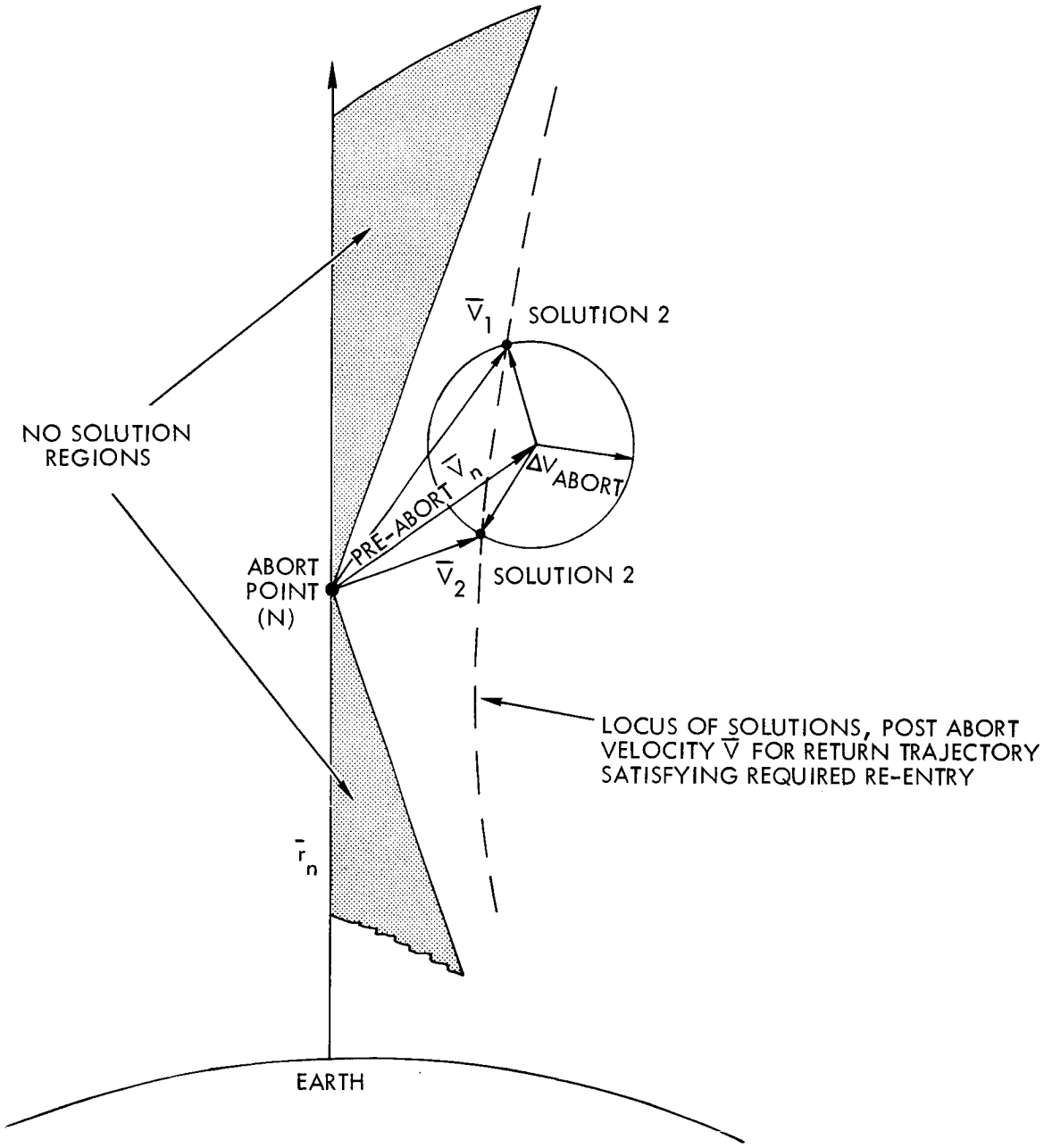

Figure 3-4. Permissible Vector Additions of the Abort Velocity Impulse ΔV_{ABORT} to the Pre-Abort Velocity Vector, $\overline{V}_n$

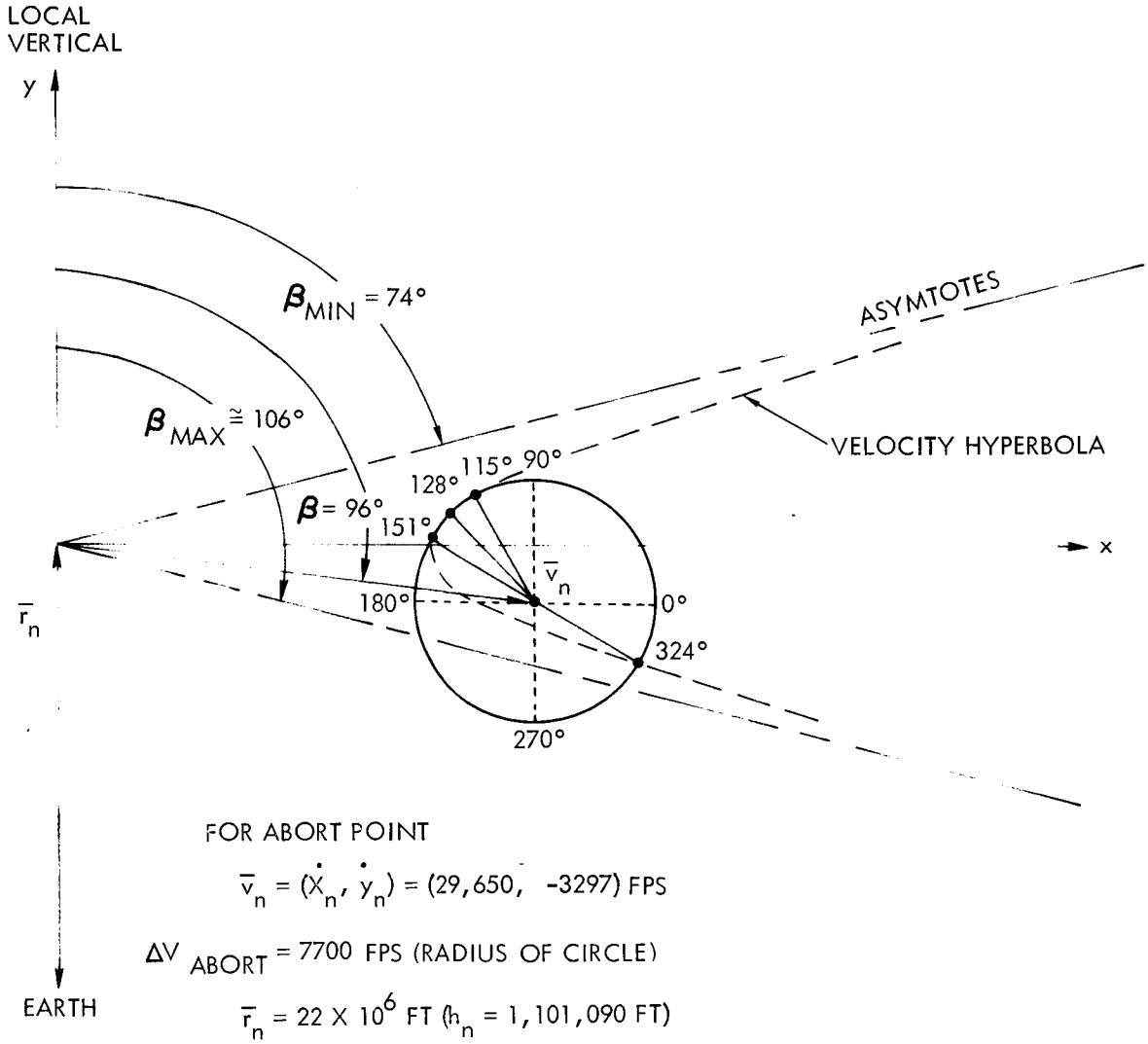

FOR ABORT POINT

$\bar{v}_n = (\dot{X}_n, \dot{y}_n) = (29,650, -3297)$ FPS

$\Delta V_{ABORT} = 7700$ FPS (RADIUS OF CIRCLE)

$\bar{r}_n = 22 \times 10^6$ FT ($h_n = 1,101,090$ FT)

Figure 3-5. Comparative Example of Planar Abort Velocity Solutions from Analytic Abort Trajectory Program

This result, in a physical interpretation, would be very favorable from the guidance standpoint, indicating that the reentry conditions are nearly insensitive to small errors in the ΔV_{ABORT} direction. This figure has been drawn for a computed abort situation; the broken lines represent the asymptotes of the hyperbola with the corresponding range of flight path angles shown.

3.3 PRE-ABORT TRAJECTORY CHARACTERISTICS

Before investigating actual abort trajectories, it is necessary to determine the characteristics of the pre-abort or free-flight trajectories resulting from premature termination of S-IVB thrust during the translunar injection. Initial efforts toward defining these characteristics made use of the powered flight data supplied by NASA/MSC which represented the typical performance of the S-IVB stage through an expected range of injection angles for a 72-hour direct ascent mission. This data was fitted to a representative 72-hour trajectory launched on January 23, 1968 using STL's analytic lunar program. From the results of this program the pre-abort trajectory data shown in Figures 3-6 through 3-14 were derived. For generating the actual abort trajectories, a more general basis, independent of a specified launch date and offering a greater range in the launch variables, was adopted. The results obtained for the specific launch date, however, remain applicable, representing a specific case in the variation of launch azimuth and injection angle over the range of the generalized study. The relationship between launch azimuth and injection angle is shown in Figure 3-6 for January 23, 1968. A more detailed discussion of launch phenomena was presented in Section 2. Table 3-2 presents the powered flight data received from NASA/MSC which serves as the basis for this study.

The variation in the size of the pre-abort trajectories with changing S-IVB burn-time-to-go covers a large range. This is readily evident in the variation of the semi-major axis and the eccentricity shown in Figure 3-7. It is important to note the effect of the last few seconds of burning on the increase in semi-major axis. In addition, note the dip in the eccentricity to near circular orbit values during the earliest cutoff interval with an attendant spread in the argument of pergee. The latter of these two areas provides an interesting aspect to the

Table 3-2. Summary of NASA/MSC Powered Flight Data

Nominal Injection Angle β_I (deg)	Selected Times-To-Go(1) Δt_{GO} (sec)	Time From Liftoff(2) $\Delta t_{c.o.}$ (hr)	S-IVB Burn Period ΔT_{BURN} (sec)	Powered Flight Angle θ_{PF} (deg)	Geocentric Radius at Cutoff $r_{c.o.}$ (10^6 ft)	Velocity at Cutoff $V_{c.o.}$ (fps)	Flight Path Angle at Cutoff $\beta_{c.o.}$ (deg)	Altitude at Cutoff $h_{c.o.}$ (ft)	Azimuth at Cutoff(2) $A_{c.o.}$ (deg)
80	0	0.28785	1036.2440	51.41	22.40380	35,175.56(2)	80.000	1,504,899	111.08
	15	0.28286	1018.2875	49.83	22.29904	34,409.61	80.691	1,400,131	110.54
	30	0.27869	1003.2875	48.53	22.21876	33,796.47	81.249	1,319,852	110.08
	60	0.27036	973.2875	45.98	22.07634	32,652.46	82.311	1,177,430	109.14
	120	0.25369	913.2875	41.07	21.85425	30,629.42	84.211	955,344	107.19
	180	0.23702	853.2875	36.39	21.69945	28,874.40	85.796	800,549	105.19
	240	0.22036	793.2875	31.94	21.59502	27,320.64	87.053	696,111	103.16
	300	0.20369	733.2875	27.70	21.52645	25,926.04	87.976	627,543	101.12
	360	0.18702	673.2875	23.66	21.48123	24,663.43	88.555	582,321	99.10
82	0	0.28783	1036.1740	51.83	22.10470	35,417.08(2)	82.000	1,205,798	110.36
	15	0.28284	1018.2182	50.22	22.02052	34,651.89	82.618	1,121,618	109.77
	30	0.27867	1003.2182	48.88	21.95657	34,038.46	83.116	1,057,660	109.27
	60	0.27034	973.2182	46.27	21.84453	32,889.76	84.060	945,627	108.25
	120	0.25367	913.2182	41.26	21.67505	30,845.48	85.731	776,148	106.15
	180	0.23701	853.2182	36.51	21.56344	29,059.88	87.107	664,534	104.02
	240	0.22034	793.2182	32.00	21.49433	27,471.74	88.179	595,424	101.87
	300	0.20367	733.2182	27.72	21.45464	26,042.63	88.941	555,731	99.72
	360	0.18701	673.2182	23.65	21.43307	24,747.67	89.387	534,169	97.61
84	0	0.28781	1036.1330	52.19	21.80590	35,662.02(2)	84.060	906,999	109.59
	15	0.28283	1018.1732	50.53	21.74339	34,895.99	84.613	844,481	108.95
	30	0.27866	1003.1732	49.17	21.69668	34,280.50	85.055	797,774	108.40
	60	0.27033	973.1732	46.50	21.61690	33,124.60	85.885	717,997	107.29
	120	0.10439	913.1732	41.40	21.50357	31,056.61	87.328	604,664	105.03
	180	0.23699	853.1732	36.58	21.43809	29,239.29	88.484	539,185	102.74
	240	0.22033	793.1732	32.02	21.40648	27,615.61	89.352	507,573	100.46
	300	0.20366	733.1732	27.70	21.39700	26,150.40	89.932	498,098	98.21
	315	0.19949	718.1732	26.66	21.39689	25,806.02	90.032	497,985	97.66
	330	0.19533	703.1732	25.63	21.39739	25,469.84	90.114	498,482	97.11
	345	0.19116	688.1732	24.61	21.39836	25,141.62	90.177	499,455	96.56
	360	0.18699	673.1732	23.61	21.39968	24,821.15	90.222	500,769	96.01
86	0	0.28782	1036.1480	52.16	21.60690	35,828.32(2)	86.000	707,998	108.88
	15	0.28283	1018.1906	50.47	21.56521	35,053.10	86.484	666,300	108.18
	30	0.27866	1003.1906	49.09	21.53499	34,429.94	86.867	636,088	107.60
	60	0.27033	973.1906	46.39	21.48585	33,258.44	87.575	586,944	106.41
	120	0.25366	913.1906	41.23	21.42483	31,158.09	88.767	525,922	104.02
	180	0.23700	853.1906	36.38	21.40071	29,307.37	89.670	501,802	101.62
	240	0.22033	793.1906	31.81	21.40080	27,650.25	90.297	501,898	99.24
	300	0.20366	733.1906	27.49	21.41478	26,152.93	90.654	515,872	96.91
	315	0.19950	718.1906	26.45	21.41940	25,800.90	90.703	520,498	96.34
	330	0.19533	703.1906	25.42	21.42423	25,457.28	90.735	525,329	95.78
	345	0.19116	688.1906	24.41	21.42916	25,121.83	90.750	530,252	95.21
	360	0.18700	673.1906	23.41	21.43406	24,794.37	90.748	535,156	94.65
88	0	0.28784	1036.2170	51.85	21.45690	35,955.28(2)	88.000	557,999	108.09
	15	0.28285	1018.2637	50.14	21.43694	35,162.23	88.413	538,038	107.35
	30	0.27868	1003.2637	48.75	21.42394	34,525.33	88.734	525,037	106.72
	60	0.27035	973.2637	46.02	21.40670	33,328.76	89.314	507,793	105.47
	120	0.25368	913.2637	40.85	21.39975	31,185.38	90.233	500,849	102.95
	180	0.23702	853.2637	35.99	21.41759	29,297.86	90.853	518,687	100.44
	240	0.22035	793.2637	31.43	21.44873	27,607.91	91.198	549,823	97.98
	300	0.20368	733.2637	27.14	21.48420	26,080.79	91.287	585,298	95.59
	315	0.19952	718.2637	26.10	21.49289	25,721.79	91.272	593,983	95.02
	330	0.19535	703.2637	25.08	21.50130	25,371.40	91.242	602,395	94.44
	345	0.19118	688.2637	24.07	21.50935	25,029.41	91.196	610.445	93.86
	360	0.18702	673.2637	23.08	21.51695	24,695.64	91.137	618,045	93.29

NOTES:

(1) Times-to-go, as selected, correspond with discrete S-IVB burn periods of the NASA/MSC computer output tape to the nearest 3 seconds.

(2) These data computed by STL with the aid of the analytic lunar program and correspond to a launch.

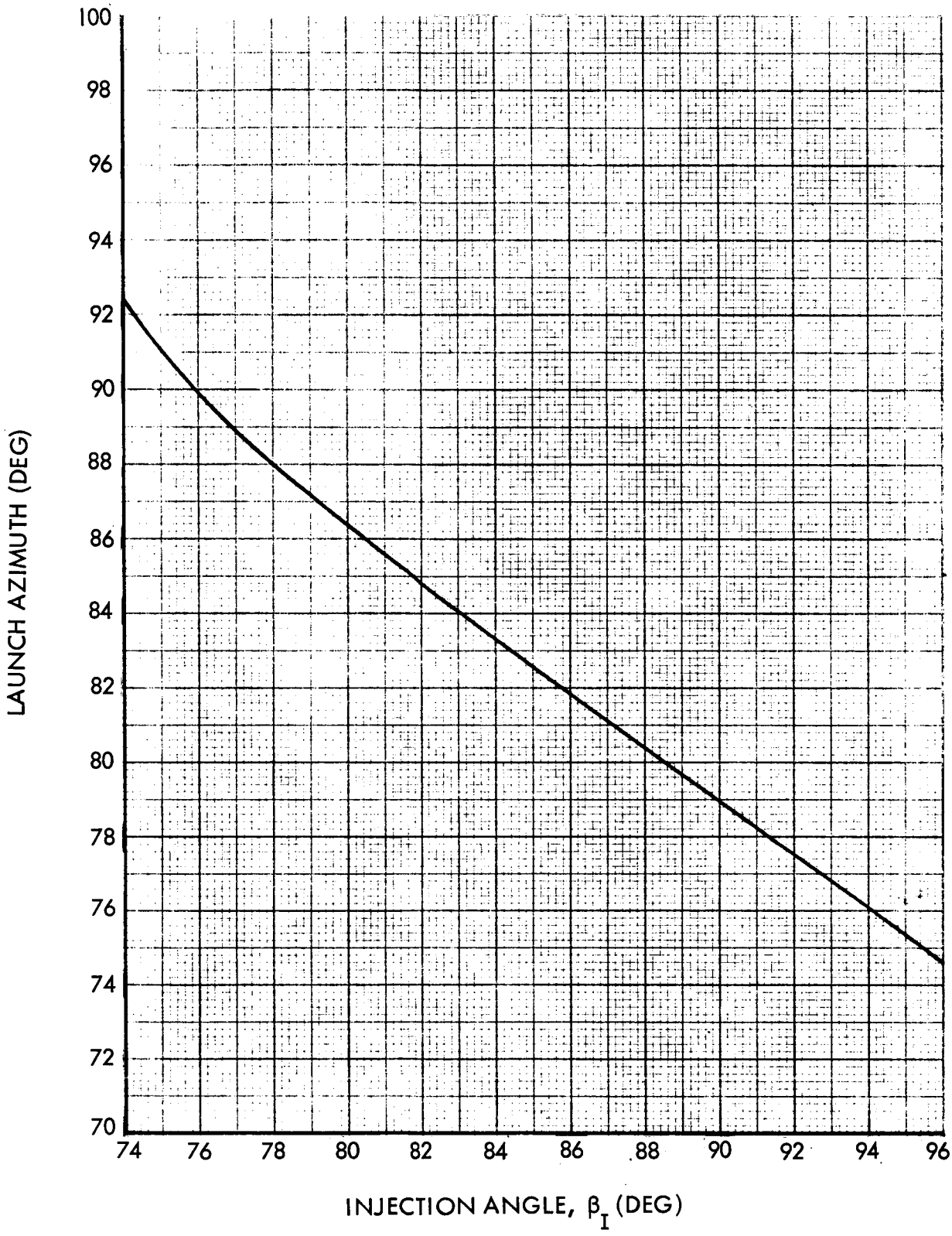

Figure 3-6. Launch Azimuth as a Function of the Injection Angle, β_I for a Direct Ascent Launch on 23 January 1968 with a 72-Hour Flight Time

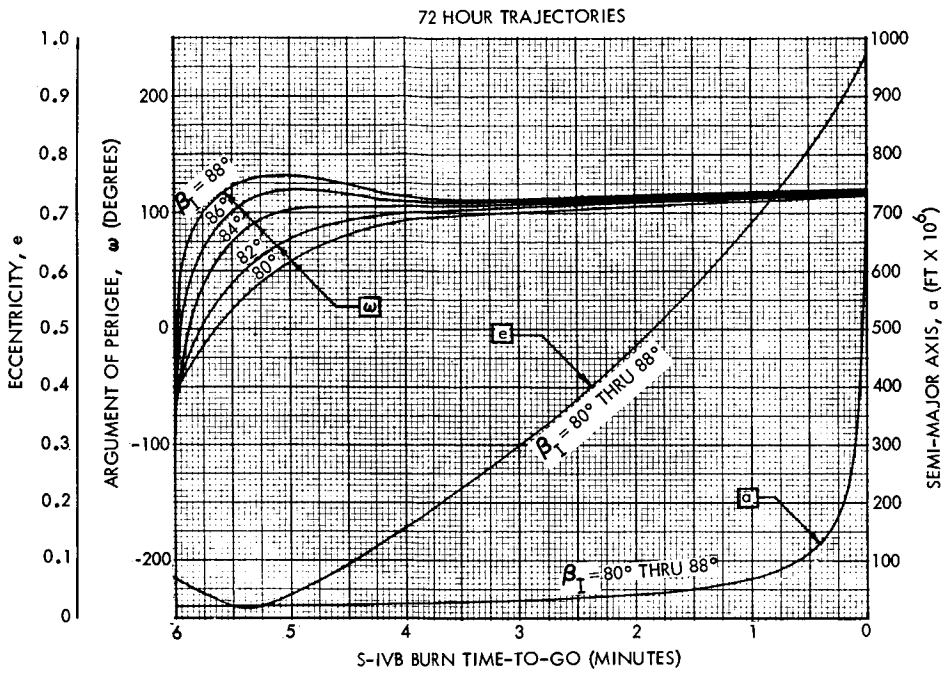

Figure 3-7. Orbit Elements as a Function of S-IVB Translunar Injection Burn Time-to-Go for a Special Earth Model

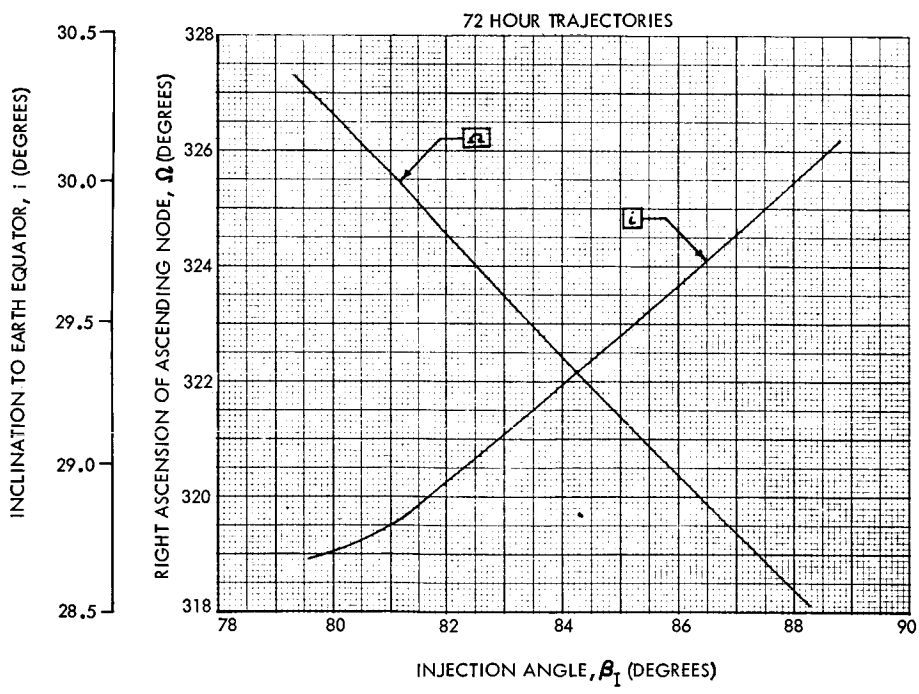

Figure 3-8. Orbit Elements that are Functions of Injection Angle β_I Only for a Spherical Earth Model

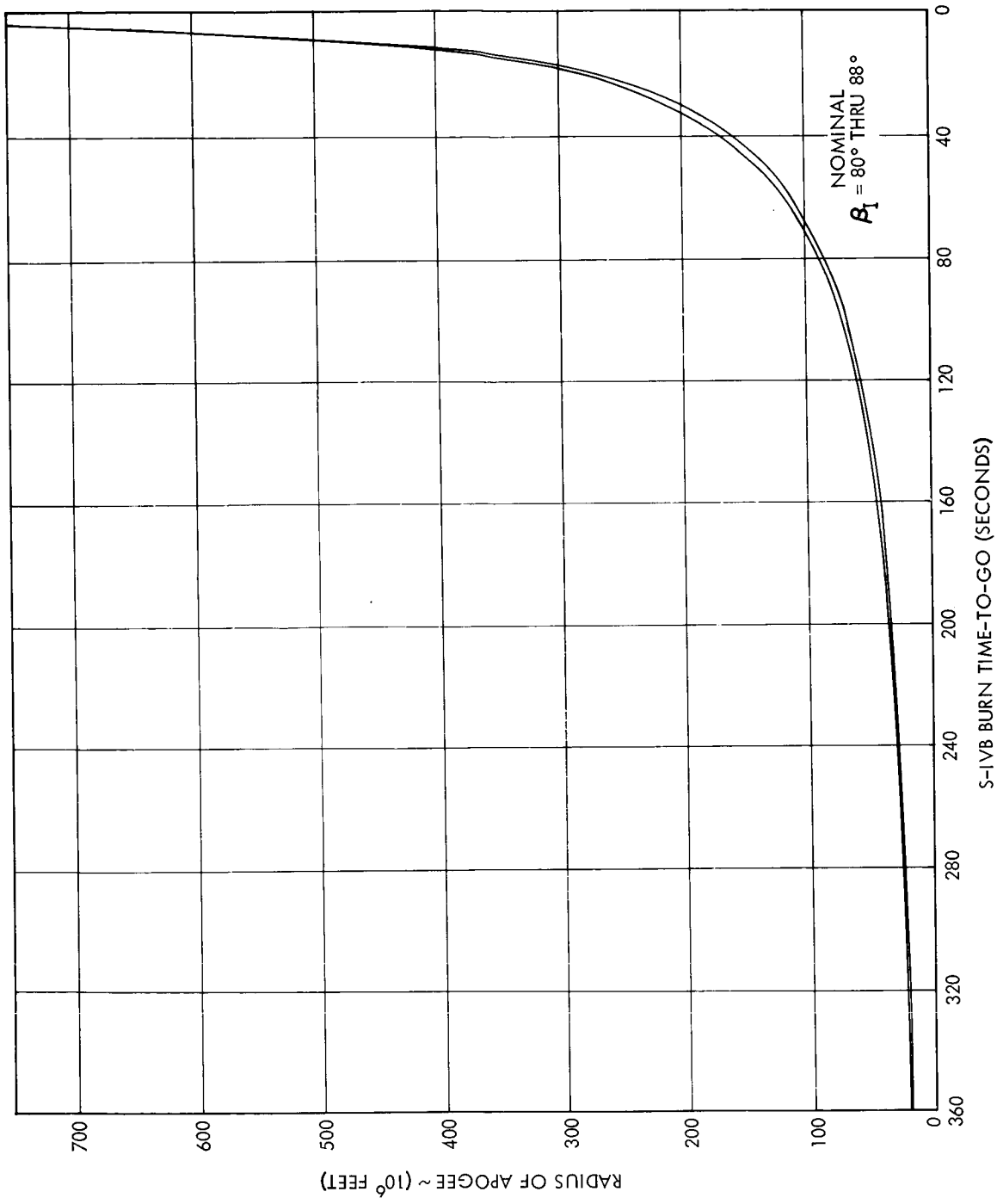

Figure 3-9. Radius of Apogee for Pre-Abort Trajectories as a Function of S-IVB Burn Time-to-Go for All Nominal Injection Angles 80° to 88°

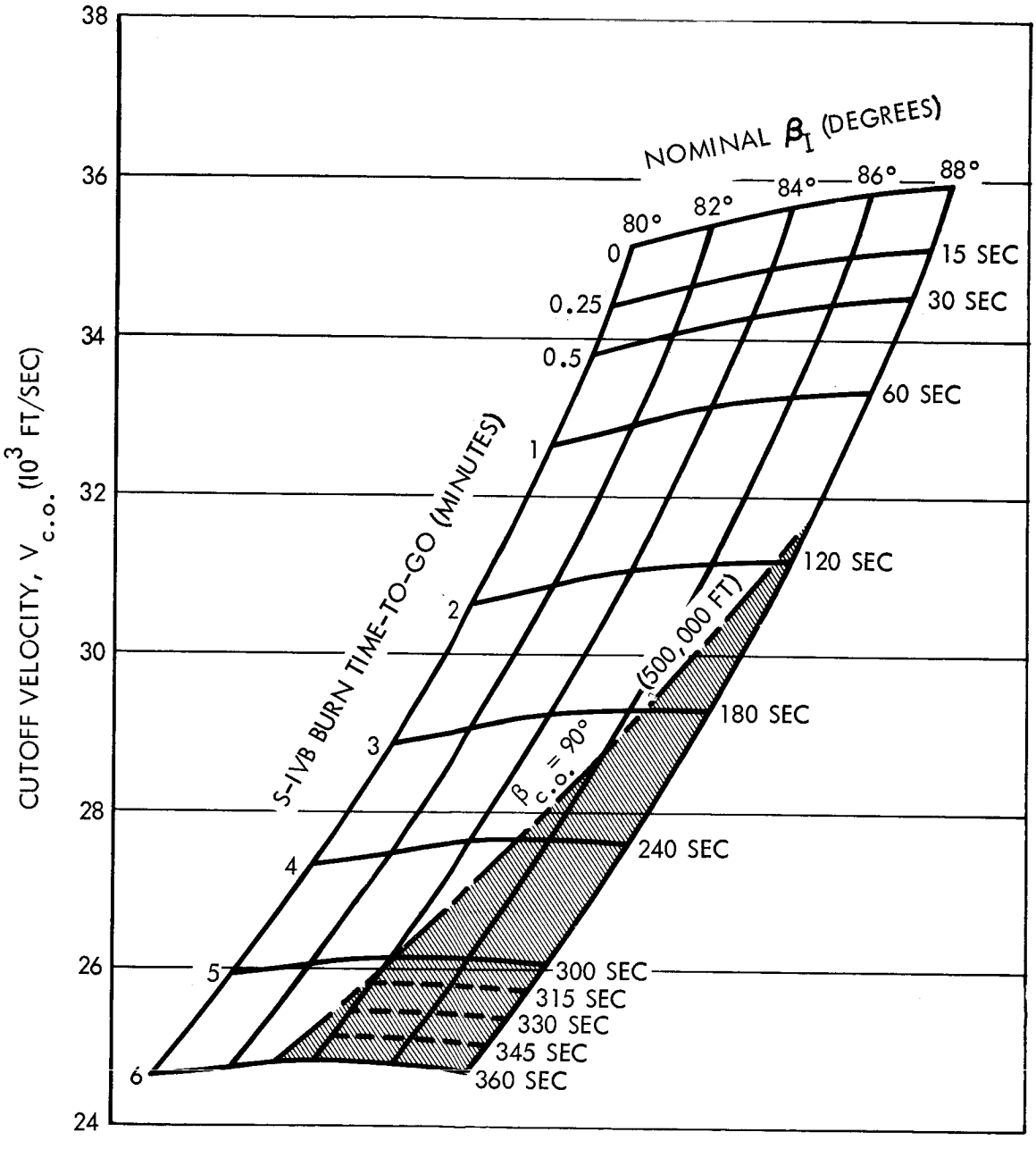

Figure 3-10. Cutoff Velocity, $V_{c.o.}$ as a Function of S-IVB Translunar Injection Burn Time-to-Go

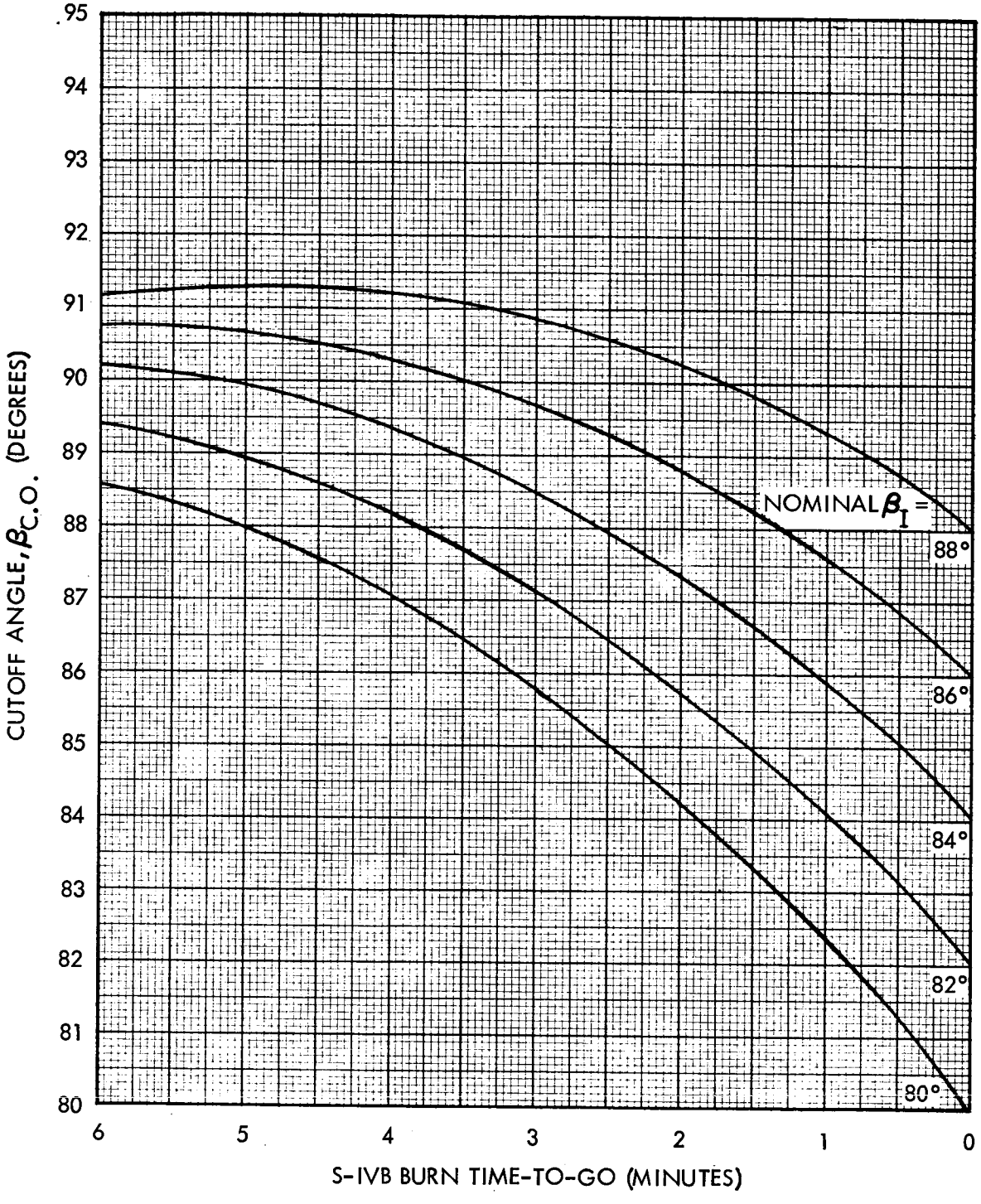

Figure 3-11. Cutoff Angle, $\beta_{c.o.}$ as a Function of S-IVB Translunar Injection Burn Time-To-Go

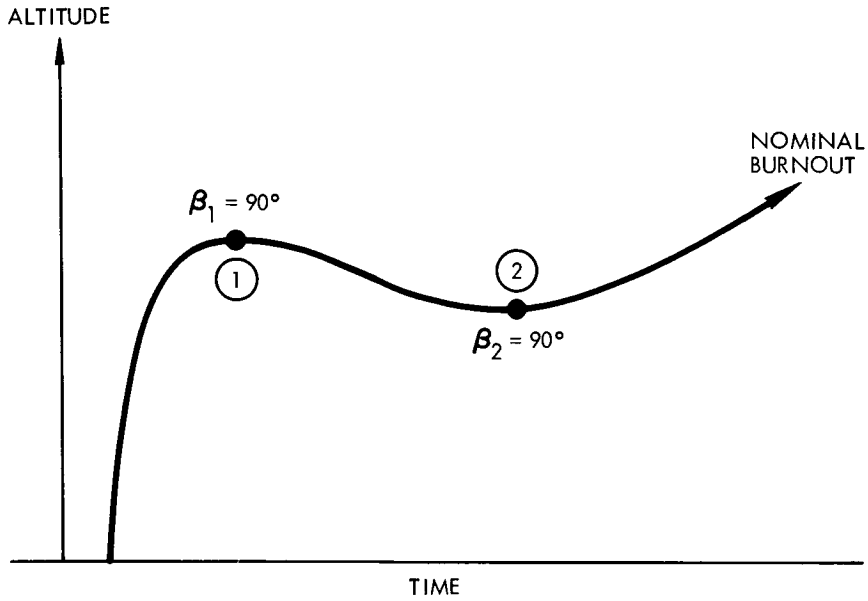

Figure 3-12. Diagrammatic Variation in Altitude and Flight Path Angle for a Typical Direct Ascent Powered Flight Trajectory

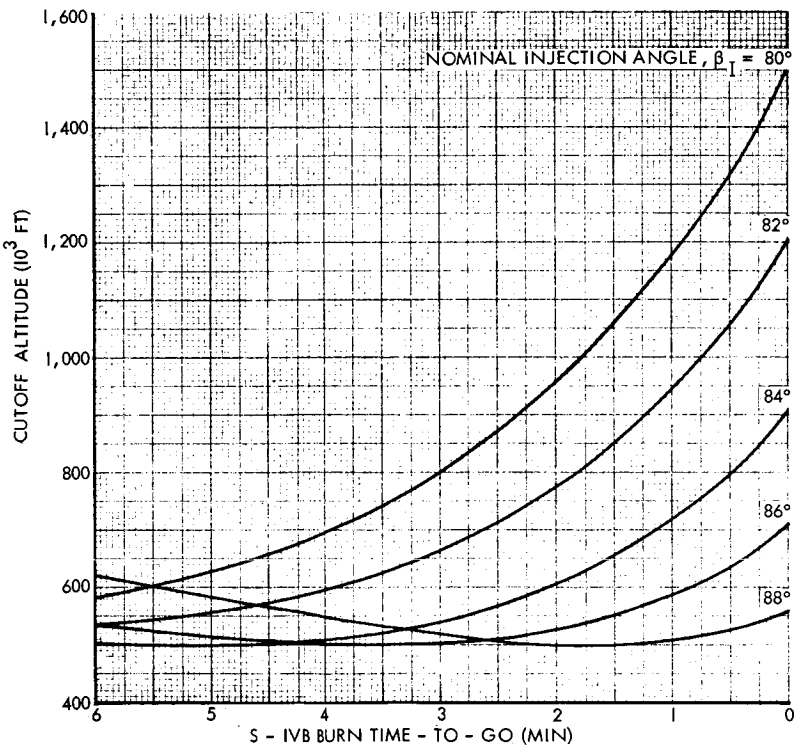

Figure 3-13. Effect of Nominal Injection Angle, β_I on the Variation in Cutoff Altitude as a Function of S-IVB Burn Time-to-Go

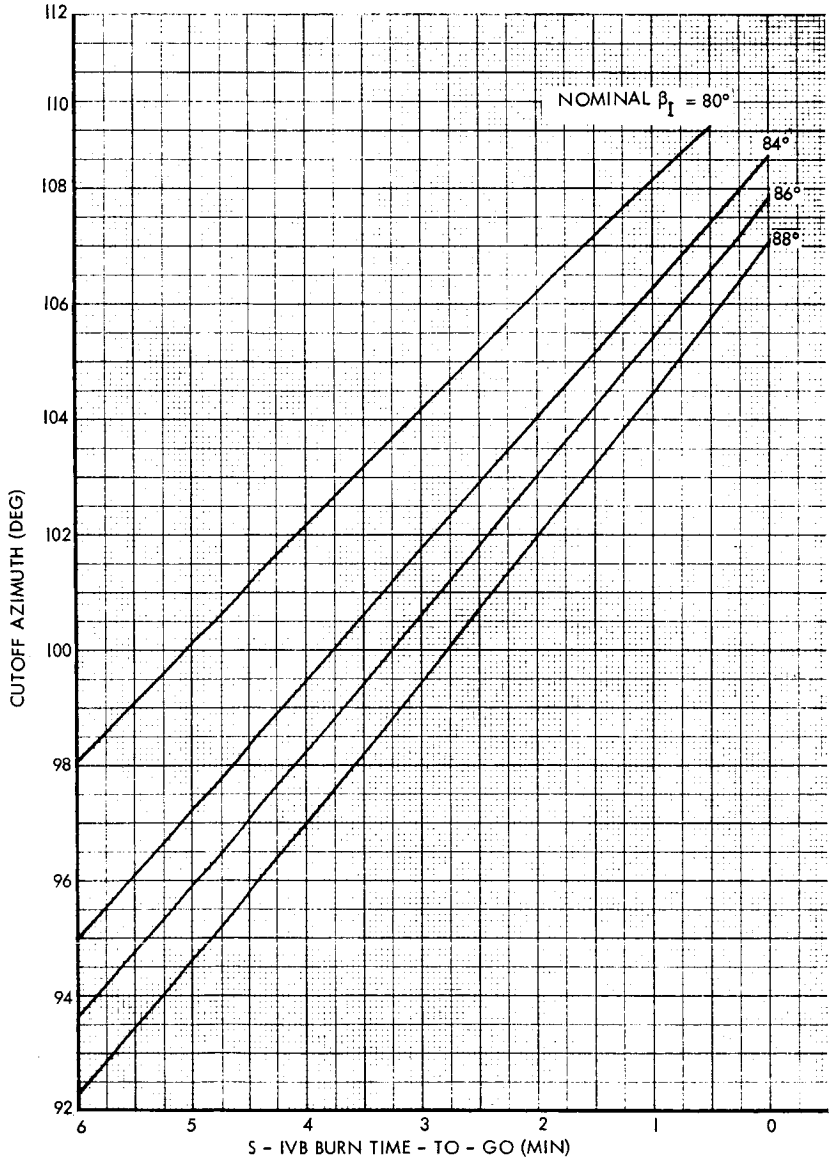

Figure 3-14. Effect of Nominal Injection Angle, β_I on the Variation of Cutoff Azimuth as a Function of S-IVB Burn Time-To-Go

abort capability of the direct ascent mode. Of interest also are the variations in inclination and right ascension shown in Figure 3-8. These are plotted against injection angle β_I inasmuch as the orientation of the free-flight orbital plane shows very little change with burn-time-to-go. On the other hand the planar elements a, e, and ω show extremely little change with β_I, except for the interval between 4 and 6 minutes where some variation in ω is indicated. Figure 3-9 shows apogee radius as a function of burn-time-to-go for the range of β_I. Here, again, the pronounced effect of the last minute of burn is evident.

For an abort problem postulated on premature termination in thrust, it is important to examine the changes in the resulting injection parameters. Of major concern are the cutoff velocity, flight path angle, and altitude. Figure 3-10 shows the effect of burn-time-to-go on injection velocity for the range of nominal injection flight path angles. β_I as used here and in subsequent figures identifies a particular nominal trajectory and not the angle associated with the cutoff velocity, except at 0 time-to-go. $\beta_{c.o.}$ defines the flight path angle at cutoff. Figure 3-10 also indicates a restricted region. Velocities in this region have an associated $\beta_{c.o.}$ that exceeds 90 degrees and yield free-flight trajectories of extremely short life span. They create, however an abort opportunity of special interest. It is observed that most of the velocities are well beyond circular orbit speed.

Figure 3-11 relates the flight path angle at cutoff to burn-time-to go. To indicate the significance of the points for which $\beta_{c.o.}$ = 90 degrees and to visualize the shape of the typical direct injection trajectory, Figure 3-12 diagrammatically depicts the characteristic variation of altitude and flight path angle. Note that there are two points of inflection ($\beta_{c.o.}$ = 90 degrees), the second of which falls within the range of interest. The pre-abort trajectories requiring special considerations are the ones for nominal β_I = 84, 86, and 88 degrees. Because of the opportunity afforded these trajectories for possible aborts to an earth orbit, discussion of their pre-abort trajectories is deferred to Section 3.4.

Figure 3-13 presents the variation of cutoff altitude with burn-time-to-go, showing computed points depicted in Figure 3-12. S-IVB thrust termination at longer burn-times-to-go occurs near 500,000 feet altitude causing the cutoff angles for these cases to be more critical in the problem of obtaining free-flight trajectories that do not violate this limit.

To the triad of V, β, h at cutoff, is added the velocity azimuth, shown as a function of burn-time-to-go in Figure 3-14. For direct ascent, all S-IVB cutoffs occur at azimuths greater than 90 degrees.

To complete the presentation of the pre-abort trajectory characteristic, Figure 3-15 shows the variation in pre-abort radius as a function of time from cutoff for various burn-times-to-go. This data represents a nominal β_I of 84 degrees. The effect of β_I on the pre-abort radius is indicated in Figure 3-16 showing radius as a function of coast time beyond cutoff for β_I = 80, 84, and 88 degrees and at burn-times-to-go of 15 and 60 seconds. Figure 3-17 shows the variation of free-flight velocity as a function of radial distance for various burn-times-to-go. Again the data represents a β_I of 84 degrees. The effect of β_I on velocity is graphically shown on a contour map in Figure 3-18 for 15 and 30 seconds burn-time-to-go.

The relative size of the resulting pre-abort trajectories may be visualized as conics in the earth-moon space, identified by their respective burn-time-to-go. Figure 3-19 diagrammatically shows these orbits relative to circles of altitude in terms of earth radii. The portions of the orbits extending into the moon's sphere of influence are, of course, not valid.

3.4 ABORTS TO ORBIT

As previously mentioned in Section 3.3, a number of free-flight trajectories resulting from early thrust termination bear special consideration in the abort problem. These trajectories are characterized by the fact that their cutoff angles reach or exceed 90 degrees within the time-to-go range of interest. References to Figure 3-11 ($\beta_{c.o.}$ versus burn-time-to-go), indicates that the particular trajectories attaining this condition are the ones for nominal β_I = 84, 86, and 88 degrees. From orbital geometry, there are two points of β = 90 degrees, apogee and perigee. If the points

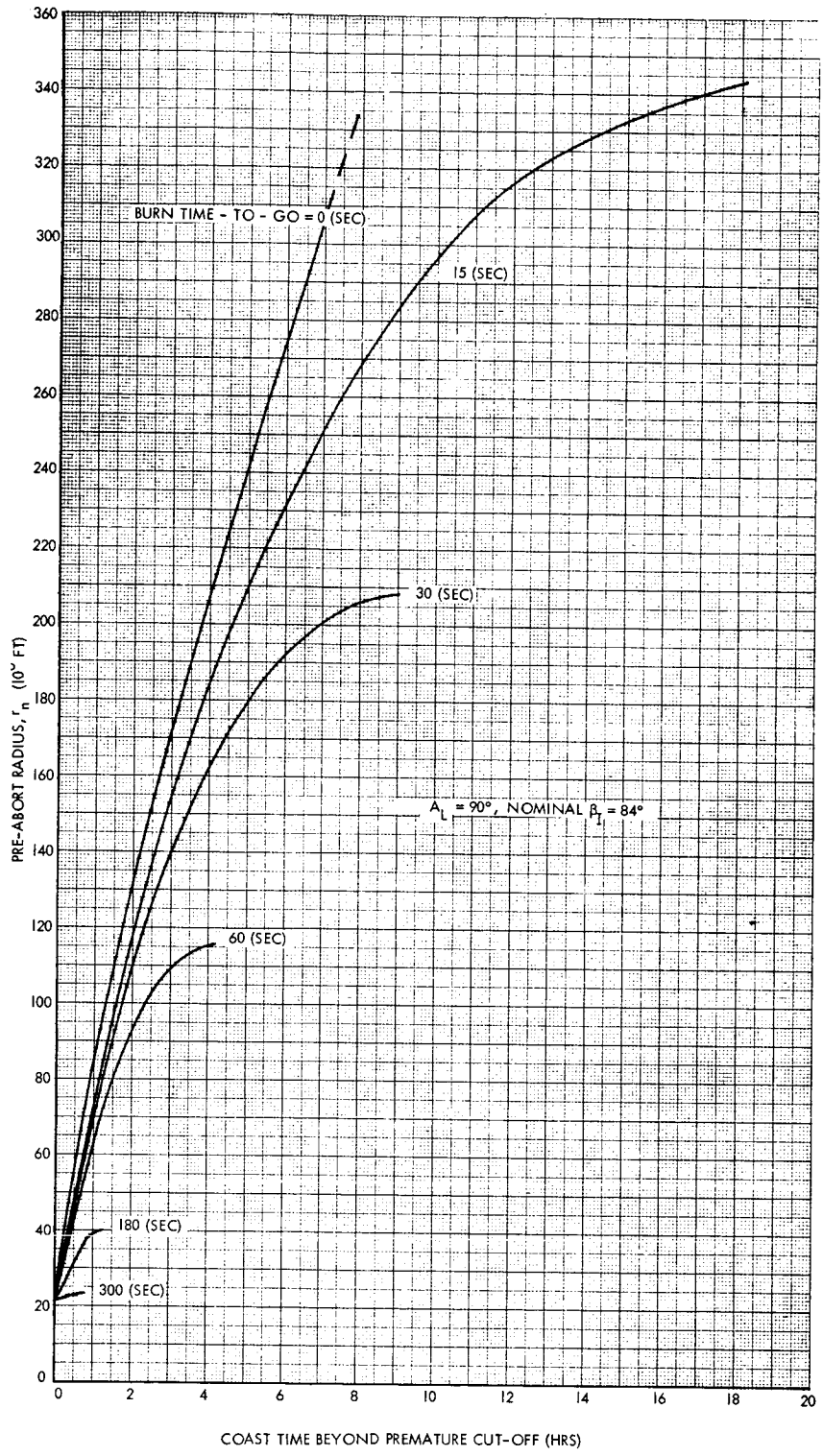

Figure 3-15. Effect of Variation in S-IVB Burn Time-To-Go on the Pre-Abort Trajectory Radius as a Function of Coast Time Beyond Premature Cutoff

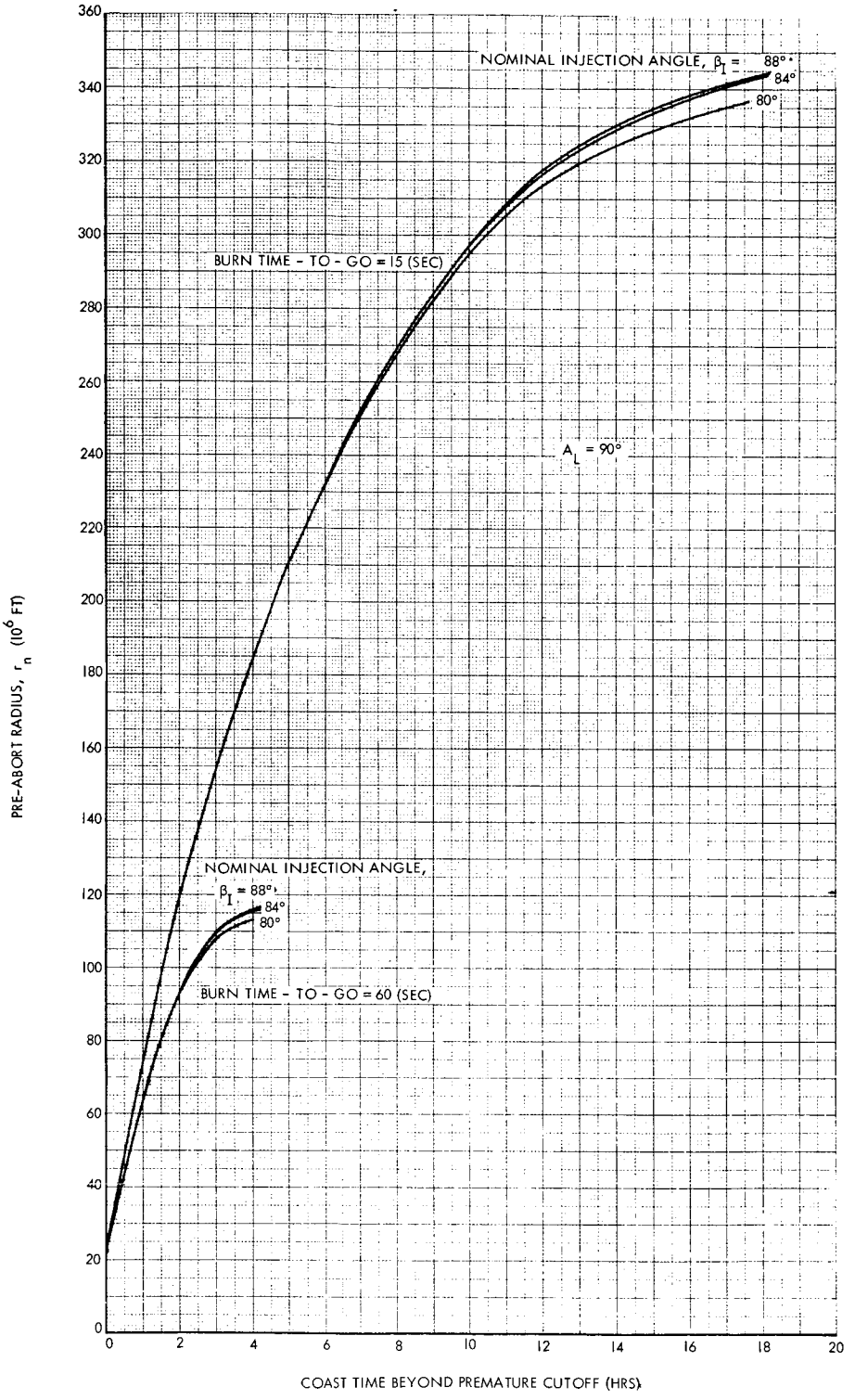

Figure 3-16. Effect of Nominal Injection Angle, β_I on the Pre-Abort Trajectory Radius as a Function of Coast Time Beyond Premature Cutoff

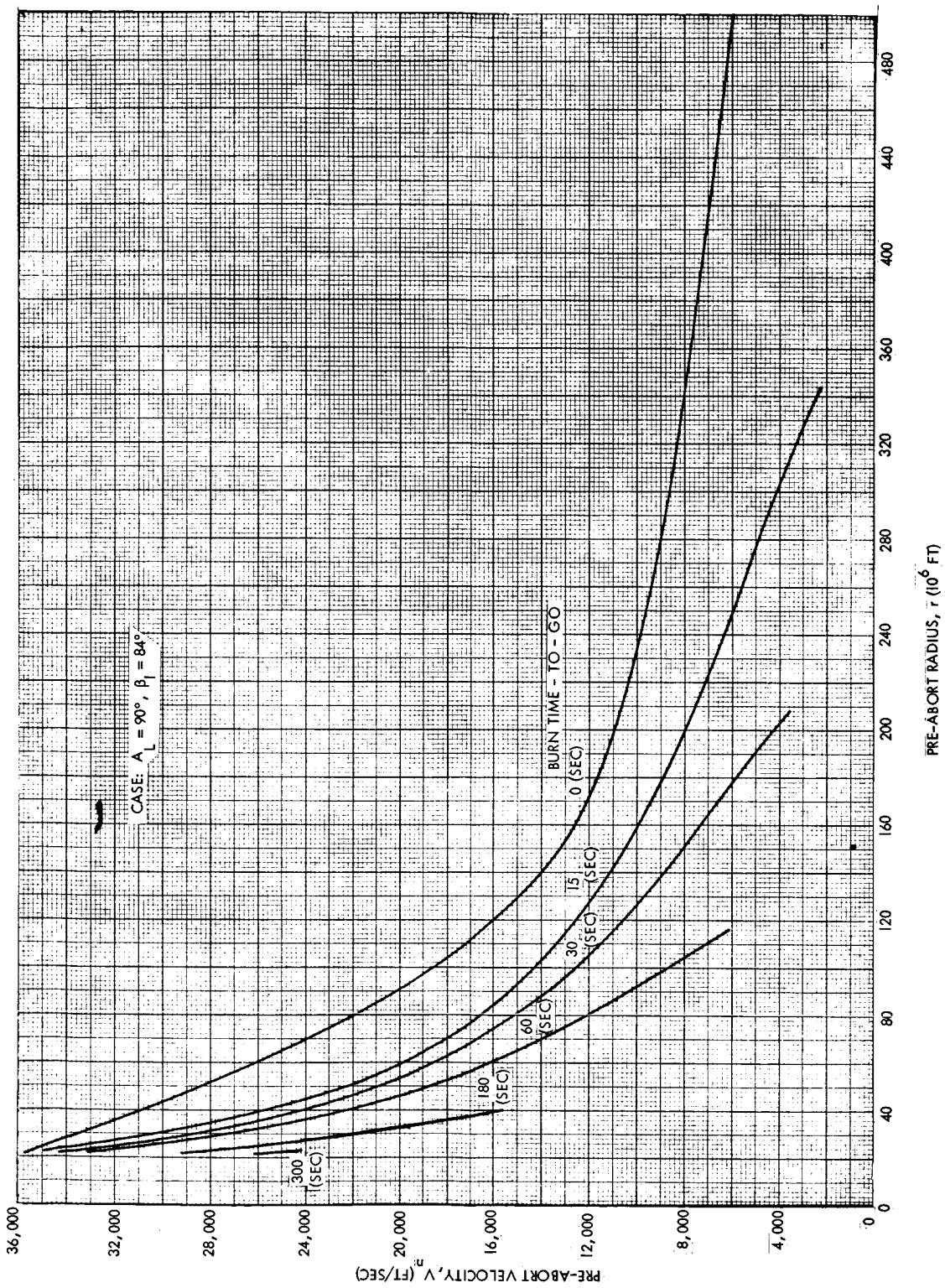

Figure 3-17. Variation of Pre-Abort Velocity With Radius for Various S-IVB Burn Time-To-Go

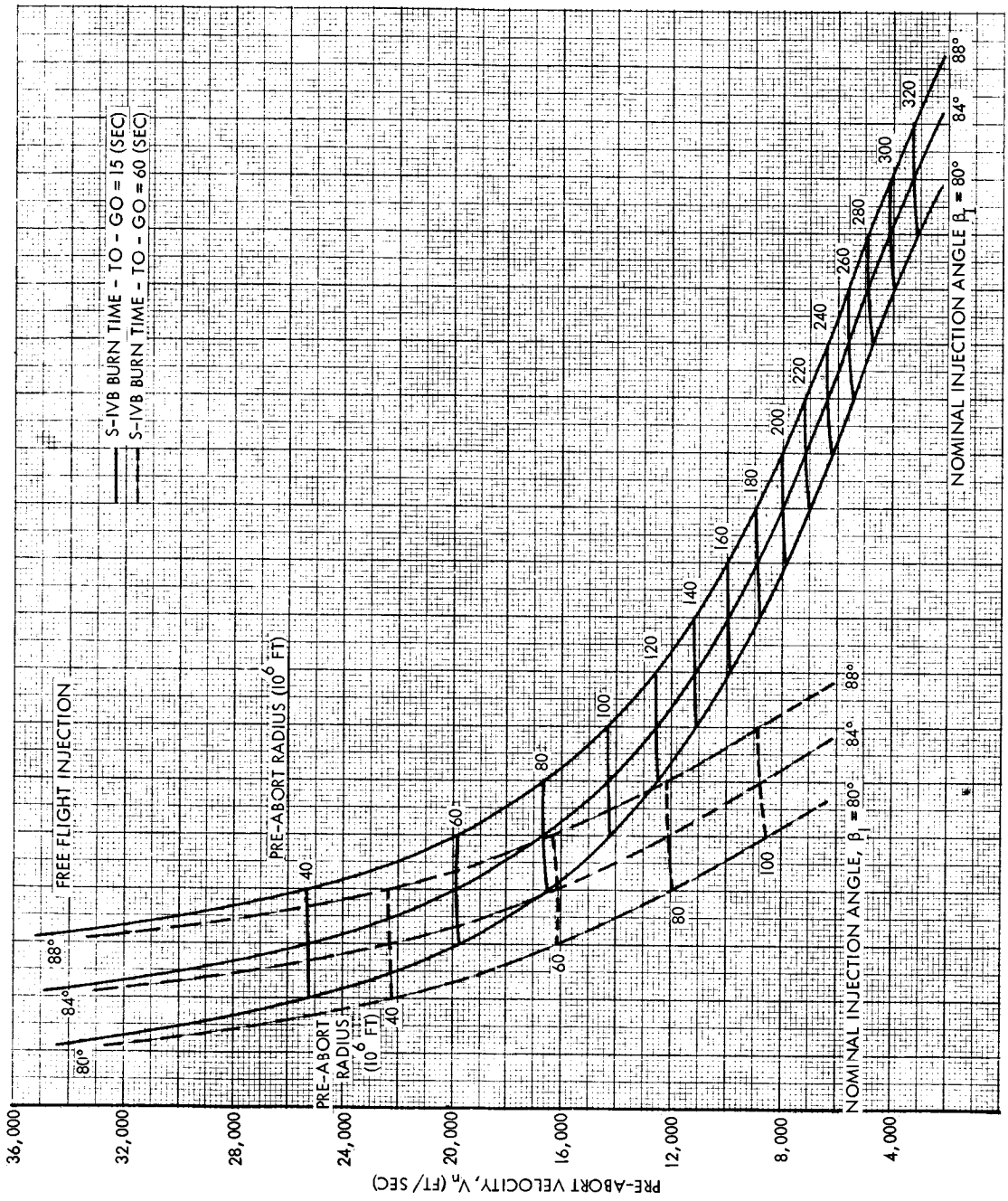

Figure 3-18. Pre-Abort Velocity Contour Indicating the Effect of Nominal Injection Angle, β_I

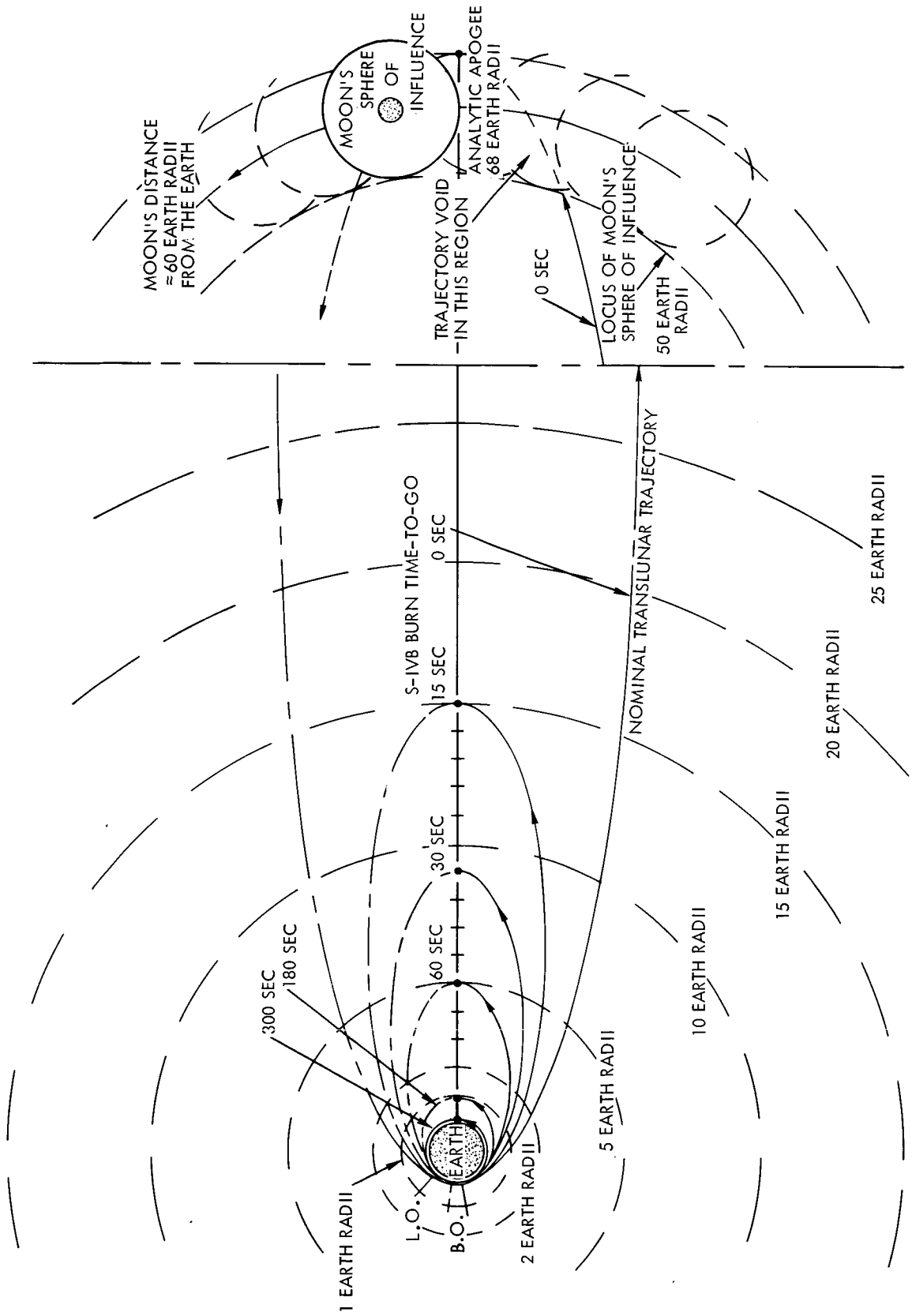

Figure 3-19. Diagrammatic Representation of Pre-Abort Trajectories Resulting from S-IVB Thrust Termination with Various Burn Times-To-Go

in question are near perigee, a periodic earth orbit will result with the closest approach altitude near that of the cutoff. However, if the points are near apogee, a ballistic trajectory with extremely short lifetime could result. The answer to this question may be reasoned as follows:

a) $\beta_{c.o.} > 90$ and decreasing ⟶ pre-perigee injection, altitude decreasing

b) $\beta_{c.o.} \leq 90$ and decreasing ⟶ post-perigee injection, altitude increasing

c) $\beta_{c.o.} \leq 90$ and increasing ⟶ pre-apogee injection, altitude increasing

d) $\beta_{c.o.} \geq 90$ and increasing ⟶ post-apogee injection, altitude decreasing

This can also be shown with the aid of Figure 3-20.

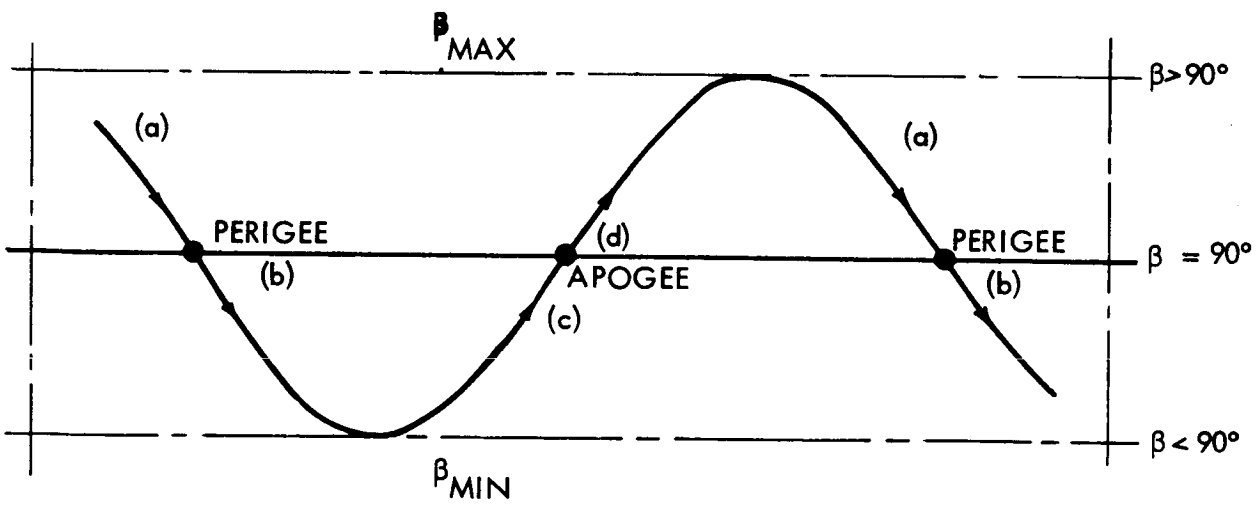

Figure 3-20. Variation in Flight Path Angle Along an Elliptical Earth Orbit

From Figure 3-21, it is apparent that all trajectories resulting from burn-times-to-go of greater than 300 seconds exhibit the characteristic of a post-apogee injection. Figure 3-22 shows the altitude variations during this time span. Most of the trajectories exhibit a decrease in altitude over the short time span shown, but altitude alone is a poor indication of what lies ahead for greater time periods. The worst of the post-apogee trajectories, that for a nominal β_I = 88 degrees, shows the largest margin in altitude above the arbitrary 500,000 foot limit. Figure 3-23 shows the altitudes of closest earth passages for nominal β_I = 80 through 88 degrees as a function of S-IVB burn-time-to-go at cutoff.

Table 3-3, presents the orbital characteristics for the free-flight trajectories in the region of possible aborts to orbit.

Table 3-3. Orbital Elements of Low Altitude Pre-Abort Trajectories Resulting From Thrust Terminations $\geq$ 300 Seconds Burn-Time-To-Go

Nominal β_I (deg)	Δt_{GO} (sec)	a (10^6 ft)	e	$V_{c.o.}$ (fps)	$\beta_{c.o.}$ (deg)	r_{apogee} (10^6 ft)	$h_{perigee}$ (ft)
84	300	22.2763	0.0395	26,150	89.932	23.1560	497,890
	315	21.6627	0.0123	25,806	90.032	21.9292	497,490
	330	21.1039	0.0140	25,470	90.114	21.3994	---*
	345	20.5929*	0.0392	25,142	90.177	21.4001	---*
	360	20.1239*	0.0635	24,821	90.222	21.4021	---*
86	300	22.3196	0.0421	26,153	90.655	23.2596	480,890
	315	21.7001	0.0178	25,801	90.703	22.0864	415,090
	330	21.1358	0.0187	25,457	90.735	21.5310	---*
	345	20.6199*	0.0414	25,122	90.750	21.4736	---*
	360	20.1464*	0.0652	24,794	90.748	21.4606	---*
88	300	22.3366	0.0443	26,081	91.287	23.3256	448,890
	315	21.7141	0.0244	25,722	91.272	22.2439	285,590
	330	21.1468	0.0274	25,371	91.242	21.7262	---*
	345	20.6278*	0.0476	25,029	91.196	21.6097	---*
	360	20.1514*	0.0706	24,696	91.137	21.5740	---*

*Below the earth's radius of 20.89871 x 10^6 feet.

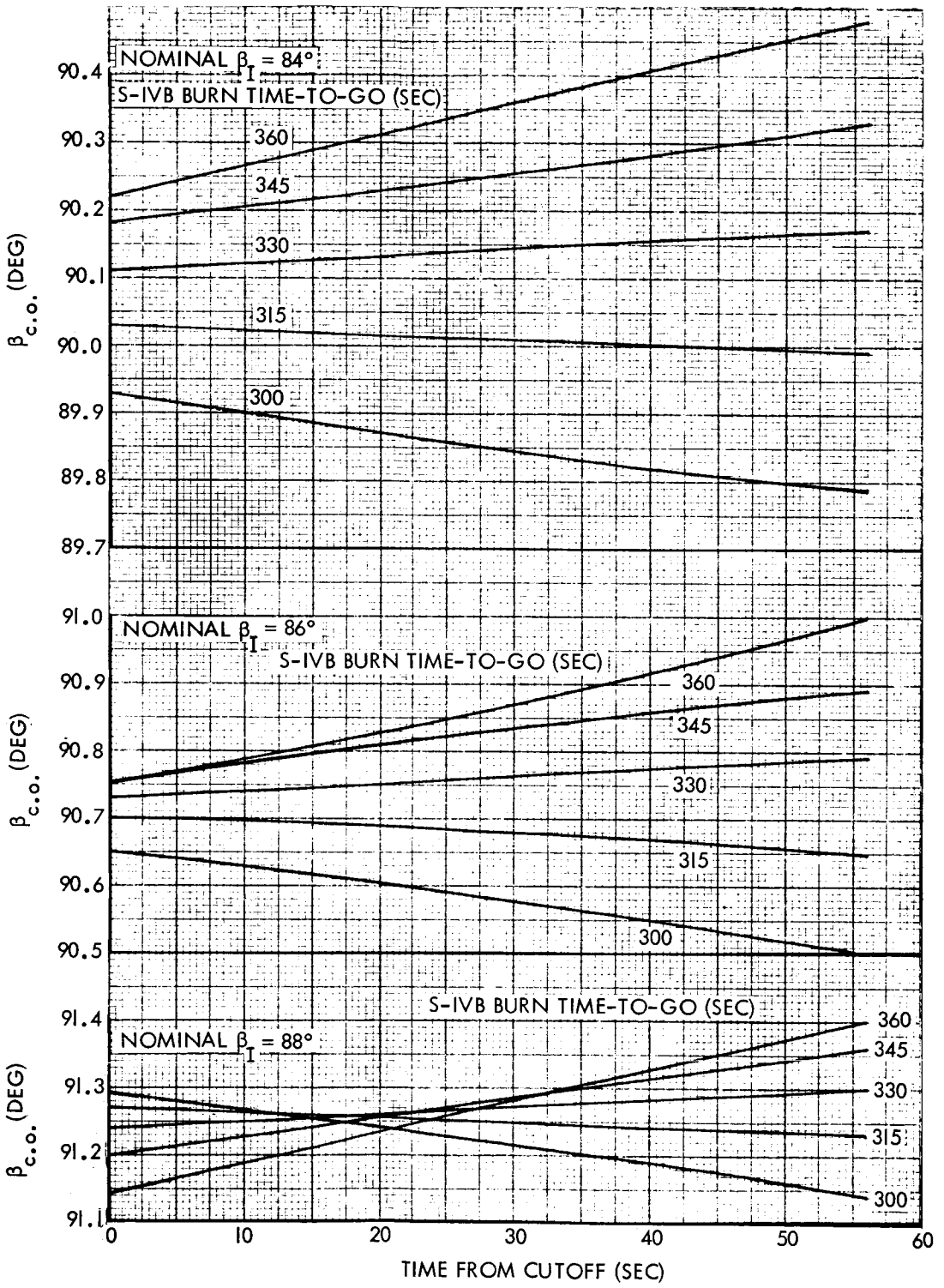

Figure 3-21. Short Time History of $\beta_{c.o.}$ for Particular Pre-Abort Trajectories Between 300 (sec) and 360 (sec) S-IVB Burn Time-to-Go

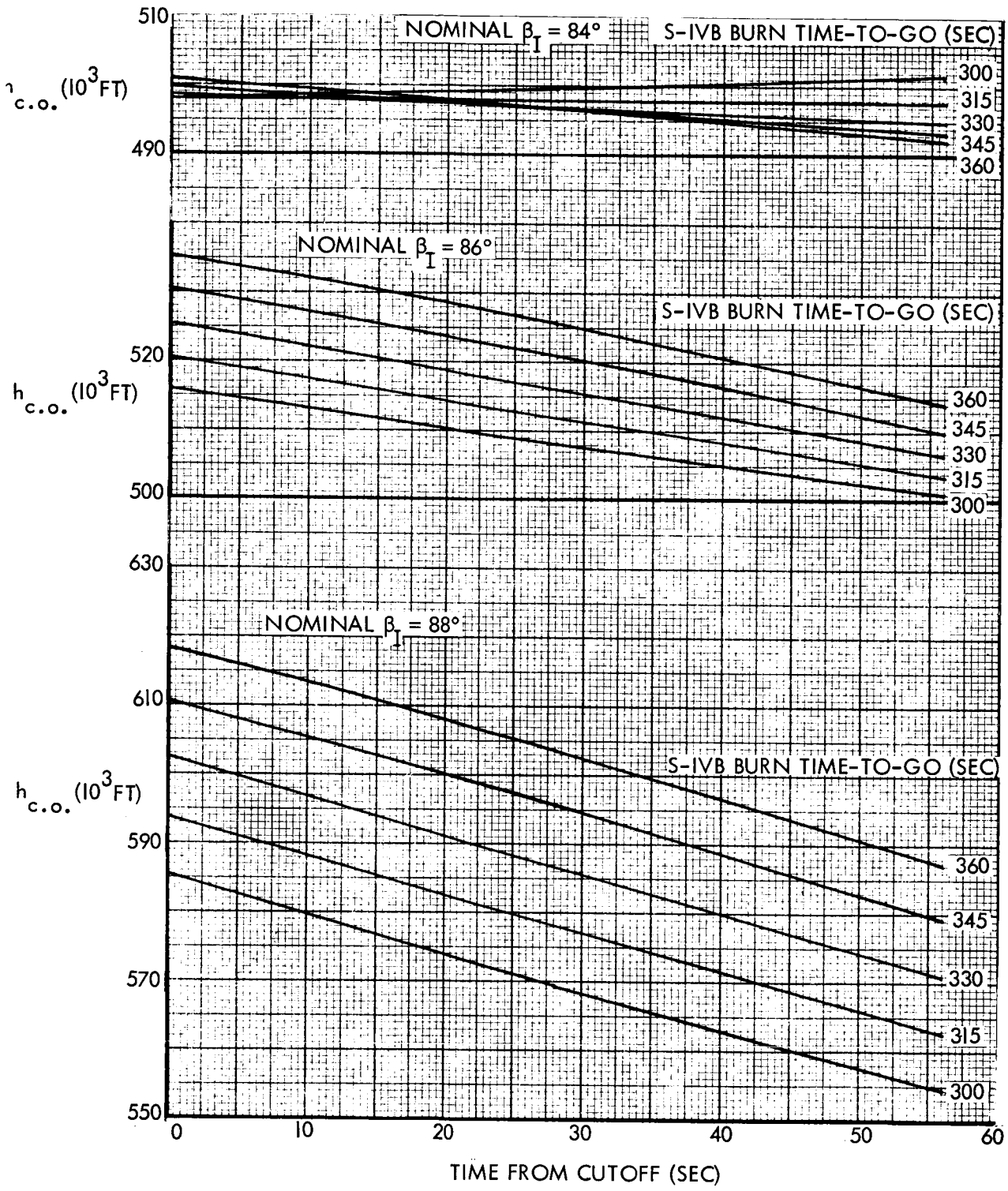

Figure 3-22. Short Time History of Cutoff Altitude, $h_{c.o.}$, for Particular Pre-Abort Trajectories Between 300 (sec) and 360 (sec) S-IVB Burn Times-To-Go

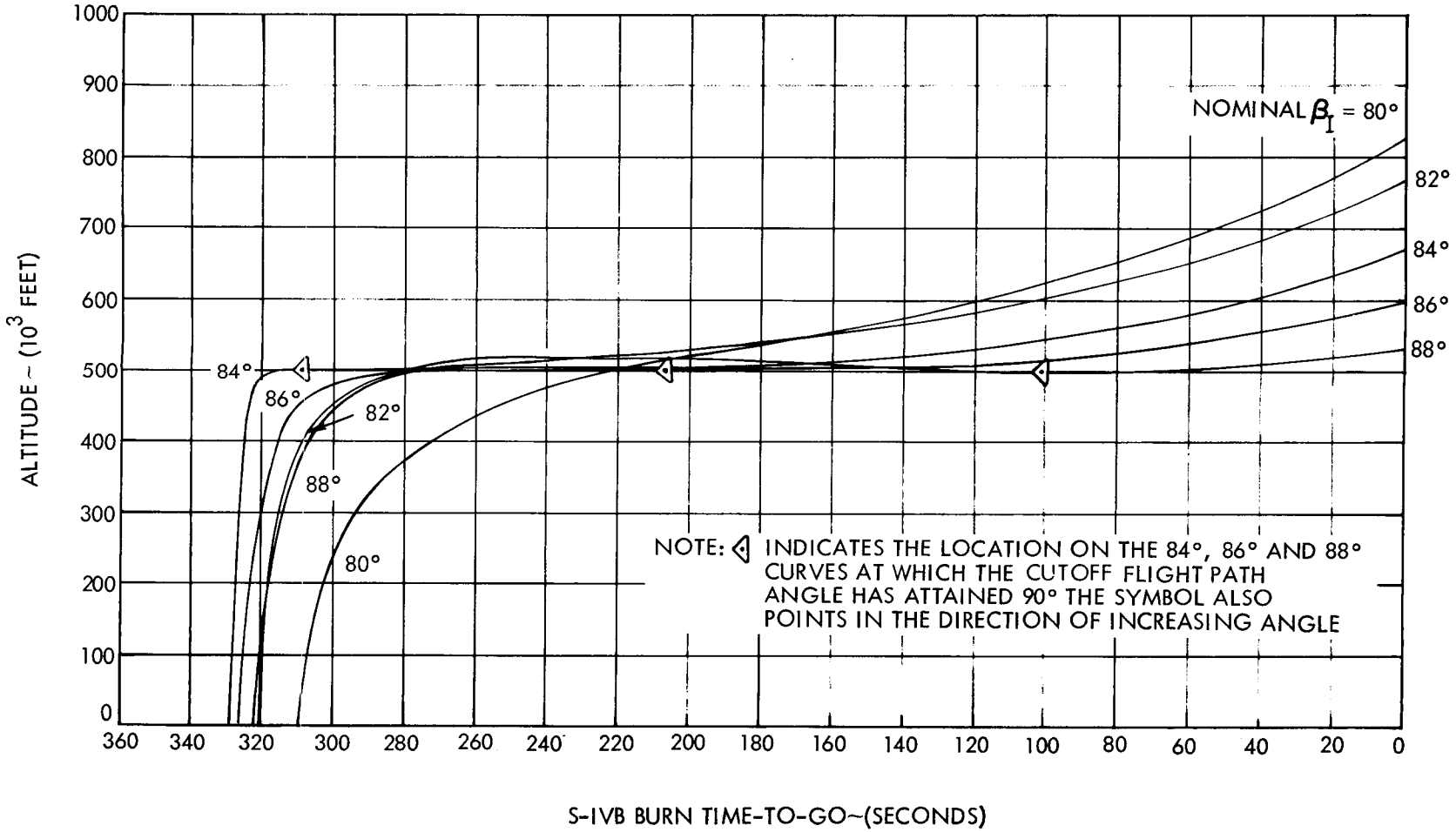

Figure 3-23. Altitude of Closest Earth Passage as a Function of S-IVB Burn Time-To-Go for a Range of Nominal Angles of Injection

In examining the relative merits of each mission prior to the injection maneuver, it must be acknowledged that a circular coast phase or parking orbit, providing as easily available alternative in the event of an emergency, is a major advantage. The trajectory shaping of the direct ascent mission is not as favorable to an abort into a circular earth orbit because of the steeper ascent path. However, with control systems operative, aborts to earth orbit for the direct ascent launch are indeed possible. This is particular true if the S-IVB cutoff is elective and is executed well before nominal burnout, as in a case of aborts necessitated by other than propulsion failure.

For the post-perigee trajectories, the abort to a circular orbit concept is most promising. In fact, the post-apogee trajectories are not ruled out. In their case, however, reaction time may prove critical. NASA/MSC has considered a mandatory minimum coast time before abort initiation to be 28 seconds after cutoff. With initial conditions specified after this time, NASA/MSC ran several abort-to-orbit trajectories for burn-times-to-go of 300, 330, and 360 seconds at nominal β_I = 84, 86, and 88 degrees using a constant angle of attack computer program with a discrete thrust period. A 24-hour orbit lifetime was required. In satisfying this condition a burnout altitude of 500,000 feet was required. For those trajectories that had attained this altitude, a constant angle of attack thrusting of the service module produced a circular orbit of satisfactory period. For the cases that did not reach 500,000 feet, NASA/MSC used two trapezoidal angle-of-attack functions during service module thrusting to obtain the desired results. Service module performance parameters used were

Thrust = 21,800 pounds

Weight = 60,200 pounds

I_{sp} = 313 seconds

For these same conditions, results were computed for impulsive velocity increments instead of the integrated values obtained by NASA/MSC. The equivalent velocity increments are shown in Figure 3-24. The perigree and apogee altitude for the resulting earth orbits are shown in Figure 3-25 as a function of burn-time-to-go at premature cutoff. Values for nominal β_I = 84 degrees are shown as estimated in Figures 3-24 and 3-25 since the complete data from NASA/MSC for this case were not available at this writing.

3.5 MINIMUM RETURN TIME ABORTS

Abort trajectories satisfying the requirement of return in the minimum possible time are now considered. From the standpoint of survival the study of this abort mode is not primarily concerned with return to a predetermined landing site although accurate knowledge of the possible landing areas is important to recovery. It is desirable that this type of return trajectory be co-planar with the free-flight trajectory because propellant required for plane change maneuvers can be used to shorten return time on the co-planar abort path.

The general approch in the following analysis was to generate a large number of abort trajectories from as few powered trajectories as would adequately define the range of mission parameters. Nine basic trajectories were selected, namely, a combination of three launch azimuths (72, 90, and 108 degrees) and three nominal injection angles, β_I (80, 84, and 88 degrees). For each of these trajectories, six points of thrust termination were selected. The latter, defined in terms of S-IVB burn-time remaining to nominal burnout, were selected to represent the wide range of free-flight trajectories resulting from different cutoff times. For the trajectories representing cutoffs near the nominal injection, burn times-to-go of 15, 30, and 60 seconds were selected. For trajectories remaining in the near vicinity of the earth and representing cutoffs with longer burn-times-to-go, 180 and 300 seconds were selected.

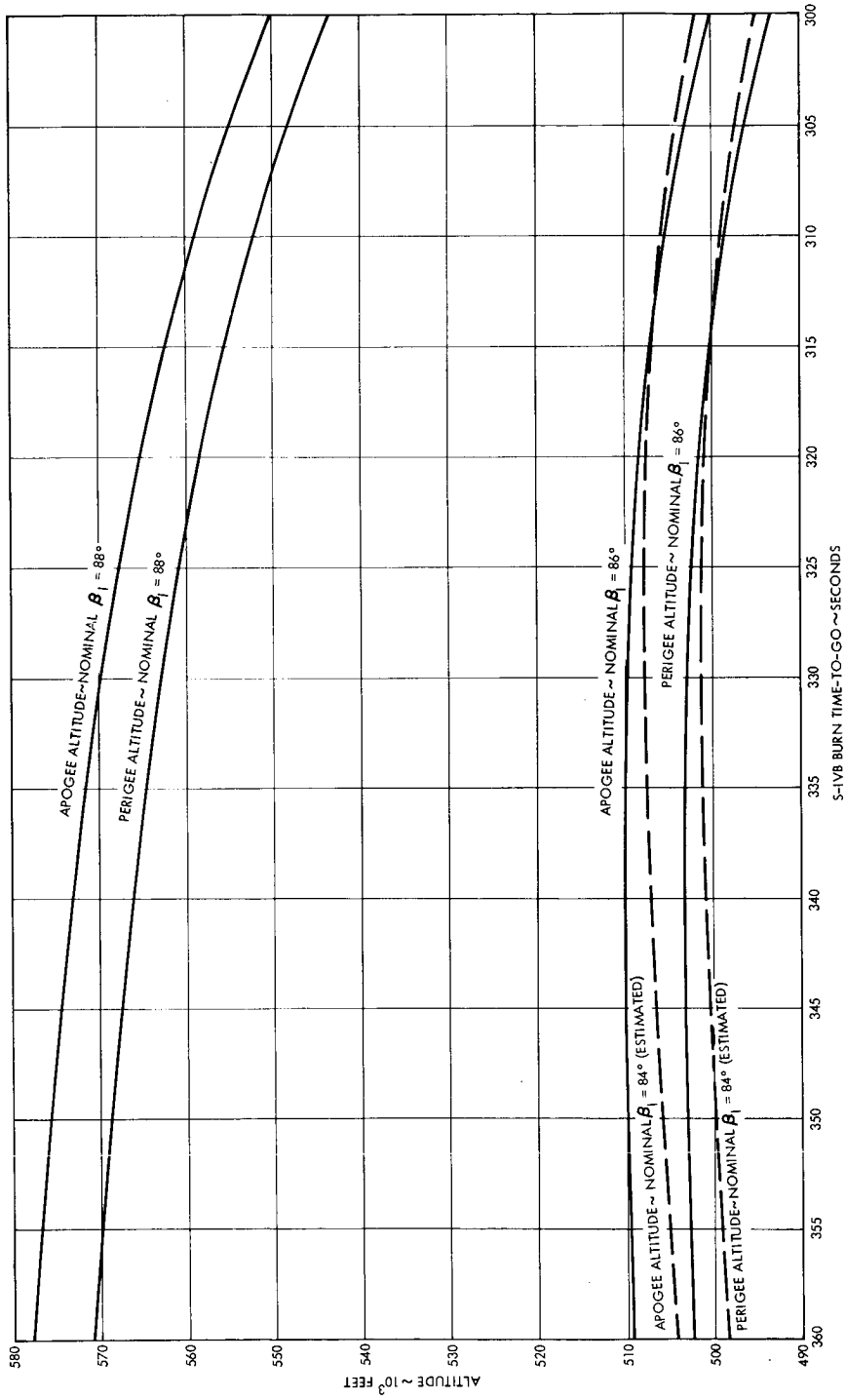

Figure 3-25. Apogee and Perigee Altitudes for a 24-Hour Life Time Earth Orbit Resulting from an Abort to Orbit 28 Seconds After a Premature Cutoff of the S-IVB

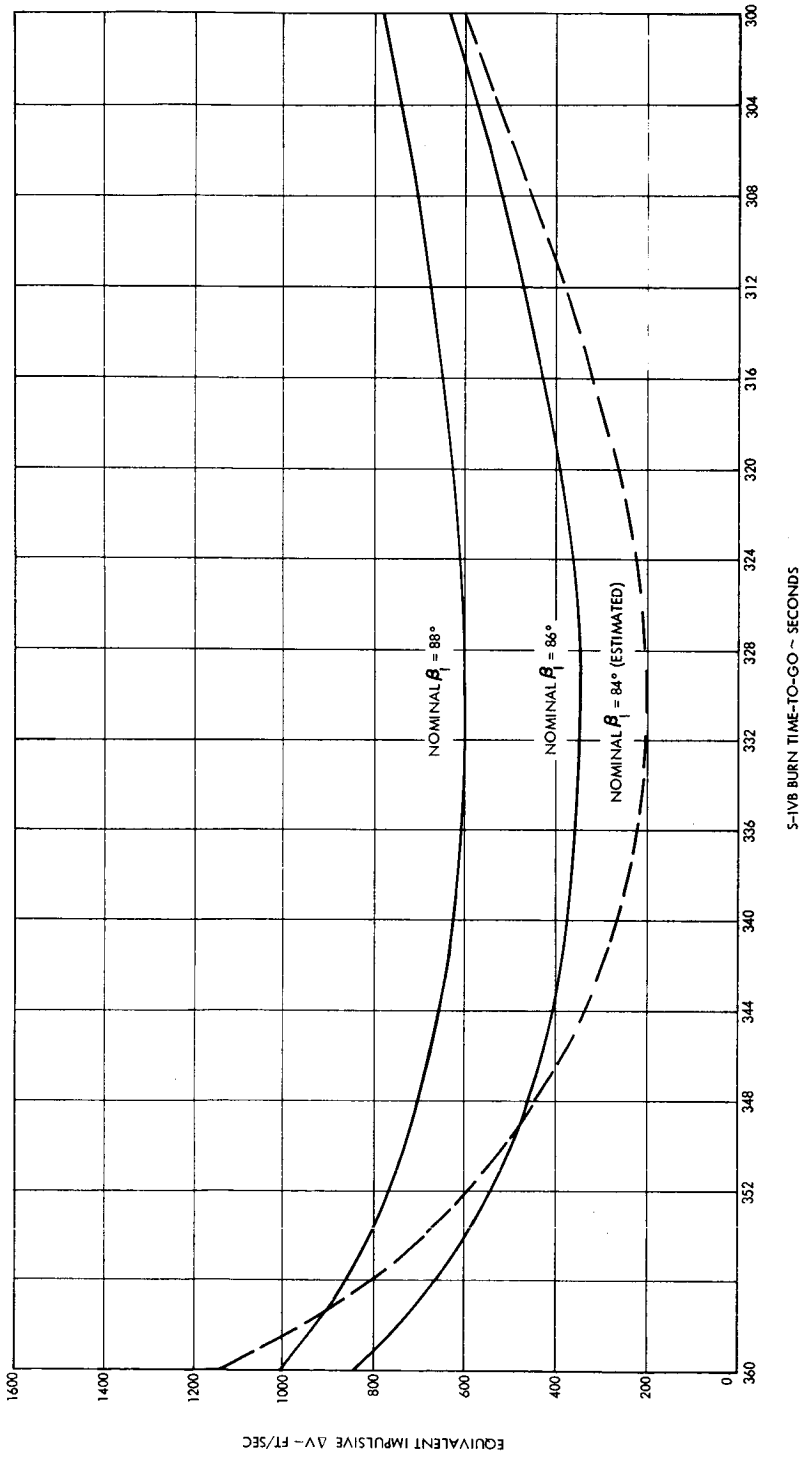

Figure 3-24. Equivalent Impulsive Velocity Increment for a 24-Hour Life Time Earth Orbit Resulting from an Abort to Orbit 28 Seconds After a Premature Cutoff of the S-IVB

Special consideration was given to these long burn-time-to-go free-flight trajectories in the previous section because of their possible entry into the atmosphere and also because their near circular orbit characteristics suggest an abort-to-orbit mode.

At 10 equal intervals in radii along each of the 54* free-flight trajectories, three values of velocity increment, impulsively applied, were considered in producing the required abort trajectory. So that the resulting abort trajectory would be compatible with current performance levels of the LEM and CSM, values of 1925, 5000, and 10,000 fps were chosen. For the extended free-flight trajectories, only that portion outside the moon's sphere of influence is considered. An inverse square force field and a spherical earth are used to approximate the earth's influence. For the number of parameters used, there exists the possibility of producing 1620 abort trajectories, some of which may yield as many as four "posigrade" solutions for the same abort velocity impulse, ΔV_{ABORT}. It may be seen that, even from a modest beginning, the abort problem expands to considerable proportions. However as more insight is gained from this and future studies into uncovering the functional relationships existing in this area, more sophisticated techniques other than the "straightforward" approach currently available can undoubtedly be applied. The current study treats each abort trajectory as a discrete entity although certain "family" relationships are in evidence.

In selecting the variables to examine the effects of the mission launch constraint, it is seen that the results are independent of the day of launch and do not depend on a "targeted reference trajectory." A potential advantage in the direct ascent missions is that the conclusions contained herein will be completely general and thus will apply to any date and launch time. In particular it will be shown that those variables related to launch conditions do not strongly influence the abort parameters.

*With six points of thrust termination specified for each of the nine basic trajectories.

The parameters entering into analysis may be written in the following order:

A.
1) Azimuth of launch (A_L)
2) Nominal trajectory defined by injection angle (nominal β_I)
3) Premature thrust termination defined by S-IVB burn-time-to-go to nominal burnout (Δt_{go})

B.
1) Impulsive abort velocity increment (ΔV_{ABORT})
2) Coast time between cutoff and abort initiation (Δt_{coast})

C.
1) Total return time from cutoff to landing including any coast time
2) Location of landing site given by latitude and longitude in a geographic coordinate system.

The above grouping of parameters is made to indicate their different roles in the abort problem. The group A parameters are initial state variables which describe the conditions at abort initiation. The group B parameters are control variables since this group contains the decision processes necessary to determine the outcome variables, group C, once the mission is underway. On the other hand, it is necessary to understand the nature of of the influence that group A variables have on the outcome, group C, from the standpoint of decisions that could be made prior to launch.

The question for minimum time aborts is: what choice of group B variables result in the fastest return? Having determined these, how are they related to the initial variables in group A?

Looking at the problem geometrically, it becomes apparent that minimum time returns for planar aborts not confined to specific landing sites involves only the in-plane elements of the trajectory. These abort modes are a function of the distance from the earth, the true anomaly, the post-abort velocity and, to some extent, the burnout flight path angle. These are independent of launch azimuth. It will also be seen that nominal β_I resulting from the trajectory shaping plays a minor role in the return time except for those aborts very near the earth and thus for early thrust

terminations. Thrust termination defined by Δt_{go}, on the other hand, plays an important role on the pre-abort trajectory and, in turn, on the return time. Again Figure 3-15 shows the large variation in radius as a function of time from cutoff for various Δt_{go}. This effect carries over into Figures 3-26 and 3-27 showing total return time as a function of coast time from cutoff. Here also can be observed the small influence played by nominal β_I. One conclusion is immediately drawn—to return in minimum time, the abort must be initiated as soon as possible. There is however, an extenuating case that will be discussed later in connection with returns using low abort velocity increments.

Having discussed the effect of the state variables group A, a discussion of the control variables group B, ΔV_{ABORT} and cost time, follows. The effect of the latter is clearly in evidence in Figures 3-26 and 3-27 and shares the same conclusions drawn for the radius at which aborts should be initiated. The effect of abort velocity increment is also evident in this figure; however, an illustrative example may be seen in Figures 3-28 and 3-29. Here an attempt is made to graphically represent the range in return times from cutoff to apogee as influenced by burn-time-to-go and abort velocity increment. Examination of the charts, done for nominal β_I = 84 degrees but equally applicable to all β_I between 72 and 108 degrees, reveals the following: the percentage improvement in return time with increase in ΔV_{ABORT} is quite large near the cutoff point but gets progressively smaller with increasing distance. This must be viewed in connection with the fact that the pre-abort velocity is higher near the cutoff than at apogee. Reference again to Figure 3-17 will show the typical plot of velocity versus radius for nominal β_I = 84 degrees. Figure 3-18 shows the typical velocity contour for various nominal β_I at burn-times-to-go of 15 and 60 seconds. It is again seen that no advantage, in general, is gained by extended coast and an early abort is more favorable. In addition, Figures 3-26 through 3-29 indicate that return time is substantially reduced with increase in the applied abort velocity increment for the one-impulse type of aborts. This fact again might have been established a priori.

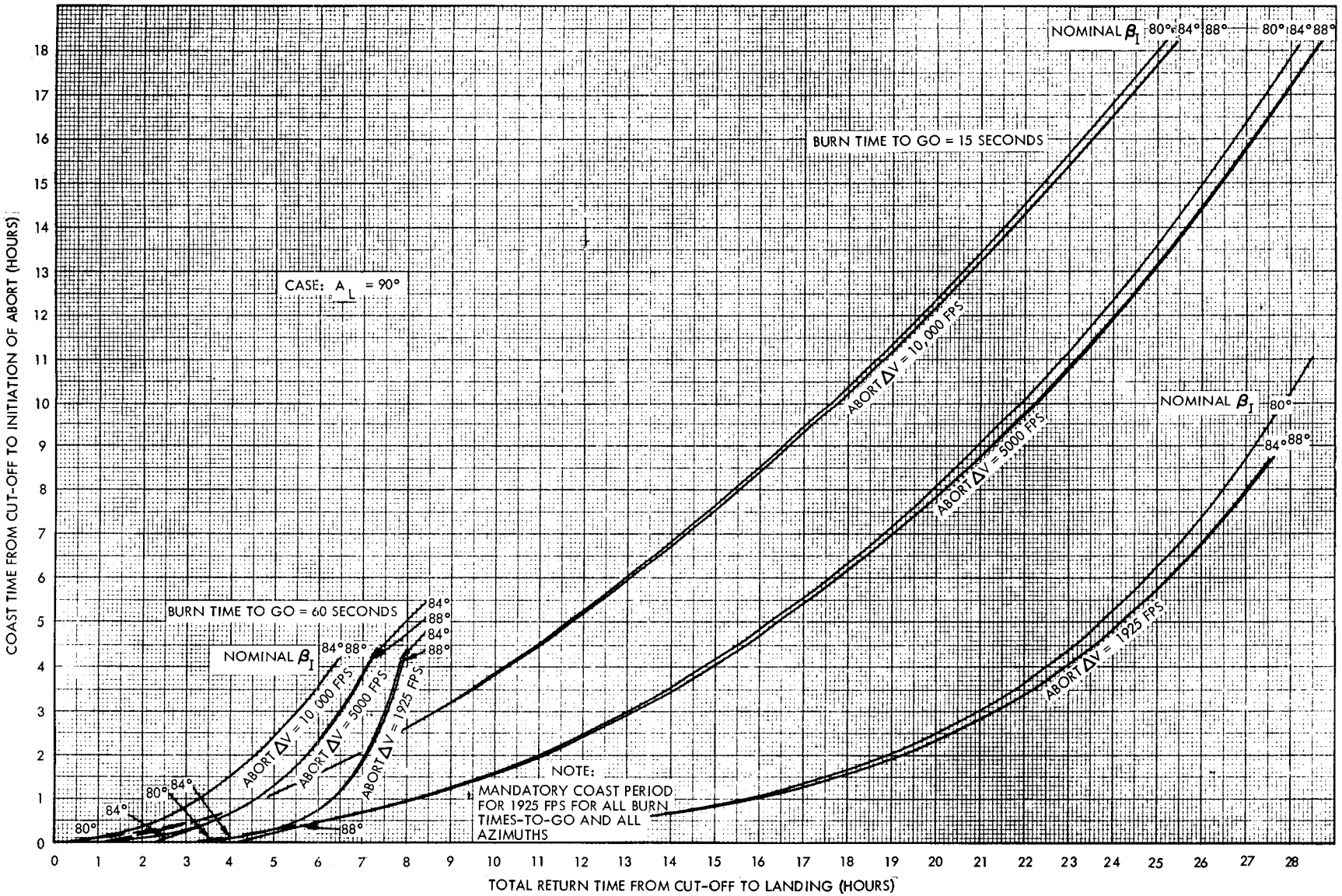

Figure 3-26. Total Return Time from Premature Cutoff to Landing as a Function of Coast Time Prior to the Abort Initiation for a Variation in Abort Velocity Increment at 15 and 60 Seconds Burn Time-To-Go

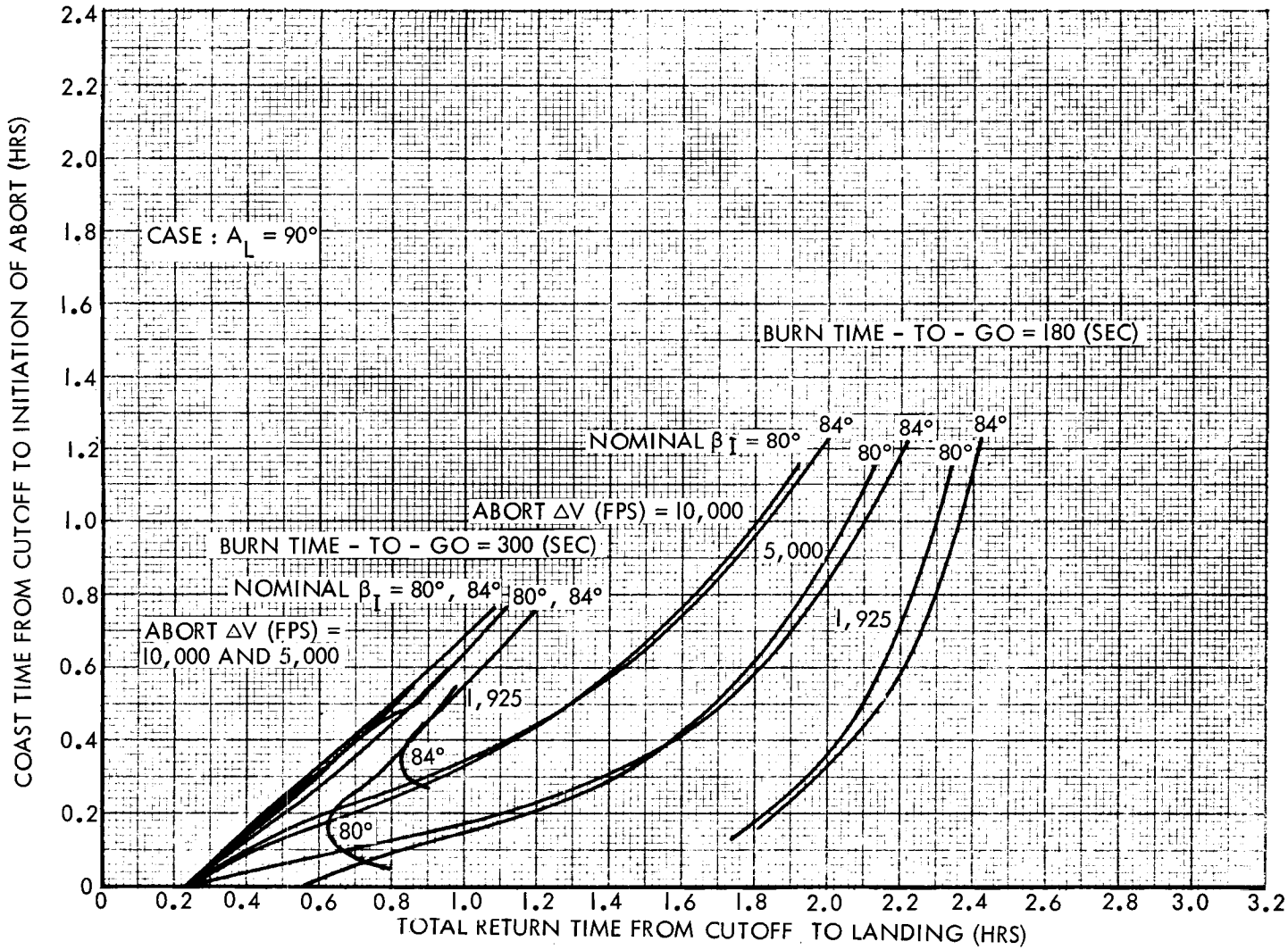

Figure 3-27. Total Return Time from Premature Cutoff to Landing as a Function of Coast Time Between Cutoff and Abort Initiation for a Variation in Abort Velocity Increment at 180 and 300 (Sec) Burn Time-To-Go

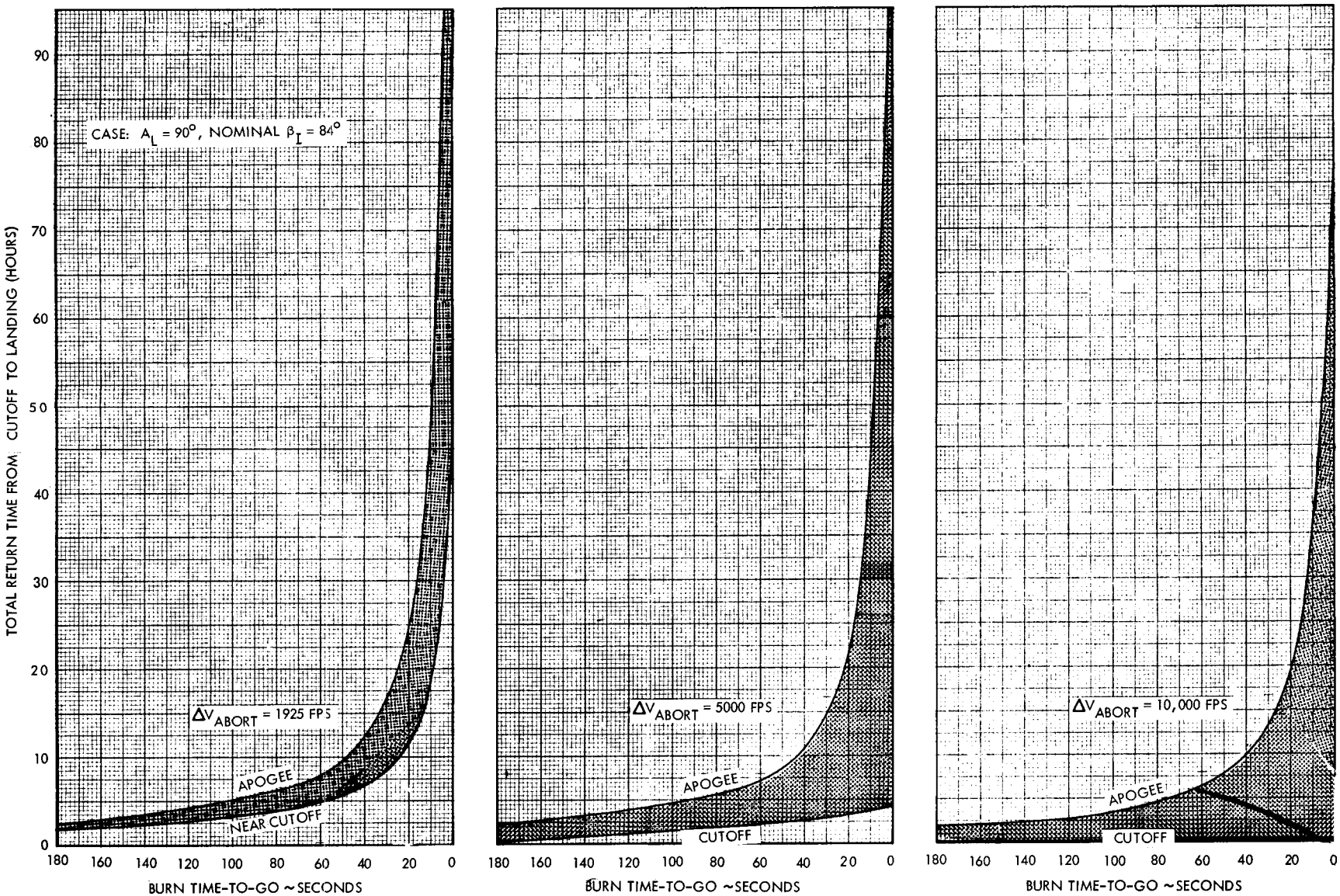

Figure 3-28. Limits of Total Return Time Variation for Burn Times-To-Go Between 0 and 180 Seconds; Planar Survival Aborts

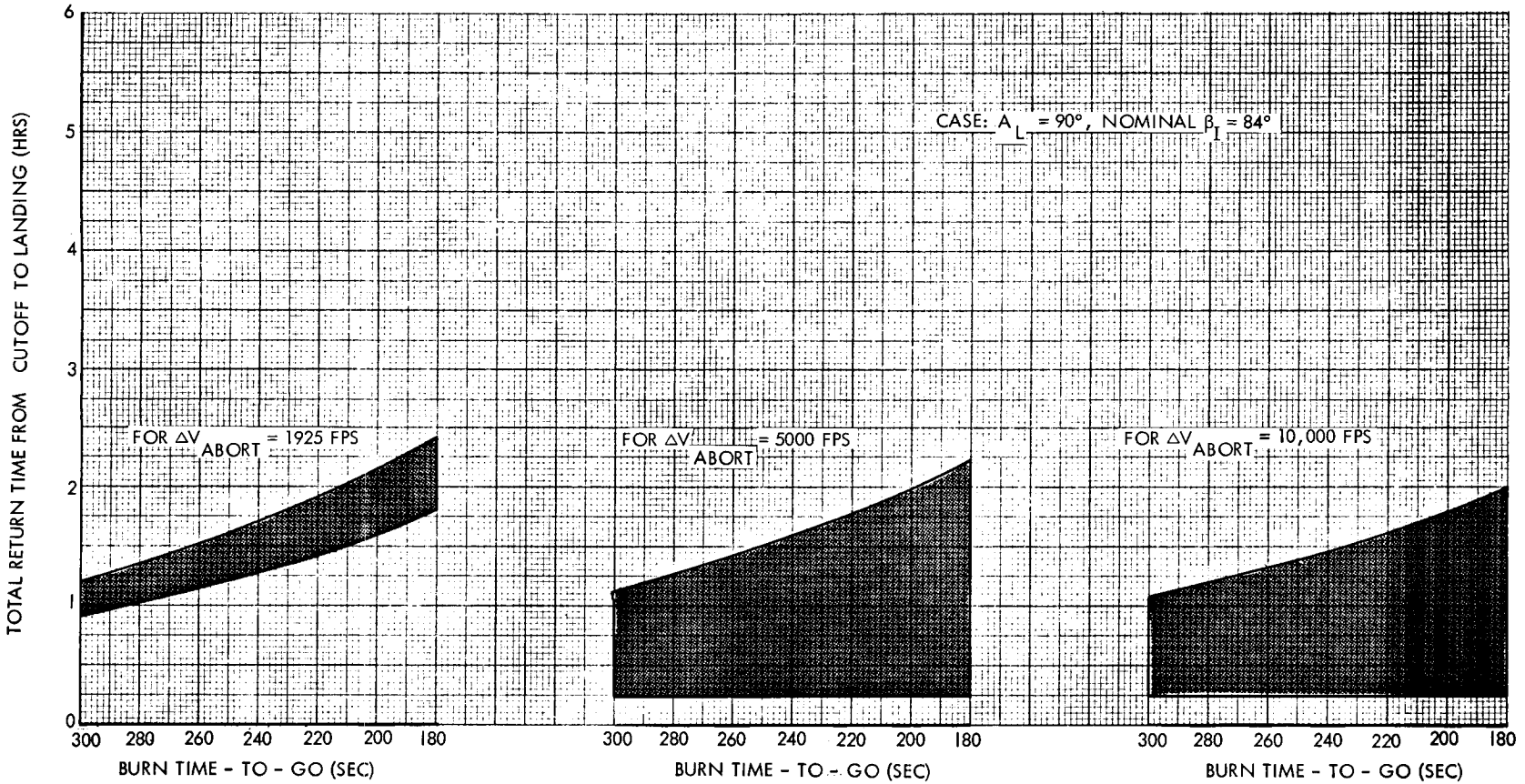

Figure 3-29. Limits of Total Return Time Variation for Burn Times-To-Go Between 180 and 300 (Sec); Planar Survival Aborts

Higher abort velocity increments provide for larger angular changes in the pre-abort velocity vector; this capability is especially important for direct returns at the lower altitudes where pre-abort velocities are large. In fact, for the lower velocity increments, returns are only possible through apogee passage trajectories with a post-abort velocity vector directed away from the earth. Reference to Table 3-4 will indicate the effect of pre-abort radius and velocity, burn-time-to-go and abort velocity increment on the type of return trajectory. These results also indicate that for the earlier cutoffs the pre-abort velocity vector is already pointed near the local horizontal; consequently, there is an increase in the number of aborts toward the earth for the smaller abort velocity increment.

It should also be noted that for the lower abort velocity increment no solutions were obtained at the zero coast or cutoff point. There is reason to believe that this region of "no abort" may extend over a meaningful time period beyond cutoff for a range of low thrust abort velocity increments. (Figure 3-30.) Figures 3-31 and 3-32 show the contrast with higher abort velocity impulses. In view of this fact, and with the conclusions reached concerning aborting as early as possible, it becomes imperative that more information be obtained in this area. The consequences of an attempted abort in this region with, say, the first stage LEM thrust should certainly be evaluated. If a mandatory coast period is required, as seems to be the case here, its extent should be carefully determined.

Figure 3-33 indicates the range of inertial reentry velocities obtained. Although this example is shown for a nominal β_I of 84 degrees, very little variation occurs for other β_I angles. Table 3-5 gives some representative values for the three values of β_I covering the range of this study at burn-times-to-go of 0, 30, and 60 seconds.

Table 3-4. Summary of Abort Trajectory Type as Indicated by the Post Abort Velocity Direction Relative to the Earth

	S-IVB Burn Time-To-Go = 0 Seconds						S-IVB Burn Time-To-Go = 15 Seconds						S-IVB Burn Time-To-Go = 30 Seconds					
Radius Increment	Radius (10^6 ft)	Velocity (fps)	True Anomaly (deg)	Abort Velocity Direction 1925 fps	5000 fps	10,000 fps	Radius (10^6 ft)	Velocity (fps)	True Anomaly (deg)	Abort Velocity Direction 1925 fps	5000 fps	10,000 fps	Radius (10^6 ft)	Velocity (fps)	True Anomaly (deg)	Abort Velocity Direction 1925 fps	5000 fps	10,000 fps
Cutoff	21.806	35,662	12.061	None	Away	Away	21.7434	34,896	11.497	None	Away	Toward	21.6967	34,281	11.033	None	Away	Toward
1	163.364	12,371	139.68	Away		Away	53.9501	21,090	106.37	Away		Away	40.3719	23,978	92.383	Away		Away
2	304.923	8,546	152.48			Toward	86.1569	15,802	126.89				59.0472	18,825	114.68			
3	446.482	6,615	158.81				118.364	12,681	138.19			Away	77.7224	15,486	127.79			
4	588.041	5,346	162.94		Away		150.570	10,484	145.94			Toward	96.3976	13,024	137.09			Away
5	729.600	4,392	166.04		Toward		182.777	8,773	151.91				115.073	11,056	144.41			Toward
6	871.158	3,608	168.58				214.984	7,341	156.91				133.748	9,386	150.62			
7	1012.720	2,916	170.83				247.191	6,069	161.40		Away		152.423	7,892	156.26		Away	
8	1154.280	2,257	172.99	Away		Toward	279.397	4,869	165.74		Toward		171.099	6,490	161.76		Toward	
9	1295.480	1,559	175.32	Toward			311.604	3,646	170.47	Away			189.774	5,092	167.78	Away		
10	1436.930	540	180.00	Toward	Toward		343.811	2,197	179.990	Toward	Toward	Toward	208.449	3,555	180.00	Toward	Toward	Toward

	S-IVB Burn Time-To-Go = 60 Seconds						S-IVB Burn Time-To-Go = 180 Seconds						S-IVB Burn Time-To-Go = 300 Seconds					
Radius Increment	Radius (10^6 ft)	Velocity (fps)	True Anomaly (deg)	Abort Velocity Direction 1925 fps	5000 fps	10,000 fps	Radius (10^6 ft)	Velocity (fps)	True Anomaly (deg)	Abort Velocity Direction 1925 fps	5000 fps	10,000 fps	Radius (10^6 ft)	Velocity (fps)	True Anomaly (deg)	Abort Velocity Direction 1925 fps	5000 fps	10,000 fps
Cutoff	21.6169	33,125	10.111	None	Away	Toward	21.4381	29,239	6.525	None	Toward	Toward	21.3970	26,150	1.770	None	Toward	Toward
1	31.0320	26,497	75.869	Away		Away	23.2968	27,389	49.381	Away	Away		21.5729	25,945	38.289			
2	40.4471	22,157	98.715				25.1554	25,708	68.952				21.7488	25,740	54.988	None		
3	49.8622	18,960	113.44				27.0141	24,163	83.833				21.9247	25,538	68.532	Away		
4	59.2774	16,426	124.46			Away	28.8728	22,733	96.424				22.1006	25,337	80.705			
5	68.6925	14,308	133.45			Toward	30.7314	21,397	107.74				22.2765	25,138	92.276	Away		
6	78.1076	12,463	141.29				32.5901	20,139	118.39				22.4524	24,940	103.76	Toward		
7	87.5227	10,795	148.54				34.4488	18,946	128.89		Away		22.6283	24,744	115.64			
8	96.9378	9,236	155.71		Away		36.3074	17,808	139.87		Toward		22.8042	24,549	128.67			
9	106.353	7,719	163.67	Away	Toward		38.1661	16,714	152.63	Away			22.9802	24,356	144.47			
10	115.768	6,169	180.00	Toward	Toward	Toward	40.0248	15,656	180.00	Toward	Toward	Toward	23.1561	24,164	179.88	Toward	Toward	Toward

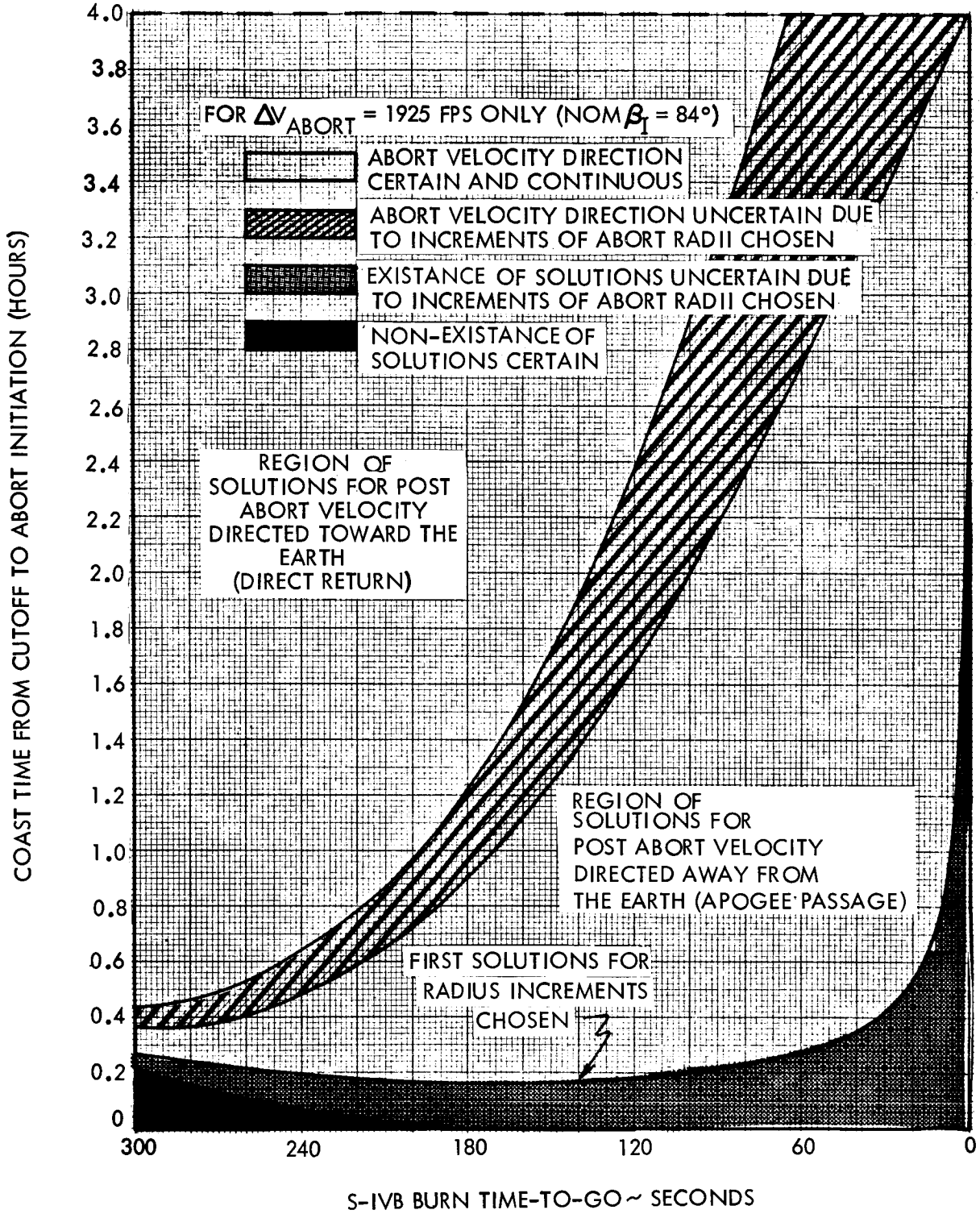

Figure 3-30. Abort Solution Contour Indicating Types of Abort Trajectories Obtained as a Function of Burn Time-To-Go and Coast Time from Cutoff; ΔV_{ABORT} = 1925 Fps

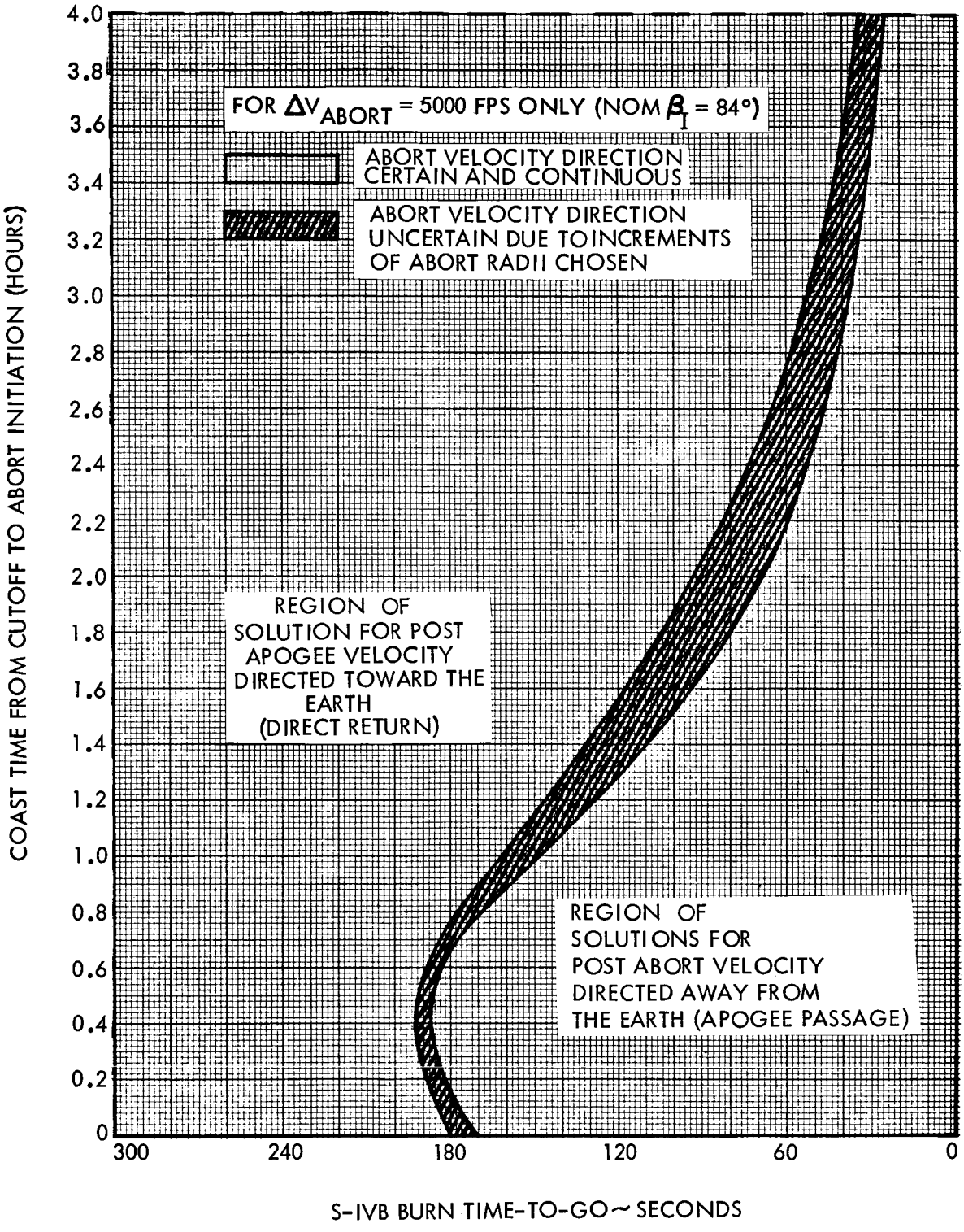

Figure 3-31. Abort Solution Contour Indicating Types of Abort Trajectories Obtained as a Function of Burn Time-To-Go and Coast Time from Cutoff; ΔV_{ABORT} = 5000 Fps

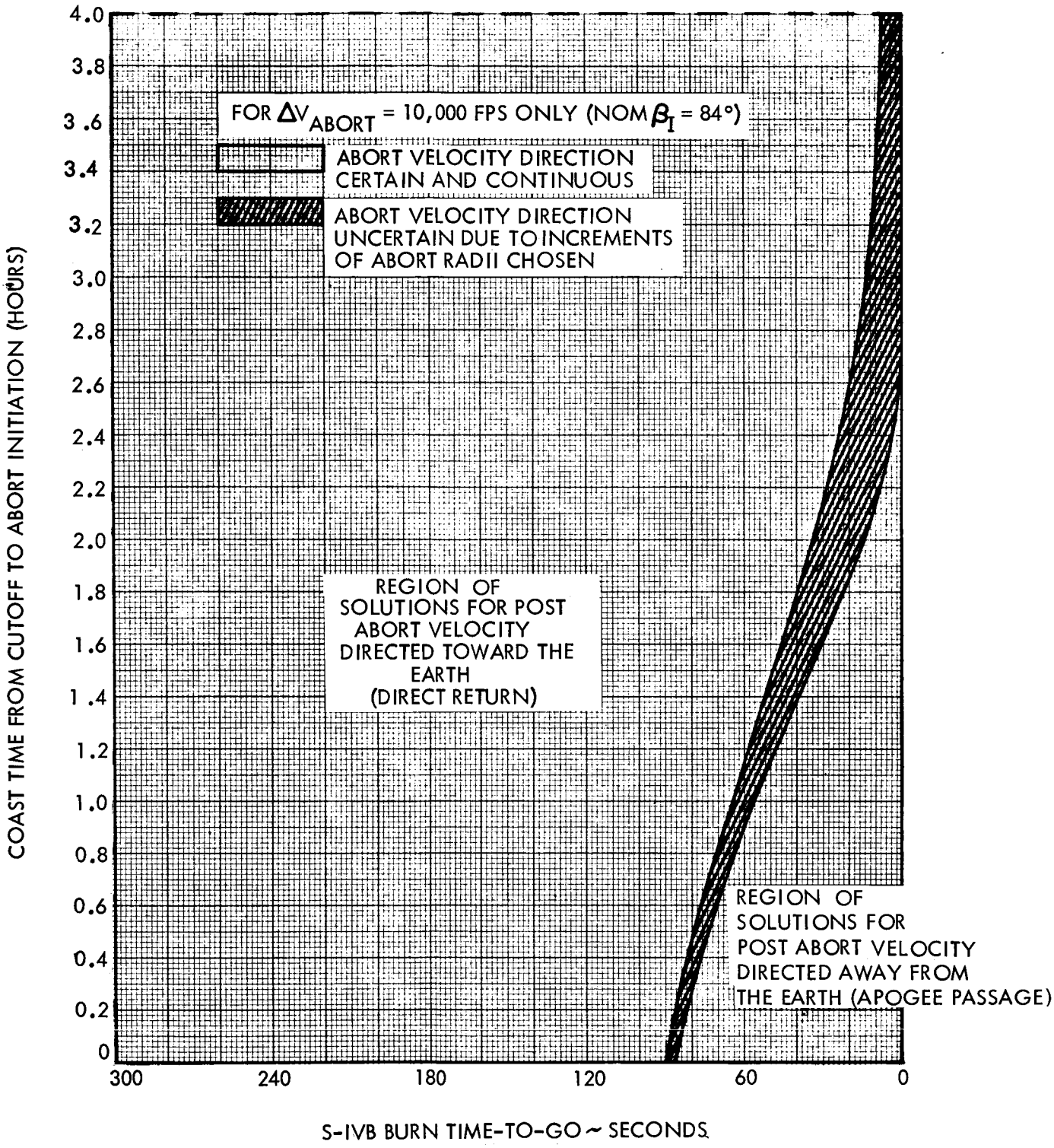

Figure 3-32. Abort Solution Contour Indication Types of Abort Trajectories Obtained as a Function of Burn Time-To-Go and Coast Time from Cutoff; ΔV_{ABORT} = 10,000 Fps

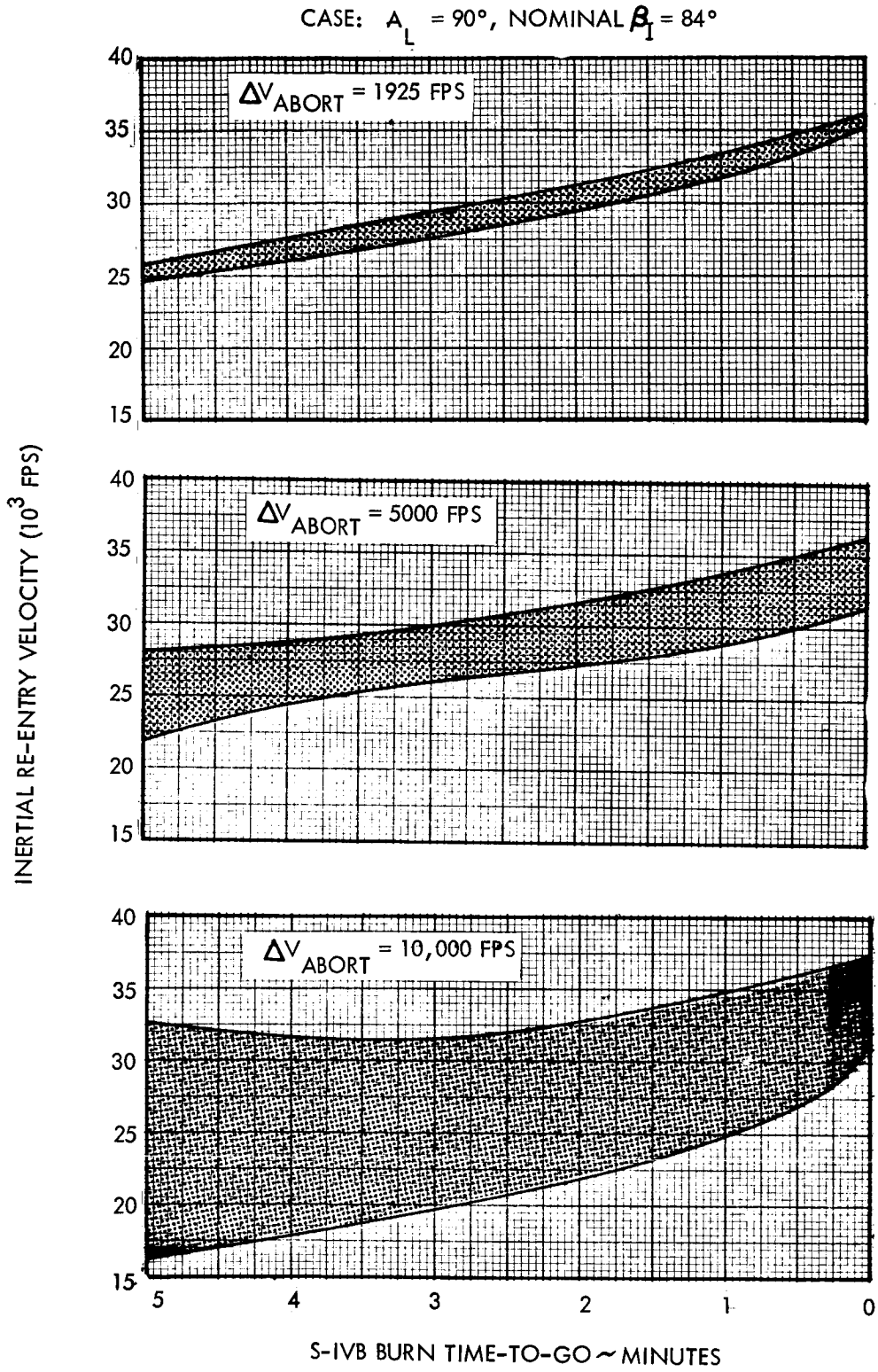

Figure 3-33. Limits of Inertial Re-entry Velocity Variation for Minimum Time Aborts

Table 3-5. Some Representative Values of the Abort Reentry Velocities

ΔT_{GO} (sec)	ΔV_{ABORT} (fps)	Limit	$\beta_I = 80^\circ$	$\beta_I = 84^\circ$	$\beta_I = 88^\circ$
0	1,925	Upper	35,968	35,968	35,968
		Lower	35,488	35,488	35,489
	5,000	Upper	36,023	36,023	36,023
		Lower	31,339	31,565	32,268
	10,000	Upper	36,668	36,668	36,668
		Lower	26,501	31,723	27,311
30	1,925	Upper	34,621	34,658	34,664
		Lower	33,386	33,436	33,451
	5,000	Upper	34,931	34,967	34,972
		Lower	29,778	30,047	30,873
	10,000	Upper	35,999	36,034	36,039
		Lower	25,090	26,967	25,448
60	1,925	Upper	33,376	33,438	33,452
		Lower	31,949	32,021	32,043
	5,000	Upper	33,705	33,766	33,779
		Lower	28,499	28,812	30,805
	10,000	Upper	34,838	34,895	34,907
		Lower	24,035	24,774	24,009

Discussing now the landing location for these type of aborts, it is observed in Figure 3-34 that the time of cutoff plays an important role in determining the form of the landing locii. Early cutoffs, represented by 180 and 300 seconds burn-time-to-go, exhibit the familiar trace of an earth orbit. This is indicative of the orbital character of the pre-abort free-flight trajectory. These trajectories indicate a uniformity in landing location, progressing in an easterly or posigrade sense from a point off the west African coast. Although they appear to terminate off the California coast at a north latitude near 28 degrees, they would in fact, continue in the orbit trace if abort points beyond apogee were included. Figure 3-34 also indicates the dispersion in landing site due to launch azimuth variation. All data presented are results of an abort velocity impulse of 10,000 fps. Figure 3-35 exhibits the effect of different velocity impulses on landing location. Aborts immediately at cutoff using 5000 fps velocity impulse, land in the Caribbean area instead of landing near the African coast as with the 10,000 fps aborts. No cutoff aborts are possible using 1925 fps. Data points are numbered for convenience in determining the direction of landing site progression. The numbers correspond to the ten ordered radius increments arbitrarily selected for abort points. To avoid clutter, all data points are not shown. The numbering, therefore, does not necessarily run in consecutive order. Point 10, in every case, represents the landing for an abort initiated at apogee of the coast trajectory.

For cutoffs between 0 and 60 seconds burn-time-to-go, aborts yield landing sites predominantly lying in the northern hemisphere because of the in-plane return angles required and the elapsed time of return. These aborts occur at considerably greater altitudes (beyond one earth radius) than those from earlier cutoff trajectories. Return angles (the change in true anomaly) generally are in the range of 160 to 360 degrees with the exception of aborts at cutoff for 10,000 fps velocity impulse which return in less than an hour with in-plane angles between 45 and 65 degrees.

Figure 3-36 shows the abort point and landing latitude dispersions representing a nominal β_I = 84 degrees and a cutoff at 15 seconds burn time remaining. The dispersion is shown to be function of the change in true

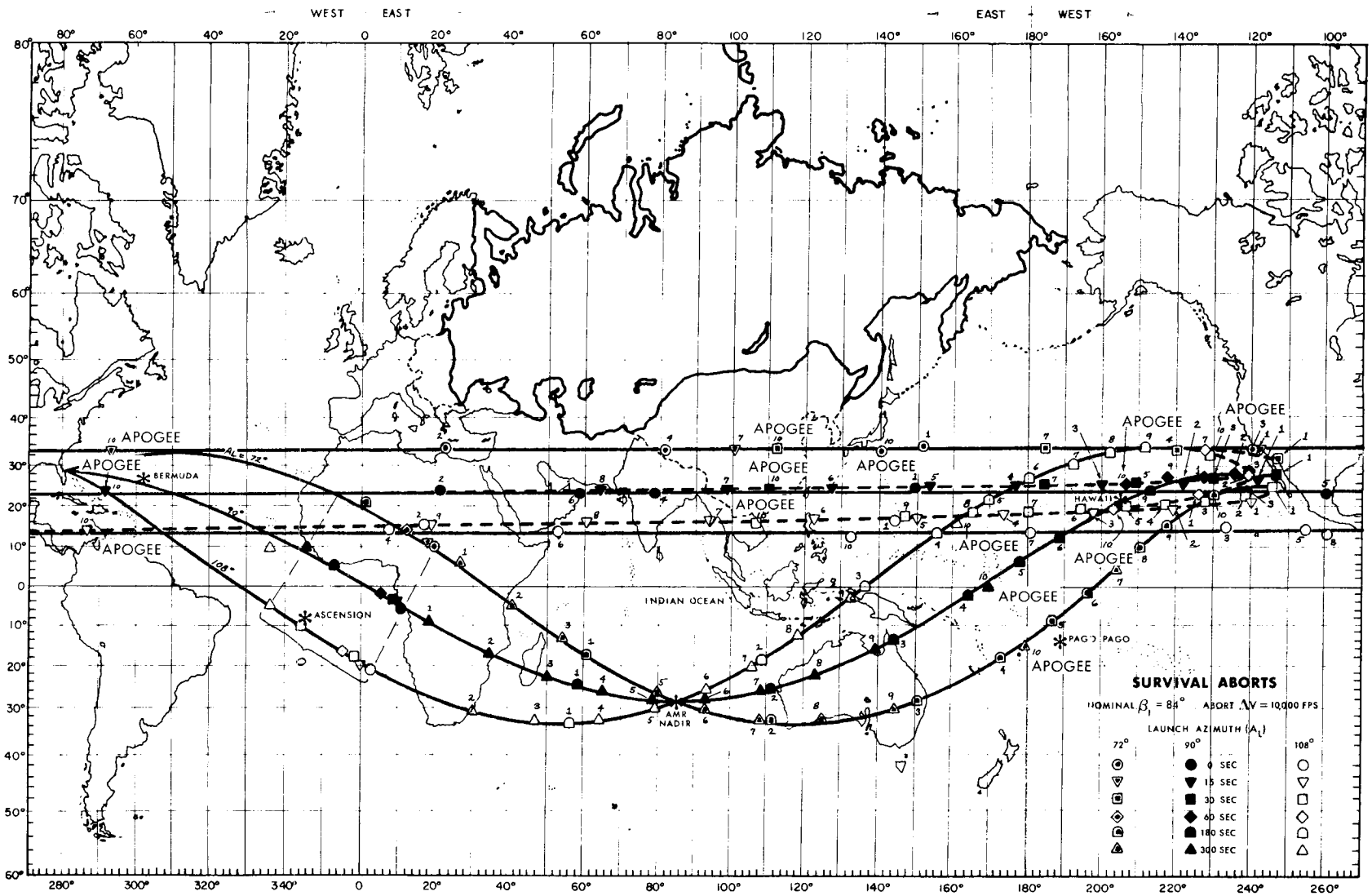

Figure 3-34. Landing Site Loci for Various Launch Azimuths as a Function of Burn Time-to-Go at Cutoff

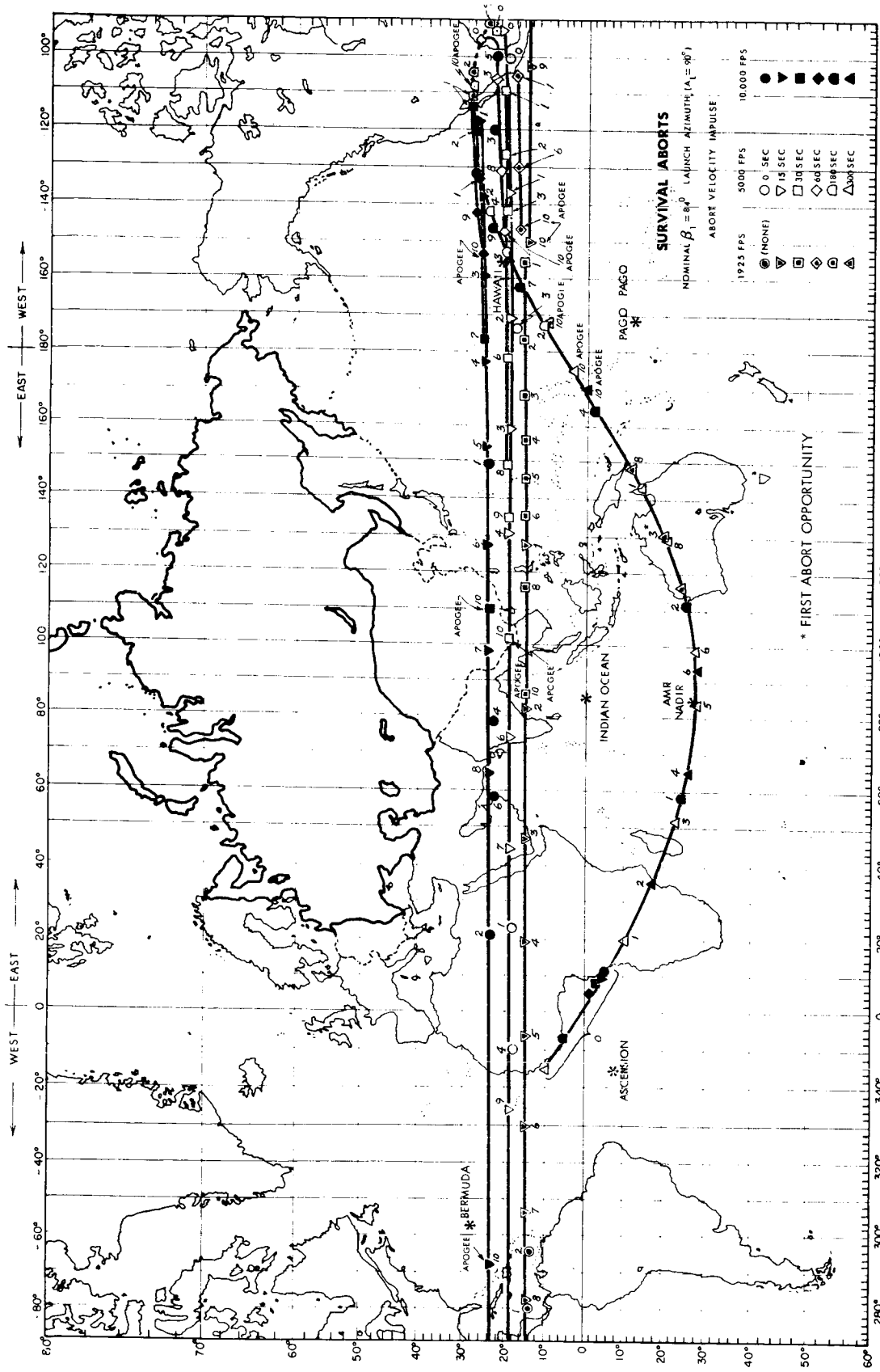

Figure 3-35. Landing Site Loci as a Function of Abort Velocity Impulse and Burn Time-to-Go at Cutoff

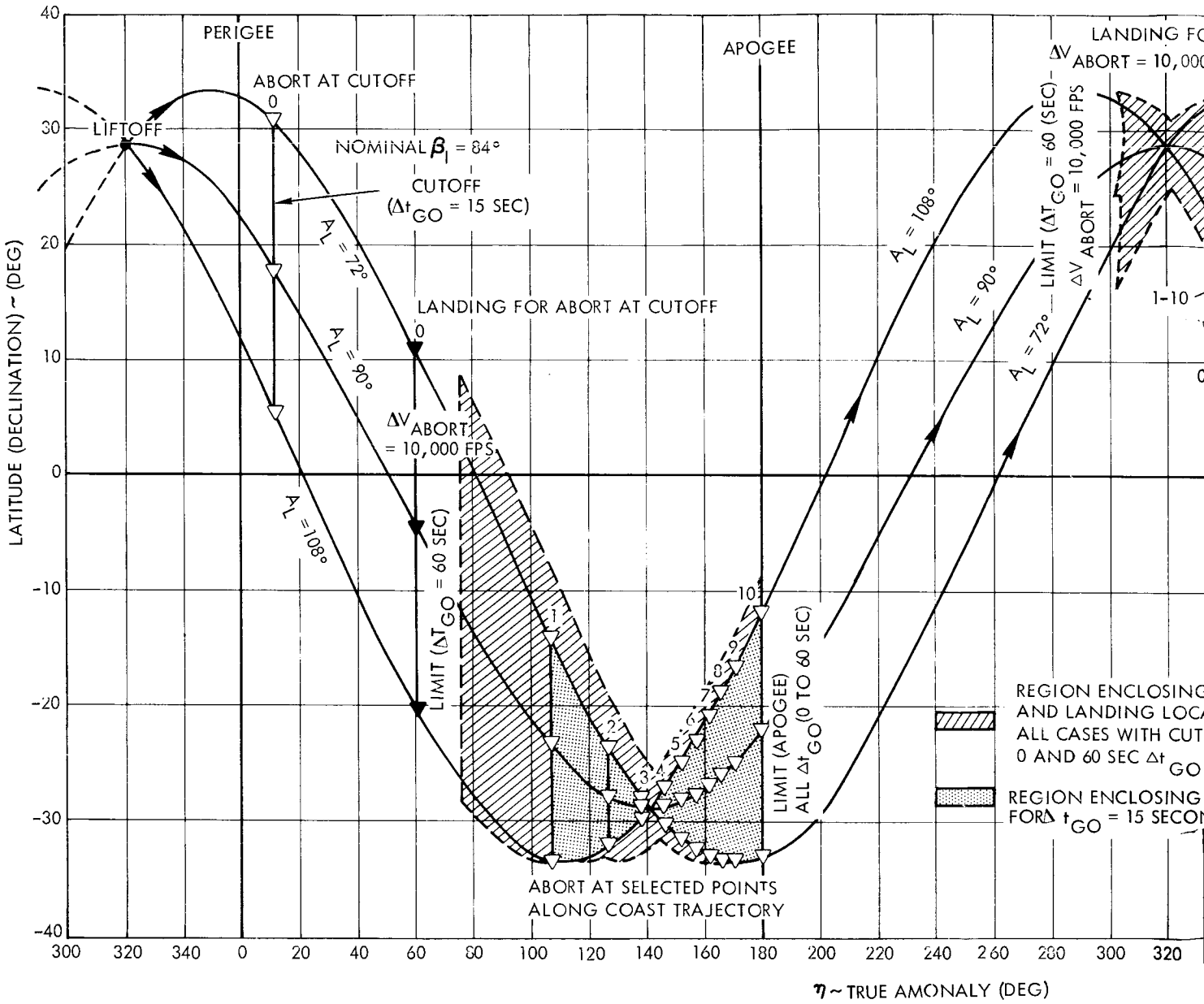
PERIGEE
APOGEE
LIFTOFF
ABORT AT CUTOFF
NOMINAL β_1 = 84°
CUTOFF (Δt_{GO} = 15 SEC)
LANDING FOR ABORT AT CUTOFF
ΔV_{ABORT} = 10,000 FPS
A_L = 72°
A_L = 90°
A_L = 108°
LIMIT (ΔT_{GO} = 60 SEC)
LIMIT (APOGEE) ALL Δt_{GO} (0 TO 60 SEC)
ABORT AT SELECTED POINTS ALONG COAST TRAJECTORY
LANDING FO
ΔV_{ABORT} = 10,000
LIMIT (ΔT_{GO} = 60 (SEC)
ΔV_{ABORT} = 10,000 FPS
1-10
REGION ENCLOSING
AND LANDING LOCA
ALL CASES WITH CUT
0 AND 60 SEC Δt_{GO}
REGION ENCLOSING
FOR Δt_{GO} = 15 SECON
LATITUDE (DECLINATION) ~ (DEG)
η ~ TRUE AMONALY (DEG)

I-159
1

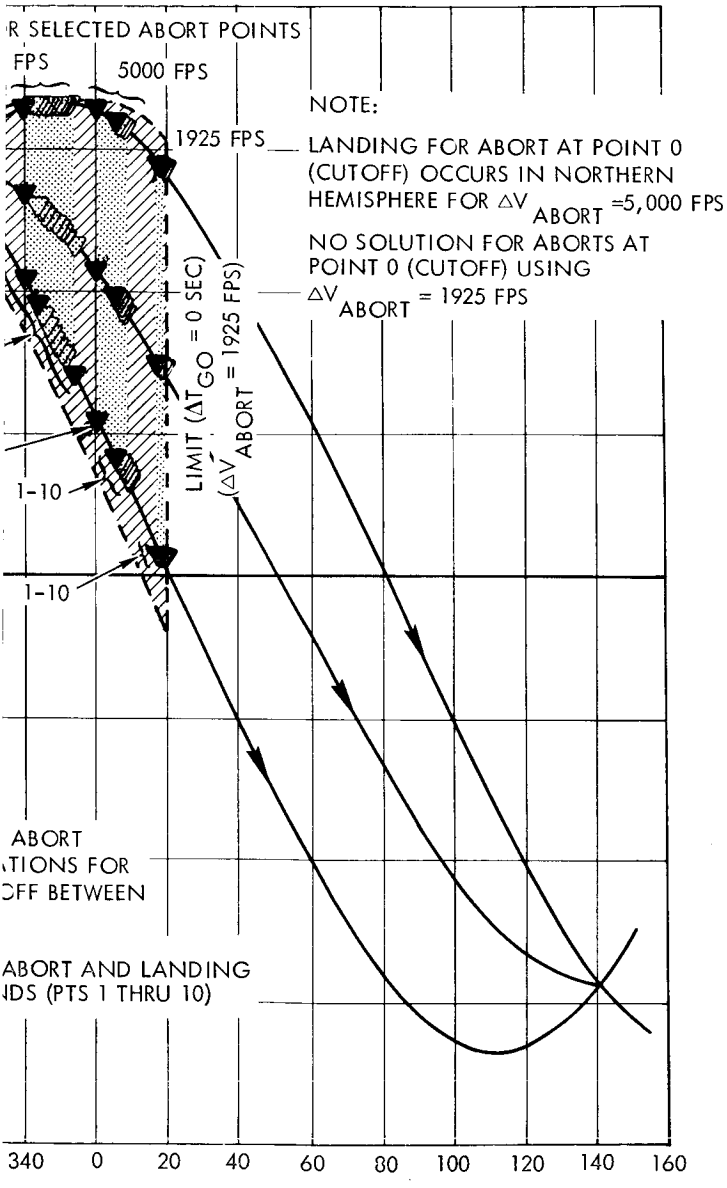

TIME OF ABORT (HRS)

POINT		TIME FROM LIFTOFF	TIME FROM CUTOFF
(CUTOFF)	0	0.28	0
	1	0.91	0.63
	2	1.53	1.25
	3	2.28	2.00
	4	3.17	2.89
	5	4.23	3.95
	6	5.50	5.22
	7	7.04	6.76
	8	8.97	8.69
	9	11.63	11.35
(APOGEE)	10	18.41	18.13

TIMES OF LANDING (HOURS)

POINT		TIME FROM CUTOFF			TIME FROM ABORT			FPS
		1925	5000	10,000	1925	5000	10,000	
(CUTOFF)	0	NONE	3.42	0.26	NONE	3.42	0.26	
	1	13.89	6.74	3.68	13.26	6.11	3.05	
	2	16.94	9.03	5.30	15.69	7.78	4.05	
	3	19.21	11.04	6.87	17.21	9.04	4.87	
	4	21.11	12.95	8.48	18.22	10.06	5.59	
	5	22.82	14.83	10.17	18.87	10.88	6.22	
	6	24.41	16.73	11.99	19.20	11.51	6.77	
	7	25.96	18.72	13.99	19.21	11.97	7.24	
	8	27.53	20.89	16.29	18.84	12.20	7.60	
	9	29.26	23.45	19.14	17.91	12.11	7.79	
(APOGEE)	10	32.41	28.60	25.36	14.29	10.48	7.24	

Figure 3-36. Abort Point and Landing Site Latitude Variation as a Function of Abort True Anomaly

anomaly as influenced by launch azimuth, radial distance (represented by the 10 selected abort points, numbered consecutively along the coast trajectory) and the velocity impulse applied. The cross hatched areas represent the range of variation for all cases between 0 and 60 seconds burn-time-to-go. The limits of these regions are identified by the constituent cases (Δt_{go} and ΔV_{ABORT}). The abort region is limited on the right by apogee of the coast trajectory since no aborts beyond this point are considered. Aborts initiated immediately at cutoff using 10,000 fps velocity impulse, land in a very short time as indicated by the 0 landing point to the left of the major abort region. The use of 5000 fps moves this landing point into the major landing region. No solution exists using 1925 fps. The difference in true anomaly between any abort point and its corresponding landing point is the in-plane return angle. These vary between 165 and 235 degrees for 10,000 fps aborts, between 190 and 350 degrees* for 5000 fps and between 200 and 270 degrees for 1925 fps.

For the case: $A_L = 90$; nominal $\beta_I = 84$ degrees; $\Delta V_{ABORT} = 10,000$ fps, Figure 3-37 presents the variation in longitude as a function of total return time from cutoff to landing. The curves representing 180 and 300 seconds burn-time-to-go terminate at then respective apogee points. The curves representing the later cutoff exhibit first a posigrade then a retrograde direction of impact as previously indicated on the map of Figure 3-34. Figures 3-38 and 3-39 show the longitude variation for launch azimuths of 72 and 108 degrees, respectively.

For near nominal cutoff, opportunities for landing in the southern hemisphere are restricted to aborts at less than one or greater than 24 hours from liftoff. Landing will be, for the most part, between 0 and 180 degrees east longitude. Abort opportunities occurring early in the S-IVB burn are more advantageous for a southern landing with the additional merit of shorter return times. One region in the northern hemisphere appears to be quite promising as a landing site. That is the Pacific Ocean area around Hawaii.

*Includes the abort from cutoff, point 0 (otherwise 190 to 259 degrees).

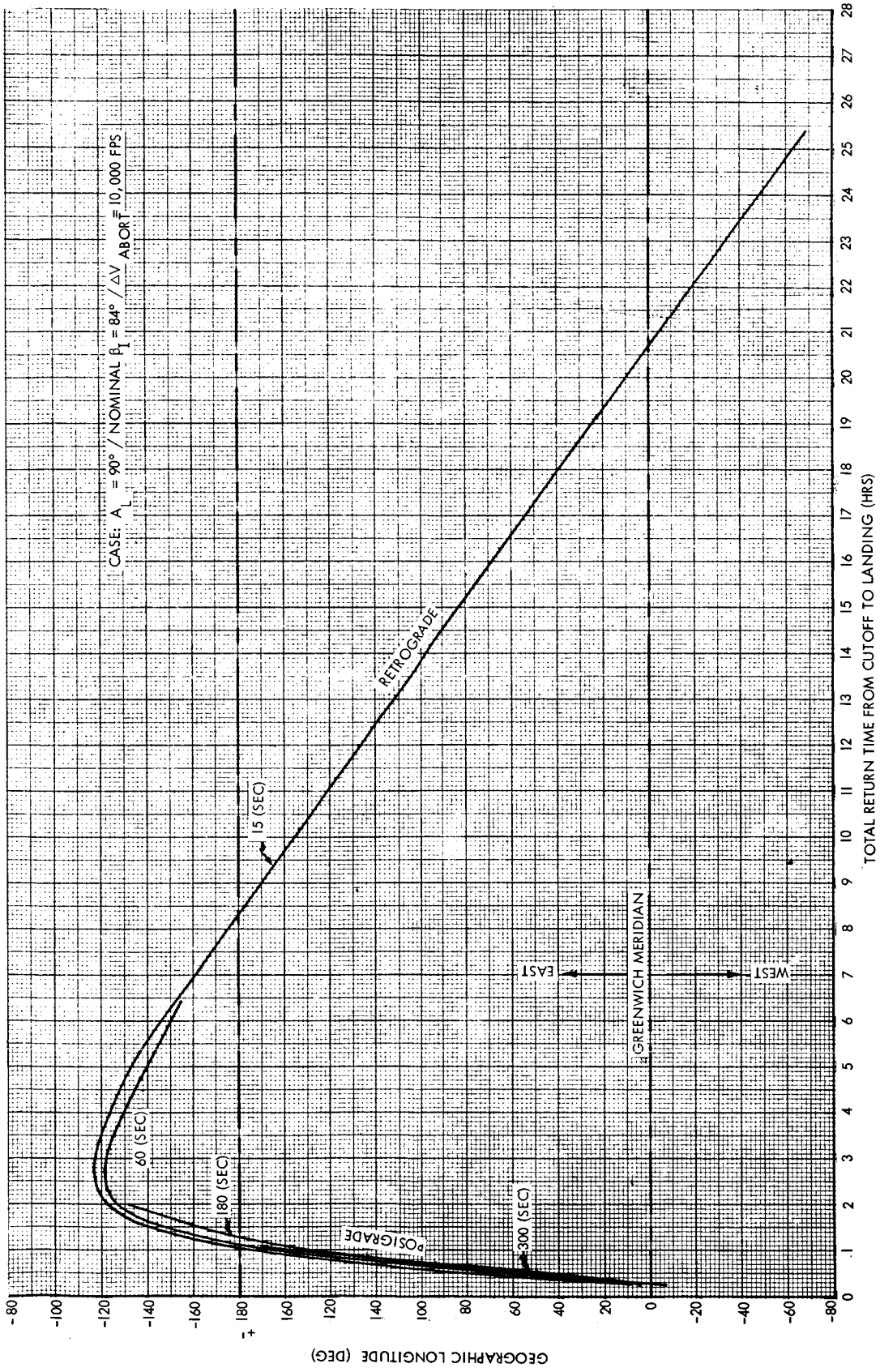

Figure 3-37. Longitude of Landing Site as a Function of Total Return Time from Cutoff to Landing for a Variation in S-IVB Burn Time-To-Go

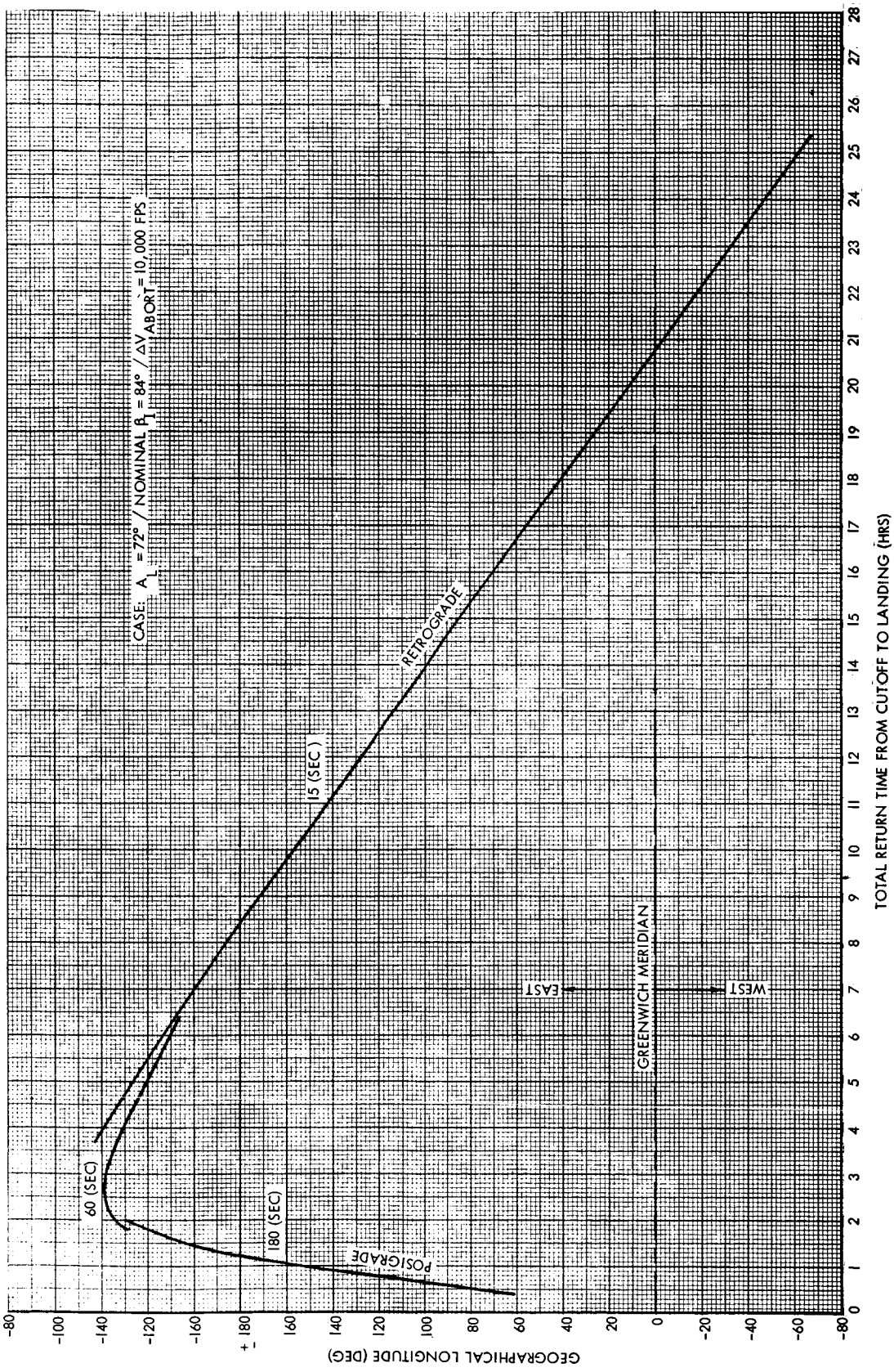

Figure 3-38. Longitude of Landing Site as a Function of Total Return Time from Cutoff to Landing for a Variation in S-IVB Burn Time-To-Go

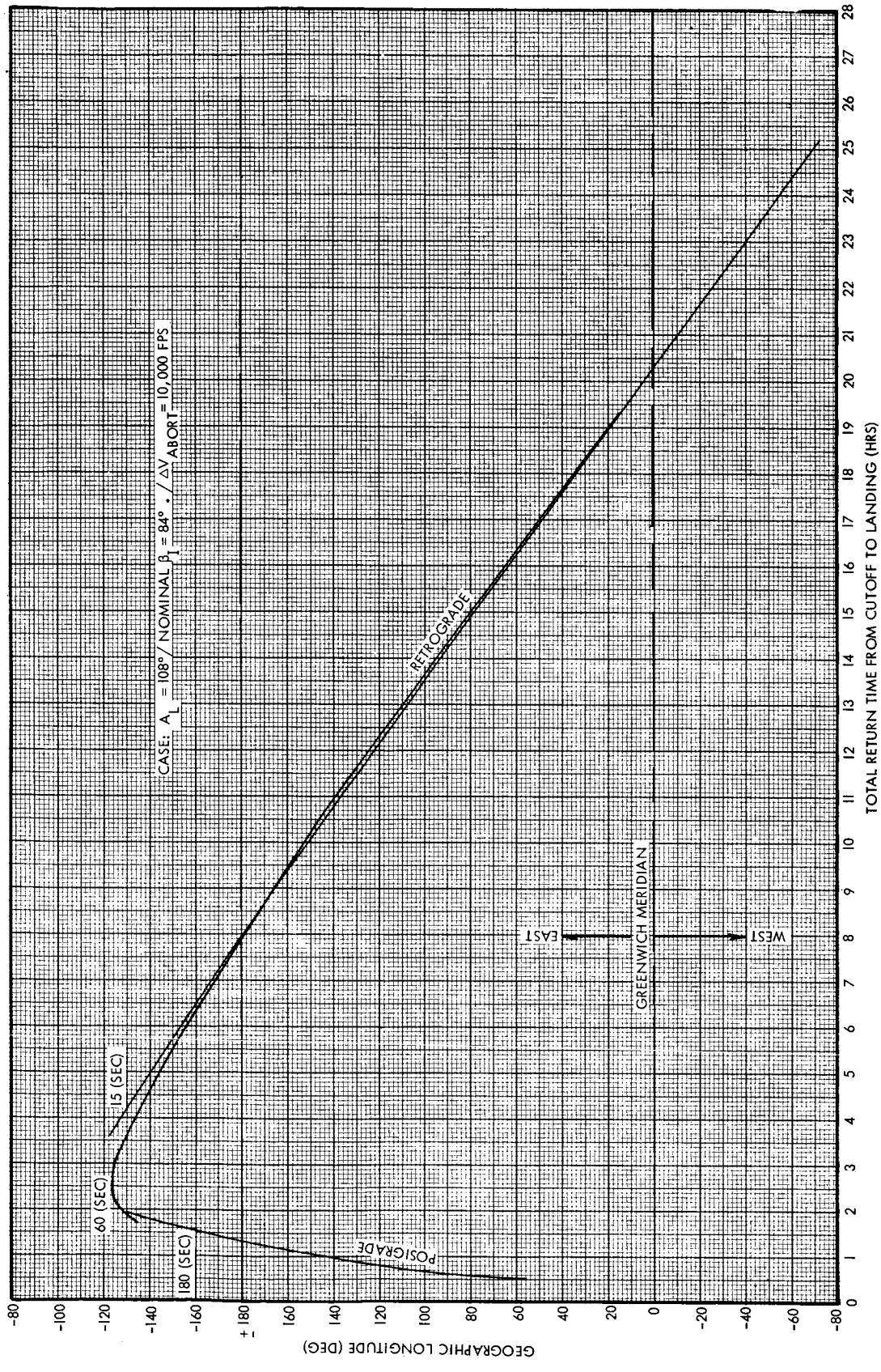

Figure 3-39. Longitude of Landing Site as a Function of Total Return Time from Cutoff to Landing for a Variation in S-IVB Burn Time-To-Go

3.6 RETURNS TO SPECIFIC LANDING AREAS

Budget does not permit a full evaluation of this area of the study. Some analysis was completed but produced only preliminary results. Additional computer programming and checkout will be necessary to facilitate further study. Some quantitative understanding can, however, be gained from the current abort program output.

The primary landing sites selected for this study were:

a)	Bermuda	58° W Longitude 27° N Latitude
b)	Ascension	14.5° W Longitude 8° S Latitude
c)	Indian Ocean	87° E Longitude 0° Latitude
d)	AMR Nadir	85° E Longitude 28° S Latitude
e)	Pago Pago	171° W Longitude 14° S Latitude
f)	Hawaii	155° W Longitude 22° N Latitude

In general, the approach taken in effecting a solution was to match the longitude of a particular site with that of the closest approaching loci of landing points from the minimum time aborts. This defines a range of radii for which abort trajectories are nearly in phase with the site at touchdown. The latitude match is obtained by a plane change. The resultant error is removed by an adjustment in flight time by an iteration on the abort velocity impulse ΔV_{ABORT}. Perhaps a more desirable method, for future studies, would be to hold return time constant at the value for the equivalent in-plane survival aborts and obtain the final match by iteration of the remaining variables—abort radius, azimuth and velocity impulse.

Some of the questions to be answered by this type of study are the following:

a) For each primary landing area, what is the earliest time after premature injection that the area can be acquired from any nominal free-flight trajectory?

b) For what period of time after first availability does landing opportunity exist for each of the primary sites, and what is the sequence in site availability for a particular free flight trajectory? What will be the transition times from one site to the next?

c) How are the objectives stated in a) and b) above affected by variations in the launch parameters AZL and β_I?

d) Is there a particular landing area that exhibits a higher probability of opportunity than the others for all pre-abort trajectories considered?

In formulating the answers to these and other possible questions, an analysis leading to the creation of "abort window" diagrams, analogous to those for launch opportunities, is suggested. Such a diagram would take into account the launch and trajectory parameters defining the free flight, time lines defining the range of landing opportunity for specific landing areas, and lines of abort velocity impulses (or firing schedules). It would yield the total return time from the point of premature cutoff in addition to coast times should any be required.

At this writing it is only possible to present some preliminary restuls. Table 3-6 shows some representative data for a nominal in-plane ΔV_{ABORT} of 1925 fps at a cutoff with 15 seconds burn time remaining. The actual values necessary to achieve a landing at the sites shown are computed for various abort radii. Figure 3-40 attempts to correlate the tradeoff in ΔV_{ABORT} for the plane changes involved.

It seems evident, from this preliminary examination, that this area of study should produce some very important and useful results.

Table 3-6. Aborts to Specified Landing Areas

$A_L = 90^\circ$, $i = 28$, Nominal $\beta_I = 84^\circ$, $\Delta T_{GO} = 15$ sec, $\Delta V_{available} = 1925$ fps

TNZ = TIME FROM ABORT TO LANDING

TNZ	Landing Area	Time of Cutoff (hrs from L.O.)	Time of Abort (hrs from L.O.)	Radius of Abort (10^6 ft)	Azimuth at Abort (deg)	Coast Time from Cutoff (hr)	Required ΔV (fps)	Plane Change ΔAZ (deg)	Total Return Time (hr)
21.39	AMR Nadir	0,283	1.72	95.0	95.66	1.44	1890	-11.33	22.83
21.55			1.84	100.0	94.68	1.56	1631	-9.35	23.11
16.00	Indian Ocean	0.283	1.30	75.0	100.39	1.02	2489	-10.39	17.02
16.11			1.43	81.3	98.75	1.15	2263	-8.75	17.26
16.28			1.84	100.0	94.68	1.56	2045	-4.68	17.84
23.57	Ascension	0.283	3.46	160.0	86.28	3.18	1050	3.72	26.75
23.17			4.17	181.0	84.25	3.89	1167	5.75	27.06
22.70			4.88	200.0	82.64	4.60	1271	7.36	27.30
19.12	Bermuda	0.283	5.29	210.0	81.85	5.01	2002	8.15	24.13
17.83			6.27	232.0	80.25	5.99	2386	9.75	23.82
17.47			6.42	235.0	80.04	6.14	2499	9.96	23.61
21.96	Hawaii	0.283	10.99	305.0	75.42	10.71	1017	14.59	32.67
14.35			16.05	340.0	72.25	15.77	2746	17.75	30.12
13.76			17.02	342.5	71.73	16.74	2822	18.27	30.50

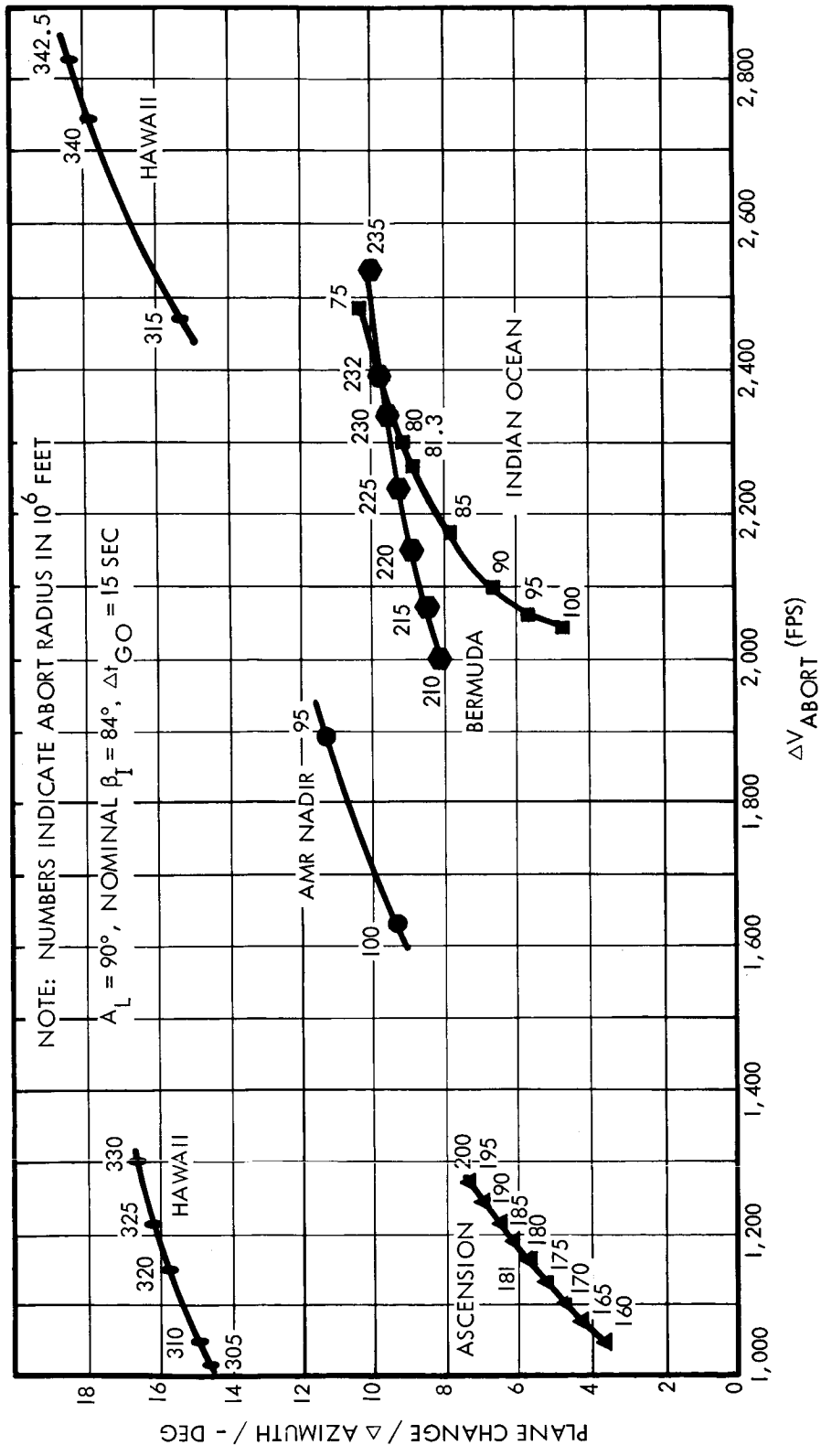

Figure 3-40. Some Values of Abort Velocity Impulse Required for Various Plane Changes to Specified Landing Sites

4. CONCLUSIONS

The most significant result derived from this study is that an increased injected payload can be gained with the direct injection mode but at a considerable reduction in the number of launch opportunities and length of the launch window. Concerning abort possibilities, two significant differences arise between the direct injection and parking orbit injection modes. The first is that the parking orbit permits abort possibilities prior to translunar injection. On the other hand, since the geographic location of translunar injection is somewhat localized, an abort philosophy (particularly to specific landing areas) may be developed independent of the day of launch. These results are summarized as follows:

a) With no lighting constraints at the launch site, the earth parking orbit injection mode offers approximately ten launch windows per month, or about 120 days per year. In contrast, the direct injection mode offers about 45 launch windows per year. If a daylight launch is required, the number of direct injection and parking orbit injection launch windows is reduced by about 50 and 20 percent respectively.

b) The typical earth parking orbit launch window is about 2.5 hours duration if the launch azimuth is varied through its range of 26 degrees. The typical direct injection window is about 1.5 hours duration, and is achieved by use of a variable injection flight path angle. The direct injection launch azimuth varies within a narrower range than the parking orbit injection launch azimuth.

c) Regardless of the location of the lunar landing site, the launch period for this site is limited to a three-day interval each month by lunar lighting constraints. Under these conditions, the earth parking orbit mode offers one opportunity each month, or 12 per year. Unlike the parking orbit mode, the direct injection mode launch opportunities are dependent on the landing site selected. The direct injection mode offers only 5 or 6 opportunities per year with a daylight launch. If the launch lighting constraint is relaxed, the direct injection mode offers from 6 to 9 opportunities per year.

d) Direct injection offers a potential payload increase only when a portion of the available window is utilized; utilizing the entire 90-minute window results in an allowable payload with direct injection which is slightly less than that for nominal parking orbit injection.

e) An intermediate trajectory mode would be the parking orbit with a short coast (less than one revolution). This mode would provide the parking orbit launch opportunities and windows without the loss of excessive boiloff. The gain in payload could then be as great as 2130 pounds over the nominal parking orbit mode.

f) For cutoff at any given burn time-to-go, the return time, measured from cutoff to landing and constrained by fixed reentry conditions, is minimized by the following:

- Abort initiated as soon as possible after cutoff
- Use of the largest abort velocity increment available
- Abort in-plane.

g) No solutions were found in the cases using 1925 fps velocity increment for aborts initiated immediately at cutoff. This suggests the existence of a mandatory coast period following cutoff for a range of low velocity increments during which an abort would be unsuccessful.

h) Landing sites are well distributed longitudinally around the earth. For cutoffs in the last 60 seconds of S-IVB burn, landing points move retrograde to the earth's rotation and are contained in a belt of northern latitudes between 10 and 30 degrees.

i) Hawaii exhibits the greatest promise as a landing site since all landing loci pass through this vicinity during some period after liftoff.

1. INTRODUCTION

This portion of the report presents a comparison of the on-time launch probability, flight success probability, mission success and crew safety for the direct injection (DI) and earth parking orbit injection (EPOI) lunar missions of the Saturn V/Apollo vehicle.

1.1 ON-TIME LAUNCH PROBABILITY

In Section 2, estimates are made of the pertinent launch probability parameters for the Saturn V/Apollo—in particular, the average number of holds per successful countdown ($\overline{h}$), the average time lost per hold (τ), and the probability that a vehicle which begins a countdown will not be scrubbed for technical reasons (P_2). Also, a comparison is given of the launch probability (i.e., the probability that liftoff of the vehicle will occur during a launch window in the firing period) for the DI and for the EPOI missions. These launch probabilities have been calculated both with and without the use of a built-in (or scheduled) hold.

The comparisons of on-time launch probability have been explicitly made for a 1.5-hour launch window for the DI mission and for the 2.5- and 4.5-hour launch windows for the EPOI mission. These particular window lengths were selected since they are the values which correspond to essentially the same nominal payload weight. The launch probability results are shown both in parametric and in continuous form so that any window length can be considered—e.g., a 30-minute window length for the DI mission. (This short window corresponds to a significant increase in the nominal payload weight for the DI mission).

The mathematical (probabilistic) model and methods (including associated parametric presentations) are given, whereby launch probabilities can be generated for any value of $\overline{h}$, τ, and P_2, for any number, length, and placement of built-in holds in the countdown, and for any length launch window.

1.2 FLIGHT SUCCESS PROBABILITY

In Section 3, the relative flight success probabilities of the DI and EPOI missions are given. These probabilities are conditional upon the attainment of liftoff by the vehicle. The relative change in flight success probability has been computed using several sets of input reliability numbers, viz., the following: a) those furnished on the Saturn V launch vehicle and the Apollo spacecraft by the Apollo Support Department of the General Electric Company at Daytona Beach, Florida; b) those furnished on the S-IVB by the Marshall Space Flight Center; c) the S-IVB reliability estimates based on Douglas Aircraft Company data; and d) the in-flight reliability data collected, analyzed, and summarized explicitly for this study by STL. This last set of numbers was obtained from relevant flight test histories and is considered to provide the most realistic comparison of the relative flight success probabilities for both missions. The first three sets of numbers represent planning numbers being used by various cognizant organizations concerned with the Saturn V/Apollo program.

Consistent with the scope of this study, the comparative flight reliabilities generated by STL's Florida Division from flight test histories were confined to the following: The reliability of the S-IVB reignition, which is required for the EPOI mission but not for the DI mission; and the reliability of the S-IVB reaction control system function, which is required for both trajectories.

1.3 MISSION SUCCESS AND CREW SAFETY PROBABILITIES

In Section 4, the launch probability of Section 2 and the flight success probabilities generated from flight reliability histories (given in Section 3) are combined to yield a comparison of mission success probabilities. This multiplication gives the relative probabilities that the vehicle will not only meet a launch window during the specified firing period but will also have a successful flight.

The General Electric Apollo Support Department, Daytona Beach, in support of the present study, utilized the four sets of input reliability numbers described in Section 1.2 to generate comparisons relative to both mission (flight) success probability and crew safety probability. This work is referenced in Sections 3 and 4 and is contained in full in Reference 5.

1.4 ADDITIONAL ITEMS

The major results are stated in Section 5, and conclusions and recommendations are given in Sections 6 and 7, respectively.

Also included are the pertinent references and an appendix which describes the Fortran computer programs and associated plotter programs used to generate launch probabilities for any set of conditions (e.g., for any number, length, and placement of built-in holds).

2. PROBABILITY OF ON-TIME LAUNCH

2.1 PREDICTION OF LAUNCH PROBABILITY PARAMETERS

2.1.1 Introduction

The purpose of this section is to estimate the pertinent launch probability parameters for the Saturn V/Apollo configuration. These pertinent parameters are the following: number of holds per successful countdown (i.e., a countdown terminating in liftoff); time lost per hold (including any associated recycle time, i.e., any time lost in recycling to an earlier point in the countdown); probability of countdown scrub; probability of slippage of the first scheduled launch attempt; and probability that a countdown would commence on a pre-specified day during the firing period conditional upon the vehicle's not yet being launched.

The pertinent launch probability parameters (together with launch probability as a function of launch window length) have previously been estimated in References 1, 2 and 3 for other space booster vehicles (in particular, the Atlas/Agena, the Atlas/Centaur, and the Titan II Gemini launch vehicle). These referenced studies were completed by collecting data on all of the schedule slippages, countdown holds, and scrubs in the following 11 missile programs at AFETR:

1) Atlas D (32 missiles, 61 countdowns)
2) Atlas E (18 missiles, 32 countdowns)
3) Atlas F (10 missiles, 16 countdowns)
4) Atlas/Agena (9 missiles, 18 countdowns)
5) Atlas/Able (3 missiles, 5 countdowns)
6) Atlas/Centaur (1 missile, 4 countdowns)
7) Atlas/Mercury (10 missiles, 15 countdowns)
8) Titan I (47 missiles, 72 countdowns)

9)	Titan II	(23 missiles, 31 countdowns)
10)	Thor (R and D)	(35 missiles, 46 countdowns)
11)	Thor/Delta	(17 missiles, 27 countdowns)
	TOTALS	(205 missiles, 327 countdowns)

The collected slippage, hold and scrub reasons were categorized as airborne, GSE, and range, and then further categorized by subsystems. The data was screened of R and D reasons. (An R and D reason was defined as that relating to any system not related to a space program; e.g., nose cone, downrange aircraft, ballistic cameras at Ascension Island, a system known to have been redesigned to alleviate a past problem area, etc.). The screened data was operated on statistically to derive the launch probability of a particular vehicle.

2.1.2 Statistical Similarity of Different Missile Programs

Table 2-1 presents a comparison of the countdown performance of the weapon system booster programs studied, considering holds and scrubs regardless of whether or not the delays were of an R and D nature. Table 2-2 shows the countdown performance of these same programs after screening out all R and D data. (The Thor booster development program could not be screened of R and D data because only the number of holds and total hold minutes were reported without a detailed discussion of the nature of the individual holds.) Inspection of these data reveals the statistical similarity between the programs. Screening the data of R and D reasons serves only to reduce the magnitude of the numbers without disturbing the statistical similarity of the programs. This fact is emphasized for the purpose of demonstrating that, to date, no one program at ETR has achieved a countdown performance record significantly different from any other.

2.1.3 Booster Holds in Successful Countdowns

From Table 2-2, $\bar{h}$ (the average number of holds per count) was 2.4, and τ (the average time lost per hold) was 37 minutes. However, closer examination of Table 2-2 indicates that the Atlas D and Titan I holds per count were significantly higher than the other values listed. The data from

Table 2-1. Comparison of the Countdown Performance During the "R and D" Development of Boosters at ETR

	Atlas D	Atlas E	Atlas F	Titan I	Titan II	Average
No. of Boosters	32	18	10	47	23	
No. of Counts	42	29	15	72	30	
Counts/Booster	1.3	1.6	1.5	1.5	1.3	1.4
Total No. of Holds	114	63	31	198	66	
Total No. of Holds Min.	4353	2940	918	7130	2278	
Min/Hold	38	47	30	36	35	37
Holds/Count	2.7	2.2	2.1	2.8	2.2	2.4
Hold Min/Count	104	101	61	99	76	88

Table 2-2. Comparison of the Countdown Performance During the "R and D" Development of Boosters at ETR (Excluding R and D Data)

	Atlas D	Atlas E	Atlas F	Thor	Titan I	Titan II	Average
No. of Boosters	32	18	10	35	47	23	
No. of Counts	61	32	16	46	72	31	
Counts/Booster	1.9	1.8	1.6	1.3	1.5	1.4	1.6
Total No. of Holds	148	73	38	138	236	85	
Minutes/Hold	6118	3389	1284	7777	8722	3010	
Hold/Coudn	41	46	34	56	37	35	42
Hold/Count	2.4	2.3	2.4	3.0	3.3	2.7	2.7
Hold Min/Count	100	106	80	169	121	97	112

32 successful countdowns of the Atlas D booster development program (screened of R and D hold reasons) indicates that the Atlas D experienced only 1.8 holds per successful countdown, as compared to 2.7 holds per count for all countdowns. In contrast, the Titan II booster development experienced 2.1 holds per successful countdown, as compared to 2.2 holds per count for all countdowns. The discrepancy in the Atlas D countdown performance, not observed in the other programs presented here, is believed to be due to the relatively large number of countdown attempts scrubbed for R and D reasons. The assumption was therefore made that an $\bar{h}$ of 2.1 holds per successful countdown is a realistic estimate for use in this study.

This assumption is substantiated by the performance of the Saturn I program to date. Although a small sample, the hold and scrub experience of the Saturn I booster program shown in Table 2-3 was 2.1 holds per count for all counts and 1.8 holds per successful count. The scrub experience is also about the same as the average scrub experience for all boosters shown in Table 2-2.

In the development of boosters, the average time lost per hold, τ, was 37 minutes; however, in the Atlas space programs (Agena and Mercury) the average time lost per hold, including associated recycle time, was 20 minutes (see Reference 1). It is believed that the discipline of meeting a launch window is the primary reason for the drop in the average time lost per hold. Also, better procedures and a better understanding of system anomalies, developed during the booster development program, probably have had some effect.

Therefore, it is estimated that 20 minutes will be the expected time lost per hold in any advanced space vehicle countdown. This estimate is based upon the assumption that the Atlas-Agena and Atlas-Mercury programs at AFETR are typical space vehicle programs whose statistics permit prediction of the countdown of future space programs employing similar systems.

Table 2-3. Saturn I Booster Development Countdown Record

Saturn Booster	Countdown Attempt	No. of Holds	Total Hold Min
SA-1	1	2	66
SA-2	1	1	30
SA-3	1	1	45
SA-4	1	3	102
SA-5	1	5	115*
	2	1	72
SA-6	1	1	0*
	2	3	173
Average	1.3	2.8 (2.1 holds/count)	100 (35 min/hold)

*The long holds that terminated in a scrub were not counted in the derivation of $\bar{h}$ and τ because of the small sample.

2.1.4 Estimated Saturn Stage S-IC Countdown Performance

Table 2-3 shows the countdown record of the Saturn I booster development through SA-6. This record indicates that the Saturn has experienced essentially the same countdown performance as the average booster shown in Table 2-2. This permits the prediction that the τ for the "advanced" Saturn boosters will drop (as was the case on the advanced Atlas), to approximately 20 minutes per hold as better procedures are developed, current subsystem anomalies are rectified, and the discipline of meeting a launch window is inserted into the program. The term "booster," as applied to Saturn and Atlas, describes the first stage of the vehicle and includes the many subsystems (airborne, GSE, and range) that are herein considered independent of additional powered-stages and spacecrafts. These subsystems are shown in Table 2-4 which gives the hold experience, by subsystem category, of several of the advanced Atlas booster programs and of the Atlas booster development. It is estimated that the Saturn booster (i.e., Stage S-IC, which includes all of the subsystems mentioned in Table 2-4) will experience, on the average, 2.1 twenty-minute holds per successful launch countdown.

2.1.5 Contribution of Other Saturn V Stages

The $\bar{h}$ for the total Saturn V/Apollo configuration must also include the contribution of the upper stages. In addition to the S-IC booster, the Saturn V/Apollo configuration is comprised of two additional cryogenic liquid propellant stages, the spacecraft command module with its many subsystems, the service module with its restartable propulsion system, and the two-stage Lunar Excursion Module (LEM). The subsystems of the S-II and S-IVB stages that contribute to the total $\bar{h}$ are: airborne and GSE hydraulics, propulsion, pneumatics, and propellant utilization. If these subsystems perform according to the average, and assuming that the subsystem totals of Table 2-4 (57 holds in 97 counts) represent the average contribution of these subsystems, then each of these stages, including their related GSE, will contribute 0.6 hold per count.

Table 2-4. Atlas Hold Recurrence (R and D hold reasons excluded)

HOLD RECURRENCE FOR AIRBORNE SYSTEMS

PROJECT	ELECTRICAL	CONTROLS	GUIDANCE	HYDRAULICS	PROPULSION	PNEUMATICS	PROPELLANT UTILIZATION	TELEMETRY	AIRFRAME	AIRBORNE RANGE (TRACKING & SAFETY)	TOTAL NUMBER OF AIRBORNE HOLDS	NUMBER OF COUNTDOWNS	AIRBORNE HOLDS PER COUNTDOWN
ATLAS D WEAP. SYSTEM	3	4	8	1	17	8	2	8	1	6	58	61	0.95
ATLAS OF ATLAS AGENA	1	1	4	2	5	0	0	1	1	2	17	18	0.94
ATLAS OF ATLAS MERCURY	2	0	2	0	2	0	0	2	0	1	9	13	0.7
ATLAS OF ATLAS ABLE	0	1	0	0	0	0	0	0	1	1	3	5	0.6
TOTAL	6	6	14	3	24	8	2	11	3	10	87	97	0.9
% OF TOTAL AIRBORNE	7	7	16	3	28	9	2	13	3	11			
% OF TOTAL AIRBORNE&GSE	3	3	8	2	14	5	1	6	2	6	50		

GSE SYSTEMS

PROJECT	ELECTRICAL		GUIDANCE	HYDRAULICS	PROPULSION	PNEUMATICS	MECHANICAL	TELEMETRY	INVESTIGATE PAST FAILURE	GSE RANGE (TRACKING & SAFETY)	TOTAL NUMBER OF GSE HOLDS	NUMBER OF COUNTDOWNS	GSE HOLDS PER COUNTDOWN
ATLAS D WEAP. SYSTEM	9	NOT REQUIRED	12	0	7	9	2	1	0	16	56	61	0.9
ATLAS AGENA	5		0	0	1	1	0	0	0	6	13	18	0.7
ATLAS MERCURY	0		2	0	1	0	3	0	0	11	17	13	1.3
ATLAS ABLE	1		0	0	1	0	0	0	0	0	2	5	0.4
TOTAL	15		14	0	10	10	5	1	0	33	88	97	0.9
% OF TOTAL GSE	17		16	0	11	11	6	1	0	38			
% OF TOTAL AIRBORNE & GSE	9		8	0	6	6	3	1	0	19	50		

AIRBORNE PLUS GSE TOTAL HOLDS	TOTAL NO. OF COUNTDOWNS	TOTAL HOLDS PER COUNTDOWN
175	97	1.8

It is anticipated that the T - 1 day checks on the LEM will essentially suffice for launch; therefore, the LEM itself is not expected to contribute significantly to $\bar{h}$ on T - 0 day. Its contribution is expected to be equivalent to that of a Ranger/Mariner spacecraft, where $\bar{h}$ = 0.1 (see Reference 1).

The command and service modules (CSM) are expected to make significant contributions to $\bar{h}$. The last five Mercury capsules contributed an average $\bar{h}$ of 1.2 to the launch countdown; however, the Apollo spacecraft, including the service module, will have essentially the same complexity as a booster. It will possess all of the airborne, GSE, and range systems shown in Table 2-4; therefore, it is estimated that its $\bar{h}$ contribution will be the same as the S-IC, or 2.1 holds per count.

2.1.6 Holds Per Count for Saturn V/Apollo Configuration

In summary, the $\bar{h}$ of the entire Saturn V/Apollo configuration is estimated to be as follows:

S-IC (including all GSE and required range systems)	2.1
S-II (including GSE systems)	0.6
S-IVB (including GSE systems)	0.6
LEM (including GSE systems)	0.1
CSM (including all GSE and required range systems)	2.1
TOTAL	5.5

It is anticipated that the average time lost per hold will be 20 minutes. It is postulated that the majority of the holds will occur in the latter part of the countdown, as has been the case in all of the programs studied (e.g., see Figures 2-1 and 2-2 and References 1, 2, 3, and 4).

2.1.7 Estimated Range of $\bar{h}$

The actual $\bar{h}$ for the S-IC (and similarly for the CSM) may easily vary from 1.8 to 2.4 (Table 2-5). The value of 1.8 is the current number of holds per successful count in the Saturn I program; however, 2.4 holds per count have been experienced by Atlas in the Atlas-Agena program, even though in its development it had 1.8 holds per successful count.

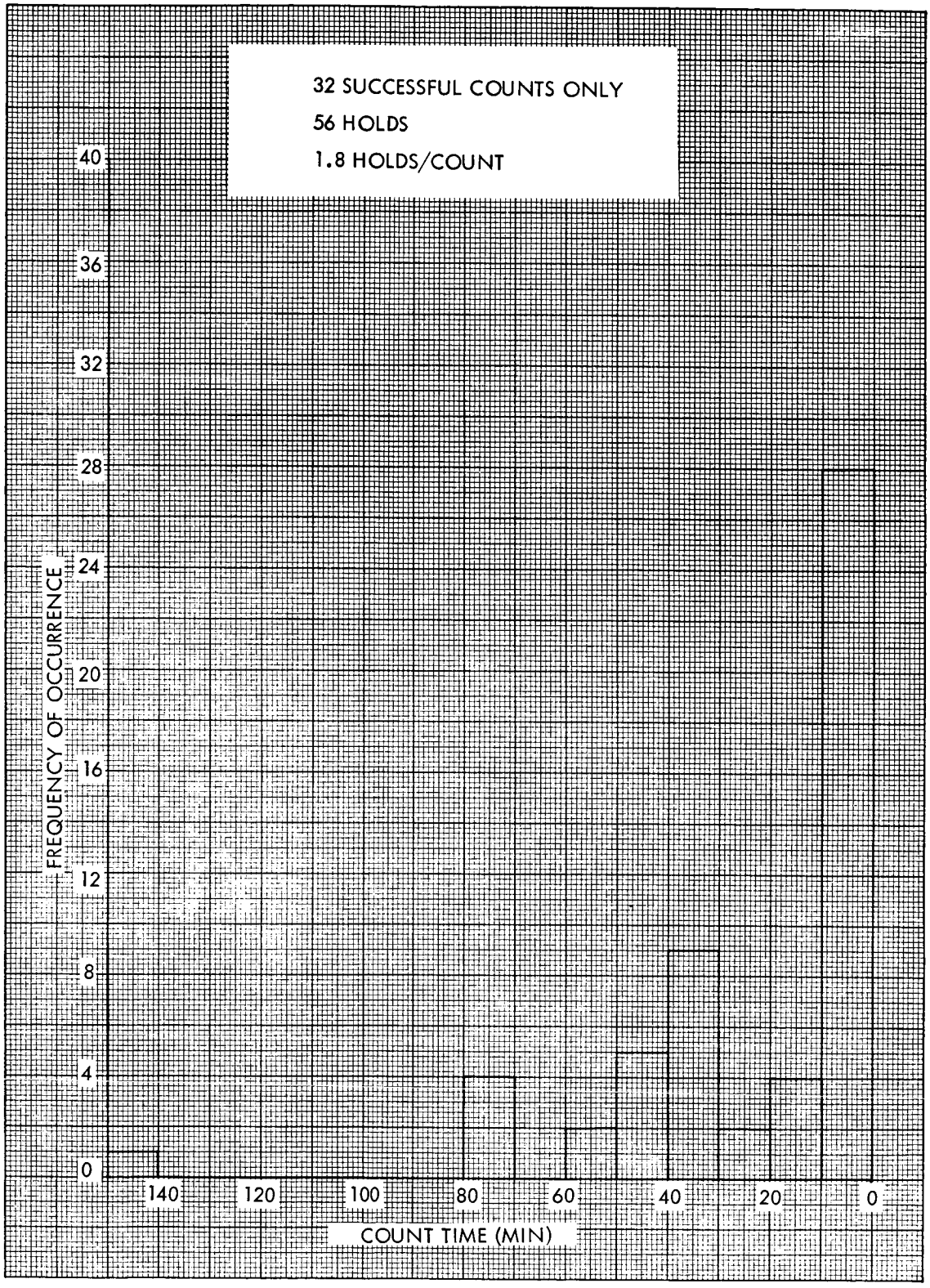

Figure 2-1. Atlas D Holds Versus Time

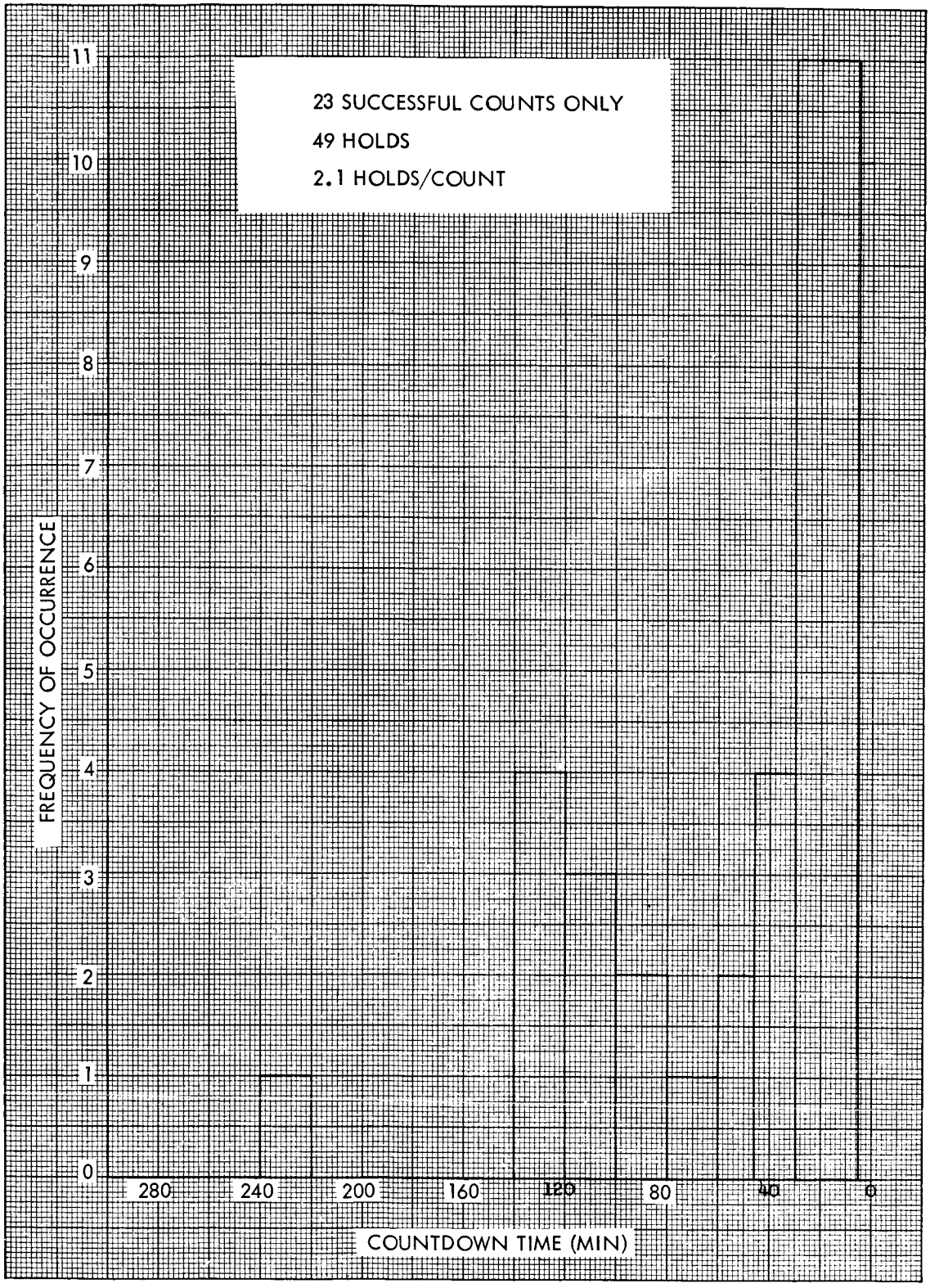

Figure 2-2. Titan II Holds Versus Time

Table 2-5. Estimated Range of $\bar{h}$

	Min $\bar{h}$	$-\Delta\bar{h}$	Expected $\bar{h}$	$+\Delta\bar{h}$	Max $\bar{h}$
S-IC	1.8	0.3	2.1	0.3	2.4
S-11	0.5	0.1	0.6	0.1	0.7
S-IVB	0.5	0.1	0.6	0.1	0.7
LEM	0.0	0.1	0.1	1.1	1.2
CSM	1.8	0.3	2.1	0.3	2.4

$$-\Delta h = \sqrt{0.09 + 0.01 + 0.01 + 0.01 + 0.09} \cong 0.5$$

$$+\Delta h = \sqrt{0.09 + 0.01 + 0.01 + 1.21 + 0.09} \cong 1.2$$

To date, the hydrogen stage of Saturn I has had only one hold in four counts. This gives an average number of holds per count of 0.25; however, the sample size is very small and therefore is not considered conclusive. In contrast, the hydrogen stage of Centaur, excluding the contributions of the guidance and control systems, has experienced an average of 0.7 hold per count in the successful counts. It is believed that ±0.1 hold per count is a reasonable tolerance to add to the 0.6 hold per count estimate for the S-II and S-IVB hydrogen stages of Saturn V.

The LEM may contribute more than 0.1 hold per count, particularly if the operational philosophy places emphasis on holding and attempting a solution instead of simply scrubbing. However, the LEM is not expected to contribute more than was experienced by the last five Mercury capsules, which averaged 1.2 holds per count.

Taking the square root of the sums of the squares of the tolerances described above, the estimated range of $\bar{h}$ for the entire Saturn space vehicle becomes 5.0 to 6.7, with 5.5 the expected value.

2.1.8 Probability of a Nonscrub

The most optimistic probability of a nonscrub* for the entire Saturn V/Apollo configuration is estimated to be 0.53. This estimate was derived by assuming that the systems of the various stages of the vehicle will behave, on the average, as similar systems have done in the Saturn, Atlas D, and Titan II; and furthermore, that the LEM will behave as well as the Mercury spacecraft. The upper and lower limits on the Saturn V/Apollo nonscrub probability are derived below.

By referring to the accumulated subsystem data categorized within Volume 2 of Reference 1, the total average scrub experience for the systems similar to the ones contained within the S-II and S-IVB stages was found to be 0.1 scrub per missile. This figure yields a nonscrub probability number of 0.9.

From Table 2-2, as well as from Reference 1, it may be observed that the average number of counts per booster system has been 1.4. If the S-IC and the CSM (each of which is estimated to have a countdown performance similar to an average booster system) experience this average, then the probability of a nonscrub for each of these two systems will be (1/1.4), or 0.7.

The LEM is not expected to contribute more than the spacecraft of the Atlas-Agena series, which have a current nonscrub probability of 0.83.

The product of these individual contributions is estimated as the overall lower limit on the probability of a nonscrub, namely:

$$\underset{\text{(S-CI)}}{0.7} \times \underset{\text{(S-II)}}{0.9} \times \underset{\text{(S-IVB)}}{0.9} \times \underset{\text{(LEM)}}{0.83} \times \underset{\text{(CSM)}}{0.7} = 0.33$$

*A nonscrub is defined as a successful countdown, i.e., a countdown which terminates in liftoff, with no consideration of launch window.

The nonscrub probability for the S-IC and CSM could go as high as 0.77, if they experience the current Saturn I booster counts-per-launch average of 1.3. This average was experienced in the Atlas D and Titan II programs.

In the current total of 13 AFETR countdowns on liquid hydrogen stages (5 Saturns and 8 Centaurs), no scrubs have been caused by the liquid hydrogen stages; however, it is believed that a nonscrub probability of 1.0 for these stages is unrealistic. The subsystem data in Reference 1, Volume 2, indicates that the possibility of a nonscrub ratio of 1.0 in such a complex system is remote. Taking into account the current records of the hydrogen stages at ETR, combined with the data of Reference 1, the most optimistic nonscrub probability for these systems is estimated as 0.95.

If the LEM countdown performance duplicates that of the Mercury spacecraft, its nonscrub ratio may be 1.0. Although the possibility of a unity nonscrub ratio in such a complex system is remote, this ratio was nevertheless used in forming the optimistic estimate of the nonscrub probability for the overall Saturn V/Apollo configuration.

The product of the individual contributions to the overall upper limit on the nonscrub probability estimate is

$$\underset{\text{(S-IC)}}{0.77} \times \underset{\text{(S-II)}}{0.95} \times \underset{\text{(S-IVB)}}{0.95} \times \underset{\text{(LEM)}}{1.0} \times \underset{\text{(CSM)}}{0.77} = 0.53$$

Thus, the nonscrub probability for the Saturn V/Apollo configuration is estimated to be between 0.33 and 0.53, with 0.43 being the average value and the assumed best estimate. This probability does not include the influences of launch window, sea state, or weather.

The one factor that may cause as many scrubs as any other is sea states and/or weather. Sea states and/or weather during the Mercury program caused a counts per launch ratio of 1.4, or a nonscrub probability of 0.71. Thus, the best estimate of the average nonscrub probability including these effects becomes

$$0.43 \times 0.71 = 0.31 \ .$$

2.1.9 Probability of Schedule Slippage

It is believed that the excellent planning and the discipline demanded by this highly complex program will assure missile readiness for launch on the scheduled day, i.e., on the first scheduled launch attempt, which is assumed to coincide with the first day of the firing period. Nevertheless, there will be the weather to consider. As an alternative to including sea states and/or weather in the scrub reasons, as above, it is believed that sea states could legitimately be considered as a reason for slipping the schedule, on the assumption that the countdown would not be started if the sea states precluded recovery in the event of an abort. A probability of no schedule slip for sea states and/or weather may then reasonably be expected to be 0.71. However, due to the long launch preparations in the precount, together with the countdown itself (viz., a total of about 16 to 18 hours, including a 6-hour terminal count in which ETR participates) and due to the short firing period (viz., three days), it is anticipated that the more likely practice will be to initiate (and hence not slip) the countdown and subsequently scrub when an unsatisfactory sea state prevails.

The turn-around (recycle) time in the event of a scrub, for any reason, is assumed to be two days. This assumption is based upon the fact that the pre-count and terminal count take so long that a one-day turn-around time for commencement of the next countdown would be very difficult to implement. However, due to the high degree of preplanning presently anticipated for the implementation of any required rework or compont replacement, it does appear that a two-day turn-around time is a reasonable assumption in the event of a countdown scrub. Thus, under this assumption, the probability that a countdown will commence on a prespecified day in the firing period (conditional upon the vehicle's not yet being launched) is as follows: 1.0 for the first day, 1.0 if the last countdown attempt was commenced two days earlier, and zero if the last countdown attempt was commenced the preceding day.

Subsequent sections present calculations of the probability of vehicle liftoff during a launch window in the firing period which were made both for a one-day and two-day turn around for the recommencement of the countdown.

The persistence effect of weather, sea states, and major technical reasons (whereby an entire firing period might be knocked out and thereby eliminated from usage) was considered beyond the scope of the present study. Instead, these phenomena have been considered herein as random from day to day, and hence their associated probabilities of occurrence are considered as independent and constant from day to day.

2.2 ON-TIME LAUNCH PROBABILITY WITHOUT BUILT-IN HOLDS

2.2.1 Introduction

This section analyzes the probability of launch of Saturn V/Apollo vehicles for lunar missions for both direct injection and earth parking orbit injection, for the situation in which no built-in (or scheduled) holds are used. The effect of built-in holds on the probability of launch is assessed in a subsequent section.

The probability of launch is defined herein as the probability of achieving liftoff prior to the expiration of the launch window. The basic assumptions and definitions employed are as follows:

a) The length of the launch window will be 1.5 hours for direct injection and 2.5 (under certain conditions, 4.5) hours for earth parking orbit injection. The mathematical (probabilistic) model is presented such that for any launch window, the probability of launch can be determined.

b) The launch window for a specific mission will be constant for each day of a given firing period. Deviations from this assumption are permissible due to the parametric presentation contained herein.

c) The firing period, that is, the number of consecutive days suitable for launch, will be three days. Lunar lighting conditions at a given landing site constrain the launching to three days per synodic month.

d) The turn-around time from countdown scrub to commencement of the next countdown is two days. This follows from the assumption that the countdown itself will consume about one day (on the order of 20 hours).

e) The probability (P_1) that the vehicle is ready to start a countdown on a prespecified day during the firing period is 1.0, conditional upon the vehicle's not yet being launched.

f) The average length of holds (τ) remains constant throughout the countdown and is equal for all three stages of the boost vehicle, and for all three modules of the spacecraft. Furthermore, this same value of τ includes both the length of the holds and any time lost due to recycling to an earlier point in the countdown.

g) No more than one firing period per synodic month exists for either the DI or the EPOI missions.

2.2.2 Mathematical Model

The mathematical model used to determine the launch probability of the Saturn V/Apollo is essentially a product of conditional probabilities. The probabilities of interest are the following:

P_1 The probability that the vehicle is ready to start a countdown on a prespecified day

P_2 The probability that the countdown, if begun, will not be scrubbed for technical reasons other than expiration of launch window

P_L The probability that the countdown, if not scrubbed for technical reasons, will be completed before the expiration of the launch window (P_L)

ρ_1 The probability of launch for a one-day firing period, or for any particular day in the entire firing period

ρ_n The probability of launch for an n-day firing period.

The number of holds per countdown and the lost time associated with these holds play a dominant role in the calculation of the probability of meeting a launch window. Thus, the average number of holds for a countdown terminating in liftoff ($\bar{h}$) and the average time lost per hold (τ) are the pertinent parameters from which P_L is estimated.

Under the assumption that ρ_1 is constant and independent from day to day, the probability that the vehicle will not be launched during a firing period of n days is given by the expression

$$1 - \rho_n = \left(1 - \rho_1\right)^m$$

where m is the number of possible launch attempts in a firing period of n days. Hence, the probability ρ_n that the vehicle will be launched during a firing period of n days is

$$\rho_n = 1 - \left(1 - \rho_1\right)^m$$

The launch probabilities are thus given by the following formulas:

$$\rho_1 = P_1 P_2 P_L$$

and

$$\rho_n = 1 - \left(1 - \rho_1\right)^m$$

where, for a turn-around time of two days

$$m = \frac{n + 1}{2} \qquad \text{for } n \text{ odd}$$

$$= \frac{n}{2} \qquad \text{for } n \text{ even}$$

(If the assumption had been made that the turn-around time was one day instead of two days, then m would equal n for all n.)

The above equations for ρ_n are general, but under the assumed lunar lighting constraints, n is equal to 3.

2.2.3 Probability Distribution of Excess Countdown Time

The excess time (Δt) required to complete a countdown can be defined as the difference between the actual countdown time and the planned countdown time. The probability that Δt will be zero is equal to the probability that no holds

will occur during the countdown, since the occurrence of a hold automatically means a loss of time. Given that exactly i holds ($i > 0$) have occurred in a countdown, the probability density of Δt is obtained as the product of the probability of occurrence of exactly i holds multiplied by the probability density of the time lost in a countdown in which exactly i holds have occurred, and thereupon summed over all values of $i > 0$ (i.e., $i = 1, 2, 3, \cdots$)

Let the probability density of the excess time (Δt), for $\Delta t > 0$, be denoted by $\Phi(\Delta t)\, d(\Delta t)$ and let the probability that Δt will equal zero be denoted by the expression

$$P(\Delta t = 0) = P(0)$$

The probability distribution of Δt is thus given by the following expression

$$\Phi(\Delta t)\, d(\Delta t) = \sum_{i=1}^{\infty} P(i)\theta_i(t)\, dt \qquad \text{for } \Delta t > 0$$

where

$P(i) \equiv$ probability of occurrence of exactly i holds ($i = 0, 1, 2, \cdots$)

and

$\theta_i(t)\, dt \equiv$ probability density of the time lost (per countdown) due to holds if exactly i holds occur in the countdown ($i = 1, 2, \cdots$)

From the above expression, one can observe that the probability P(0) will occur in the probability distribution of Δt is a Dirac Delta function at the value of $\Delta t = 0$. Associated with the occurrence of exactly one hold will be a portion of the probability distribution of Δt attributable to the probability distribution of the lengths of holds (including any associated recycling times), possessing mean μ and standard deviation σ. The area under this portion of the probability distribution would be equal to P(1). Similarly, there would be a portion associated with exactly r holds (for $r = 1, 2, 3 \cdots$) with mean equal to $r\mu$ and with standard deviation $\rho\sqrt{r}$, and the area under this portion would be equal to P(r).

The statistical analysis of countdown hold data obtained from space programs indicates that the assumption that P(i) follows a Poisson distribution appears valid for the Saturn V/Apollo vehicle, i.e.,

$$P(i) = \frac{(\bar{h})^i e^{\bar{h}}}{i!}$$

where

$\bar{h} \equiv$ average number of holds per successful countdown (i.e., a countdown terminating in liftoff),

and furthermore, θ_1 follows a negative-exponential distribution; that is,

$$\theta_1(t)\, dt = \frac{1}{\tau} e^{-t/\tau}\, dt,$$

where τ is the average time lost per hold.

The statistical analysis of the hold times on space vehicles indicates that the above assumption concerning the probability density, viz.,

$$\theta_1(t)\, dt = \frac{1}{\tau} e^{-t/\tau}\, dt$$

is a reasonable one for the Saturn V/Apollo vehicle. In regard to $\theta_1(t)\, dt$, the variable $2t/\tau$ is distributed as a chi-square variate with two degrees of freedom.

Since the sum of two independent chi-square variates with m_1 and m_2 degrees of freedom is a chi-square variate with $\overline{m_1 + m_2}$ degrees of freedom, then in regard to $\theta_i(t)\, dt$ the variable $2t/\tau$ is distributed as a chi-square variate with 2i degrees of freedom.

Thus,

$$\theta_i(t)\, dt = \frac{t^{i-1}}{(i-1)!\, \tau^i} e^{-t/\tau}\, dt$$

The probability of launch (P_L) within a launch window of length W (where $W \geq 0$), conditional upon the countdown not being scrubbed for technical reasons (as opposed to being late in meeting the launch window), can be obtained by integration of $\Phi(\Delta t)\, d\,(\Delta t)$ from zero to W and subsequently adding P(0) to the result, thereby giving

$$P_L = P(0) + \int_0^W \Phi(\Delta t)\, d\,(\Delta t)$$

$$= 1 - e^{-K}\left(\sum_{i=1}^{\infty} P_i + K \sum_{i=2}^{\infty} P_i + \frac{K^2}{2} \sum_{i=3}^{\infty} P_i + \frac{K^3}{3!} \sum_{i=4}^{\infty} P_i + \frac{K^4}{4!} \sum_{i=5}^{\infty} P_i + \cdots\right)$$

where

$$K = \frac{W}{\tau}, \quad P_i = P(i)$$

and

$$\sum_{i=1}^{\infty} P_i = 1 - P_0 = 1 - e^{-\bar{h}}$$

$$\sum_{i=2}^{\infty} P_i = 1 - P_0 - P_1 = 1 - \left(e^{-\bar{h}} + \bar{h}e^{-\bar{h}}\right)$$

$$\sum_{i=3}^{\infty} P_i = 1 - P_0 - P_1 - P_2 = 1 - \left(e^{-\bar{h}} + \bar{h}e^{-\bar{h}} + \frac{\bar{h}}{2!}\, e^{-\bar{h}}\right)$$

and so on.

2.2.4 Convolution of Stages and Modules

The mathematical method by which the excess time and thereby the P_L's of the S-IC (first stage), S-II (second stage), S-IVB (third stage), and the spacecraft modules are combined is by means of the addition of their respective $\bar{h}$'s; that is, $\bar{h}$ (S-IC + S-II) = $\bar{h}$(S-IC) + $\bar{h}$(S-II). The third stage and spacecraft are combined in the same way. That is, $\bar{h}$(S-IC + S-II + S-IVB + spacecraft) = $\bar{h}$(S-IC) + $\bar{h}$(S-II) + $\bar{h}$(S-IVB) + $\bar{h}$ (spacecraft).

The P_L for the Saturn V/Apollo vehicle could also have been obtained as the convolution of the integrals of their respective excess time probability densities—viz.,

$$\theta_{S\text{-}IC}(t)\,dt \text{ and } \theta_{S\text{-}II}(t)\,dt$$

where for simplicity, Δt has been replaced by t, giving the expression

$$P_L(S\text{-}IC + S\text{-}II) = \int_0^W \theta_{S\text{-}IC}(t)\left[\int_0^{W-t} \theta_{S\text{-}II}(x)\,dx\right] dt$$

A similar convolution could be used to incorporate the complete Saturn V/Apollo vehicle, leading to the following

P_L(S-IC + S-II + S-IVB + spacecraft)

$$= \int_0^W \theta_{S\text{-}IC}(t)\left(\int_0^{W-t} \theta_{S\text{-}II}(x)\left\{\int_0^{W-x-t} \theta_{S\text{-}IVB}(y)\left[\int_0^{W-y-x-t} \theta_{SP}(z)\,dz\right] dy\right\} dx\right) dt$$

Instead of using this formula, we can obtain the effect of each of the separate probability distributions of excess times, simply by making use of the fact that, for the sum of independent Poisson variables, the $\overline{h}$(sum) is equal to the sum of the individual $\overline{h}$'s.

2.2.5 Parametric Presentation of Launch Probabilities

Figure 2-3 gives a parametric presentation of the conditional probability of launch (P_L) versus the dimensionless ratio, W/τ, where W is the launch window length and τ is the average time lost per hold (including any associated recycle time). The set of parametric curves shown in Figure 2-3 are for the following values of the average number of holds per successful countdown ($\overline{h}$): 1.0 (1.0) 10. That is, all values of $\overline{h}$ from 1.0 to 10 inclusive, in increments of 1.0 are shown. This figure is directly applicable to countdown situations in which no build-in holds are used. In space programs studied to date, the numerical value of τ has

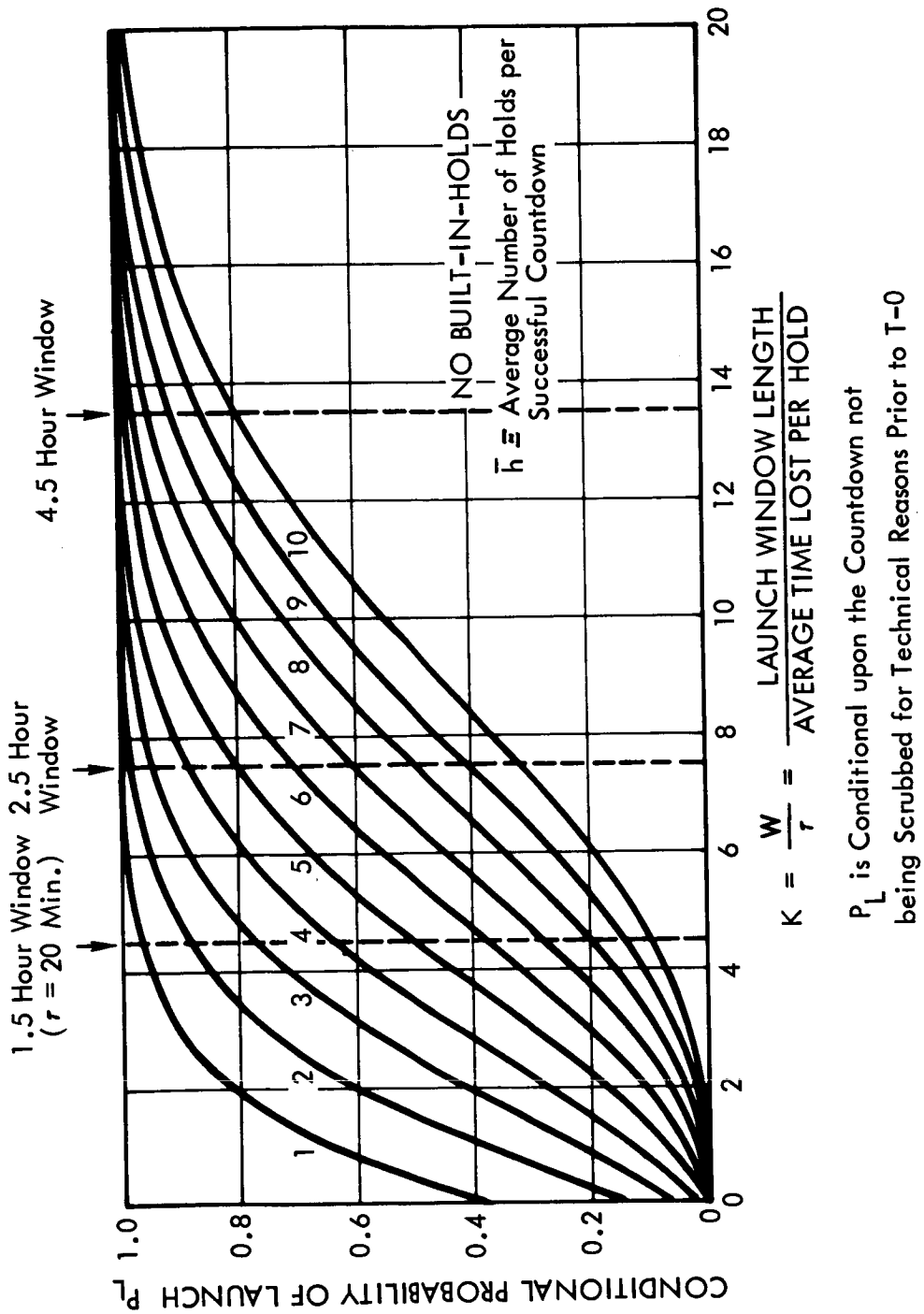

Figure 2-3. Probability of Launch (P_H) as a Function of Launch Window Length

been 20 minutes, or very close to it. Although τ = 20 minutes is considered to be a reasonable assumption for the Saturn V/Apollo vehicle, the effect of other values for τ can be studied by the use of Figure 2-3, due to the fact that the abscissa employs the dimensionless ratio, W/τ.

2.2.6 Numerical Calculation of Launch Probability

In order to demonstrate the influence of P_L on ρ_n, three examples follow: Let

$$\bar{h} = 5.5$$

$$\tau = 20 \text{ minutes}$$

and

$$W = 90 \text{ minutes}$$

Hence

$$\frac{W}{\tau} = \frac{90}{20} = 4.5$$

Furthermore, let $P_1 = 1.0$ and $P_2 = 0.43$.

From Figure 2-3, at K = 4.5 and $\bar{h} = 5.5$

$$P_L = 0.44$$

Hence,

$$\rho_1 = P_1 P_2 P_L = (1.0)(0.43)(0.44) = 0.19$$

That is, 0.19 would be the probability of launch given a 1.5 hour window for a specific day, for τ = 20 minutes, $\bar{h} = 5.5$, $P_1 = 1.0$, and $P_2 = 0.43$. These values of the parameters τ, $\bar{h}$, P_1, and P_2 represent best estimates of the Saturn V/Apollo countdown performance, excluding a consideration of sea states.

For launch windows of 2.5 and 4.5 hours duration

$$\frac{W}{\tau} = \frac{150}{20} = 7.5$$

and

$$\frac{W}{\tau} = \frac{270}{20} = 13.5$$

respectively.

Hence, from Figure 2-3, $P_L = 0.76$ and 0.98, respectively. Therefore,

$$\rho_1 = (1.0)(0.43)(0.76) = 0.33$$

for a launch window of 2.5 hours and

$$\rho_1 = (1.0)(0.43)(0.98) = 0.42$$

for a launch window of 4.5 hours. That is, 0.33 would be the probability of launch given a 2.5 hour window for a specific day, and 0.42 would be the probability of launch given a 4.5 hour window for a specific day. For a firing period of three days, launch probabilities for the 1.5, 2.5, and 4.5 hour launch windows discussed above would be given by

$$\rho_3 = 1 - \left(1 - \rho_1\right)^2, \quad \text{since } m = \frac{3+1}{2} = 2.$$

Thus

$$\rho_3 = 0.34 \text{ for } \rho_1 = 0.19 \text{ (1.5 hour window)}$$

$$\rho_3 = 0.55 \text{ for } \rho_1 = 0.33 \text{ (2.5 hour window)}$$

and

$$\rho_3 = 0.66 \text{ for } \rho_1 = 0.42 \text{ (4.5 hour window)}$$

That is, 0.34 would be the probability of launch given a 1.5 hour window and a 3-day firing period; 0.55 would be the probability of launch given 2.5 hour window and a 3-day firing period; and 0.66 would be the probability of launch given a 4.5 hour window and a 3-day firing period.

Under the assumption that the recycle time is one day instead of two days,

$$\rho_n = 1 - \left(1 - \rho_1\right)^3$$

for a 3-day firing period, and thus

$$\rho_3 = 0.47 \text{ for } \rho_1 = 0.19 \text{ (1.5 hour window)}$$

$$\rho_3 = 0.70 \text{ for } \rho_1 = 0.33 \text{ (2.5 hour window)}$$

and

$$\rho_3 = 0.80 \text{ for } \rho_1 = 0.42 \text{ (4.5 hour window).}$$

2.3 SATURN V/APOLLO ON-TIME LAUNCH PROBABILITY WITH BUILT-IN HOLDS

2.3.1 Improvement in Probability of Launch

The use of built-in (scheduled) holds can lead to an increase in the probability of launch. A "built-in hold" is defined as a length of time in a countdown within which no work has been scheduled, the function of which is to provide time for "on schedule" completion of scheduled work that was delayed by previous unplanned holds.

Under the assumption that the failure rate is zero during the built-in holds under consideration, a value of P_L equal to 1.0 (or virtually so) could be attained by the use of built-in holds sufficiently close to T - 0 in the countdown. There are, however, certain practical restrictions and considerations which may place a limit on the length of the built-in holds and also on where they may be placed in the countdown.

Analysis of the various weapon and space vehicles reveals that, in general, the hold rate increases as the countdown nears T - 0; thus a large built-in hold near T - 0 would be very advantageous. This, however, cannot always be accomplished. In the case of the Atlas D, for example, a hold after T - 3.5 minutes necessitates a recycle to T - 3.5 minutes or earlier in the countdown sequence.

Let T' be the number of minutes prior to T - 0 where a built-in hold is to be placed, and let b be the time (in minutes) of the built-in hold. The countdown must start b minutes earlier than if no built-in hold were used. That is, if b equals 60 minutes, the countdown would start one hour earlier. If 40 minutes of unscheduled hold time occurred prior to T - T', the count would remain at T - T' for 20 minutes before continuing. Only if there were no unplanned holds called prior to T - T' would the count remain at T - T' for the entire hour.

2.3.2 Mathematical Model and Convolution Method

The mathematical expression for the implementation of built-in holds follows for all values logically admissible

$$P_L = P(\Delta t < b \text{ for } \bar{h}_2 \text{ and } \Delta t \leq W \text{ for } \bar{h}_1) + P\left[b < \Delta t < (b+W) \text{ for } \bar{h}_2 \text{ and } 0 < \Delta t < W \text{ for } \bar{h}_1\right]$$

where

$b \equiv$ length of built-in hold

$\Delta t \equiv$ excess time $= \Delta t_1 + \Delta t_2$

$\bar{h}_2 \equiv$ average number of holds prior to the built-in hold

$\bar{h}_1 \equiv$ average number of holds after (or subsequent to) the built-in hold

$W \equiv$ length of launch window

and logically admissible is defined as follows:

Let

$$\Delta t_1 = \text{excess time for } \bar{h}_1$$

and

$$\Delta t_2 = \text{excess time for } \bar{h}_2$$

then for

$$b < \Delta t_2 < b + W \text{ and } 0 < \Delta t_1 < W$$

we must always have,

$$\Delta t_2 - b + \Delta t_1 \leq W$$

or

$$\Delta t_2 + \Delta t_1 \leq W + b$$

That is, if $\Delta t_2 = b + (3/4)W$, then Δt_1 can only have values in the range $(0, W/4)$. Mathematically speaking, the convolution integral which is discussed below is computed numerically as follows:

$$P_L = \sum_{i=1}^{N} \Delta p_{1i} \bar{p}_{2i} + p_1(W)\, p_2(b)$$

where

$$\Delta p_{1i} = p_1(b + i + 1) - p_1(b + i)$$

and

$$\bar{p}_{2i} = \frac{p_2(k - i + 1) + p_2(k - i)}{2}$$

for

$$p_1 = P_{L_{\bar{h}_1}} \text{ and } P_2 = P_{L_{\bar{h}_2}}, \text{ and } N = \frac{W}{\Delta k}$$

Now we have that

$$P_L(\Delta t) = P_{L_{\bar{h}_1}}(W) \cdot P_{L_{\bar{h}_2}}(b) + \int_b^{b+W} P'_{L_{\bar{h}_2}}(k) P_{L_{\bar{h}_1}}(W + b - k)\, dk$$

where

$\tau \equiv$ average time lost per hold

$k \equiv W/\tau$

$P'_{L_{\bar{h}_2}} \equiv$ probability density function for the probability of launch for $\bar{h}_2$

$P_{L_{\bar{h}_1}} \equiv$ cumulative distribution function for the probability of launch for $\bar{h}_1$

For two built-in holds, the mathematics follow:

Let

$P_{LC} \equiv$ the probability distribution function computed by convoluting $P_{L_{\bar{h}_1}}$ with $P_{L_{\bar{h}_2}}$, where the first built-in hold $\equiv$ length b_1

$b_2 \equiv$ length of second built-in hold

$P_{L_{\bar{h}_3}} \equiv$ average number of holds subsequent to the second built-in hold.

Then,

$$P_L \equiv P_{LC}(W) \cdot P_{L_{\bar{h}_3}}(b_2) + \int_{b_2}^{b_2+W} P'_{LC}(k) P_{L_{\bar{h}_3}}(W + b_2 - k)\, dk$$

This procedure can be extended for any number of built-in holds.

2.3.3 Calculation of Launch Probability With and Without Built-in Hold

Figure 2-4 shows eight examples of the effect of built-in holds (BIH) for the Saturn V/Apollo vehicle with $\tau = 20$ minutes and $\bar{h} = 5.5$ for the total countdown. The eight cases are explained in the legend on the right-hand side of the figure. Also shown is the case of no BIH, and it is easily seen that the probability of launch is much greater using built-in holds. For instance, with a window of 1.5 hours (DI mission) P_L is 0.44 if no BIH is used, whereas P_L is 0.92 for the convolution of $\bar{h}_1 = 1.0$ with $\bar{h}_2 = 4.5$ using a BIH of 135 minutes. The 135-minute BIH thus accomplishes an increase of 110 percent in P_L over the value associated with no BIH.

To see the effect this has on ρ_n for a window of 1.5 hours, we use the formula

$$\rho_n = 1 - (1 - \rho_1)^m$$

where as before,

$$m = \frac{n+1}{2} \text{ for } n \text{ odd}$$

and

$$m = \frac{n}{2} \text{ for } n \text{ even}$$

$$\rho_1 = P_1 P_2 P_L = (1.0)(0.43)(0.44)$$

as before, with no built-in hold, for $\bar{h} = 5.5$ and

$$\rho_1 = P_1 P_2 P_L = (1.0)(0.43)(0.92) \text{ for the convolution of } \bar{h}_1 = 1.0$$

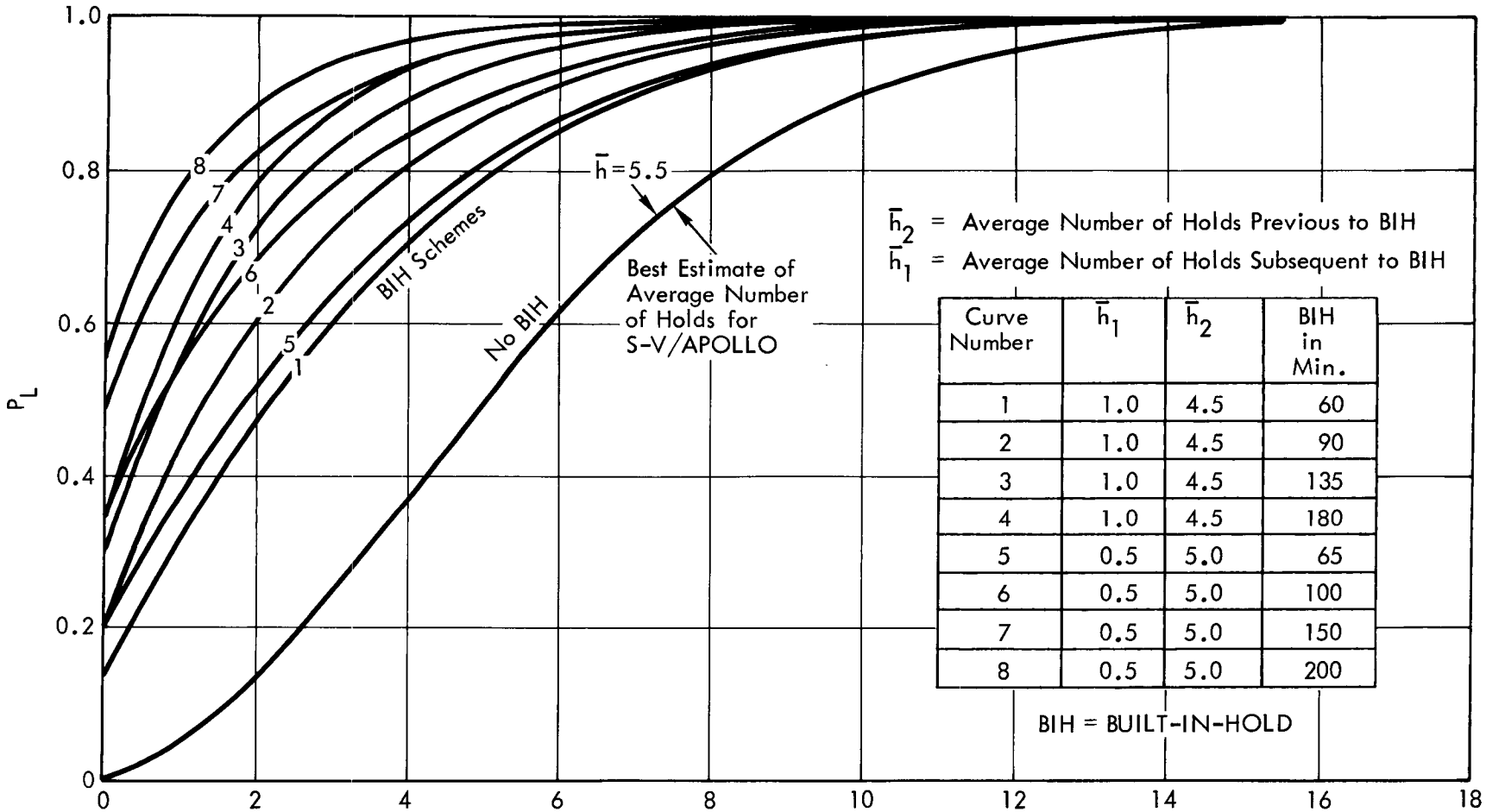

Curve Number	$\bar{h}_1$	$\bar{h}_2$	BIH in Min.
1	1.0	4.5	60
2	1.0	4.5	90
3	1.0	4.5	135
4	1.0	4.5	180
5	0.5	5.0	65
6	0.5	5.0	100
7	0.5	5.0	150
8	0.5	5.0	200

$$K = \frac{W}{\tau} = \frac{\text{LAUNCH WINDOW LENGTH}}{\text{AVERAGE TIME LOST PER HOLD}}$$

P_L is Conditional upon the Countdown not being Scrubbed for Technical Reasons Prior to T-0

Figure 2-4. Probability of Launch (P_L) as a Function of Window Length for Various Built-In Holds

with

$$\bar{h}_2 = 4.5 \text{ for a BIH of 135 minutes,}$$

and

$$m = \frac{n+1}{2} = \frac{3+1}{2} = 2 \text{ for } n = 3$$

Thus,

$\rho_1 = 0.19$ for $\bar{h} = 5.5$, as before, with no built-in hold (for a launch window of 1.5 hours)

and

$\rho_1 = 0.40$ for the convolution of the $\bar{h}_1 = 1.0$ and $\bar{h}_2 = 4.5$ curves using a 135-minute BIH inserted at the point in the countdown where there is one hold to go on the average (for a launch window of 1.5 hours).

Hence,

$$\rho_3 = 1 - (0.81)^2 = 0.34 \text{ for } \bar{h} = 5.5 \text{ and no BIH,}$$

and

$\rho_3 = 1 - (0.60)^2 = 0.64$ for the convolution of $\bar{h}_1 = 1.0$ with $\bar{h}_2 = 4.5$ for the BIH of 135 minutes.

This BIH hence increases ρ_3 by a factor of almost 2 over the no BIH scheme.

2.3.4 Launch Probability Using Built-In Holds

Experience from other space programs indicates that a built-in hold can, in general, be placed at the point in the countdown at which the expected number of holds remaining is only about 0.5 to 0.75. The $\bar{h}$ for the Saturn space vehicle is larger than the $\bar{h}$ for these other programs, i.e., 5.5 versus about 3.5. It therefore appears reasonable to assume that the built-in hold could be inserted where there is only one hold to go, on the average.

A built-in hold of 135 minutes produces a very large increase in the probability of launch, while at the same time it appears to have a tolerable amount of idle time associated with it. Hence, for comparison with the results obtained using no built-in hold, a 135 minute built-in hold, inserted at that point in the countdown subsequent to which there is an average of one hold to go (i.e., $\bar{h}_1 = 1.0$), has been used. This corresponds to curve number 3 in Figure 2-4.

It is emphasized there is no loss of generality in such an assumption because all of the built-in hold time does not have to be inserted at one point. That is, there are equivalent schemes, using more than one built-in hold, that produce the same launch probability as the 135 minute built-in hold which we have inserted. In general, these equivalent schemes require an increase in the built-in hold time; however, they are often preferred since they are frequently more compatible with operational constraints which must be satisfied during the countdown.

In Section 2.4, the probabilities of launch for both the DI and EPOI missions are summarized in tabular form under the following conditions: both with and without the use of built-in holds; for the range of values which can reasonably be expected for $\bar{h}$ (i.e., 5.0, 5.5, and 6.7); for the estimated probability of nonscrub, both including and excluding a consideration of sea states; and for both one-day and two-day turn-around (recycle) times of the countdown in the event of a scrub.

2.4 COMPARATIVE SUMMARY OF LAUNCH PROBABILITIES

2.4.1 Conditional Probability of Meeting Launch Window

Table 2-6 gives the conditional probability (P_L) of meeting a launch window if the countdown begins and is not scrubbed for technical reasons. The probabilities are given for both direct injection (1.5-hour window) and the earth parking orbit, and also with and without a built-in hold. The values used for the average number of holds per successful countdown ($\bar{h}$) are 5.0, 5.5, and 6.7. Figure 2-5 provides the same information for any length launch window. The idle times associated with the 135-minute built-in holds inserted close to T - 0 are also shown in Figure 2-5. The idle time varied from 62 minutes (for $\bar{h}$ = 5.0) to 40 minutes (for $\bar{h}$ = 6.7), and was equal to 55 minutes for the best estimate ($\bar{h}$ = 5.5).

It can be observed that without a built-in hold the EPOI mission has a P_L which varies from approximately 60 percent to 100 percent higher than the launch probability (P_L) for the DI mission. However, with a 135-minute built-in hold inserted at that point in the countdown where there is an average of one hold to go until T - 0 (vehicle liftoff) is reached, the P_L for the EPOI mission varies from only about 5 percent to 10 percent higher than the corresponding P_L for the DI mission.

Table 2-6. Conditional Probability of Meeting Launch Window if Countdown Begins and is Not Scrubbed for Technical Reasons

	P_L					
	No BIH			With BIH*		
Window Length W(hr) / Ave. No. of Holds per Countdown ($\bar{h}$)	1.5	2.5	4.5	1.5	2.5	4.5
$\bar{h} = 5.0$	0.51	0.81	0.99	0.935	0.99	1.00
$\bar{h} = 5.5$	0.44	0.76	0.98	0.92	0.985	1.00
$\bar{h} = 6.7$	0.31	0.64	0.95	0.87	0.965	1.00
Mission	Direct Injection	Earth Parking Orbit		Direct Injection	Earth Parking Orbit	

*Built-in hold (BIH) is 135 minutes in length and is inserted at that point in the countdown subsequent to which there is only one hold to go, on the average.

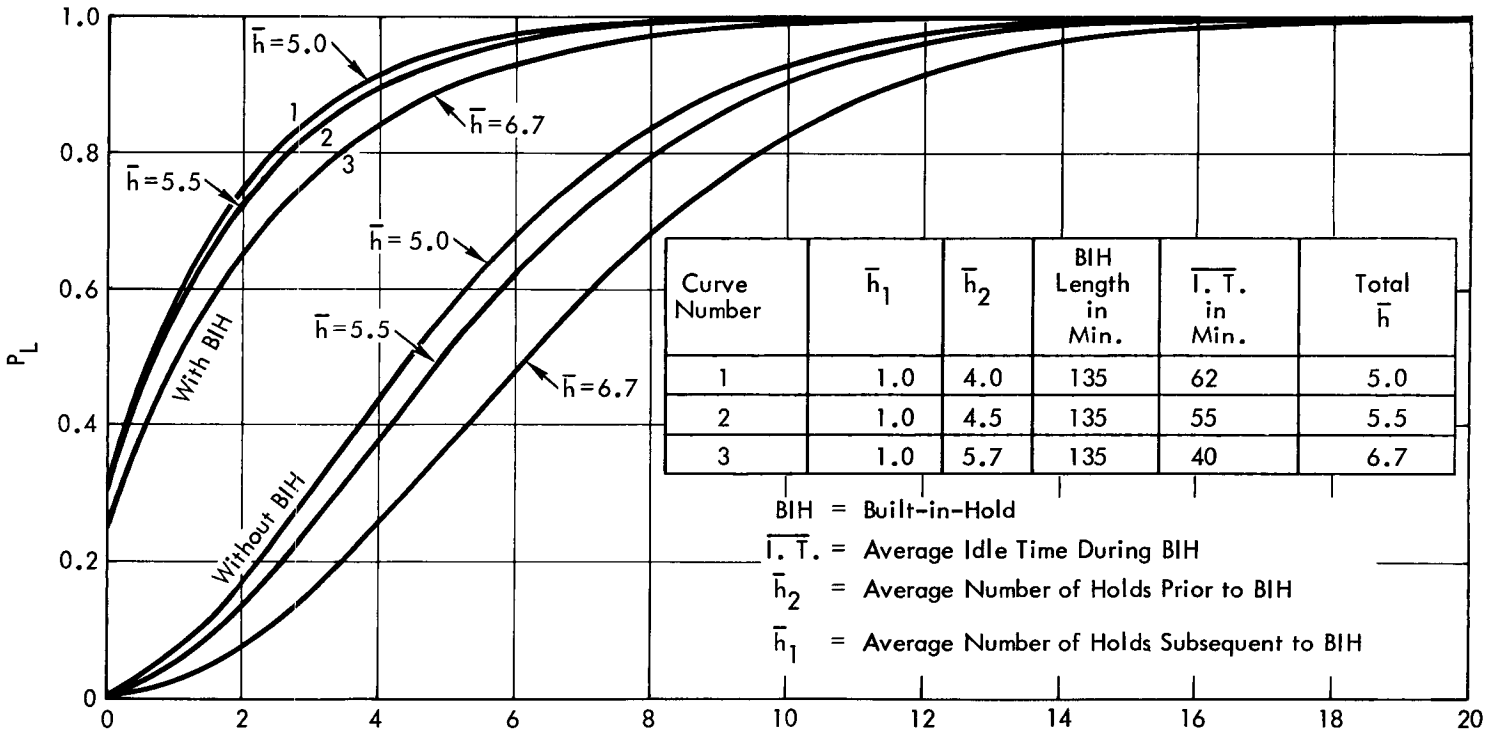

Curve Number	$\bar{h}_1$	$\bar{h}_2$	BIH Length in Min.	$\overline{I.T.}$ in Min.	Total $\bar{h}$
1	1.0	4.0	135	62	5.0
2	1.0	4.5	135	55	5.5
3	1.0	5.7	135	40	6.7

$$K = \frac{W}{\tau} = \frac{\text{LAUNCH WINDOW LENGTH}}{\text{AVERAGE TIME LOST PER HOLD}}$$

P_L is Conditional upon the Countdown not being Scrubbed for Technical Reasons Prior to T-0

Figure 2-5. Probability of Launch (P_L) as a function of Window Length for the Range of Values Estimated for $\bar{h}$ With and Without Built-In Holds

2.4.2 Two-Day Turn Around for Recommencement of Countdown

Tables 2-7 and 2-8 provide a comparative summary of the probabilities of launch during a three-day firing period (ρ_3) for the DI and EPOI missions, both with and without the use of built-in holds. These tables were based upon a two-day turn-around (recycle) time for the next commencement of the countdown in the event of a scrub. Table 2-7 employed a nonscrub probability of 0.43 (and hence excluded a consideration of sea states), whereas Table 2-8 employed a nonscrub probability of 0.31 (and hence included the consideration of sea states). An unsatisfactory sea state can, of course, cause scrubs and schedule slippages due to the necessity for successful recovery of the astronauts in the event of an abort.

These tables indicate that without a built-in hold the EPOI mission has a launch probability (ρ_3) which ranges from approximately 50 to 100 percent higher than the ρ_3 for the DI mission. With the built-in hold, however, the earth parking orbit varies from only about 5 percent to 10 percent higher than the ρ_3 for the direct injection mission.

2.4.3 One-Day Turn Around for Recommencement of Countdown

Tables 2-9 and 2-10 provide a comparative summary, similar to Tables 2-7 and 2-8, but for a one-day instead of a two-day turn around (recycle) time to the next commencement of the countdown in the event of a scrub.

2.4.4 Turn-Around Time in Excess of Two Days for Recommencement of Countdown

In the event that it is desired to determine launch probabilities (for the 3-day firing period) for the situation in which it is assumed that the turn-around time for the next commencement of the countdown (in case of a scrub) exceeds two days, these launch probabilities are readily ascertained since they are equal to ρ_1. The values of ρ_1 can readily be obtained from Tables 2-7 and 2-8, or alternatively from Tables 2-9 and 2-10.

Table 2-7. Probability of Launch During Three Day Firing Period (Excludes Consideration of Sea States)*
Two-Day Turn Around

ρ_3

Ave. No. of Holds per Countdown ($\bar{h}$) \ Window Length W(hr)	No BIH			With BIH**		
	1.5	2.5	4.5	1.5	2.5	4.5
$\bar{h} = 5.0$	0.390	0.575	0.671	0.642	0.671	0.675
$\bar{h} = 5.5$	0.342	0.547	0.665	0.635	0.668	0.675
$\bar{h} = 6.7$	0.248	0.474	0.651	0.608	0.658	0.675
Mission	Direct Injection	Earth Parking Orbit		Direct Injection	Earth Parking Orbit	

*$P_1 = 1.0$, $P_2 = 0.43$; 2-day turn around in event of scrub

$\rho_1 = P_1 P_2 P_L$

$\rho_3 = 1 - (1 - \rho_1)^2$

**The built-in hold (BIH) is 135 minutes in length and is inserted at that point in the countdown subsequent to which there is only one hold to go, on the average.

Table 2-8. Probability of Launch During Three Day Firing Period (Includes Consideration of Sea States)*
Two-Day Turn-Around

	ρ_3					
	No BIH			With BIH**		
Window Length W(hr) / Ave. No. of Holds per Countdown ($\bar{h}$)	1.5	2.5	4.5	1.5	2.5	4.5
$\bar{h} = 5.0$	0.291	0.439	0.520	0.496	0.520	0.524
$\bar{h} = 5.5$	0.254	0.416	0.516	0.489	0.517	0.524
$\bar{h} = 6.7$	0.183	0.357	0.503	0.467	0.509	0.524
Mission	Direct Injection	Earth Parking Orbit		Direct Injection	Earth Parking Orbit	

*$P_1 = 1.0$, $P_2 = 0.31$; 2-day turn around in event of scrub

$\rho_1 = P_1 P_2 P_L$

$\rho_3 = 1 - (1 - \rho)^2$

**The built-in hold (BIH) is 135 minutes in length and is inserted at that point in the countdown subsequent to which there is only one hold to go, on the average.

Table 2-9. Probability of Launch During Three Day Firing Period (Excludes Consideration of Sea States)*
One-Day Turn-Around

	ρ_3					
	No BIH			With BIH**		
Window Length W(hr) / Ave. No. of Holds per Countdown ($\bar{h}$)	1.5	2.5	4.5	1.5	2.5	4.5
$\bar{h} = 5.0$	0.524	0.723	0.811	0.786	0.811	0.815
$\bar{h} = 5.5$	0.466	0.695	0.806	0.780	0.809	0.815
$\bar{h} = 6.7$	0.348	0.619	0.794	0.755	0.800	0.815
Mission	Direct Injection	Earth Parking Orbit		Direct Injection	Earth Parking Orbit	

*$P_1 = 1.0$, $P_2 = 0.43$; 1-day turn around in event of scrub

$\rho_1 = P_1 P_2 P_L$

$\rho_3 = 1 - (1 - \rho_1)^3$

**The built-in hold (BIH) is 135 minutes in length and is inserted at that point in the countdown subsequent to which there is only one hold to go, on the average.

Table 2-10. Probability of Launch During Three Day Firing Period (Includes Consideration of Sea States)*
One-day Turn-Around

	ρ_3					
	No BIH			With BIH**		
Window Length W (hr) / Ave. No. of Holds per Countdown ($\bar{h}$)	1.5	2.5	4.5	1.5	2.5	4.5
$\bar{h} = 5.0$	0.403	0.580	0.667	0.642	0.667	0.672
$\bar{h} = 5.5$	0.355	0.554	0.663	0.635	0.664	0.672
$\bar{h} = 6.7$	0.261	0.484	0.650	0.611	0.656	0.672
Mission	Direct Injection	Earth Parking Orbit		Direct Injection	Earth Parking Orbit	

*$P_1 = 1.0$, $P_2 = 0.31$; 1-day turn around in event of scrub

$\rho_1 = P_1 P_2 P_L$

$\rho_3 = 1 - (1 - \rho_1)^3$

**The built-in hold (BIH) is 135 minutes in length and is inserted at that point in the countdown subsequent to which there is only one hold to go, on the average.

2.4.5 Best Estimates of Launch Probabilities

Best estimates of the launch probabilities (P_L and ρ_3) of the Saturn V/Apollo are summarized in Table 2-11. From this table it can be noted that the built-in hold produces a significant increase in the probability of on-time launch for the DI mission. With the use of the built-in hold, the difference in on-time launch probability (between the two injection modes) is significantly reduced.

2.4.6 Launch Probability Computer Programs

In Appendix A, the computer programs and associated plotter programs for obtaining and displaying launch probabilities are described. Using these programs, one can obtain the launch probabilities for any value of h, τ, and the window length, for any number, length, and placement of built-in holds. One of the outputs of the computer programs is the average idle time associated with the built-in holds. Appendix A also includes a rule-of-thumb approximation to the launch probability when a built-in hold is used.

Table 2-11. Comparison of Best Estimates of Launch Probabilities

	Launch Probabilities Without Built-In Hold			Launch Probabilities With Built-In Hold***		
	Direct Injection (1.5-hr window)	Earth Parking Orbit Injection (2.5-hr window)	Earth Parking Orbit Injection (4.5-hr window)	Direct Injection (1.5-hr window)	Earth Parking Orbit Injection (2.5-hr window)	Earth Parking Orbit Injection (4.5-hr window)
Conditional Probability of Launch if Countdown Begins and Is Not Scrubbed for Technical Reasons (P_L)*	0.44	0.76	0.98	0.92	0.985	1.00
Probability of Launch During 3-Day Firing Period (ρ_3)**	0.25	0.42	0.52	0.49	0.52	0.52

*See Table 2-6 for $\bar{h} = 5.5$.

**See Table 2-8 for $\bar{h} = 5.5$ (this includes consideration of sea states, and assumes a two-day turn around in the event of scrub).

***The built-in hold (BIH) is 135 minutes in length and is inserted at that point in the countdown subsequent to which there is only one hold to go, on the average.

3. IN-FLIGHT RELIABILITY COMPARISON

3.1 INTRODUCTION

In-flight reliability, or flight success probability, provides an excellent measure of the relative attributes of the direct injection (DI) and the earth parking orbit injection (EPOI) missions. Several different data sources have been employed to draw reliability comparisons between the Saturn V/Apollo mission with an earth parking orbit injection and the same mission utilizing direct injection.

3.2 COMPARISON OF EQUIPMENT OPERATING TIME

Since, in general, reliability can be considered a function of operating time, it is desirable to first obtain a comparison of equipment operating time (Table 3-1), for the two types of missions. Due to the operating characteristics of certain equipment, it is necessary to list not only the overall time that the equipment is in a state available for operation, but also the number of cycles, switching operations, etc., and the actual cycle time involved for the two types of missions. The attitude control subsystem of the S-IVB is an example of this. From Table 3-1, it is apparent that while some equipment operating times are unchanged, the majority are in use for less time in the DI mission, and the time is increased in only one instance, S-IVB burn time.

3.3 RELIABILITY COMPARISONS

The initial reliability comparison was made utilizing Douglas Aircraft Company (DAC) reliability data for the S-IVB subsystems. The DAC reliability work sheets provided a convenient means of deriving reliability estimates suitable for comparison purposes for both types of mission. The comparison based on these work sheets did not include estimates for the thrust generation, airframe, data acquisition, and command destruct subsystems. However, assuming that thrust generation (J-2 engine) is the most serious omission, it should be pointed out that inclusion of the additional burn time, using DAC reliability design goals, results in a decrease in a total DI reliability figure of only 0.00003.

Information obtained from Marshall Space Flight Center (MSFC) on the S-IVB provided the data from which two additional comparisons were made. Unreliability and criticality* were obtained by much the same manner as reliability was obtained from the DAC work sheets. The subsystem data on thrust generation, airframe, data acquisition, and command destruct were not available from the Marshall Space Flight Center data, but the assumption made above with regard to the DAC reliability numbers should also be applicable with the Marshall Space Flight Center data. It should be noted that data from both sources (DAC and MSFC) are based on a 4.5-hour earth parking orbit.

The General Electric Apollo Support Department reliability comparison was made using the GE/SOAR III/Cindy I computer program. This program included the entire Saturn V/Apollo mission, whereas the DAC and MSFC data were concerned only with the S-IVB stage and did not consider any change in the success probability of the mission after transposition. The GE reliability figures presented in this section are component reliability figures and are not representative of mission success. It is believed, however, that they are pertinent for comparison purposes. This particular computer program used a 77-minute earth parking orbit.

The compilation, analysis, and summary of historical flight reliability data by STL's Florida Division represents the most up-to-date, relevant historical information available at this time, and is the only information based on actual flight performance.

Tables 3-1 through 3-8 presented at the end of this section give the relevant comparisons of in-flight reliability associated with the DI and EPOI missions. A description of these tables follows.

---

*Criticality is defined as the probability of an item contributing to stage loss and is the product of the conditional probability of stage loss associated with the type of failure times the mission unreliability times 10^6. Reference: Reliability Mathematical Model Saturn S-IVB Stage, Douglas Report SM 43610, dated 15 April 1963.

S-IVB equipment operating time through transposition is shown in Table 3-1. These operating times have been extracted from Douglas Report SM-44748 utilizing Douglas reliability work sheets, revised July 1964, and are derived from the Douglas assumption of a 4.5-hour parking orbit. Operating times for direct injection were obtained by deletion of Phase E (Douglas definition: 1st Coast Phase) equipment operating time provided in the Douglas work sheets.

Comparison of DAC S-IVB reliability estimates is shown in Table 3-2. The EPOI reliability was obtained by a serial multiplication of the subsystem component mission reliabilities through transposition. DI reliability was obtained by adding the Phase E unreliabilities to the component mission reliabilities and then performing the same multiplication as stated above. The Douglas reliability estimates were based on a 4.5-hour earth parking orbit and no attempt was made to time-scale these reliabilities to any other orbital time duration. Douglas component criticalities are not summed by mission phase to obtain mission criticality, but rather the phase which has the highest criticality is used to represent mission criticality which in turn is subtracted from 1.0 to obtain mission probability of stage loss. As a result of this, it is not permissible to subtract Phase E criticality from mission criticality to arrive at a number which represents mission probability of stage loss during direct injection.

Table 3-3 is a tabulation of the MSFC S-IVB Criticality Ranking Summary providing unreliability and criticality figures for components of the S-IVB and S-IC ignition cycle start through transposition. Unreliability and criticality for the direct injection mission were obtained by deleting mission events 32 through 43 in the MSFC mission events list (earth parking orbit of 4.5 hours).

Table 3-4 presents a summary of GE/ASD/SOAR III/Cindy I component reliabilities for the entire Apollo mission, including a 77-minute earth parking orbit (sub-phases 11 through 24 of the Cindy event list). Reliability figures for a DI mission were obtained by extracting those unreliabilities that occurred during sub-phases 11 through 24 and adding them to the total EPOI mission. It should be noted that these are component reliabilities only, and a direct comparison with mission success cannot be drawn.

Data from the Able Star, Agena, and Titan I missile systems have been collected and studied. Areas of interest were the number of failures during three periods of operation; namely, ignition, steady state burning, and shutdown. Figures have been gathered to show the number of successful tests, no-test cases, and failures. A reliability figure has been derived by dividing the number of successful tests by the total number of applicable tests (successes plus failures). The values of reliability for each of the three modes of operation have been multiplied to give an overall reliability. A summary of this information is listed in Table 3-5.

The Able-Star vehicle, which uses pressure-fed hypergolic propellants (UDMH/IRFNA), has restart capability. The results of 13 flights from 13 April 1960 through 5 December 1963 are shown in Table 3-5. The one failure during first burning was the result of a propulsion problem. Problems associated with the second burning of the stage are explained in Table 3-6.

There is known to have been a propulsion anomaly (a momentary flameout due to a bubble in the propellant) during the second ignition of one vehicle. This propulsion problem did not result in a failure, and was not considered to be a failure; however, if the propellants had not been hypergolic, a failure could have occurred. Hence the value shown in Table 3-5 for the reliability of restart could realistically be lowered.

The Agena vehicle also uses pressure-fed hypergolic (UDMH/IRFNA) propellants. There have been three series of Agena vehicles A, B, and D. The B can be programmed to restart once, and the D vehicles can have a restart capability of up to four times.

The first Agena launch was in February 1959 and 123 have been launched through March 1964. Reliability for the Agena during both first and second burn is shown in Table 3-5. Flight test result information for the classified programs is limited, but it appears that only 39 of the flights planned to use restarts of the Agena. Eighty-four flights had only a single burn. Failures during first burn were attributable to several subsystems including propulsion, guidance, electrical, AGC, and hydraulics.

Reasons for failures during second burn of the Agena are listed in Table 3-6. It can be observed that for the 39 vehicles which had a multiple burn capability, none had a failure during the first burning period. Six cases are not applicable due to five booster failures and one guidance failure which was present before launch and which precluded a successful second ignition.

The Titan I is a two-stage cryogenic pump-fed propulsion system. Only the G, J, and M series were evaluated in Table 3-5. First stage failures were due to propellant, pressurization, and flight control problems.

Second stage failures are listed in Table 3-6. Although neither stage of this vehicle had a restart capability, it does resemble the S-IVB stage in that it uses cryogenic propellants (LOX and RP-1) and the second stage is ignited in a space environment. It will be noted that the second stage reliability is the lowest of all vehicles shown.

The Agena vehicle has been used in many instances to provide a proper orientation for the payload by use of its attitude control system (ACS) for the entire mission. The ACS also provides vehicle stabilization during the shorter burn time and coast phase (if applicable). Of the 123 flight tests which were analyzed, the ACS function was successful on 86 flights, failed on 13, was not applicable on 24, and hence had a reliability per flight of $86/(86 + 13) = 0.868$. These flights did not all have the same planned duration of operation for the ACS. The greater number of Agena vehicles have been launched in the Discoverer Program, in which most vehicles were placed into a nominal 90-minute orbit with a planned orbit lifetime of from 17 to as many as 64 orbits. As a result, where no information could be found concerning the planned ACS operating time, a mission duration of 17 orbits and an orbital period of 90 minutes was assumed.

Table 3-7 lists the failures of the ACS function. For those flights which did have a failure, it occurred on the average during the 11th orbit after about 990 minutes of operation. There were five failures during the first 105 minutes of operation. Since the time in an

earth parking orbit for the S-IVB is presently planned to be of about this same duration, we may apply the Agena ACS value of reliability (1-5/99 = 0.9499) to the S-IVB in the EPOI mission.

Table 3-7 also itemizes the failure areas. There were only four failures of the attitude control system. Other failures were due to support or peripheral equipment and systems. A histogram (Figure 3-1) shows time of occurrence of the ACS failures.

Table 3-7 lists the total operating time before failure for the 13 vehicles where failure occurred. Data about the planned duration of operation of ACS was not always available. Where data was not available, a 17-orbit mission of 90 minutes per orbit was again assumed. This time totaled 133,560 minutes for the 86 successful missions, and the total time before failure of the unsuccessful missions was 12,870 minutes. Therefore, the total number of minutes of successful operation of ACS = 133,560 + 12,870 = 146,430.

Mean time before failure in ACS mode = (146,430/13) = 11,265 minutes.

Mean time before failure of ACS only = (146,430/4) = 36,608 minutes.

Table 3-8 provides a listing suitable for quick comparison of reliabilities, unreliabilities, and criticalities for the two types of missions discussed in this report. The last column on the right lists the percentage of improvement of the Direct Injection versus Earth Parking Orbit Injection missions.

The following is a brief description of the source of information summarized in the table.

a) Reliability estimates based on DAC data represent the final product of the reliabilities listed in Table 3-2 (4.5-hour EPO).

b) GE/SOAR III/Cindy I represents the final product of the reliabilities listed in Table 3-4. These reliabilities are based on a 77-minute orbit. As stated previously, the reliability product is based upon individual component reliability and is not representative of mission success.

c) Same as b), but scaled to a 2-hour, 48-minute, 50.6-second orbit.

d) Summation of MSFC (Table 3-3) unreliability (4.5-hour earth parking orbit).

e) Summation of MSFC (Table 3-3) criticality (4.5-hour earth parking orbit).

f) Flight results of Missile System A (Able Star) mission success during second burn (analogous to earth parking orbit with reignition), versus first burn (analogous to direct injection).

g) Flight results of Missile System B (Agena) mission success during second burn (analogous to earth parking orbit), versus first burn (analogous to direct injection).

h) Flight results of Missile System C (Titan I) second stage. Although this system did not have reignition capabilities the functional aspects more closely resemble the S-IVB than the previous missile Systems A and B, and at the time of ignition the environment approximates that of the S-IVB.

The reliabilities listed in a) and the unreliabilities and criticalities listed in d) and e) do not contain the unreliability of the thrust generation (J-2 engine) subsystem. In view of the actual flight analysis of missile systems A, B, and C, it would appear erroneous to assume a reliability of 1.0 for this portion of the S-IVB. Another inconsistency, borne out by f) and g) is reignition reliability. It appears that at least 30 discrete events must be completed over a period of approximately 6 seconds to achieve proper ignition and reignition of the S-IVB. Relays, logic circuitry and electrical times must operate properly. Numerous solenoid control valves and pneumatic valves must be energized and de-energized, and at various steps temperatures and pressures must be sampled.

It appears that the complexity of the J-2 (S-IVB) start requirement is greater than the sequences used during the early R and D flights of the second stages of Titan I and II, and the F1 and AC2 Centaur, and as such, a reliability consistent with this complexity should be used.

Table 3-1. Equipment Operating Time

SUBSYSTEM	EPO OPERATIONAL TIME*	DIRECT INJECTION TIME*	DIFFERENCE* + (INCREASE) - (DECREASE)
S-IC Burn Time	150.6 sec.	150.6 sec.	-0.1 sec.
S-II Burn Time	388.9 sec.	388.9 sec.	0
S-IVB Burn Time	480.0 sec.	493.0 sec.	+13
Fuel Fill & Drain 21.1	4.79	.29	-4.5
Oxidizer Fill & Drain 21.1	4.79	.29	-4.5
Fuel Tank Pressurization (V-IVB-22.1)	4.64	.14	-4.5
Oxidizer Tank Pressurization (V-IVB-22.2)	4.79	.29	-4.5
Propellant Pressurization Control (V-IVB-22.3)	4.79	.29	-4.5
Fuel Tank Re-Pressurization (V-IVB-22.4)	4.70	.20	-4.5
Oxidizer Tank Re-Pressurization (V-IVB-22.4)	4.70	.20	-4.5
Oxidizer Tank Re-Pressurization (V-IVB-22.5)	4.70	.20	-4.5
Pneumatic Control (23)	4.70	.20	-4.5
Fuel Feed & Chilldown (25.1)	4.79	.29	-4.5
Oxidizer Feed & Chilldown (25.2)	4.79	.29	-4.5
Ullage Positioning (V-IVB-26.1)	4.79 630 sec. 11 cycles	.29 618 sec. 10 cycles	-4.5 -12 sec. - 1 cycle
Oxidizer Tank Vent Control (V-IVB-27.1)	4.79	.29	-4.5
LO_2 Tank Vent Control	6.79	2.29	-4.5
Fuel Tank Vent Control (V-IVB-27.2)	6.79	2.29	-4.5
Propellant Utilization (V-IVB-30)	.14	.14	0
Propellant Mass Sensing (V-IVB-31)	.14	.14	0

*Time in hours unless otherwise specified.

[redacted]

Table 3-1. Equipment Operating Time (Continued)

SUBSYSTEM	EPO OPERATIONAL TIME *	DIRECT INJECTION TIME *	DIFFERENCE * + (INCREASE) - (DECREASE)
Path Control (V-IVB-41)	4.79	.29	-4.5
Attitude Control (V-IVB-42)	6.79 200.2 sec. 2002 cycles	2.29 135 sec. 652 cycles	-4.5 -65.2 sec. -1350 cycles
Electrical Power Supply (V-IVB-51)	6.79	2.29	-4.5
Hydraulic Power Supply (V-IVB-52)	4.79 12 cycles	.29 3 cycles	-4.5 -9 cycles
S-II to S-IVB Separation (V-IVB-61)	.15	.15	0
Electrical Distribution (V-IVB-71)	6.79	.29	-4.5
Electrical Command (V-IVB-72)	6.79	2.29	-4.5
Internal Power	6.79	2.29	-4.5
Forward Skirt Environmental Control (V-IVB-91)	6.79	2.29	-4.5
Aft Skirt Environmental Control (V-IVB-92)	2.15	.15	-2.00
Safe & Arm (V-IVB-102)	.20	.20	0

*Time in hours unless otherwise specified.

[redacted]

[redacted]

Table 3-2. Comparison of DAC S-IVB Reliability Estimates for Earth Parking Orbit Versus Direct Injection

SUBSYSTEM	EPO RELIABILITY	DI RELIABILITY	
Airframe	*	*	
Fuel Fill & Drain	0.998955	0.999720	
Oxidizer Fill & Drain	0.998955	0.999096	
Fuel Pressurization	0.996269	0.996737	
Oxidizer Pressurization	0.996507	0.997317	
Propellant Pressurization	0.990048	0.990334	
Fuel Re-Pressurization	0.997649	0.998124	
Oxidizer Re-Pressurization	0.997649	0.998124	
Pneumatic Control	0.987212	0.989781	
Fuel Feed & Chilldown	0.997761	0.999153	
Oxidizer Feed & Chilldown	0.997527	0.998061	
Ullage Positioning	0.979322	0.986292	
Oxidizer Tank Vent Control	0.998739	0.998909	
Fuel Tank Vent Control	0.990368	0.992357	
Thrust Generation	*	*	
Propellant Utilization	0.996761	0.996761	
Propellant Mass Sensing	0.999272	0.999272	
Path Control	0.997891	0.998184	
Attitude Control	0.982857	0.981855	
Electrical Power Supply	0.937532	0.950073	
Hydraulic Power Supply	0.976565	0.979032	
Separation	0.981120	0.981120	
Electrical Distribution	0.993498	0.994185	
Electrical Command	0.922482	0.932188	
Data Acquisition	*	*	
Internal Power	0.996236	0.996711	
Forward Skirt Environmental Control	0.998597	0.998617	
Aft Skirt Environmental Control	0.999848	0.999850	
Command Destruct	*	*	
Safe and Arm	0.998394	0.998394	
TOTAL	0.742108	0.775464	4.3% Increase in Reliability

*Reliability figures are not available and were assumed to be 1.0 for this comparison.

[redacted]

[redacted]

Table 3-3. MSFC Criticality Ranking Summary

COMPONENT	ALPHA	ENV. ADJ.FAC.	FAILURE RATE	ADJ. UNREL.	CRIT.	ADJ. CRIT.	UNREL.
Fuel Shut Off Valve	.200	1000.	4.6	690.00	317.4	317.4	726.80
Fuel Fill & Drain Piping	1.000	1000.	5.48	1342.60	272.62	272.62	1835.80
Oxidizer Shut Off Valve	.200	1000.	4.6	717.6	278.76	278.76	800.40
Oxid. Fill & Drain Piping	1.000	1000.	4.66	1352.40	239.99	239.99	1561.10
Solenoid Valve Control	.300	1000.	4.6	552.00	55.2	55.2	552.00
Pressure Switch	.400 .300	1000.	20.0	2800.00	280.0	280.0	2800.00
Solenoid Valve Stop	.300	1000.	4.6	599.70	361.95	361.95	723.9
Pressure Switch Stop	.500	1000.	20.0	2900.00	1675.00	1675.00	3350.0
Subsystem Plumbing	1.000	1000.	8.6	2494.0	442.9	442.9	2881.0
Pressure Spheres	.990	1000.	.24	68.90	12.23	12.23	79.59
Relief Valve	.400 .300	1000.	5.70	1157.1	583.96	583.96	1336.65
Dump Valve Solenoid	.500	1000.	4.60	667.00	118.45	118.45	770.50
Pressure Regulator	.500	1000.	2.14	310.3	132.72	132.72	358.45
He_2 Supply Shut Off Valve	.500	1000.	.56	162.40	110.6	110.6	187.60
Pressure Switch	.300	1000.	20.00	1740.0	1065.0	1065.0	2010.00
Pressure Switch Flight Control & Pre-Press.	.300 .400	1000.	20.00	4060.0	1941.0	1941.0	4690.00
Low Pressure Plumbing	1.000	1000.	1.43	414.70	253.82	253.82	479.05
By-Pass Control Valve	.500	1000.	2.24	324.80	57.68	57.68	375.20
Vent Valve Pneumatic	.400 .300	1000.	6.50	1319.50	1524.25	1524.25	1524.25
Relief Valve	.400 .300	1000.	6.50	1319.50	1524.25	1524.25	1524.25
Pressure Sphere	1.000	1000.	.08	116.0	13.4	13.4	134.00
Relief Valve	.400 .300	1000.	3.90	791.70	561.79	561.79	914.55
Dump Valve Solenoid	.500	1000.	.22	31.90	18.42	18.42	36.85
Solenoid Valve Re-Press	.200 .300	1000.	6.50	942.50	500.82	500.82	1088.75
Pressure Sphere	1.000	1000.	.08	23.20	2.68	2.68	26.00
Relief Valve	.300 .200	1000.	3.90	565.50	222.10	222.10	653.25
Dump Valve Solenoid	.400	1000.	.22	25.52	2.94	2.94	29.48
Solenoid Control Valve	.200	1000.	6.50	377.00	435.5	435.5	435.5
Subsystem Plumbing	1.000	1000.	8.60	2494.0	288.1	288.1	2881.00
Pneu. Power Control Mod. Switch	.100	1000.	3.27	65.73	80.44	80.44	80.44
Pneu. Power Control Mod. Switch	.100	1000.	20.00	402.0	492.0	492.0	492.0
Pneu. Power Control Mod. Valve	.200	1000.	4.60	184.92	226.32	226.32	226.32
Actuator Vent Control Mod.	.400	1000.	4.60	369.84	452.64	452.64	452.64
Pneu. Control Piping	1.000	1000.	8.60	2494.0	288.1	288.1	2881.0
Check Valve	.500	1000.	2.30	667.0	310.5	310.5	770.50

[redacted]

[redacted]

Table 3-3. (Continued)

COMPONENT	ALPHA	ENV. ADJ.FAC.	FAILURE RATE	ADJ. UNREL.	CRIT.	ADJ. CRIT.	UNREL.
Chill Down Pump	.300 .200	900.	13.50	911.25	689.17	689.17	922.72
Fuel Piping	1.000	1000.	16.44	4767.60	846.66	846.66	5507.40
Check Valve	.500	1000.	2.30	667.0	770.50	770.50	770.5
Oxidizer Piping	1.000	1000.	13.98	4054.20	719.97	719.97	4683.30
Chill Down Pump	.300 .200	900.	13.50	911.25	689.17	689.17	922.72
Engine 1750 LB Thrust	.300 .400	1000.	.10 1.00 1.08	292.66	126.86	109.28	229.29
Engine 150 LB Thrust	.400	1000.	1.000	232.00	66.14	49.22	268.00
Fuel Tank Relief Valve	.940 .010	1000.	3.90	1074.99	1230.11	1230.11	1228.11
Fuel Vent Relief Valve	.010	1000.	3.90	11.31	2.0	2.0	13.06
Vent Relief Valve Vent Function	.090 .900 .010	1000.	5.70	62.70	241.01	239.63	319.19
Vent Relief Valve Relief Function	.090 .900 .010	1000.	5.70	1653.00	1151.34	1151.34	1909.49
Low Pressure Sensing Switch	.600 .200	1000.	12.0	432.00	388.8	64.8	972.0
Venting System Plumbing	1.000	1000.	5.75	1667.50	475.43	353.82	1926.25
Subsystem Wiring	.700 .300	1000.	8.10	1134.00	149.84	149.84	1134.00
Electric Assy Function C&D	.400 .600	1000.	14.4	2016.0	266.40	266.40	2016.00
Oxidizer Mass Sensor	.700 .300	1000.	2.6	364.0	121.81	121.81	364.00
Fuel Mass Sensor	.700	1000.	2.6	364.0	48.10	48.10	364.00
Servo Cylinder Assy 2	.070 .925 .005	1000.	5.10	2958.0	539.77	539.77	3416.99
Servo Valve 2	.100 .400	1000.	5.10	2957.99	2049.4	2049.4	3416.50
Fuel Shut-off Valve	.200	1000.	4.60	46.00	46.00	46.00	46.00
Cylinder By-Pass Valve	.400 .200	1000.	2.24	779.50	392.44	392.44	900.48
Subsystem Plumbing	1.000	1000.	1.00	290.0	51.5	51.5	335.0
Feed Back Transducer 2	.010 .002	1000.	5.10	49.78	40.48	40.48	55.28
Subsystem Plumbing	1.000	1000.	.30	93.0	32.96	26.62	106.50
Subsystem Plumbing	1.000	1000.	.30	93.0	30.01	23.26	106.50
Helium Fill Disconnect Vehicle Half	.100	1000.	.40	12.40	4.00	3.1	14.20
Helium Sphere	.990	1000.	.07	42.97	13.85	10.74	49.20
Helium Dump Valve	.200	1000.	5.70	353.40	114.08	91.43	404.70

[redacted]

[redacted]

Table 3-3. (Continued)

COMPONENT	ALPHA	ENV. ADJ.FAC.	FAILURE RATE	ADJ. UNREL.	CRIT.	ADJ. CRIT.	UNREL.
Pressure Relief Valve	.300 .400	1000.	3.90	846.30	591.90	452.48	969.15
Helium Fill Subsystem Plumbing	1.000	1000.	.30	93.0	30.01	23.26	106.50
Helium Pressure Reg. Subsystem Plumbing	1.000	1000.	.20	62.0	20.01	15.51	71.00
Solenoid Pressure Relief Valve 2	.600	1000.	4.60	1504.20	481.22	375.65	1752.60
Vent Line Disconnect	.300	1000.	.40	74.40	24.01	18.61	85.20
Propellant Press. Sub-System Plumbing	1.000	1000.	.30	93.0	30.01	23.26	106.50
Engine 150 LB Thrust	.10 .30 .60	1000.	.10 1.00 1.08	4006.21	1342.56	1180.32	4249.89
Fwd. Battery No. 1 Cell Assy	.490	1.0	288.0	646.32	424.84	292.76	1916.40
Fwd. Battery No. 1 Box Assy.	.100	1000.	.38	11.78	3.79	2.94	13.49
Fwd. Battery No. 1 Ext.-Int. Switch	.020	1000.	10.68	132.50	42.74	37.58	151.72
Fwd. Power Dist. Box Assy.	.100	1000.	.38	11.78	3.79	2.94	13.49
Fwd. Battery No. 2 Cell Assy.	.500	1.0 1000.	144.0	22484.88	3743.78	3743.78	26048.88
Fwd. Battery No. 2 Box Assy.	.100	1000.	.19	5.51	.97	.97	6.36
Fwd. Battery No. 2 Ext.-Int. Switch	.020	1000.	10.68	128.22	22.00	22.00	147.44
Aft. Battery No. 1 Cell Assy.	.490	1.	288.0	646.32	424.84	292.76	1916.40
Aft. Battery No. 1 Box Assy.	.100	1000.	.38	11.78	3.79	2.94	13.49
Aft. Battery No. 1 Heater Assy.	1.000	100. 1000.	9.62 1.40	732.22	236.35	183.21	838.51
Aft. Battery No. 1 Ext.-Int. Switch	.040	1000.	10.68	132.94	42.75	33.14	151.72
Aft. Power Distribution Box Assy.	.100	1000.	.38	11.78	3.79	2.94	13.49
Aft. Battery No. 2 Cell Assy	.490	1.	288.0	81.84	140.26	140.26	1351.92
Aft. Battery No. 2 Heater Assy.	1.000	1000. 100.	1.40 9.62	684.98	121.64	121.64	791.27
Aft. Battery No. 2 Ext.-Int. Switch	.040	1000.	10.68	123.94	22.00	22.00	143.17
Relay Power Switching Input S-S Transmitter	.190	1000.	.21	4.39	1.23	1.06	6.18
Relay Power Switching Flight Transmitter Group	.190 .310	1000.	.21	7.17	1.43	1.26	11.88

[redacted]

[redacted]

Table 3-3. (Continued)

COMPONENT	ALPHA	ENV. ADJ.FAC.	FAILURE RATE	ADJ. UNREL.	CRIT.	ADJ. CRIT.	UNREL.
Relay Power Switching In-Orbit Transmitter Group	.190 .310	1000.	.21	7.17	1.43	.97	11.88
Relay Switching In Orbit SCO Group	.190 .310	1000.	.21	2.00	.66	0.00	6.71
Relay Power Switching In-Flight SCO Group	.190 .310	1000.	.26	14.3	2.53	1.95	20.14
Relay Power Switching In Rec. & Meas. Group	.190 .310	1000.	.26	14.29	2.46	2.46	14.29
Relay Power Switching In DDA Power	.310	1000.	.21	7.16	1.23	1.23	7.16
Relay Power Switching In Single-Sideband Group	.310	1000.	.21	7.17	2.02	1.73	10.09
Relay Power Supply Input C.O. Meas. Group	.310	1000.	.21	20.19	7.13	5.76	23.11
Inverter Converter Assy.	1.000	1000.	27.15	7873.50	1398.22	1398.22	9095.25
Inverter Converter Power Distr. Relay In.	.190 .310	1000.	.21	45.16	6.78	6.78	54.58
Inverter Converter Box Assy.	.100	1000.	.19	2.66	.43	.43	3.51
Relay 28 VDC Power Supply Input PU & DU Oven	.190 .310	1000.	.21	30.16	4.93	4.93	39.56
Relay Power Supply Input Hydraulic Motor Pump	.310 .190	1000.	.21	9.45	2.17	2.17	17.08
Relay Power Supply Input Press. & Temp. Switch	.310	1000.	.21	20.19	7.13	5.76	23.11
Relay Power Supply Input LOX Chilldown Motor Pump	.190 .310	1000.	.21	15.01	2.65	1.16	17.93
Relay Power Supply Input H_2 Chilldown Pump Bleed VLV	.190 .310	1000.	.21	15.01	2.65	1.16	17.93
Subsystem Wiring	.700 .300	1000.	10.85	3363.50	1217.80	978.08	2851.74
Electric Motor 3 HP	1.0	1000.	9.36	2714.40	2749.96	2749.96	2749.96
Hydraulic Pump	.750 .500 .250	1000.	13.50 13.50 2.00	4495.0	2055.09	2055.09	4550.09
Thermal Switch	.50	1000.	.16	483.0	497.48	497.48	497.48
Check Valve High Press.	.001	1000.	2.3	.21	.31	.31	.31
Check Valve Low Press.	.999	1000.	2.3	666.33	769.72	459.54	769.72
Pump Engine Driven	.75 .25	1000.	13.50	1890.00	857.24	857.24	2497.49

[redacted]

[redacted]

Table 3-3. (Continued)

COMPONENT	ALPHA	ENV. ADJ.FAC.	FAILURE RATE	ADJ. UNREL.	CRIT.	ADJ. CRIT.	UNREL.
Check Valve	.001	1000.	2.30	207.00	500.51	500.51	770.49
Check Valve	.001 .999	1000.	2.30	667.0	119.09	119.09	770.49
Bleed & Sample Valve	.500	1000.	5.00	725.0	128.75	128.75	837.50
Accumulator Reservoir Assy.	.970 .010	1000.	5.00	1421.0	260.64	260.64	1641.50
Nitrogen Fill Valve	1.000	1000.	.11	32.48	5.76	5.76	37.52
High Press. Relief Valve	.999	1000.	5.00	1448.55	1086.41	1086.41	1673.32
Subsystem Plumbing	.990	1000.	25.00	7177.50	1274.62	1274.62	8291.25
Tension Plate	1.000	1.	1.0	.15	.15	.15	.15
S-IV B Wiring & Conn. To S-IV B Switch Selector	.330	1.	.80	82.35	81.78	67.51	94.30
S-IV B Wiring & Conn. To S-IV B Switch Selector	.330	1.	2.10	214.83	214.15	176.91	246.01
S-IV B Wiring & Conn. To S-IV B Switch Selector	.330	1.	.88	90.03	89.74	74.14	103.09
Sequencer	.050 .250	1000.	.34	10.88	2.79	2.41	14.70
Sequencer	.250	10.	.34	1.70	.89	.51	5.52
Sequencer	.250	10.	.34	0.00	.38	0.00	3.82
Sequencer	.250	1000.	.34	9.35	2.64	2.26	13.17
Sequencer	.050	1000.	.34	1.53	.15	.15	1.53
Sequencer	.250	10.	.34	0.00	.38	0.00	3.82
Sequencer	.250	10.	.34	1.70	.17	.17	1.70
Sequencer	.050 .250	10.	.34	0.00	.24	0.00	4.58
Sequencer	.050 .250	1000.	.34	29.75	10.64	8.09	41.21
Sequencer	.250	1000.	.34	26.35	9.32	7.53	30.17
Sequencer	.050 .250	1000.	.34	31.45	11.20	8.30	43.67
Sequencer	.050 .250	1000.	.34	4.08	1.86	.88	13.24
Sequencer	.050 .250	1000.	.34	14.02	3.88	2.86	14.78
Sequencer	.050	1000.	.34	2.55	2.29	1.27	3.31
Sequencer	.050	10.	.34	0.00	.76	0.00	.76

[redacted]

[redacted]

Table 3-3. (Continued)

COMPONENT	ALPHA	ENV. ADJ.FAC.	FAILURE RATE	ADJ. UNREL.	CRIT.	ADJ. CRIT.	UNREL.
Sequencer	.050 .100	1000.	.34	5.10	1.57	.89	8.15
Sequencer	.050 .100	1000.	.34	12.41	2.29	1.38	14.70
Sequencer	.050 .100	1000.	.34	7.05	9.56	6.12	10.87
Sequencer	.100 .050	1000.	.34	6.29	1.14	.99	7.90
Sequencer	.050 .100	1000.	.34	5.44	.67	.60	6.20
Sequencer	.050 .250	1000.	.34	8.50	8.17	3.90	16.90
Sequencer	.050 .100 .250	10.	.34	0.00	2.98	0.00	6.11
Sequencer	.050 .250	1000.	.34	10.71	9.33	9.33	10.71
Sequencer	.250	1000.	.34	7.65	3.82	3.82	7.65
Sequencer	.250 .050	1000.	.34	5.10	.50	.50	5.10
Sequencer	.050 .100	1000.	.34	7.65	3.80	3.65	9.18
Sequencer	.050 .100	1000.	.34	7.14	.92	.92	7.14
Sequencer	.050 .100	1000.	.34	14.28	1.64	1.64	14.28
Sequencer	.050 .100	1000.	.34	1.53	.75	.15	7.65
Sequencer	.050 .100	1000.	.34	22.27	23.63	19.52	26.09
Sequencer	.100 .050	1000.	.34	3.40	3.39	2.33	5.69
Manifold	.990	1000.	1.00	289.08	47.56	27.32	293.53
Couplings	1.000	1000.	.64	186.88	30.74	17.66	189.76
Flexible Hose	1.000	1000.	2.10	613.20	100.91	57.97	622.65
Cold Plates.	.400	1000.	1.00	116.80	19.22	11.04	118.60
Valves	1.000	1000.	4.60	1343.20	221.05	126.98	1363.90

[redacted]

Table 3-4. General Electric/Daytona SOAR III/Cindy I Component Reliability Summary

SOAR III NAME	SUBPHASE	COMPONENT	PARK REL.	Δ RELX10^{-4}	D.I. REL.	K_1	P_1(MTBF)	$P_3(K_2)$
1C3-1	12-31	SENSORS (A)	1.0	NO CHANGE				
1C3-4	12-31	SIGNAL CONDITIONER (A)	.99517729	4.7289	.99565018	3.8000E00	1.0000E04	1.000E00
1C3-7	12-31	PCM/FM TELEMETER	1.0	NO CHANGE				
1C3-10	12-31	PCM/FM TRANSMITTER	.99597957	3.9419	.99637376	3.8	1.2000E04	1.0E00
1C3-13	12-31	TELEMETRY ANTENNA (A)	.99985699	.3110	.99988809	2.5	1.0000E05	1.0E00
1C4-16	12-31	SENSORS (A)	1.0	NO CHANGE				
1C4-19	12-31	SIGNAL CONDITIONER (A)	.99517729	4.7289	.99565018	3.8	1.0000E04	1.0E00
1C4-24	12-31	PCM/FM TELEMETER	1.0	NO CHANGE				
1C4-27	12-31	PCM/FM TRANSMITTER	.99597957	3.9419	.99637376	3.8	1.2000E04	1.0E00
1C4-28	12-31	TELEMETRY ANTENNA (A)	.99985699	.3110	.99988809	2.5	1.0000E05	1.0E00
1C6-40	12-31	C-BAND TRANSPONDER	.99379280	6.0843	.99440123	3.8	7.7640E03	1.0E00
1C6-41	12-31	C-BAND ANTENNA (A)	.99951679	.4736	.99956415	3.8	1.0000E05	1.0E00
1C6-42	12-31	C-BAND ANTENNA (B)	.99951679	.4736	.99956415	3.8	1.0000E05	1.0E00
1C6-43	12-31	C-BAND ANTENNA (C)	.99951679	.4736	.99956415	3.8	1.0000E05	1.0E00
1C6-44	12-31	C-BAND ANTENNA (D)	.99951679	.4736	.99956415	3.8	1.0000E05	1.0E00
1C6-45	12-120	HEADSET (A)	.98913562	1.8952	.98932514	3.8	2.5000E04	1.0E00
1C6-46	12-76	HEADSET (B)	.99558134	1.8952	.99577086	3.8	2.5000E04	1.0E00
1C6-47	12-76	HEADSET (C)	.99558134	1.8952	.99577086	3.8	2.5000E04	1.0E00
1C6-48	12-120	AUDIO CENTER (A)	.99909055	.1567	.99910622	3.8	3.0000E05	1.0E00
1C6-49	12-108	AUDIO CENTER (B)	.99984244	.1567	.99985811	3.8	3.0000E05	1.0E00
1C6-50	12-108	AUDIO CENTER (C)	.99931696	.1567	.99933263	3.8	3.0000E05	1.0E00
1C6-51	12-120	AUDIO CONTROL (A)	.99941359	.1013	.99942372	3.8	4.6512E05	1.0E00
1C6-52	12-108	AUDIO CONTROL (B)	.99955954	.1013	.99956967	3.8	4.6512E05	1.0E00
1C6-53	12-108	AUDIO CONTROL (C)	.99955954	.1013	.99956967	3.8	4.6512E05	1.0E00
1C6-54	12-120	VHF/AM TRANSCEIVER	.99563590	.2118	.99565708	3.8	3.4785E04	1.0E00
1C6-55	12-120	VHF/UHF DIPLEXER	.99696179	.9480	.99705659	3.8	5.0000E04	1.0E00
1C6-56	12-120	VHF MULTIPLEXER AND FILTER	1.0	NO CHANGE				
1C6-57	12-120	VHF/UHF SCIMITAR ANTENNA (A)	.99177305	3.1182	.99208487	2.5	1.0000E04	1.0E00
1C6-58	12-120	VHF/UHF SCIMITAR ANTENNA (B)	.99177305	3.1182	.99208487	2.5	1.0000E04	1.0E00
1C6-60	12-120	MANUAL RF SWITCH	.99995235	.0176	.99995411	2.5	1.7200E06	1.0E00
1C6-61	12-31	VHF/FM TRANSMITTER	.99612894	.5411	.99618305	3.8	1.2464E04	1.0E00
1C6-62	12-76	PCM TELEMETRY	.97945444	8.8421	.98033865	3.8	5.3330E03	1.0E00
1C6-63	12-76	SIGNAL CONDITIONER	.99163736	3.5889	.99199625	3.8	1.3183E04	1.0E00
1C6-64	12-76	PCM SENSORS	1.0	NO CHANGE				
1C6-65	12-120	DISTRIBUTION PANEL	.99420085	.6230	.99426315	2.5	5.0000E04	1.0E00
1C6-66	12-120	DISPLAYS	.99738654	.2800	.99741454	2.5	1.1111E05	1.0E00
1C6-67	12-108	COMMUNICATION CONTROL PANEL	.99960622	.0791	.99961413	2.5	3.9000E05	1.0E00
1C6-69	12-120	CENTRAL TIMING	.99839043	.1617	.99840660	3.8	2.9150E05	1.0E00
1C6-71	12-76	PREMODULATION PROCESSOR LOW-PASS FILTER	.99998219	.0093	.99998312	2.5	3.0000E06	1.0E00

Table 3-4. (Continued)

COMTRACK - ELECTRICAL POWER

SOAR III NAME	SUBPHASE	COMPONENT	PARK REL.	Δ REL.X10^{-4}	D.I.REL.	K_1	P_1(MTBF)	$P_3(K_2)$
1C6-72	32-141	S-BAND TRANSPONDER (A)	.98836168		.98836168	3.8	2.6250E04	1.0E00
1C6-74	32-141	S-BAND POWER AMPLIFIER (A)	.98255090		.98255090	3.8	1.7457E04	1.0E00
1C6-75	32-103	S-BAND POWER AMPLIFIER (B)	.99298858		.99298858	3.8	1.7457E04	1.0E00
1C6-76	32-141	MANUAL RF SWITCH	.99988304		.99988304	2.5	1.7200E06	1.0E00
1C6-77	32-141	PREMODULATION PROCESSOR	.99228599		.99228599	3.8	3.9682E04	1.0E00
1C6-78	32-141	ANTENNA CONTROL	.90367542		.90367542	3.8	3.0340E03	1.0E00
1C6-81	32-141	S-BAND HI GAIN ANTENNA	.98003361		.98003361	2.5	1.0000E04	1.0E00
1C7-87	78-120	HEADSET (A)	.99896967		.99896967	2.5	2.5000E04	1.0E00
1C7-88	78-120	HEADSET (B)	.99896967		.99896967	2.5	2.5000E04	1.0E00
1C7-89	78-120	AUDIO CENTER (A)	.99802879		.99802879	3.8	2.3894E04	1.0E00
1C7-90	78-120	AUDIO CENTER (B)	.99802879		.99802879	3.8	2.3894E04	1.0E00
1C7-91	78-120	AUDIO CONTROL (A)	.99982305		.99982305	3.8	2.6596E05	1.0E00
1C7-92	78-120	AUDIO CONTROL (B)	.99982305		.99982305	3.8	2.6596E05	1.0E00
1C7-93	78-120	VHF/AM TRANSCEIVER (A)	.99440262		.99440262	3.8	8.4000E03	1.0E00
1C7-95	78-120	DIPLEXER	.99905753		.99905753	3.8	5.0000E04	1.0E00
1C7-97	78-120	POWER DIVIDER	.95394301		.95394301	3.8	1.0000E03	1.0E00
1C7-98	78-120	VHF OMNI ANTENNA (A)	.99976839		.99976839	2.5	1.1111E05	1.0E00
1C7-99	78-120	VHF OMNI ANTENNA (B)	.99976839		.99976839	2.5	1.1111E05	1.0E00
1C7-107	78-120	CENTRAL TIMING	.97414498		.97414498	3.8	1.8000E03	1.0E00
1C8-125	28-30	CAPE CANAVERAL ANTENNA &MICROWAVE COMPONENTS	1.0	NO CHANGE				
1C8-126	28-30	CAPE CANAVERAL C-BAND TRANSMITTER	1.0	NO CHANGE				
1C8-127	28-30	CAPE CANAVERAL C-BAND RECEIVER	1.0	NO CHANGE				
1C8-128	28-30	CAPE CANAVERAL ANGLE TRACKING	1.0	NO CHANGE				
1C8-129	28-30	CAPE CANAVERAL RANGE TRACKING	1.0	NO CHANGE				
1C8-130	28-30	CAPE CANAVERAL DIGITAL DATA	1.0	NO CHANGE				
1C8-131	28-30	CAPE CANAVERAL POWER DISTRIBUTION AND SUPPLIES	1.0	NO CHANGE				
1C8-132	28-30	CAPE CANAVERAL VHF/AM TRANSMITTER	1.0	NO CHANGE				
1C8-133	28-30	CAPE CANAVERAL TRANSMITTING ANTENNA	1.0	NO CHANGE				
1C8-134	28-30	CAPE CANAVERAL RECEIVING ANTENNA SYS.	1.0	NO CHANGE				
1C8-135	28-30	CAPE CANAVERAL HYBRID RINGS AND MULTICOUPLERS	1.0	NO CHANGE				
1C8-136	28-30	CAPE CANAVERAL VOICE RECEIVER	1.0	NO CHANGE				
1C8-137	28-30	CAPE CANAVERAL TIMING EQUIPMENT	1.0	NO CHANGE				
1C8-138	28-30	CAPE CANAVERAL DATA TRANSMISSION EQUIP.	1.0	NO CHANGE				
1C8-139	28-30	CAPE CANAVERAL DATA PROCESSING EQUIP.	1.0	NO CHANGE				
1C8-140	28-30	CAPE CANAVERAL PCM/FM RECEIVER	1.0	NO CHANGE				
1C8-141	28-30	CAPE CANAVERAL PCM/FM DATA HANDLING	1.0	NO CHANGE				
1C8-142	28-30	CAPE CANAVERAL PAM/FM/FM RECEIVER	1.0	NO CHANGE				
1C8-143	28-30	CAPE CANAVERAL PAM/FM/FM DATA HANDLING	1.0	NO CHANGE				

Table 3-4. (Continued)

COMTRACK - ELECTRICAL POWER

SOAR III NAME	SUBPHASE	COMPONENT	PARK REL.	λ.REL.X10^{-4}	D.I.REL.	K_1	P_1(MTBF)	P_3 (K_2)
1C8-144	28-30	CAPE CANAVERAL COMPUTER	1.0	NO CHANGE				
1C8-145	28-30	CAPE CANAVERAL INPUT/OUTPUT REGISTER AND DECODER	1.0	NO CHANGE				
1C8-146	28-30	CAPE CANAVERAL COMMAND TRANSMITTER	1.0	NO CHANGE				
1C8-147	28-30	CAPE CANAVERAL COMMAND ANTENNA	1.0	NO CHANGE				
1C8-155	12-30	BERMUDA VHF/AM TRANSMITTER	1.0	NO CHANGE				
1C8-156	12-30	BERMUDA TRANSMITTING ANTENNA	1.0	NO CHANGE				
1C8-157	12-30	BERMUDA RECEIVING ANTENNA SYSTEM	1.0	NO CHANGE				
1C8-158	12-30	BERMUDA HYBRID RINGS AND MULTICOUPLERS	1.0	NO CHANGE				
1C8-159	12-30	BERMUDA VOICE RECEIVER	1.0	NO CHANGE				
1C8-160	12-30	BERMUDA TIMING EQUIPMENT	1.0	NO CHANGE				
1C8-161	12-30	BERMUDA DATA TRANSMISSION EQUIPMENT	1.0	NO CHANGE				
1C8-162	12-30	BERMUDA DATA PROCESSOR	1.0	NO CHANGE				
1C8-163	12-30	BERMUDA PCM/FM RECEIVER	1.0	NO CHANGE				
1C8-164	12-30	BERMUDA PCM/FM DATA HANDLING	1.0	NO CHANGE				
1C8-165	12-30	BERMUDA PAM/FM/FM RECEIVER	1.0	NO CHANGE				
1C8-166	12-30	BERMUDA PAM/FM/FM DATA HANDLING	1.0	NO CHANGE				
1C8-167	12-30	BERMUDA COMPUTER	1.0	NO CHANGE				
1C8-168	12-30	BERMUDA INPUT/OUTPUT REGISTER + ENCODER	1.0	NO CHANGE				
1C8-169	12-30	BERMUDA COMMAND TRANSMITTER	1.0	NO CHANGE				
1C8-170	12-30	BERMUDA COMMAND ANTENNA	1.0	NO CHANGE				
1C8-171	12-31	ANTIGUA VHF/AM TRANSMITTER	1.0	NO CHANGE				
1C8-172	12-31	ANTIGUA TRANSMITTING ANTENNA	1.0	NO CHANGE				
1C8-173	12-31	ANTIGUA RECEIVING ANTENNA SYSTEM	1.0	NO CHANGE				
1C8-174	12-31	ANTIGUA HYBRID RINGS & MULTICOUPLERS	1.0	NO CHANGE				
1C8-175	12-31	ANTIGUA VOICE RECEIVER	1.0	NO CHANGE				
1C8-176	12-31	ANTIGUA TIMING EQUIPMENT	1.0	NO CHANGE				
1C8-177	12-31	ANTIGUA DATA TRANSMISSION EQUIPMENT	1.0	NO CHANGE				
1C8-178	12-31	ANTIGUA DATA PROCESSOR	1.0	NO CHANGE				
1C8-179	12-31	ANTIGUA PCM/FM RECEIVER	1.0	NO CHANGE				
1C8-180	12-31	ANTIGUA PCM/FM DATA HANDLING	1.0	NO CHANGE				
1C8-181	12-31	ANTIGUA PAM/FM/FM RECEIVER	1.0	NO CHANGE				
1C8-182	12-31	ANTIGUA PAM/FM/FM DATA HANDLING	1.0	NO CHANGE				
1C8-183	12-13	RANGE TRACKER VHF/AM TRANSMITTER	1.0	NO CHANGE				
1C8-184	12-13	RANGE TRACKER TRANSMITTING ANTENNA	1.0	NO CHANGE				
1C8-185	12-13	RANGE TRACKER RECEIVING ANTENNA SYSTEM	1.0	NO CHANGE				
1C8-186	12-13	RANGE TRACKER HYBRID RINGS & MULTI-COUPLERS	1.0	NO CHANGE				
1C8-187	12-13	RANGE TRACKER VOICE RECEIVER	1.0	NO CHANGE				
1C8-188	12-13	RANGE TRACKER TIMING EQUIPMENT	1.0	NO CHANGE				
1C8-189	12-13	RANGE TRACKER DATA TRANSMISSION EQUIP.	1.0	NO CHANGE				

Table 3-4. (Continued)

COMTRACK - ELECTRICAL POWER

SOAR III NAME	SUBPHASE	COMPONENT	PARK REL.	Δ REL.X10^{-4}	D.I.REL.	K_1	P_1(MTBF)	$P_3(K_2)$
IC8-190	12-13	RANGE TRACKER DATA PROCESSOR	1.0	NO CHANGE				
IC8-191	12-13	RANGE TRACKER PCM/FM RECEIVER	1.0	NO CHANGE				
IC8-192	12-13	RANGE TRACKER PCM/FM DATA HANDLING	1.0	NO CHANGE				
IC8-193	12-13	RANGE TRACKER PAM/FM/FM RECEIVER	1.0	NO CHANGE				
IC8-194	12-13	RANGE TRACKER PAM/FM/FM DATA HANDLING	1.0	NO CHANGE				
IC8-195	12-13	RANGE TRACKER ANTENNA AND MICROWAVE COMPONENTS	1.0	NO CHANGE				
IC8-196	12-13	RANGE TRACKER C-BAND TRANSMITTER	1.0	NO CHANGE				
IC8-197	12-13	RANGE TRACKER C-BAND RECEIVER	1.0	NO CHANGE				
IC8-198	12-13	RANGE TRACKER ANGLE TRACKING	1.0	NO CHANGE				
IC8-199	12-13	RANGE TRACKER RANGE TRACKING	1.0	NO CHANGE				
IC8-200	12-13	RANGE TRACKER DIGITAL DATA	1.0	NO CHANGE				
IC8-201	12=13	RANGE TRACKER POWER DISTRIBUTION & SUPPLIES	1.0	NO CHANGE				
IC8-202	13	ROSE KNOT VICTORY VHF/AM TRANSMITTER	1.0	NO CHANGE				
IC8-203	13	ROSE KNOT VICTORY TRANSMITTING ANTENNA	1.0	NO CHANGE				
IC8-204	13	ROSE KNOT VICTORY RECEIVING ANTENNA SYSTEM	1.0	NO CHANGE				
IC8-205	13	ROSE KNOT VICTORY HYBRID RINGS AND MULTICOUPLERS	1.0	NO CHANGE				
IC8-206	13	ROSE KNOT VICTORY VOICE RECEIVER	1.0	NO CHANGE				
IC8-207	13	ROSE KNOT VICTORY TIMING EQUIPMENT	1.0	NO CHANGE				
IC8-208	13	ROSE KNOT VICTORY DATA TRANSMISSION EQUIPMENT	1.0	NO CHANGE				
IC8-209	13	ROSE KNOT VICTORY DATA PROCESSOR	1.0	NO CHANGE				
IC8-210	13	ROSE KNOT VICTORY PCM/FM RECEIVER	1.0	NO CHANGE				
IC8-211	13	ROSE KNOT VICTORY PCM/FM DATA HANDLING	1.0	NO CHANGE				
IC8-212	13	ROSE KNOT VICTORY PAM/FM/FM RECEIVER	1.0	NO CHANGE				
IC8-213	13	ROSE KNOT VICTORY PAM/FM/FM DATA HANDLING	1.0	NO CHANGE				
IC8-214	13	ROSE KNOT VICTORY COMPUTER	1.0	NO CHANGE				
IC8-215	13	ROSE KNOT VICTORY INPUT/OUTPUT REGISTERS AND ENCODERS	1.0	NO CHANGE				
IC8-216	13	ROSE KNOT VICTORY COMMAND TRANSMITTER	1.0	NO CHANGE				
IC8-217	13	ROSE KNOT VICTORY COMMAND ANTENNA	1.0	NO CHANGE				
IC8-218	13	KANO VHF/AM TRANSMITTER	1.0	NO CHANGE				
IC8-219	13	KANO TRANSMITTING ANTENNA	1.0	NO CHANGE				
IC8-220	13	KANO RECEIVING ANTENNA SYSTEM	1.0	NO CHANGE				
IC8-221	13	KANO HYBRID RINGS AND MULTICOUPLERS	1.0	NO CHANGE				
IC8-222	13	KANO VOICE RECEIVER	1.0	NO CHANGE				
IC8-223	13	KANO TIMING EQUIPMENT	1.0	NO CHANGE				
IC8-224	13	KANO DATA TRANSMISSION EQUIPMENT	1.0	NO CHANGE				
IC8-225	13	KANO DATA PROCESSOR	1.0	NO CHANGE				

Table 3-4. (Continued)

COMTRACK - ELECTRICAL POWER

SOAR III NAME	SUBPHASE	COMPONENTS	PARK REL	Δ REL.X10^{-4}	D.I. REL.	K_1	P_1(MTBF)	$P_3(K_2)$
IC8-226	13	KANO PAM/FM/FM RECEIVER	1.0	NO CHANGE				
IC8-227	13	KANO PAM/FM/FM DATA HANDLING	1.0	NO CHANGE				
IC8-228	14-16	ZANZIBAR VHF/AM TRANSMITTER	1.0	NO CHANGE				
IC8-229	14-16	ZANZIBAR TRANSMITTING ANTENNA	1.0	NO CHANGE				
IC8-230	14-16	ZANZIBAR RECEIVING ANTENNA SYSTEM	1.0	NO CHANGE				
IC8-231	14-16	ZANZIBAR HYBRID RINGS & MULTICOUPLERS	1.0	NO CHANGE				
IC8-232	14-16	ZANZIBAR VOICE RECEIVER	1.0	NO CHANGE				
IC8-233	14-16	ZANZIBAR TIMING EQUIPMENT	1.0	NO CHANGE				
IC8-234	14-16	ZANZIBAR DATA TRANSMISSION EQUIPMENT	1.0	NO CHANGE				
IC8-235	14-16	ZANZIBAR DATA PROCESSOR	1.0	NO CHANGE				
IC8-236	14-16	ZANZIBAR PAM/FM/FM RECEIVER	1.0	NO CHANGE				
IC8-237	14-16	ZANZIBAR PAM/FM/FM DATA HANDLING	1.0	NO CHANGE				
IC8-238	14-16	JOHANNESBURG RECEIVING ANTENNA SYSTEM	1.0	NO CHANGE				
IC8-239	14-16	JOHANNESBURG HYBRID RINGS & MULTI-COUPLERS	1.0	NO CHANGE				
IC8-240	14-16	JOHANNESBURG TIMING EQUIPMENT	1.0	NO CHANGE				
IC8-241	14-16	JOHANNESBURG DATA TRANSMISSION EQUIP.	1.0	NO CHANGE				
IC8-242	14-16	JOHANNESBURG DATA PROCESSOR	1.0	NO CHANGE				
IC8-243	14-16	JOHANNESBURG PAM/FM/FM RECEIVER	1.0	NO CHANGE				
IC8-244	14-16	JOHANNESBURG PAM/FM/FM DATA HANDLING	1.0	NO CHANGE				
IC8-245	16-18	COASTAL SENTRY QUEBEC VHF/AM TRANS-MITTER	1.0	NO CHANGE				
IC8-246	16-18	COASTAL SENTRY QUEBEC TRANSMITTING ANTENNA	1.0	NO CHANGE				
IC8-247	16-18	COASTAL SENTRY QUEBEC RECEIVING ANTENNA SYSTEM	1.0	NO CHANGE				
IC8-248	16-18	COASTAL SENTRY QUEBEC HYBRID RINGS & MULTICOUPLERS	1.0	NO CHANGE				
IC8-249	16-18	COASTAL SENTRY QUEBEC VOICE RECEIVER	1.0	NO CHANGE				
IC8-250	16-18	COASTAL SENTRY QUEBEC TIMING EQUIPMENT	1.0	NO CHANGE				
IC8-251	16-18	COASTAL SENTRY QUEBEC DATA TRANS-MISSION EQUIPMENT	1.0	NO CHANGE				
IC8-252	16-18	COASTAL SENTRY QUEBEC DATA PROCESSOR	1.0	NO CHANGE				
IC8-253	16-18	COASTAL SENTRY QUEBEC PCM/FM RECEIVER	1.0	NO CHANGE				
IC8-254	16-18	COASTAL SENTRY QUEBEC PCM/FM DATA HANDLING	1.0	NO CHANGE				
IC8-255	16-18	COASTAL SENTRY QUEBEC PAM/FM/FM RECEIVER	1.0	NO CHANGE				
IC8-256	16-18	COASTAL SENTRY QUEBEC PAM/FM/FM DATA HANDLING	1.0	NO CHANGE				
IC8-257	18	MUCHEA VHF/AM TRANSMITTER	1.0	NO CHANGE				
IC8-258	18	MUCHEA TRANSMITTING ANTENNA	1.0	NO CHANGE				
IC8-259	18	MUCHEA RECEIVING ANTENNA SYSTEM	1.0	NO CHANGE				

Table 3-4. (Continued)

COMTRACK - ELECTRICAL POWER

SOAR III NAME	SUBPHASE	COMPONENTS	PARK REL.	Σ REL.X10^{-4}	D.I. REL.	K_1	P_1(MTBF)	$P_3(P_2)$
IC8-299	21	CANTON ISLAND TIMING EQUIPMENT	1.0	NO CHANGE				
IC8-300	21	CANTON ISLAND DATA TRANSMISSION EQUIP.	1.0	NO CHANGE				
IC8-301	21	CANTON ISLAND DATA PROCESSOR	1.0	NO CHANGE				
IC8-302	21	CANTON ISLAND PAM/FM/FM RECEIVER	1.0	NO CHANGE				
IC8-303	21	CANTON ISLAND PAM/FM/FM DATA HANDLING	1.0	NO CHANGE				
IC8-304	21-22	KAUAI VHF/AM TRANSMITTER	1.0	NO CHANGE				
IC8-305	21-22	KAUAI TRANSMITTING ANTENNA	1.0	NO CHANGE				
IC8-306	21-22	KAUAI RECEIVING ANTENNA SYSTEM	1.0	NO CHANGE				
IC8-307	21-22	KAUAI HYBRID RINGS & MULTICOUPLERS	1.0	NO CHANGE				
IC8-308	21-22	KAUAI VOICE RECEIVER	1.0	NO CHANGE				
IC8-309	21-22	KAUAI TIMING EQUIPMENT	1.0	NO CHANGE				
IC8-310	21-22	KAUAI DATA TRANSMISSION EQUIPMENT	1.0	NO CHANGE				
IC8-311	21-22	KAUAI DATA PROCESSOR	1.0	NO CHANGE				
IC8-312	21-22	KAUAI PCM/FM RECEIVER	1.0	NO CHANGE				
IC8-313	21-22	KAUAI PCM/FM DATA HANDLING	1.0	NO CHANGE				
IC8-314	21-22	KAUAI PAM/FM/FM RECEIVER	1.0	NO CHANGE				
IC8-315	21-22	KAUAI PAM/FM/FM DATA HANDLING	1.0	NO CHANGE				
IC8-316	21-22	KAUAI COMPUTER	1.0	NO CHANGE				
IC8-317	21-22	KAUAI INPUT/OUTPUT REGISTER & DECODER	1.0	NO CHANGE				
IC8-318	21-22	KAUAI COMMAND TRANSMITTER	1.0	NO CHANGE				
IC8-319	21-22	KAUAI COMMAND ANTENNA	1.0	NO CHANGE				
IC8-320	21-22	KAUAI ANTENNA & MICROWAVE COMPONENTS	1.0	NO CHANGE				
IC8-321	21-22	KAUAI C-BAND TRANSMITTER	1.0	NO CHANGE				
IC8-322	21-22	KAUAI C-BAND RECEIVER	1.0	NO CHANGE				
IC8-323	21-22	KAUAI ANGLE TRACKING	1.0	NO CHANGE				
IC8-324	21-22	KAUAI RANGE TRACKING	1.0	NO CHANGE				
IC8-325	21-22	KAUAI DIGITAL DATA	1.0	NO CHANGE				
IC8-326	21-22	KAUAI POWER DISTRIBUTION & SUPPLIES	1.0	NO CHANGE				
IC8-327	22-25	TWIN FALLS VICTORY VHF/AM TRANSMITTER	1.0	NO CHANGE				
IC8-328	22-25	TWIN FALLS VICTORY TRANSMITTING ANTENNA	1.0	NO CHANGE				
IC8-329	22-25	TWIN FALLS VICTORY RECEIVING ANTENNA SYSTEM	1.0	NO CHANGE				
IC8-330	22-25	TWIN FALLS VICTORY HYBRID RINGS & MULTICOUPLERS	1.0	NO CHANGE				
IC8-332	22-25	TWIN FALLS VICTORYTIMING EQUIPMENT	1.0	NO CHANGE				
IC8-333	22-25	TWIN FALLS VICTORY DATA TRANSMISSION EQUIPMENT	1.0	NO CHANGE				
IC8-334	22-25	TWIN FALLS VICTORY DATA PROCESSOR	1.0	NO CHANGE				
IC8-335	22-25	TWIN FALLS VICTORY PCM/FM RECEIVER	1.0	NO CHANGE				
IC8-336	22-25	TWIN FALLS VICTORY PCM/FM DATA HANDLING	1.0	NO CHANGE				
IC8-337	22-25	TWIN FALLS VICTORY PAM/FM/FM RECEIVER	1.0	NO CHANGE				
IC8-331	22-25	TWIN FALLS VICTORY VOICE RECEIVER	1.0	NO CHANGE				

Table 3-4. (Continued)

COMTRACK - ELECTRICAL POWER

SOAR III NAME	SUBPHASE	COMPONENT	PARK REL.	ΔREL.X10^{-4}	D.I.REL.	K_1	P_1(MTBF)	$P_3(K_2)$
1C8-260	18	MUCHEA HYBRID RINGS & MULTICOUPLERS	1.0	NO CHANGE				
1C8-261	18	MUCHEA VOICE EQUIPMENT	1.0	NO CHANGE				
1C8-262	18	MUCHEA TIMING EQUIPMENT	1.0	NO CHANGE				
1C8-263	18	MUCHEA DATA TRANSMISSION EQUIPMENT	1.0	NO CHANGE				
1C8-264	18	MUCHEA DATA PROCESSOR	1.0	NO CHANGE				
1C8-265	18	MUCHEA PCM/FM RECEIVER	1.0	NO CHANGE				
1C8-266	18	MUCHEA PCM/FM DATA HANDLING	1.0	NO CHANGE				
1C8-267	18	MUCHEA PAM/FM/FM RECEIVER	1.0	NO CHANGE				
1C8-268	18	MUCHEA PAM/FM/FM DATA HANDLING	1.0	NO CHANGE				
1C8-269	18	MUCHEA COMPUTER	1.0	NO CHANGE				
1C8-270	18	MUCHEA INPUT/OUTPUT REGISTER + ENCORDER	1.0	NO CHANGE				
1C8-271	18	MUCHEA COMMAND TRANSMITTER	1.0	NO CHANGE				
1C8-272	18	MUCHEA COMMAND ANTENNA	1.0	NO CHANGE				
1C8-273	18	MUCHEA ANTENNA + MICROWAVE COMPONENTS	1.0	NO CHANGE				
1C8-274	18	MUCHEA C-BAND TRANSMITTER	1.0	NO CHANGE				
1C8-275	18	MUCHEA C-BAND RECEIVER	1.0	NO CHANGE				
1C8-276	18	MUCHEA ANGLE TRACKING	1.0	NO CHANGE				
1C8-277	18	MUCHEA RANGE TRACKING	1.0	NO CHANGE				
1C8-278	18	MUCHEA DIGITAL DATA	1.0	NO CHANGE				
1C8-279	18	MUCHEA POWER DISTRIBUTION & SUPPLIES	1.0	NO CHANGE				
1C8-280	19-20	WOOMERA RECEIVING ANTENNA SYSTEM	1.0	NO CHANGE				
1C8-281	19-20	WOOMERA HYBRID RINGS & MULTICOUPLERS	1.0	NO CHANGE				
1C8-282	19-20	WOOMERA TIMING EQUIPMENT	1.0	NO CHANGE				
1C8-283	19-20	WOOMERA DATA TRANSMISSION EQUIPMENT	1.0	NO CHANGE				
1C8-284	19-20	WOOMERA DATA PROCESSOR	1.0	NO CHANGE				
1C8-285	19-20	WOOMERA PAM/FM/FM RECEIVER	1.0	NO CHANGE				
1C8-286	19-20	WOOMERA PAM/FM/FM DATA HANDLING	1.0	NO CHANGE				
1C8-287	19-20	WOOMERA ANTENNA AND MICROWAVE COMPONENTS	1.0	NO CHANGE				
1C8-288	19-20	WOOMERA C-BAND TRANSMITTER	1.0	NO CHANGE				
1C8-289	19-20	WOOMERA C-BAND RECEIVER	1.0	NO CHANGE				
1C8-290	19-20	WOOMERA ANGLE TRACKING	1.0	NO CHANGE				
1C8-291	19-20	WOOMERA RANGE TRACKING	1.0	NO CHANGE				
1C8-292	19-20	WOOMERA DIGITAL DATA	1.0	NO CHANGE				
1C8-293	19-20	WOOMERA POWER DISTRIBUTION & SUPPLIES	1.0	NO CHANGE				
1C8-294	21	CANTON ISLAND VHF/AM TRANSMITTER	1.0	NO CHANGE				
1C8-295	21	CANTON ISLAND TRANSMITTING ANTENNA	1.0	NO CHANGE				
1C8-296	21	CANTON ISLAND RECEIVING ANTENNA SYSTEM	1.0	NO CHANGE				
1C8-297	21	CANTON ISLAND HYBRID RINGS AND MULTI-COUPLERS	1.0	NO CHANGE				
1C8-298	21	CANTON ISLAND VOICE RECEIVER	1.0	NO CHANGE				

Table 3-4. (Continued)

COMTRACK - ELECTRICAL POWER

SOAR III NAME	SUBPHASE	COMPONENT	PARK REL	Δ REL.X10^{-4}	D.I.REL.	K_1	P_1(MTBF)	$P_3(K_2)$
1C8-338	22-25	TWIN FALLS VICTORY PAM/FM/FM DATA HANDLING	1.0	NO CHANGE				
1C8-339	22-25	TWIN FALLS VICTORY COMPUTER	1.0	NO CHANGE				
1C8-340	22-25	TWIN FALLS VICTORY INPUT/OUTPUT REGISTER AND DECODER	1.0	NO CHANGE				
1C8-341	22-25	TWIN FALLS VICTORY COMMAND TRANSMITTER	1.0	NO CHANGE				
1C8-342	22-25	TWIN FALLS VICTORY COMMAND ANTENNA	1.0	NO CHANGE				
1C8-343	23-25	TWIN FALLS VICTORY ANTENNA & MICROWAVE COMPONENTS	1.0	NO CHANGE				
1C8-344	23-25	TWIN FALLS VICTORY C-BAND TRANSMITTER	1.0	NO CHANGE				
1C8-345	23-25	TWIN FALLS VICTORY C-BAND RECEIVER	1.0	NO CHANGE				
1C8-346	23-25	TWIN FALLS VICTORY ANGLE TRACKING	1.0	NO CHANGE				
1C8-347	23-25	TWIN FALLS VICTORY RANGE TRACKING	1.0	NO CHANGE				
1C8-348	23-25	TWIN FALLS VICTORY DIGITAL DATA	1.0	NO CHANGE				
1C8-349	23-25	TWIN FALLS VICTORY POWER DISTRIBUTION AND SUPPLIES	1.0	NO CHANGE				
1C8-350	23-25	POINT ARGUELLO VHF/AM TRANSMITTER	1.0	NO CHANGE				
1C8-351	23-25	POINT ARGUELLO TRANSMITTING ANTENNA	1.0	NO CHANGE				
1C8-352	23-25	POINT ARGUELLO RECEIVING ANTENNA SYS.	1.0	NO CHANGE				
1C8-353	23-25	POINT ARGUELLO HYBRID RINGS AND MULTI-COUPLERS	1.0	NO CHANGE				
1C8-354	23-25	POINT ARGUELLO VOICE RECEIVER	1.0	NO CHANGE				
1C8-355	23-25	POINT ARGUELLO TIMING EQUIPMENT	1.0	NO CHANGE				
1C8-356	23-25	POINT ARGUELLO DATA TRANSMISSION EQUIP.	1.0	NO CHANGE				
1C8-357	23-25	POINT ARGUELLO DATA PROCESSOR	1.0	NO CHANGE				
1C8-358	23-25	POINT ARGUELLO PCM/FM RECEIVER	1.0	NO CHANGE				
1C8-359	23-25	POINT ARGUELLO PCM/FM DATA HANDLING	1.0	NO CHANGE				
1C8-360	23-25	POINT ARGUELLO PAM/FM/FM RECEIVER	1.0	NO CHANGE				
1C8-361	23-25	POINT ARGUELLO PAM/FM/FM DATA HANDLING	1.0	NO CHANGE				
1C8-362	23-25	POINT ARGUELLO COMPUTER	1.0	NO CHANGE				
1C8-363	23-25	POINT ARGUELLO INPUT/OUTPUT REGISTER AND DECODER	1.0	NO CHANGE				
1C8-364	23-25	POINT ARGUELLO COMMAND TRANSMITTER	1.0	NO CHANGE				
1C8-365	23-25	POINT ARGUELLO COMMAND ANTENNA	1.0	NO CHANGE				
1C8-366	23-25	POINT ARGUELLO ANTENNA & MICROWAVE COMPONENTS	1.0	NO CHANGE				
1C8-367	23-25	POINT ARGUELLO C-BAND TRANSMITTER	1.0	NO CHANGE				
1C8-368	23-25	POINT ARGUELLO C-BAND RECEIVER	1.0	NO CHANGE				
1C8-369	23-25	POINT ARGUELLO ANGLE TRACKING	1.0	NO CHANGE				
1C8-370	23-25	POINT ARGUELLO RANGE TRACKING	1.0	NO CHANGE				
1C8-371	23-25	POINT ARGUELLO DIGITAL DATA	1.0	NO CHANGE				
1C8-372	23-25	POINT ARGUELLO POWER DISTRIBUTION & SUPPLIES	1.0	NO CHANGE				

Table 3-4. (Continued)

COMTRACK - ELECTRICAL POWER

SOAR III NAME	SUBPHASE	COMPONENTS	PARK REL.	Δ REL.X10^{-4}	D.I.REL.	K_1	P_1(MTBF)	$P_3(K_2)$
1C8-373	25-28	Guaymas VHF/Am Transmitting	1.0	NO CHANGE				
1C8-374	25-28	GUAYMAS TRANSMITTING ANTENNA	1.0	NO CHANGE				
1C8-375	25-28	GUAYMAS RECEIVING ANTENNA SYSTEM	1.0	NO CHANGE				
1C8-376	25-28	GUAYMAS HYBRID RINGS & MULTICOUPLER	1.0	NO CHANGE				
1C8-377	25-28	GUAYMAS VOICE RECEIVER	1.0	NO CHANGE				
1C8-378	25-28	GUAYMAS TIMING EQUIPMENT	1.0	NO CHANGE				
1C8-379	25-28	GUAYMAS DATA TRANSMISSION EQUIPMENT	1.0	NO CHANGE				
1C8-380	25-28	GUAYMAS DATA PROCESSOR	1.0	NO CHANGE				
1C8-381	25-28	GUAYMAS PCM/FM RECEIVER	1.0	NO CHANGE				
1C8-382	25-28	GUAYMAS PCM/FM DATA HANDLING	1.0	NO CHANGE				
1C8-383	25-28	GUAYMAS COMPUTER	1.0	NO CHANGE				
1C8-384	25-28	GUAYMAS INPUT/OUTPUT REGISTER & DECODER	1.0	NO CHANGE				
1C8-385	25-28	GUAYMAS COMMAND TRANSMITTER	1.0	NO CHANGE				
1C8-386	25-28	GUAYMAS COMMAND ANTENNA	1.0	NO CHANGE				
1C8-387	25-28	GUAYMAS VERLORT RADAR	1.0	NO CHANGE				
1C8-388	25-28	WHITE SANDS RECEIVING ANTENNA SYSTEM	1.0	NO CHANGE				
1C8-389	25-28	WHITE SANDS HYBRID RINGS & MULTICOUPLER	1.0	NO CHANGE				
1C8-390	25-28	WHITE SANDS TIMING EQUIPMENT	1.0	NO CHANGE				
1C8-391	25-28	WHITE SANDS DATA TRANSMISSION EQUIPMENT	1.0	NO CHANGE				
1C8-392	25-28	WHITE SANDS DATA PROCESSOR	1.0	NO CHANGE				
1C8-393	25-28	WHITE SANDS PCM/FM RECEIVER	1.0	NO CHANGE				
1C8-394	25-28	WHITE SANDS PCM/FM DATA HANDLING	1.0	NO CHANGE				
1C8-395	25-28	WHITE SANDS ANTENNA & MICROWAVE COMPONENTS	1.0	NO CHANGE				
1C8-396	25-28	WHITE SANDS C-BAND TRANSMITTER	1.0	NO CHANGE				
1C8-397	25-28	WHITE SANDS C-BAND RECEIVER	1.0	NO CHANGE				
1C8-398	25-28	WHITE SANDS ANGLE TRACKING	1.0	NO CHANGE				
1C8-399	25-28	WHITE SANDS RANGE TRACKING	1.0	NO CHANGE				
1C8-400	25-28	WHITE SANDS DIGITAL DATA	1.0	NO CHANGE				
1C8-1401	25-28	WHITE SANDS POWER DISTRIBUTION AND SUPPLIES	1.0	NO CHANGE				
1C8-1402	25-28	CORPUS CHRISTI VHF/AM TRANSMITTER	1.0	NO CHANGE				
1C8-1403	25-28	CORPUS CHRISTI TRANSMITTING ANTENNA	1.0	NO CHANGE				
1C8-1404	25-28	CORPUS CHRISTI RECEIVING ANTENNA SYS.	1.0	NO CHANGE				
1C8-1405	25-28	CORPUS CHRISTI HYBRID RINGS & MULTI-COUPLERS	1.0	NO CHANGE				
1C8-1406	25-28	CORPUS CHRISTI VOICE RECEIVER	1.0	NO CHANGE				
1C8-1407	25-28	CORPUS CHRISTI TIMING EQUIPMENT	1.0	NO CHANGE				
1C8-1408	25-28	CORPUS CHRISTI DATA TRANSMISSION EQUIPMENT	1.0	NO CHANGE				
1C8-1409	25-28	CORPUS CHRISTI DATA PROCESSOR	1.0	NO CHANGE				
1C8-1410	25-28	CORPUS CHRISTI PCM/FM RECEIVER	1.0	NO CHANGE				

Table 3-4. (Continued)

COMTRACK - ELECTRICAL POWER

SOAR III NAME	SUBPHASE	COMPONENT	PARK REL.	Δ REL.X10^{-4}	D.I.REL.	K_1	P_1(MTBF)	$P_3(K_2)$
IC8-1411	25-28	CORPUS CHRISTI PCM/FM DATA HANDLING	1.0	NO CHANGE				
IC8-1412	25-28	CORPUS CHRISTI PAM/FM/FM DATA HANDLING	1.0	NO CHANGE				
IC8-1413	25-28	CORPUS CHRISTI PAM/FM/FM RECEIVER	1.0	NO CHANGE				
IC8-1414	25-28	CORPUS CHRISTI COMPUTER	1.0	NO CHANGE				
IC8-1415	25-28	CORPUS CHRISTI INPUT/OUTPUT REGISTER AND DECODER	1.0	NO CHANGE				
IC8-1416	25-28	CORPUS CHRISTI COMMAND TRANSMITTER	1.0	NO CHANGE				
IC8-1417	25-28	CORPUS CHRISTI COMMAND ANTENNA	1.0	NO CHANGE				
IC8-1418	25-28	CORPUS CHRISTI VERLORT RADAR	1.0	NO CHANGE				
IC8-1419	27-30	EGLIN ANTENNA & MICROWAVE COMPONENTS	1.0	NO CHANGE				
IC8-1420	27-30	EGLIN C-BAND TRANSMITTER	1.0	NO CHANGE				
IC8-1421	27-30	EGLIN C-BAND RECEIVER	1.0	NO CHANGE				
IC8-1422	27-30	EGLIN ANGLE TRACKING	1.0	NO CHANGE				
IC8-1423	27-30	EGLIN RANGE TRACKING	1.0	NO CHANGE				
IC8-1424	27-30	EGLIN DIGITAL DATA	1.0	NO CHANGE				
IC8-1425	27-30	EGLIN POWER DISTRIBUTION & SUPPLIES	1.0	NO CHANGE				
IC8-1426	25-30	EGLIN VHF/AM TRANSMITTER	1.0	NO CHANGE				
LC8-1427	25-30	EGLIN TRANSMITTING ANTENNA	1.0	NO CHANGE				
IC8-1428	25-30	EGLIN RECEIVING ANTENNA SYSTEM	1.0	NO CHANGE				
IC8-1429	25-30	EGLIN HYBRID RINGS & MULTICOUPLER	1.0	NO CHANGE				
IC8-1430	25-30	EGLIN VOICE RECEIVER	1.0	NO CHANGE				
IC8-1431	25-30	EGLIN TIMING EQUIPMENT	1.0	NO CHANGE				
IC8-1432	25-30	EGLIN DATA TRANSMISSION EQUIPMENT	1.0	NO CHANGE				
IC8-1433	25-30	EGLIN DATA PROCESSOR	1.0	NO CHANGE				
IC8-1434	29-30	ANTIGUA ANTENNA & MICROWAVE COMPONENTS	1.0	NO CHANGE				
IC8-1435	29-30	ANTIGUA C-BAND TRANSMITTER	1.0	NO CHANGE				
IC8-1436	29-30	ANTIGUA C-BAND RECEIVER	1.0	NO CHANGE				
IC8-1437	29-30	ANTIGUA ANGLE TRACKING	1.0	NO CHANGE				
IC8-1438	29-30	ANTIGUA RANGE TRACKING	1.0	NO CHANGE				
IC8-1439	29-30	ANTIGUA DIGITAL DATA	1.0	NO CHANGE				
IC8-1440	29-30	ANTIGUA POWER DISTRIBUTION & SUPPLIES	1.0	NO CHANGE				
IC8-1441	32-141	JOHANNESBURG S-BAND ANTENNA	1.0	NO CHANGE				
IC8-1442	32-141	JOHANNESBURG ANTENNA SERVO SYSTEM	1.0	NO CHANGE				
IC8-1443	32-141	JOHANNESBURG UNIFIED S-BAND RECEIVER	1.0	NO CHANGE				
IC8-1444	32-141	JOHANNESBURG RANGING RECEIVER SYSTEM	1.0	NO CHANGE				
IC8-1445	32-141	JOHANNESBURG TELEMETRY RECEIVER SYSTEM	1.0	NO CHANGE				
IC8-1446	32-141	JOHANNESBURG AUDIO RECEIVER SYSTEM	1.0	NO CHANGE				
IC8-1447	32-141	JOHANNESBURG DATA PROCESSING EQUIPMENT	1.0	NO CHANGE				
IC8-1448	32-141	JOHANNESBURG DIGITAL CLOCK SYSTEM	1.0	NO CHANGE				
IC8-1449	32-141	JOHANNESBURG MODULATION SYSTEM	1.0	NO CHANGE				

Table 3-4. (Continued)

COMTRACK - ELECTRICAL POWER

SOAR III NAME	SUBPHASE	COMPONENT	PARK REL.	ΔREL.X10^{-4}	D.I.REL.	K_1	P_1(MTBF)	$P_3(K_2)$
IC8-1450	32-141	JOHANNESBURG S-BAND TRANSMITTER SYS.	1.0	NO CHANGE				
IC8-1451	41-141	GOLDSTONE S-BAND ANTENNA	1.0	NO CHANGE				
IC8-1452	41-141	GOLDSTONE ANTENNA SERVO SYSTEM	1.0	NO CHANGE				
IC8-1453	41-141	GOLDSTONE UNIFIED S-BAND RECEIVER	1.0	NO CHANGE				
IC8-1454	41-141	GOLDSTONE RANGING RECEIVER SYSTEM	1.0	NO CHANGE				
IC8-1455	41-141	GOLDSTONE TELEMETRY RECEIVER SYSTEM	1.0	NO CHANGE				
IC8-1456	41-141	GOLDSTONE AUDIO RECEIVER SYSTEM	1.0	NO CHANGE				
IC8-1457	41-141	GOLDSTONE DATA PROCESSING EQUIPMENT	1.0	NO CHANGE				
IC8-1458	41-141	GOLDSTONE DIGITAL CLOCK SYSTEM	1.0	NO CHANGE				
IC8-1459	41-141	GOLDSTONE MODULATION SYSTEM	1.0	NO CHANGE				
IC8-1460	41-141	GOLDSTONE S-BAND TRANSMITTER SYSTEM	1.0	NO CHANGE				
IC8-1461	46-141	WOOMERA S-BAND ANTENNA	1.0	NO CHANGE				
IC8-1462	46-141	WOOMERA ANTENNA SERVO SYSTEM	1.0	NO CHANGE				
IC8-1463	46-141	WOOMERA UNIFIED S-BAND RECIEVER	1.0	NO CHANGE				
IC8-1464	46-141	WOOMERA RANGING RECEIVER SYSTEM	1.0	NO CHANGE				
IC8-1465	46-141	WOOMERA TELEMETRY RECEIVER SYSTEM	1.0	NO CHANGE				
IC8-1466	46-141	WOOMERA AUDIO RECEIVER SYSTEM	1.0	NO CHANGE				
IC8-1467	46-141	WOOMERA DATA PROCESSING EQUIPMENT	1.0	NO CHANGE				
IC8-1468	46-141	WOOMERA DIGITAL CLOCK SYSTEM	1.0	NO CHANGE				
IC8-1469	46-141	WOOMERA MODULATION SYSTEM	1.0	NO CHANGE				
IC8-1470	46-141	WOOMERA S-BAND TRANMITTER SYSTEM	1.0	NO CHANGE				
IC7-1471	78-120	CONTROLS AND DISPLAYS	.99995136		.99995136	2.5000E00	5.2600E05	1.0E00
E1-501	2-4	BATTERY #1	.99939123		.99939123	1.5000E02	1.0000E04	1.0E00
E1-502	2-4	BATTERY #2	.99939123		.99939123	1.5000E02	1.0000E04	1.0E00
E1-509	2-4	INVERTER	.99998939		.99998939	4.5000E01	1.7200E05	1.0E00
E1-511	2-4	DISTRIBUTION SYSTEM (A) CABLING	.99999698		.99999698	1.5000E02	2.0000E06	1.0E00
E1-512	2-4	DISTRIBUTION SYSTEM (B) CABLING	.99999698		.99999698	1.5000E02	2.0000E06	1.0E00
* E1-513	2-4	DISTRIBUTION SYSTEM (C) CABLING	.99999698		.99999698	1.5000E02	2.0000E06	1.0E00
* E1-515	2-4	DISTRIBUTION SYSTEM (E) CABLING	.99999698		.99999698	1.5000E02	2.0000E06	1.0E00
E1-516	2-4	DISTRIBUTION SYSTEM (F) CABLING	.99999698		.99999698	1.5000E02	2.0000E06	1.0E00
E1-517	2-4	DISTRIBUTORS	.99999240		.99999240	1.5000E02	8.0000E05	1.0E00
E2-518	4-8	INSTRUMENT BATTERY	.99838629		.99839629	3.8000E00	1.0000E04	1.0E00
E2-519	4-8	MAIN BATTERY	.99838629		.99838629	3.8	1.0000E04	1.0E00
E2-520	4-8	BATTERY HEATER (I.B.)	.99987581		.99987581	3.8	1.3000E05	1.0E00
E2-521	4-8	BATTERY HEATER (M.B.)	.99987581		.99987581	3.8	1.3000E05	1.0E00
E2-524	4-8	MAIN DC BUS	.99997984		.99997984	3.8	8.0000E05	1.0E00
E2-525	4-8	INSTRUMENT DC BUS	.99997984		.99997984	3.8	8.0000E05	1.0E00
E2-526	4-8	VOLTAGE DIVIDER	.99993542		.99993542	3.8	2.5000E05	1.0E00
E2-527	4-8	INSTRUMENT POWER DISTRIBUTION J-BOX	.99997984		.99997984	3.8	8.0000E05	1.0E00
E3-528	8-35	FORWARD BATTERY #1	.99711095	4.8653	.99759748	3.8	1.0000E04	1.0E00
E3-529	8-35	FORWARD BATTERY #2	.99711095	4.8653	.99759748	3.8	[illegible]	

Table 3-4. (Continued)

COMTRACL - ELECTRICAL POWER

SOAR III NAME	SUBPHASE	COMPONENT	PARK REL.	Δ REL.X10^{-4}	D.I.REL.	K_1	P_1(MTBF)	$P_3(K_2)$
E3-530	8-35	AFTER BATTERY #1	.99711095	4.8653	.99759748	3.8000E00	1.0000E04	1.0E00
E3-531	8-35	AFTER BATTERY #2	.99711095	4.8653	.99759748	3.8	1.0000E04	1.0E00
E3-532	8-35	AFTER BATTERY HEATER #1	.99977764	.3738	.99981502	3.8	1.3000E05	1.0E00
E3-533	8-35	AFTER BATTERY HEATER #2	.99977764	.3738	.99981502	3.8	1.3000E05	1.0E00
E3-534	8-35	FORWARD BATTERY HEATER #1	.99977764	.3738	.99981502	3.8	1.3000E05	1.0E00
E3-535	8-35	FORWARD BATTERY HEATER #2	.99977764	.3738	.99981502	3.8	1.3000E05	1.0E00
E3-536	8-35	INVERTER-CONVERTER	.99988329	.3130	.99991459	2.5	1.0200E05	1.0E00
E3-541	8-35	FORWARD POWER DISTRIBUTION ON BOX	.99996401	.0599	.99997000	3.8	8.0000E05	1.0E00
E3-542	8-35	AFTER POWER DISTRIBUTION ON BOX	.99996401	.0599	.99997000	3.8	8.0000E05	1.0E00
E3-543	8-35	CABLING	.99998574	.0232	.99998806	3.8	2.0000E06	1.0E00
E3-544	8-35	SWITCH SELECTOR	1.0	NO CHANGE				
E5-545	2-145	FUEL CELL SUBSYSTEM (A)	.96241734	2.2096	.96263830	3.8	2.2000E04	1.0E00
E5-546	2-145	FUEL CELL SUBSYSTEM (B)	.96241734	2.2096	.96263830	3.8	2.2000E04	1.0E00
E5-547	2-145	FUEL CELL SUBSYSTEM (C)	.96241734	2.2096	.96263830	3.8	2.2000E04	1.0E00
E5-548	2-145	D-C DISTRIBUTION SYSTEM (A)	.99894795	.0599	.99895394	3.8	8.0000E05	1.0E00
E5-549	2-145	D-C DISTRIBUTION SYSTEM (B)	.99894795	.0599	.99895394	3.8	8.0000E05	1.0E00
E5-550	2-145	OXYGEN TANK SYSTEM #1	.98566594	.8332	.98574926	3.8	5.8370E04	1.0E00
E5-551	2-145	OXYGEN TANK SYSTEM #2	.98566594	.8332	.98574926	3.8	5.8370E04	1.0E00
E5-552	2-145	HYDROGEN TANK SYSTEM #1	.98566594	.8332	.98574926	3.8	5.8370E04	1.0E00
E5-553	2-145	HYDROGEN TANK SYSTEM #2	.98566594	.8332	.98574926	3.8	5.8370E04	1.0E00
E6-554	66145	PYRO BATTERY (A)	.99999574	------	.99999574	1.5000E02	1.0000E04	1.0E00
E6-555	66145	PYRO BATTERY (B)	.99999574	------	.99999574	1.5000E02	1.0000E04	1.0E00
E6-556	41-162	BATTERY (A)	.99391402	------	.99391402	3.8000E00	1.0000E04	1.0E00
E6-557	41-162	BATTERY (B)	.99391402	------	.99391402	3.8	1.0000E04	1.0E00
E6-359	41-110	BATTERY CHARGER	.99992201	------	.99992201	2.5000E00	2.1000E05	1.0E00
E6-560	2-162	MAIN DC BUS A	.99888369	.0599	.99888968	3.8	8.0000E05	1.0E00
E6-561	2-162	MAIN DC BUS B	.99888369	.0599	.99888968	3.8	8.0000E05	1.0E00
E6-563	41-162	BATTERY BUS A	.99992403	------	.99992403	3.8	8.0000E05	1.0E00
E6-564	41-162	BATTERY BUS B	.99992403	------	.99992403	3.8	8.0000E05	1.0E00
E6-565	2-112	NON-ESSENTIAL D.C.BUS	.99942070	.0599	.99942669	3.8	8.0000E05	1.0E00
E6-566	2-162	BATTERY RELAY BUS	.99888369	.0599	.99888968	3.8	8.0000E05	1.0E00
E6-567	2-162	AC BUS 1	.99888369	.0599	.99888968	3.8	8.0000E05	1.0E00
E6-568	2-162	AC BUS 2	.99888369	.0599	.99888968	3.8	8.0000E05	1.0E00
E6-569	2-162	INVERTER 1	.99678090	.1854	.99679944	2.5000E00	1.7200E05	1.0E00
FE7-572	75-124	FUEL CELL SUBSYSTEM (A)	.99684002	------	.99684002	3.8	2.2000E04	1.0E00
FE7-573	75-124	FUEL CELL SUBSYSTEM (B)	.99684002	------	.99684002	3.8	2.2000E04	1.0E00
FE7-574	75-124	FUEL CELL SUBSYSTEM (C)	.99684002	------	.99684002	3.8	2.2000E04	1.0E00
FE7-575	75-124	OXYGEN TANK SYSTEM	.99880794	------	.99880794	3.8	5.8370E04	1.0E00
FE7-576	75-124	HYDROGEN TANK SYSTEM	.99880794	------	.99880794	3.8	5.8370E04	1.0E00
FE7-577	81-110	PYRO BATTERY (A)	.99998744	------	.99998744	3.8	1.0000E04	1.0E00

Table 3-4. (Continued)

COMTRACK - ELECTRICAL POWER

SOAR III NAME	SUBPHASE	COMPONENT	PARK REL.	ΔREL.X10^{-4}	D.I. REL.	K_1	P_1(MTBF)	$P_3(K_2)$
FE7-578	81-110	PYRO BATTERY (B)	.99998744	------	.99998744	3.8000E00	1.0000E04	1.0E00
FE7-579	81-110	PYRO DISTRIBUTION BUS (A)	.99999997	------	.99999997	2.5000E00	8.0000E05	1.0E00
FE7-580	81-110	PYRO DISTRIBUTION BUS (B)	.99999997	------	.99999997	2.5	8.0000E05	1.0E00
FE7-582	75-124	D-C BUS DISTRIBUTION (A)	.99991344	------	.99991344	3.8	8.0000E05	1.0E00
FE7-583	75-124	D-C BUS DISTRIBUTION (B)	.99991344	------	.99991344	3.8	8.0000E05	1.0E00
FE7-586	75-124	INVERTER	.99976447	------	.99976447	2.5	1.7200E05	1.0E00
E7-587	75-111	NON-ESSENTIAL DC BUS	.99993756	------	.99993756	3.8	8.0000E05	1.0E00
FE7-588	75-124	ESSENTIAL AC BUS	.99991344	------	.99991344	3.8	8.0000E05	1.0E00
E7-589	75-111	NON-ESSENTIAL AC BUS	.99993756	------	.99993756	3.8	8.0000E05	1.0E00

Table 3-4. (Continued)

PROPULSION SYSTEM - GUIDANCE AND NAVIGATION

SOAR III NAME	SUBPHASE	COMPONENT	PARK REL.	ΔRELX10^{-4}	D.I.REL.	K_1	P_1(MTBF)	$P_3(K_2)$
P1-1001	2-3	ENGINE 1	.99662494	------	.99662494	1.0000E00	1.0000E06	8.3333E04
P1-1002	2-3	ENGINE 2	.99662494	------	.99662494	1.0	1.0000E06	8.3333E04
P1-1003	2-3	ENGINE 3	.99662494	------	.99662494	1.0	1.0000E06	8.3333E04
P1-1004	2-3	ENGINE 4	.99662494	------	.99662494	1.0	1.0000E06	8.3333E04
P1-1005	2-3	ENGINE 5 (CENTER ENGINE)	.99662494	------	.99662494	1.0	1.0000E06	8.3333E04
P1-1006	2-3	FUEL FEED 1	.99853122	------	.99853122	1.0	1.0000E06	3.6231E04
P1-1007	2-3	FUEL FEED 2	.99853122	------	.99853122	1.0	1.0000E06	3.6231E04
P1-1008	2-3	FUEL FEED 3	.99853122	------	.99853122	1.0	1.0000E06	3.6231E04
P1-1009	2-3	FUEL FEED 4	.99853122	------	.99853122	1.0	1.0000E06	3.6231E04
P1-1010	2-3	FUEL FEED 5	.99853122	------	.9985122	1.0	1.0000E06	3.6231E04
P1-1011	2-3	OXIDIZER FEED 1	.99880401	------	.99880401	1.0	1.0000E06	2.9498E04
P1-1012	2-3	OXIDIZER FEED 2	.99880401	------	.99880401	1.0	1.0000E06	2.9498E04
P1-1013	2-3	OXIDIZER FEED 3	.99880401	------	.99880401	1.0	1.0000E06	2.9498E04
P1-1014	2-3	OXIDIZER FEED 4	.99880401	------	.99880401	1.0	1.0000E06	2.9498E04
P1-1015	2-3	OXIDIZER FEED 5	.99880401	------	.99880401	1.0	1.0000E06	2.9498E04
P1-1016	2-3	GAS GENERATOR 1	.99884157	------	.99884157	1.0	1.0000E06	2.8571E04
P1-1017	2-3	GAS GENERATOR 2	.99884157	------	.99884157	1.0	1.0000E06	2.8571E04
P1-1018	2-3	GAS GENERATOR 3	.99884157	------	.99884157	1.0	1.0000E06	2.8571E04
P1-1019	2-3	GAS GENERATOR 4	.99884157	------	.99884157	1.0	1.0000E06	2.8571E04
P1-1020	2-3	GAS GENERATOR 5	.99884157	------	.99884157	1.0	1.0000E06	2.8571E04
P1-1021	2-3	TURBOPUMP ASSEMBLY 1	.99864862	------	.99864862	1.0	1.0000E06	3.3333E04
P1-1022	2-3	TURBOPUMP ASSEMBLY 2	.99864862	------	.99864862	1.0	1.0000E06	3.3333E04
P1-1023	2-3	TURBOPUMP ASSEMBLY 3	.99864862	------	.99864862	1.0	1.0000E06	3.3333E04
P1-1024	2-3	TURBOPUMP ASSEMBLY 4	.99864862	------	.99864862	1.0	1.0000E06	3.3333E04
P1-1025	2-3	TURBOPUMP ASSEMBLY 5	.99864862	------	.998864862	1.0	1.0000E06	3.3333E04
P1-1026	2-3	FUEL PRESSURIZATION	.99726262	------	.99726262	1.0	1.0000E06	6.7567E04
P1-1027	2-3	OXIDIZER PRESSURAZATION	.99545204	------	.99545204	1.0	1.0000E06	1.1236E05
P1-1028	2-3	CONTROL PRESSURE SYSTEM 1	.99620360	------	.99620360	---	-----	-----
P1-1029	2-3	CONTROL PRESSURE SYSTEM 2	.99620360	------	.99620360	---	-----	-----
P1-1030	2-3	CONTROL PRESSURE SYSTEM 3	.99620360	------	.99620360	---	-----	-----
P1-1031	2-3	CONTROL PRESSURE SYSTEM 4	.99620360	------	.99620360	---	-----	-----
P1-1032	2-3	CONTROL PRESSURE SYSTEM 5	.99620360	------	.99620360	---	-----	-----
P1-1033	2-3	THRUST VECTOR CONTROL SYSTEM 1	.99817847	------	.99817847	1.0	1.0000E06	4.4940E04
P1-1034	2-3	THRUST VECTOR CONTROL SYSTEM 2	.99817847	------	.99817847	1.0	1.0000E06	4.4940E04
P1-1035	2-3	THRUST VECTOR CONTROL SYSTEM 3	.99817847	------	.99817847	1.0	1.0000E06	4.4940E04
P1-1036	2-3	THRUST VECTOR CONTROL SYSTEM 4	.99817847	------	.99817847	1.0	1.0000E06	4.4940E04
P1-1037	2-3	ELECTRICAL HARNESS	.99960003	------	.99960003	---	-----	-----
P1-1038	2-3	ENGINE SEQUENCER	.99669289	------	.99669289	---	-----	-----
P1-1039	2-3	FOUR-WAY CONTROL VALVE 1	.99999665	------	.99999665	1.0	1.0000E06	8.3000E01
P1-1040	2-3	FOUR-WAY CONTROL VALVE 2	.99999665	------	.99999665	1.0	1.0000E06	8.3000E01

Table 3-4. (Continued)

PROPULSION SYSTEM - GUIDANCE AND NAVIGATION

SOAR III NAME	SUBPHASE	COMPONENTS	PARK REL.	ΔREL.X10^{-4}	D.I.REL.	K_1	P_1(MTBF)	$P_3(K_2)$
P1-1041	2-3	FOUR-WAY CONTROL VALVE 3	.99999665	------	.99999665	1.0000E00	1.0000E06	8.3000E01
P1-1042	2-3	FOUR-WAY CONTROL VALVE 4	.99999665	------	.99999665	1.0000E00	1.0000E06	8.3000E01
P1-1043	2-3	FOUR-WAY CONTROL VALVE 5	.99999665	------	.99999665	1.0000E00	1.0000E06	8.3000E01
P1-1044	4	SEPARATION SYSTEM	.99900000	------	.99900000	-----	-----	-----
P1-1045	2-3	PROPULSION (NO EXPLOSION)	.99860049	------	.99860049	-----	-----	-----
P2-1046	5-7	ENGINE NO .1	.99103698	------	.99103698	1.0000E00	1.0000E06	8.3333E04
P2-1047	5-7	ENGINE NO. 2	.99103698	------	.99103698	1.0	1.0000E06	8.3333E04
P2-1048	5-7	ENGINE NO. 3	.99103698	------	.99103698	1.0	1.0000E06	8.3333E04
P2-1049	5-7	ENGINE NO. 4	.99103698	------	.99103698	1.0	1.0000E06	8.3333E04
P2-1050	5-7	ENGINE NO. 5 (CENTER ENGINE)	.99103698	------	.99103698	1.0	1.0000E06	8.3333E04
P2-1051	5	IGNITION SYSTEM 1	.99999793	------	.99999793	1.0	1.0000E06	5.0000E03
P2-1052	5	IGNITION SYSTEM 2	.99999793	------	.99999793	1.0	1.0000E06	5.0000E03
P2-1053	5	IGNITION SYSTEM 3	.99999793	------	.99999793	1.0	1.0000E06	5.0000E03
P2-1054	5	IGNITION SYSTEM 4	.99999793	------	.99999793	1.0	1.0000E06	5.0000E03
P2-1055	5	IGNITION SYSTEM	.99999793	------	.99999793	1.0	1.0000E06	5.0000E03
P2-1056	5-7	FUEL FEED 1	.99609321	------	.99609321	1.0	1.0000E06	3.6231E04
P2-1057	5-7	FUEL FEED 2	.99609321	------	.99609321	1.0	1.0000E06	3.6231E04
P2-1058	5-7	FUEL FEED 3	.99609321	------	.99609321	1.0	1.0000E06	3.6231E04
P2-1059	5-7	FUEL FEED 4	.99609321	------	.99609321	1.0	1.0000E06	3.6231E04
P2-1060	5-7	FUEL FEED 5	.99609321	------	.9960931	1.0	1.0000E06	3.6231E04
P2-1061	5-7	OXIDIZER FEED 1	.99681808	------	.99681808	1.0	1.0000E06	2.9498E04
P2-1062	5-7	OXIDIZER FEED 2	.99681808	------	.99681808	1.0	1.0000E06	2.9498E04
P2-1063	5-7	OXIDIZER FEED 3	.99681808	------	.98681808	1.0	1.0000E06	2.9498E04
P2-1064	5-7	OXIDIZER FEED 4	.99681808	------	.99681808	1.0	1.0000E06	2.9498E04
P2-1065	5-7	OXIDIZER FEED 5	.99681808	------	.98681808	1.0	1.0000E06	2.9498E04
P2-1066	5-7	GAS GENERATOR 1	.99691793	------	.99691793	1.0	1.0000E06	2.8571E04
P2-1067	5-7	GAS GENERATOR 2	.99691793	------	.99691793	1.0	1.0000E06	2.8571E04
P2-1068	5-7	GAS GENERATOR 3	.99691793	------	.99691793	1.0	1.0000E06	2.8571E04
P2-1069	5-7	GAS GENERATOR 4	.99691793	------	.99691793	1.0	1.0000E06	2.8571E04
P2-1070	5-7	GAS GENERATOR 5	.99691793	------	.99691793	1.0	1.0000E06	2.8571E04
P2-1071	5-7	OXIDIZER TURBOPUMP 1	.99640512	------	.99640512	1.0	1.0000E06	3.3333E04
P2-1072	5-7	OXIDIZER TURBOPUMP 2	.99640512	------	.99640512	1.0	1.0000E06	3.3333E04
P2-1073	5-7	OXIDIZER TURBOPUMP 3	.99640512	------	.99640512	1.0	1.0000E06	3.3333E04
P2-1074	5-7	OXIDIZER TURBOPUMP 4	.99640512	------	.99640512	1.0	1.0000E06	3.3333E04
P2-1075	5-7	OXIDIZER TURBOPUMP 5	.99640512	------	.99640512	1.0	1.0000E06	3.3333E04
P2-1076	5-7	FUEL TURBOPUMP 1	.99640512	------	.99640512	1.0	1.0000E06	3.3333E04
P2-1077	5-7	FUEL TURBOPUMP 2	.99640512	------	.99640512	1.0	1.0000E06	3.3333E04
P2-1078	5-7	FUEL TURBOPUMP 3	.99640512	------	.99640512	1.0	1.0000E06	3.3333E04
P2-1079	5-7	FUEL TURBOPUMP 4	.99640512	------	.99640512	1.0	1.0000E06	3.3333E04
P2-1080	5-7	FUEL TURBOPUMP 5	.99640512	------	.99640512	1.0	1.0000E06	3.3333E04

Table 3-4. (Continued)

PROPULSION SYSTEM - GUIDANCE AND NAVIGATION

SOAR III NAME	SUBPHASE	COMPONENTS	PARK REL.	Δ REL.X10^{-4}	D.I.REL.	K_1	P_1(MTBF)	P_2(K_2)
P2-1081	4	START TANK SYSTEM 1	.99999960	------	.99999960	1.0	1.0000E06	10.0000E00
P2-1082	4	START TANK SYSTEM 2	.99999960	------	.99999960	1.0	1.0000E06	10.0000E00
P2-1083	4	START TANK SYSTEM 3	.99999960	------	.99999960	1.0	1.0000E06	10.0000E00
P2-1084	4	START TANK SYSTEM 4	.99999960	------	.99999960	1.0	1.0000E06	10.0000E00
P2-1085	4	START TANK SYSTEM 5	.99999960	------	.99999960	1.0	1.0000E06	10.0000E00
P2-1086	4	OXIDIZER PRE-IGNITION TANK PRESSURE	.99839821	------	.99839821	1.0	1.0000E06	3.8461E04
P2-1087	4	FUEL PRE-IGNITION TANK PRESSURE	.99839821	------	.99839821	1.0	1.0000E06	3.8461E04
P2-1088	5-7	PRESSURIZATION FUEL TANK-MAIN STAGE	.99630686	------	.99630686	1.0	1.0000E06	3.4246E04
P2-1089	5-7	PRESSURIZATION OXIDIZER TANK-MAIN STAGE	.99630686	------	.99630686	1.0	1.0000E06	3.4246E04
P2-1090	4-8	ENGINE PNEUMATIC CONTROL 1	.99838466	------	.99838466	1.0	1.0000E06	10.0000E00
P2-1091	4-8	ENGINE PNEUMATIC CONTROL 2	.99838466	------	.99838466	1.0	1.0000E06	10.0000E00
P2-1092	4-8	ENGINE PNEUMATIC CONTROL 3	.99838466	------	.99838466	1.0	1.0000E06	10.0000E00
P2-1093	4-8	ENGINE PNEUMATIC CONTROL 4	.99838466	------	.99838466	1.0	1.0000E06	10.0000E00
P2-1094	4-8	ENGINE PNEUMATIC CONTROL 5	.99838466	------	.99838466	1.0	1.0000E06	10.0000E00
P2-1095	4	ENGINE PURGE SYSTEM 1	.99999960	------	.99999960	1.0	1.0000E06	10.0000E00
P2-1096	4	ENGINE PURGE SYSTEM 2	.99999960	------	.99999960	1.0	1.0000E06	10.0000E00
P2-1097	4	ENGINE PURGE SYSTEM 3	.99999960	------	.99999960	1.0	1.0000E06	10.0000E00
P2-1098	4	ENGINE PURGE SYSTEM 4	.99999960	------	.99999960	1.0	1.0000E06	10.0000E00
P2-1099	4	ENGINE PURGE SYSTEM 5	.99999960	------	.99999960	1.0	1.0000E06	10.0000E00
P2-1100	5-7	THRUST VECTOR CONTROL SYSTEM 1	.99930329	------	.99930329	1.0	1.0000E06	6.4510E03
P2-1101	5-7	THRUST VECTOR CONTROL SYSTEM 2	.99930329	------	.99930329	1.0	1.0000E06	6.4510E03
P2-1102	5-7	THRUST VECTOR CONTROL SYSTEM 3	.99930329	------	.99930329	1.0	1.0000E06	6.4510E03
P2-1103	5-7	THRUST VECTOR CONTROL SYSTEM 4	.99930329	------	.99930329	1.0	1.0000E06	6.4510E03
P2-1104	5-7	PROPELLANT UTILIZATION SYSTEM 1	.99998653	------	.99998653	1.0	1.0000E06	1.2500E02
P2-1105	5-7	PROPELLANT UTILIZATION SYSTEM 2	.99998653	------	.99998653	1.0	1.0000E06	1.2500E02
P2-1106	5-7	PROPELLANT UTILIZATION SYSTEM 3	.99998653	------	.99998653	1.0	1.0000E06	1.2500E02
P2-1107	5-7	PROPELLANT UTILIZATION SYSTEM 4	.99998653	------	.99998653	1.0	1.0000E06	1.2500E02
P2-1108	5-7	PROPELLANT UTILIZATION SYSTEM 5	.99998653	------	.99998653	1.0	1.0000E06	1.2500E02
P2-1109	5-7	PROPULSION (NO EXPLOSION)	.98537190	------	.98537190	-----	-----	-----
P2-1110	4	SEPARATION (FROM S-IC)	.999975600	------	.99975600	-----	-----	-----
P2-1111	5	SEPARATION (AFT-INTERSTAGE)	.99980800	------	.99980800	-----	-----	-----
P2-1112	8	SEPARATION (FROM S-IVB)	.99979300	------	.99979300	-----	-----	-----
P3-1113	9-25	ENGINE	.98897450	.4565	.98902015	1.0	1.0000E06	8.3333E04
P3-1114	9-24	IGNITION SYSTEM	.99999720	------	.99999994	1.0	1.0000E06	5.0000E03
P3-1116	9-25	FUEL FEED	.99519140	.2089	.99521229	1.0	1.0000E06	3.6231E04
P3-1117	9-25	OXIDIZER FEED	.99608324	.1620	.99609944	1.0	1.0000E06	2.9498E04
P3-1118	9-25	GAS GENERATOR	.99620610	.1569	.99622179	1.0	1.0000E06	2.8571E04
P3-1119	9-25	OXIDIZER TURBOPUMP	.99557515	.1831	.99559346	1.0	1.0000E06	3.3333E04
P3-1120	9-25	FUEL TURBOPUMP	.99557515	.1831	.99559346	1.0	1.0000E06	3.3333E04

Table 3-4. (Continued)

PROPULSION SYSTEM - GUIDANCE AND NAVIGATION

SOAR III NAME	SUBPHASE	COMPONENT	PARK REL.	Δ REL.X10^{-4}	D.I.REL.	K_1	P_1(MTBF)	$P_3(K_2)$
P3-1121	8-24	START TANK SYSTEM	.99852383	12.8037	.99980420	1.0000E00	1.0000E06	1.0000E03
P3-1122	8-23	OXIDIZER PRE-IGNITION TANK PRESSURE	.99423540	.1268	.99424808	1.0	1.0000E06	10.0000E00
P3-1123	8-23	FUEL PRE-IGNITION TANK PRESSURE	.99423540	.1268	.99424808	1.0	1.0000E06	10.0000E00
P3-1124	9-25	PRESSURIZATION FUEL TANK-MAINSTAGE	.99545425	.1880	.99547305	1.0	1.0000E06	3.4246E04
P3- 1125	9-25	PRESSURIZATION OXIDIZER TANK-MAINSTAGE	.99545425	.1880	.99547305	1.0	1.0000E06	3.4246E04
P3-1126	8-25	ENGINE PNEUMATIC CONTROL	.99801037	.1270	.99802307	1.0	1.0000E06	10.0000E00
P3-1127	9&24	ENGINE PURGE SYSTEM	.99999161	------	.99999981	1.0	1.0000E06	1.4925E04
P3-1128	9-25	THRUST VECTOR CONTROL SYSTEM	.99914213	.0356	.99914569	1.0	1.0000E06	6.4510E03
P3-1129	9-25	PROPELLANT UTILIZATION SYSTEM	.99998339	.0006	.99998345	1.0	1.0000E06	1.2500E02
P3-1130	9-25	PROPULSION (NO EXPLOSION)	.99720294	6.9902	.99790196	-----	-----	-----
P5-1131	11-144	HELIUM SUPPLY SYSTEM	.99791320	.1270	.99792590	1.0	1.0000E06	10.0000E00
P5-1132	11-144	SOLENOID SHUT OFF VALVE 1	.84604663	.2449	.84607112	1.0	1.0000E06	8.0000E02
P5-1134	11-144	PRIMARY REGULATOR 1	.99707935	.1782	.99709717	1.0	1.0000E06	1.4000E01
P5-1136	11-144	SECONDARY REGULATOR 1	.99707935	.1782	.99709717	1.0	1.0000E06	1.4000E01
P5-1138	11-144	REGULATED HELIUM SUPPLY 1	.93277738	4.2638	.93320376	1.0	1.0000E06	3.3300E02
P5-1139	11-144	REGULATED HELIUM SUPPLY 2	.93277738	4.2638	.93320376	1.0	1.0000E06	3.3300E02
P5-1140	38-144	ENGINE	.98829597	------	.98829597	1.0	1.0000E06	8.3333E04
P5-1141	38-144	FUEL FEED	.99997804	------	.99997804	1.0	1.0000E06	1.5600E02
P5-1142	38-144	OXIDIZER FEED	.99997804	------	.99997804	1.0	1.0000E06	1.5600E02
P5-1143	38-144	SOLENOID TCV PILOT VALVE 1	.99982347	------	.99982347	1.0	1.0000E06	1.2500E03
P5-1144	38-144	SOLENOID TCV PILOT VALVE 2	.99982347	------	.99982347	1.0	1.0000E06	1.2500E03
P5-1145	38-144	MAIN PROPELLANT VALVE 1	.99296103	------	.99296103	1.0	1.0000E06	5.0000E04
P5-1146	38-144	MAIN PROPELLANT VALVE 2	.99296103	------	.99296103	1.0	1.0000E06	5.0000E04
P5-1147	38-144	MAIN PROPELLANT VALVE 3	.99296103	------	.99296103	1.0	1.0000E06	5.0000E04
P5-1148	38-144	MAIN PROPELLANT VALVE 4	.99296103	------	.99296103	1.0	1.0000E06	5.0000E04
P5-1149	38-144	THRUST VECTOR CONTROL SYSTEM	.99908907	------	.99908907	1.0	1.0000E06	6.4510E03
P5-1150	38-144	PROPULSION (NO EXPLOSION)	.99792185	------	.99792185	-----	-----	-----
FP7-1151	112&115	ENGINE	.99169651	------	.99169651	1.0	1.0000E06	8.3333E04
FP7-1152	112&115	FUEL FEED	.99998440	------	.99998440	1.0	1.0000E06	1.5600E02
FP7-1153	112&115	OXIDIZER FEED	.99998440	------	.99998440	1.0	1.0000E06	1.5600E02
FP7-1154	78-115	ENGINE PURGE SUBSYSTEM	.99854185	------	.99854185	1.0	1.0000E06	10.0000E00
FP7-1155	78-115	OXIDIZER + FUEL PRESSURIZATION	.99958238	------	.99958238	1.0	1.0000E06	10.0000E00
FP7-1156	112&115	THRUST VECTOR CONTROL SYSTEM	.99935474	------	.99935474	1.0	1.0000E06	6.4510E03
FP7-1157	78-115	ENGINE CONTROL SYSTEM	.99997419	------	.99997419	1.0	1.0000E06	10.0000E00
P7-1158	112&115	PROPULSION (NO EXPLOSION)	.99948006	------	.99948006	-----	-----	-----
FP7-1159	82-96	ENGINE	.98837832	------	.98837832	1.0	1.0000E06	8.3333E04
FP7-1160	82-96	FUEL FEED	.99999866	------	.99999866	1.0	1.0000E06	10.0000E00
FP7-1161	82-96	OXIDIZER FEED	.99999866	------	.99999866	1.0	1.0000E06	10.0000E00
FP7-1162	78-96	ENGINE PURGE SUBSYSTEM	.99926004	------	.99926004	1.0	1.0000E06	10.0000E00
FP7-1163	78-96	OXIDIZER + FUEL PRESSURIZATION	.99986768	------	.99986768	1.0	1.0000E06	10.0000E00

Table 3-4. (Continued)

PROPULSION SYSTEM - GUIDANCE AND NAVIGATION

SOAR III NAME	SUBPHASE	COMPONENT	PARK REL.	Δ REL.X10^{-4}	D.I.REL.	K_1	P_1(MTBF)	P_3(K_2)
FP7-1164	82-96	THRUST VECTOR CONTROL SYSTEM	.99909551	------	.99909551	1.0000E00	1.0000E06	6.4[illegible]E03
FP7-1165	78-96	ENGINE CONTROL SYSTEM	.99999607	------	.99999607	1.0000E00	1.0000E06	10.0000E01
P7-1166	82-96	PROPULSION (NO EXPLOSION)	.99844099	------	.99844099	-----	-----	-----
FP4-1179	2-7	THRUST OK LOGIC CIRCUITRY	.99984385	------	.99984385	4.5000E01	4.2700E04	1.0E00
FP1-1180	2-3	S-IC STRUCTURAL INTEGRITY SYSTEM	.99997328	------	.99997328	4.5000E01	6.8300E04	1.0E00
FP2-1181	5-6	S-II STRUCTURAL INTEGRITY SYSTEM	.99999662	------	.99999662	2.5000E00	6.8300E04	1.0E00
FP1-1192	2-3	S-IC THRUST OK DETECTION TRANSDUCER	.99999568	------	.99999568	4.5000E01	4.2200E05	1.0E00
FP1-1193	2-3	S-IC THRUST OK DETECTION TRANSDUCER	.99999568	------	.99999568	4.5000E01	4.2200E05	1.0E00
FP1-1194	2-3	S-IC THRUST OK DETECTION TRANSDUCER	.99999568	------	.99999568	4.5000E01	4.2200E05	1.0E00
FP1-1195	2-3	S-IC THRUST OK DETECTION TRANSDUCER	.99999568	------	.99999568	4.5000E01	4.2200E05	1.0E00
FP1-1196	2-3	S-IC THRUST OK DETECTION TRANSDUCER	.99999568	------	.99999568	4.5000E01	4.2200E05	1.0E00
FP4-644	2	OVER-RATE GYRO LOGIC CIRCUIT	.99998592	------	.99998592	4.5000E01	6.8300E04	1.0E00
FP4-645	2	OVER-RATE GYRO PACKAGE	.99912140	------	.99912140	4.5000E01	1.0950E03	1.0E00
FP2-646	5-7	S-II THRUST OK DETECTION TRANSDUCER	.99998854	------	.99998854	2.5000E00	4.2200E05	1.0E00
FP2-647	5-7	S-II THRUST OK DETECTION TRANSDUCER	.99998854	------	.99998854	2.5000E00	4.2200E05	1.0E00
FP2-648	5-7	S-II THRUST OK DETECTION TRANSDUCER	.99998854	------	.99998854	2.5000E00	4.2200E05	1.0E00
FP2-649	5-7	S-II THRUST OK DETECTION TRANSDUCER	.99998854	------	.99998854	2.5000E00	4.2200E05	1.0E00
FP2-650	5-7	S-II THRUST OK DETECTION TRANSDUCER	.99998854	------	.99998854	2.5000E00	4.2200E05	1.0E00
GH-901	66-153	AGC HISTORY	.93271115	------	.93271115	2.5000E00	2.0000E03	4.0000E01
G4-801	2-34	INERTIAL MEASUREMENT UNIT	.96086572	37.2944	.96459516	3.8000E00	1.2738E03	1.0E00
G4-802	2-34	IMU ELECTRONICS	.99898356	.9733	.99908089	3.8000E00	5.0000E04	1.0E00
G4-803	2-34	GUIDANCE COMPUTER	.99853027	2.5605	.99878632	2.5000E00	1.2500E04	1.0E00
G4-804	2-34	DATA ADAPTER	.98235085	16.8573	.98404458	3.8000E00	2.8570E03	1.0E00
FG4-805	2-34	FLIGHT CONTROL COMPUTER	.99944098	.5350	.99949448	3.8	9.0909E04	1.0E00
G4-806	2-34	GN2 BEARING SUPPLY	.99746077	2.4309	.99770386	3.8	2.0000E04	1.0E00
G4-807	2-34	FLIGHT SEQUENCER	.99746077	2.4309	.99770386	3.8	2.0000E04	1.0E00
G4-808	2-8	CONTROL ACCELEROMETER	.99888884	------	.99888884	1.5000E02	2.0000E04	1.0E00
FG4-809	2-4	RATE GYRO-1	.99969558	------	.99969558	1.5000E02	2.0000E04	1.0E00
G4-810	2-8	RATE GYRO-2	.99888884	------	.99888884	1.5000E02	2.0000E04	1.0E00
G4-811	2-34	RATE GYRO-3	.99746077	2.4309	.99770386	3.8000E00	2.0000E04	1.0E00
G4-812	2-4	FLIGHT CONTROL SWITCH 1	.99969558	------	.99969558	1.5000E02	2.0000E04	1.0E00
G4-813	2-8	FLIGHT CONTROL SWITCH 2	.99888884	------	.99888884	1.5000E02	2.0000E04	1.0E00
G4-814	2-34	FLIGHT CONTROL SWITCH 3	.99746077	2.4309	.99770386	3.8000E00	2.0000E04	1.0E00
G6-815	2-159	INERTIAL MEASUREMENT UNIT	.86988191	19.2345	.87180536	3.8000E00	2.5000E03	1.0E00
G6-816	12-141	SEXTANT	.99736694	.6881	.99743575	3.8	1.9560E04	1.0E00
G6-817	12-141	SCANNING TELESCOPE	.99585178	1.0859	.99596037	3.8	1.2406E04	1.0E00
G6-818	2-159	GUIDANCE COMPUTER 1	.87498121	15.9360	.87657481	2.5000E00	2.0000E03	1.0E00
G6-819	2-153	GUIDANCE COMPUTER 2	.89544814	6.3940	.89608754	2.5000E00	2.0000E03	4.0000E01
G6-820	2-159	COUPLING DISPLAY UNIT (IMU) 1	.98587687	1.9848	.98607535	3.8000E00	2.4500E04	1.0E00
G6-821	2-159	COUPLING DISPLAY UNIT (IMU) 2	.98587687	1.9848	.98607535	3.8	2.4500E04	1.0E00

Table 3-4. (Continued)

PROPULSION SYSTEM - GUIDANCE AND NAVIGATION

SOAR III NAME	SUBPHASE	COMPONENT	PARK REL.	REL.$\times 10^{-4}$	D.I.REL.	K_1	P_1(MTBF)	$P_3(K_3)$
G6-822	2-159	COUPLING DISPLAY UNIT (IMU) 3	.98587687	1.9848	.98607505	3.8000E00	2.4500E04	1.0E00
G6-823	12-141	COUPLING DISPLAY UNIT (OPTICS) 1	.99789746	.5494	.99795240	3.8	2.4500E04	1.0E00
G6-824	12-141	COUPLING DISPLAY UNIT (OPTICS) 2	.99789746	.5494	.99795240	3.8	2.4500E04	1.0E00
G6-825	2-159	PSA-IMU ELECTRONICS	.92037433	11.5073	.92152506	3.8	4.2000E03	1.0E00
G6-826	12-141	PSA-OPTICS ELECTRONICS	.99574720	1.1125	.99585845	3.8	1.2100E04	1.0E00
G6-827	2-159	RATE GYRO ASSEMBLY	.91449486	4.8546	.91498032	3.8	1.0000E04	1.0E00
G6-828	2-159	RATE GYRO ELECTRONICS	.99580857	.2275	.99583132	3.8	2.1276E05	1.0E00
G6-829	2-159	ATTITUDE GYRO ASSEMBLY	.98373319	.8930	.98382249	3.8	5.4460E04	1.0E00
G6-830	8-144	ACCELEROMETER ASSEMBLY	.99453155	2.4333	.99962804	3.8	2.0000E04	1.0E00
G6-831	2-159	SCS CONTROL PANEL	.91817921	4.6362	.92540326	3.8	1.0471E04	1.0E00
G6-832	2-144	DISPLAY + CONTROL ELECTRONICS	.99436991	.9124	.99446115	3.8	5.3300E04	1.0E00
G6-833	2-159	ELECTRONIC CONTROL ASSEMBLY	.71755120	17.8716	.71923836	3.8	2.6930E03	1.0E00
G6-834	2-159	ELECTRONIC CONTROL ASSEMBLY-DISPLAYS	.87505562	7.2369	.87577931	3.8	6.6970E03	1.0E00
G6-835	2-152	ELECTRONIC CONTROL ASSEMBLY-AUXILIARY	.86720110	5.6372	.86776482	3.8	5.9950E03	1.0E00
G6-836	2-159	IMU CONTROL PANEL	.99812567	.2612	.99815179	3.8	1.8570E05	1.0E00
G6-837	12-14	INDICATOR CONTROL PANEL	.99597928	1.0518	.99608446	3.8	1.2800E04	1.0E00
G6-838	2-159	DISPLAY AND KEYBOARD (NAVIGATION)	.88030658	7.7187	.88107845	2.5000E00	4.1400E03	1.0E00
G6-839	2-159	DISPLAY AND KEYBOARD (MAIN)	.88030658	7.7187	.88107845	2.5000E00	4.1400E03	1.0E00
G6-843	12-159	ROTATIONAL CONTROLS NORMAL 1	.99729615	.2287	.99731902	3.8	5.8823E04	1.0E00
G6-844	12-159	ROTATIONAL CONTROLS NORMAL 2	.99729615	.2287	.99731902	3.8	5.8823E04	1.0E00
G6-845	33-124	TRANSLATIONAL CONTROLS 1	.99999705	------	.99999705	3.8	1.6474E06	1.0E00
G6-846	33-124	TRANSLATIONAL CONTROLS 2	.99999705	------	.99999705	3.8	1.6474E06	1.0E00
FG6-847	30-152	FLIGHT DIRECTORS ALTITUDE INDICATOR	.89222965	------	.89222965	3.8	5.6520E03	1.0E00
FG6-848	37-144	GIMBAL POSITION INDICATOR	.99871353	------	.99871353	3.8	4.4920E04	1.0E00
FG6-849	38-144	DELTA-V DISPLAY	.99699156	------	.99699156	2.0000E01	1.4771E04	1.0E00
FG6-852	80-120	LIGHTS ---FLASHING	1.0	NO CHANGE				
G7-853	78-120	INERTIAL MEASUREMENT UNIT 1	.98722185	------	.98722185	3.8000E00	2.5000E03	1.0E00
G7-854	78-120	INERTIAL MEASUREMENT UNIT 2	.96917892	------	.96917892	3.8	1.0270E03	1.0E00
G7-855	78-120	GUIDANCE COMPUTER	.99116801	------	.99116801	2.5000E00	2.0600E03	1.0E00
G7-856	78-96	RADAR ALTIMETER	.99645104	------	.99645104	3.8	5.0300E03	1.0E00
G7-857	78-120	POWER + SERVO ASSEMBLY-OPTICS	.99920461	------	.99920461	3.8	4.0400E04	1.0E00
G7-858	78-120	POWER + SERVO ASSEMBLY-IMU	.99300481	------	.99300481	3.8	4.5800E03	1.0E00
G7-859	78-120	COUPLING DISPLAY UNITS-IMU 1	.99868869	------	.99868869	3.8	2.4500E04	1.0E00
G7-860	78-120	COUPLING DISPLAY UNITS-IMU 2	.99868869	------	.99868869	3.8	2.4500E04	1.0E00
G7-861	78-120	COUPLING DISPLAY UNITS-IMU 3	.99868869	------	.99868869	3.8	2.4500E04	1.0E00
G7-862	78-120	COUPLING DISPLAY UNIT-OPTICS 1	.99868869	------	.99868869	3.8	2.4500E04	1.0E00
G7-863	78-120	COUPLING DISPLAY UNIT -OPTICS 2	.99868869	------	.99868869	3.8	2.4500E04	1.0E00
G7-865	78-120	DISPLAY + CONTROL ELECTRONICS	.99940652	------	.99940652	3.8	5.3300E04	1.0E00
G7-866	78-120	INDICATOR CONTROL PANEL	.99847749	------	.99847749	3.8	1.8570E05	1.0E00
G7-868	78-120	COMPUTER DISPLAY + KEYBOARD	.99565571	------	.99565571	2.5000E00	4.1400E03	1.0E00

Table 3-4. (Continued)

PROPULSION SYSTEM - GUIDANCE AND NAVIGATION

SOAR III NAME	SUBPHASE	COMPONENT	PARK REL.	Δ REL.X10^{-4}	D.I.REL.	K_1	P_1(MTBF)	$P_3(K_2)$
G7-869	78-120	OPTICAL MEASUREMENT UNIT	.99860891	------	.99860891	3.8000E00	2.3094E04	1.0E00
G7-870	78-120	RENDEZVOUS RADAR	.97611596	------	.97611596	3.8000E00	1.3300E03	1.0E00
G7-873	78-120	RATE GYRO PACKAGE -1	.99903604	------	.99903604	3.8000E00	3.3333E04	1.0E00
G7-874	78-120	RATE GYRO PACKAGE -2	.99903604	------	.99903604	3.8000E00	3.3333E04	1.0E00
G7-875	78-120	TRANSLATION CONTROL	.99788517	------	.99788517	3.8000E00	1.2987E04	1.0E00
G7-876	78-120	GUIDANCE COUPLER ASSEMBLY	.99865391	------	.99865391	3.8000E00	2.3866E04	1.0E00
G7-877	78-120	ATTITUDE + TRANSLATIONAL ASSEMBLY	.99743133	------	.99743133	3.8000E00	1.2500E04	1.0E00
G7-878	78-96	DESCENT ENFINE CONTROL ASSEMBLY	.99824902	------	.99824902	3.8000E00	1.0204E04	1.0E00
G7-879	78-120	COMPUTER AND PROGRAMMER	.98811027	------	.98811027	3.8000E00	2.6880E03	1.0E00
G7-880	78-120	CONTROL PANEL	.99333477	------	.99333477	3.8000E00	4.8076E03	1.0E00
G7-881	78-120	ROTATIONAL CONTROLS	.99346546	------	.99346546	3.8000E00	3.9525E03	1.0E00
G7-882	78-120	DISPLAYS	.99850299	------	.99850299	3.8000E00	2.1459E04	1.0E00
G7-883	78-120	RADAR ANALOG DISPLAY	.99888241	------	.99888241	3.8000E00	2.8750E04	1.0E00
G7-867	78-120	IMU CONTROL PANEL	.99982715	------	.99982715	3.8	1.8570E05	1.0E00

Table 3-4. (Continued)

REACTION CONTROL SYSTEM

SOAR III NAME	SUBPHASE	COMPONENTS	PARK REL.	λ REL.X10^{-4}	D. I. REL.	K_I	P_I(MTBF)	F_{S_I}
A5-1201	8-145	PRESSURIZATION SYSTEM	.99987261	.1269	.99988530	1.0000E00	1.0000E06	[illegible]
A5-1202	8-145	OXIDIZER FEED	.99991295	.1269	.99992564	1.0000E00	1.0000E06	[illegible]
A5-1203	8-145	FUEL FEED	.99991295	.1269	.99992564	1.0000E00	1.0000E06	[illegible]
A5-1204	8-145	4 OXIDIZER VALVES	.99987580	.1269	.99988849	1.0000E00	1.0000E06	10.0000E00
A5-1205	8-145	4 FUEL VALVES	.99987580	.1269	.99988849	1.0000E00	1.0000E06	10.0000E00
A5-1206	8-145	PRESSURIZATION SYSTEM	.99987261	.1269	.99988530	1.0	1.0000E06	10.0000E00
A5-1207	8-145	OXIDIZER FEED	.99991295	.1269	.99992564	1.0	1.0000E06	10.0000E00
A5-1208	8-145	FUEL FEED	.99991295	.1269	.99992564	1.0	1.0000E06	10.0000E00
A5-1209	8-145	4 OXIDIZER VALVES	.99987580	.1269	.99988849	1.0	1.0000E06	10.0000E00
A5-1210	8-145	4 FUEL VALVES	.99987580	.1269	.99988849	1.0	1.0000E06	10.0000E00
A5-1211	8-145	PRESSURIZATION SYSTEM	.99987261	.1269	.99988530	1.0	1.0000E06	10.0000E00
A5-1212	8-145	OXIDIZER FEED	.99991295	.1269	.99992564	1.0	1.0000E06	10.0000E00
A5-1213	8-145	FUEL FEED	.99991295	.1269	.99992564	1.0	1.0000E06	10.0000E00
A5-1214	8-145	4 OXIDIZER VALVES	.99987580	.1269	.99988530	1.0	1.0000E06	10.0000E00
A5-1215	8-145	4 FUEL VALVES	.99987580	.1269	.99988530	1.0	1.0000E06	10.0000E00
A5-1216	8-145	PRESSURIZATION SYSTEM	.99987261	.1269	.99988530	1.0	1.0000E06	10.0000E00
A5-1217	8-145	OXIDIZER FEED	.99991295	.1269	.99992564	1.0	1.0000E06	10.0000E00
A5-1218	8-145	FUEL FEED	.99991295	.1269	.99992564	1.0	1.0000E06	10.0000E00
A5-1219	8-145	4 OXIDIZER VALVES	.99987580	.1269	.99988849	1.0	1.0000E06	10.0000E00
A5-1220	8-145	4 FUEL VALVES	.99987580	.1269	.99988849	1.0	1.0000E06	10.0000E00
A5-1221	8-145	OX BLADDER	1.0	NO CHANGE				
A5-1222	8-145	OX BLADDER	1.0	NO CHANGE				
A5-1223	8-145	OX BLADDER	1.0	NO CHANGE				
A5-1224	8-145	OX BLADDER	1.0	NO CHANGE				
A5-1225	8-145	FUEL BLADDER	1.0	NO CHANGE				
A5-1226	8-145	FUEL BLADDER	1.0	NO CHANGE				
A5-1227	8-145	FUEL BLADDER	1.0	NO CHANGE				
A5-1228	8-145	FUEL BLADDER	1.0	NO CHANGE				
A5-1237	34-145	ENGINE QUAD I	.98039208	-----	.98039208	1.0000E00	1.0000E06	2.5000E05
A5-1238	34-145	ENGINE QUAD II	.98039208	-----	.98039208	1.0000E00	1.0000E06	2.5000E05
A5-1239	34-145	ENGINE QUAD III	.98039208	-----	.98039208	1.0000E00	1.0000E06	2.5000E05
A5-1240	34-145	ENGINE QUAD IV	.98039208	-----	.98039208	1.0000E00	1.0000E06	2.5000E05
A7-1241	78-124	PRESSURIZATION SUBSYSTEM	.99973522	-----	.99983522	1.0000E00	1.0000E06	10.0000E00
A7-1242	78-124	PRESSURIZATION SUBSYSTEM	.99973522	-----	.99973522	1.0000E00	1.0000E06	10.0000E00
A7-1243	78-124	FUEL FEED No. 1	.99973997	-----	.99973997	1.0000E00	1.0000E06	10.0000E00
A7-1244	78-124	FUEL FEED No. 2	.99973997	-----	.99973997	1.0000E00	1.0000E06	10.0000E00
A7-1245	78-124	OXIDIZER FEED NO. 1	.99973997	-----	.99973997	1.0000E00	1.0000E06	10.0000E00
A7-1246	78-124	OXIDIZER FEED NO. 2	.99973997	-----	.99973997	1.0000E00	1.0000E06	10.0000E00
A7-1254	78-124	OX. VALVE NO. 1	.99973996	-----	.99973996	1.0000E00	1.0000E06	10.0000E00
A7-1255	78-124	OX. VALVE NO. 3	.99974069	-----	.99974069	1.0000E00	1.0000E06	10.0000E00

Table 3-4. (Continued)

REACTION CONTROL SYSTEM

SOAR III NAME	SUBPHASE	COMPONENTS	PARK REL.	Δ REL.X10^{-4}	D. I. REL.	K_1	P_1(WTGF)	$P_3(K_2)$
A7-1257	78-124	FUEL VALVE NO. 1	.99973996	-----	.99973996	1.0000E00	1.0000E06	10.0000E00
A7-1258	78-124	FUEL VALVE NO.3	.99974069	-----	.99974069	1.0000E00	1.0000E06	10.0000E00
A7-1259	80-124	ENGINE NO. 1	.99841269	-----	.99841269	1.0	1.0000E06	8.3333E04
A7-1260	80-120	ENGINE NO. 3	.99923372	-----	.99923372	1.0	1.0000E06	8.3333E04
A7-1262	78-124	OX. VALVE NO. 2	.99973980	-----	.99973980	1.0	1.0000E06	10.0000E00
A7-1263	78-124	OX. VALVE NO. 4	.99974069	-----	.99974069	1.0	1.0000E06	10.0000E00
A7-1265	78-124	FUEL VALVE NO. 2	.99973980	-----	.99973980	1.0	1.0000E06	10.0000E00
A7-1266	78-124	FUEL VALVE NO. 4	.99974069	-----	.99974069	1.0	1.0000E06	10.0000E00
A7-1267	80-120	ENGINE NO. 2	.99841384	-----	.99841384	1.0	1.0000E06	8.3333E04
A7-1268	80-120	ENGINE NO. 4	.99923372	-----	.99923372	1.0	1.0000E06	8.3333E04
A7-1270	78-124	OX. VALVE NO. 5	.99973996	-----	.99973996	1.0	1.0000E06	10.0000E00
A7-1271	78-124	OX. VALVE NO. 8	.99974069	-----	.99974069	1.0	1.0000E06	10.0000E00
A7-1273	78-124	FUEL VLAVE NO. 5	.99973996	-----	.99973996	1.0	1.0000E06	10.0000E00
A7-1274	78-124	FUEL VALVE NO. 8	.99974069	-----	.99974069	1.0	1.0000E06	10.0000E00
A7-1275	80-124	ENGINE No. 5	.99841269	-----	.99841269	1.0	1.0000E06	8.3333E04
A7-1276	80-120	ENGINE No. 8	.99923372	-----	.99923372	1.0	1.0000E06	8.3333E04
A7-1278	78-124	OX. VALVE NO. 6	.99973980	-----	.99973980	1.0	1.0000E06	10.0000E00
A7-1279	78-124	OX. VALVE NO. 7	.99974069	-----	.99974069	1.0	1.0000E06	10.0000E00
A7-1281	78-124	FUEL VALVE NO. 6	.99973980	-----	.99973980	1.0	1.0000E06	10.0000E00
A7-1282	78-124	FUEL VALVE NO. 7	.99974069	-----	.99974069	1.0	1.0000E06	10.0000E00
A7-1283	80-120	ENGINE NO. 6	.99841384	-----	.99841384	1.0	1.0000E06	8.3333E04
A7-1284	80-120	ENGINE NO. 7	.99923372	-----	.99923372	1.0	1.0000E06	8.3333E04
A7-1286	78-124	OX. VALVE NO. 9	.99973996	-----	.99973996	1.0	1.0000E06	10.0000E00
A7-1287	78-124	OX. VALVE NO. 12	.99974069	-----	.99974069	1.0	1.0000E06	10.0000E00
A7-1289	78-124	FUEL VALVE NO. 9	.99973996	-----	.99973996	1.0	1.0000E06	10.0000E00
A7-1290	78-124	FUEL VALVE NO. 12	.99974069	-----	.99974069	1.0	1.0000E06	10.0000E00
A7-1291	80-124	ENGINE NO. 9	.99841269	-----	.99841269	1.0	1.0000E06	8.3333E04
A7-1292	80-120	ENGINE NO. 12	.99923372	-----	.99923372	1.0	1.0000E06	8.3333E04
A7-1294	78-124	OX. VALVE NO. 10	.99973980	-----	.99973980	1.0	1.0000E06	10.0000E00
A7-1295	78-124	OX. VALVE NO. 11	.99974069	-----	.99974069	1.0	1.0000E06	10.0000E00
A7-1297	78-124	FUEL VALVE NO. 10	.99973980	-----	.99973980	1.0	1.0000E06	10.0000E00
A7-1298	78-124	FUEL VALVE NO. 11	.99974069	-----	.99974069	1.0	1.0000E06	10.0000E00
A7-1299	80-120	ENGINE NO. 10	.99841384	-----	.99841384	1.0	1.0000E06	8.3333E04
A7-1300	80-120	ENGINE NO. 11	.99923372	-----	.99923372	1.0	1.0000E06	8.3333E04
A7-1302	78-124	OX. VALVE NO. 13	.99973996	-----	.99973996	1.0	1.0000E06	10.0000E00
A7-1303	78-124	OX. VALVE NO. 15	.99974069	-----	.99974069	1.0	1.0000E06	10.0000E00
A7-1305	78-124	FUEL VALVE NO. 13	.99973996	-----	.99973996	1.0	1.0000E06	10.0000E00
A7-1306	78-124	FUEL VALVE NO. 15	.99974069	-----	.99974069	1.0	1.0000E06	10.0000E00
A7-1307	80-124	ENGINE NO. 13	.99841269	-----	.99841269	1.0	1.0000E06	8.3333E04
A7-1308	80-120	ENGINE NO. 15	.99923372	-----	.99923372	1.0	1.0000E06	8.3333E04

Table 3-4. (Continued)

REACTION CONTROL SYSTEM

SOAR III NAME	SUBPHASE	COMPONENTS	PARK REL.	Δ REL.X10^{-4}	D.I.REL.	K_1	P_1(MTBF)	$P_{3(MTBF)}$
A7-1310	78-124	OX. VALVE NO. 14	.99973980	-----	.99973980	1.0000E00	1.0000E06	10.0000E00
A7-1311	78-124	OX. VALVE NO. 16	.99974069	-----	.99974069	1.0	1.0000E06	10.0000E00
A7-1313	78-124	FUEL VALVE NO. 14	.99973980	-----	.99973980	1.0	1.0000E06	10.0000E00
A7-1314	78-124	FUEL VALVE NO. 16	.99974069	-----	.99974069	1.0	1.0000E06	10.0000E00
A7-1315	80-120	ENGINE NO. 14	.99841384	-----	.99841384	1.0	1.0	8.3333E04
A7-1316	80-120	ENGINE NO. 16	.99923372	-----	.99923372	1.0	1.0	8.3333E04
A6-1321	145-159	PRESSURIZATION SUBSYSTEM	.99994048	-----	.99994048	1.0	1.0	10.0000E00
A6-1322	145-159	PRESSURIZATION SUBSYSTEM	.99994048	-----	.99994048	1.0	1.0	10.0000E00
A6-1323	145-159	FUEL FEED NO. 1	.99998295	-----	.99998295	1.0	1.0	10.0000E00
A6-1324	145-159	FUEL FEED NO. 2	.99998295	-----	.99998295	1.0	1.0	10.0000E00
A6-1325	145-159	OXIDIZER FEED NO. 1	.99998295	-----	.99998295	1.0	1.0	10.0000E00
A6-1326	145-159	OXIDIZER FEED NO. 2	.99998295	-----	.99998295	1.0	1.0	10.0000E00
A6-1327	145-159	6 OXIDIZER CONTROL VALVES	.99966262	-----	.99966262	1.0	1.0	10.0000E00
A6-1328	145-159	6 OXIDIZER CONTROL VALVES	.99966262	-----	.99966262	1.0	1.0	10.0000E00
A6-1329	145-159	6 FUEL CONTROL VALVES	.99966262	-----	.99966262	1.0	1.0	10.0000E00
A6-1330	145-159	6 FUEL CONTROL VALVES	.99966262	-----	.99966262	1.0	1.0	10.0000E00
A6-1331	145-159	ENGINE NO. 1	.99912815	-----	.99912815	1.0	1.0	10.0000E00
A6-1332	145-159	ENGINE NO. 2	.99912815	-----	.99912815	1.0	1.0	10.0000E00
A6-1333	145-159	ENGINE NO. 3	.99912815	-----	.99912815	1.0	1.0	10.0000E00
A6-1334	145-159	ENGINE NO. 4	.99912815	-----	.99912815	1.0	1.0	10.0000E00
A6-1335	145-159	ENGINE NO. 5	.99912815	-----	.99912815	1.0	1.0	10.0000E00
A6-1336	145-159	ENGINE NO. 6	.99912815	-----	.99912815	1.0	1.0	10.0000E00
A6-1337	145-159	ENGINE No. 7	.99912815	-----	.99912815	1.0	1.0	10.0000E00
A6-1338	145-159	ENGINE NO. 8	.99912815	-----	.99912815	1.0	1.0	10.0000E00
A6-1339	145-159	ENGINE NO. 9	.99912815	-----	.99912815	1.0	1.0	10.0000E00
A6-1340	145-159	ENGINE NO. 10	.99912815	-----	.99912815	1.0	1.0	10.0000E00
A6-1341	145-159	ENGINE NO. 11	.99912815	-----	.99912815	1.0	1.0	10.0000E00
A6-1342	145-159	ENGINE NO. 12	.99912815	-----	.99912815	1.0	1.0	10.0000E00
A3-1343	8-34	PRESSURIZATION SUBSYSTEM NO. 1	.99614753	.3924	.99618677	1.0	1.0	3.3333E04
A3-1344	8-34	PRESSURIZATION SUBSYSTEM NO. 2	.99614753	.3924	.99618677	1.0	1.0	1.0000E03
A3-1347	8-34	FUEL FEED No. 1	.99807794	.1461	.99809255	1.0	1.0	1.0000E03
A3-1348	8-34	FUEL FEED NO. 2	.99807794	.1461	.99809255	1.0	1.0	1.0000E03
A3-1349	8-34	FUEL EXPULSION BLADDER NO. 1	1.0	NO CHANGE				
A3-1350	8-34	FUEL EXPULSION BLADDER NO. 2	1.0	NO CHANGE				
A3-1351	8-34	FUEL CONTROL VALVE ASSEMBLY NO. 1	.99996838	.0067	.99996905	1.0	1.0	2.0000E02
A3-1352	8-34	FUEL CONTROL VALVE ASSEMBLY NO. 2	.99996838	.0067	.99996905	1.0	1.0	2.0000E02
A3-1353	8-34	FUEL CONTROL VALVE ASSEMBLY NO. 3	.99996838	.0067	.99996905	1.0	1.0	2.0000E02
A3-1354	8-34	FUEL CONTROL VALVE ASSEMBLY NO. 4	.99996838	.0067	.99996905	1.0	1.0	2.0000E02
A3-1355	8-34	FUEL CONTROL VALVE ASSEMBLY NO. 5	.99994271	.0021	.99994292	1.0	1.0	2.0000E02
A3-1356	8-34	FUEL CONTROL VALVE ASSEMBLY NO. 6	.99994271	.0021	.99994292	1.0	1.0	2.0000E02

Table 3-4. (Continued)

REACTION CONTROL SYSTEM

SOAR III NAME	SUBPHASE	COMPONENT	PARK REL.	Δ REL. $\times 10^{-4}$	D.I. REL.	K_1	P. (°F)	$P_3(K_2)$
A3-1357	8-34	FUEL CONTROL VALVE ASSEMBLY NO. 7	.99931326	2.5659	.99956985	1.0000E00	[illegible]E06	2.0000E02
A3-1358	8-34	FUEL CONTROL VALVE ASSEMBLY NO. 8	.99931326	2.5659	.99956985	1.0	[illegible]	2.0000E02
A3-1361	8-34	OXIDIZER FEED NO. 1	.99807794	.1461	.99809255	1.0	[illegible]	1.0000E03
A3-1362	8-34	OXIDIZER FEED NO. 2	.99807794	.1461	.99809255	1.0	[illegible]	1.0000E03
A3-1363	8-34	OXIDIZER EXPULSION BLADDER NO. 1	1.0	NO CHANGE				
A3-1364	8-34	OXIDIZER EXPULSION BLADDER NO. 2	1.0	NO CHANGE				
A3-1365	8-34	OX. CONTROL VALVE ASSEMBLY NO. 1	.99996838	.0067	.99996905	1.0	[illegible]	2.0000E02
A3-1366	8-34	OX. CONTROL VALVE ASSEMBLY NO. 2	.99996838	.0067	.99996905	1.0	[illegible]	2.0000E02
A3-1367	8-34	OX. CONTROL VALVE ASSEMBLY NO. 3	.99996838	.0067	.99996905	1.0	[illegible]	2.0000E02
A3-1368	8-34	OX. CONTROL VALVE ASSEMBLY NO. 4	.99996938	.0067	.99996905	1.0	[illegible]	2.0000E02
A3-1369	8-34	OX. CONTROL VALVE ASSEMBLY NO. 5	.99994271	.0021	.99994292	1.0	[illegible]	2.0000E02
A3-1370	8-34	OX. CONTROL VALVE ASSEMBLY NO. 6	.99994271	.0021	.99994292	1.0	[illegible]	2.0000E02
A3-1371	8-34	OX. CONTROL VALVE ASSEMBLY NO. 7	.99931326	2.5659	.99956985	1.0	[illegible]	2.0000E02
A3-1372	8-34	OX. CONTROL VALVE ASSEMBLY NO. 8	.99931326	2.5659	.99956985	1.0	[illegible]	2.0000E02
A3-1375	10-34	150 = RC ENGINE NO. 2 R+Y	.99990384	.5271	.99995655	1.0	[illegible]	8.3333E04
A3-1376	10-34	150 = RC ENGINE NO. 3 R+Y	.99990384	.5271	.99995655	1.0	[illegible]	8.3333E04
A3-1377	10-34	150 = RC ENGINE NO. 4 R+Y	.99990384	.5271	.99995655	1.0	[illegible]	8.3333E04
A3-1378	11-34	150 = RC ENGINE NO. 5 PITCH	.99996080	.2190	.99998270	1.0	[illegible]	8.3333E04
A3-1379	11-34	150 = RC ENGINE NO. 6 PITCH	.99996080	.2190	.99998270	1.0	[illegible]	8.3333E04
A3-1382	8-24	1750 = PROPELLANT ULLAGE NO. 1	.99993220	-----	.99993220	1.0	[illegible]	8.3333E04
A3-1383	8-24	1750 = PROPELLANT ULLAGE NO. 2	.99993220	-----	.99993220	1.0	1.0	8.3333E04
A3-1384	35	SEPARATION SUBSYSTEM	.99979300	-----	.99979300	-----	-----	-----
A3-1385	10-34	150 = RC ENGINE NO. 1 R+Y	.99990384	.5271	.99995655	1.0	1.0	8.3333E04

Table 3-4. (Continued)

ENVIRONMENTAL CONTROL SYSTEM [illegible] LANDING - LAUNCH ESCAPE - CREW

SUBSYSTEM NAME	SUBPHASE	COMPONENTS	PARK REL.	FAIL RATE $\times 10^{-4}$	D. I. REL.	K_1	P_1(MTBF)	$P_3(K_2)$
FL6-651	9-162	LEM SUITAIR THERMAL CONTROL	.98996322	.5484	.99001806	3.8000E00	8.8650E04	1.0000E00
L6-652	9-162	SUIT HUMIDITY CONTROL	.99008656	.5418	.99014074	3.8	8.9760E04	1.0E00
L6-653	9-162	NOXIOUS SUBSTANCE REMOVAL	.99108847	.4866	.99113713	3.8	9.9900E04	1.0E00
L6-654	9-162	PRESSURE COMPRESSOR NO. 1	.98183389	.9969	.98193358	3.8	4.8780E04	1.0E00
L6-657	9-162	FLOW CONTROL	.98306429	.9287	.98315716	3.8	5.2356E04	1.0E00
L6-660	9-162	CABIN PRESSURE REGULATORS (2 REGS)	.99720522	.1516	.99722038	3.8	3.1948E05	1.0E00
L6-661	9-162	CABIN PRESSURE RELIEF (2VALVES)	.99287145	.3888	.99291033	3.8	1.2500E05	1.0E00
L6-662	9-162	CABIN TEMPERATURE CONTROL	.97719108	1.2546	.97731654	3.8	3.8759E04	1.0E00
L6-663	9-162	CABIN TEMPERATURE CONTROL VALVE	.98999803	.5466	.99005269	3.8	8.8960E04	1.0E00
L6-664	9-162	CABIN TO SUIT CKT AIR CHECK VALVES (2)	.99642956	.1941	.99644899	3.8	2.5000E05	1.0E00
L6-665	9-162	GLYCOL AUTOMATIC TEMPERATURE CONTROL	.99825824	.0944	.99826768	3.8	5.1282E05	1.0E00
L6-666	9-162	GLYCOL-H_2O EVAPORATIVE HEAT EXCHANGER	.99926152	.1483	.99927635	3.8	3.2679E05	1.0E00
L6-667	9-162	GLYCOL FLOW CONTROL VALVE	.99975957	.0125	.99976082	3.8	3.7037E06	1.0E00
L6-669	11-145	RADIATOR COOLING SYSTEM	.96530317	1.9915	.96550232	3.8	2.3041E04	1.0E00
L6-670	9-162	EQUIPMENT COOLING SYSTEM	.99687549	.1696	.99683245	3.8	2.8571E05	1.0E00
L6-671	9-162	FLOW CONTROL	.98169259	1.0050	.98179309	3.8	4.8400E04	1.0E00
L6-672	9-162	PUMP 1	.99535194	.2528	.99537722	3.8	1.9193E05	1.0E00
FL6-674	9-162	SUIT CKT, EVAP. HEAT EXCHANGER H_2O	.99275614	1.4635	.99290249	3.8	3.3222E04	1.0E00
L6-675	9-162	GLYCOL EVAP. HEAT EXC. H_2O FLOW	.99926152	.1483	.99927635	3.8	3.2679E05	1.0E00
L6-676	9-162	PORTABLE H_2O SUPPLY	.98183389	.9969	.98193356	3.8	4.8780E04	1.0E00
L6-677	9-162	WASTE WATER SUPPLY	.99852821	.2958	.99855779	3.8	1.6393E05	1.0E00
L6-678	9-145	FIRST STAGE PRESSURE REGULATION	.99529199	.2720	.99531919	3.8	1.7857E05	1.0E00
L6-682	146-162	RE-ENTRY O2 SUPPLY	.99946418	-----	.99946418	3.8	9.6153E04	1.0E00
L6-685	163-165	CABIN GROUND VENTILATION SYSTEM (USED AFTER LANDING)	.99993272	-----	.99993272	3.8	6.1349E04	1.0E00
L7-686	75-120	LEM SUIT AIR THERMAL CONTROL	.99927571	-----	.99927571	3.8	7.9740E04	1.0E00
L7-687	75-120	LEM SUIT HUMIDITY CONTROL	.99971139	-----	.9971139	3.8	2.0000E05	1.0E00
L7-688	75-120	LEM SUIT PRESSURIZATION CONTROL	.99846438	-----	.99846438	3.8	3.7600E04	1.0E00
L7-689	75-120	LEM SUIT NOXIOUS SUBSTANCE REMOVAL	.99942246	-----	.9994226	3.8	1.0000E05	1.0E00
L7-690	75-121	PRESSURE SUIT = 2 +CKT.	.99984182	-----	.99984182	3.8	3.7453E05	1.0E00
L7-691	75-121	PRESSURE SUIT = 3 +CKT.	.99984182	-----	.99984182	3.8	3.7453E05	1.0E00
L7-692	76-120	LEM CABIN PRESSURIZATION CONTROL	.99940810	-----	.99940810	3.8	8.9760E04	1.0E00
L7-693	76-120	LEM CABIN ATMOSPHERE REVITALIZATION CONTROL	.99990192	-----	.99990192	3.8	5.0000E05	1.0E00
L7-694	76-120	LEM CABIN THERMAL CONTROL	.99877360	-----	.99877360	3.8	4.0060E04	1.0E00
L7-695	75-120	LEM GLYCOL TEMPERATURE CONTROL	.99964662	-----	.99964662	3.8	1.6339E05	1.0E00
L7-696	[illegible]	LEM H_2O EVAPORATIVE HEAT EXCHANGER	.99855288	-----	.99855288	3.8	3.9900E04	1.0E00
[illegible]	[illegible]	[illegible] PRES	.9906898		.9906898	3.8	[illegible]	1.0E00
[illegible]	[illegible]	[illegible]	[illegible]		[illegible]	[illegible]	[illegible]	1.0E00
[illegible]	[illegible]	[illegible]	[illegible]		[illegible]	[illegible]	[illegible]	[illegible]

Table 3-4. (Continued)

ENVIRONMENTAL CONTROL SYSTEM - EARTH LANDING - LAUNCH ESCAPE - CREW

SOAR III NAME	SUBPHASE	COMPONENT	PARK REL.	Δ REL.X10^{-4}	D.I. REL.	K_1	P_1(MTBF)	$P_3(K_2)$
L7-702	75-120	LEM OXYGEN SUPPLY	.99866827	-----	.99866827	3.8000E00	4.3360E04	1.0000E00
L6-705	9-10	CM FREON COOLING CIRCUIT	.99990019	-----	.99990019	3.8	1.3755E05	1.0E00
L4-706	2-34	IU PRESSURE REGULATION	.99804620	1.8703	.99823323	3.8	2.6000E04	1.0E00
L4-707	2-34	IU LIQUID N2 COOLING SYSTEM	.98691269	12.5128	.98816397	3.8	3.8600E03	1.0E00
L4-708	2-34	IU CIRCULATION SYSTEM	.98620255	13.1903	.98634158	3.8	3.6600E03	1.0E00
2TO-954	6	NON-ABORT SEQUENCER	.99959110	-----	.99959110	1.5000E02	1.7421E04	1.0E00
2TO-955	6	NON-ABORT SEQUENCER	.99959110	-----	.99959110	1.5000E02	1.7421E04	1.0E00
2TO-956	6	SHAPE CHARGE (OUTER)	.99900000	-----	.99900000	-----	-----	-----
2TO-957	6	CABLE CUTTER	.99580000	-----	.99580000	-----	-----	-----
2TO-958	6	SHAPE CHARGE (OUTER)	.99900000	-----	.99900000	-----	-----	-----
2TO-959	6	CABLE CUTTER	.99580000	-----	.99580000	-----	-----	-----
2TO-960	6	SHAPE CHARGE (OUTER)	.99990000	-----	.99990000	-----	-----	-----
2TO-961	6	EXPLOSIVE BOLT	.99999990	-----	.99999990	-----	-----	-----
2TO-962	6	EXPLOSIVE BOLT	.99999990	-----	.99999990	-----	-----	-----
2TO-963	6	EXPLOSIVE BOLT	.99999990	-----	.99999990	-----	-----	-----
2TO-964	6	EXPLOSIVE BOLT	.99999990	-----	.99999990	-----	-----	-----
2TO-967	6	JETTISON MOTOR	.99980000	-----	.99980000	-----	-----	-----
2TO-970	6	IGNITER	.99999999	-----	.99999999	-----	-----	-----
2TO-971	6	SHAPE CHARGE (OUTER)	.99900000	-----	.99900000	-----	-----	-----
2TO-972	6	SHAPE CHARGE (INNER)	.99900000	-----	.99900000	-----	-----	-----
2TO-973	6	SHAPE CHARGE (INNER)	.99900000	-----	.99900000	-----	-----	-----
2TO-974	6	SHAPE CHARGE (INTER)	.99900000	-----	.99900000	-----	-----	-----
2TO-975	6	SHAPE CHARGE (INNER)	.99900000	-----	.99900000	-----	-----	-----
R6-453	156-160	AUTOMATIC SEQUENCER	.99970002	-----	.99970002	-----	-----	-----
R6-454	156-160	AUTOMATIC SEQUENCER	.99970002	-----	.99970002	-----	-----	-----
R6-455	156	BARDSWITCH 25000 FT.	.99700000	-----	.99700000	-----	-----	-----
R6-456	156	BARDSWITCH 25000 FT.	.99700000	-----	.99700000	-----	-----	-----
R6-457	159-160	BARDSWITCH 15000 FT.	.99400900	-----	.99400900	-----	-----	-----
R6-458	159-160	BARDSWITCH 15000 FT.	.99400900	-----	.99400900	-----	-----	-----
R6-459	156	AUTOMATIC FORWARD HEAT SHIELD JETTISON SYSTEM	.97310000	-----	.97310000	-----	-----	-----
R6-460	156	AUTOMATIC FORWARD HEAT SHIELD JETTISON SYSTEM	.97300000	-----	.97300000	-----	-----	-----
R6-463	159	DROGUE CHUTE	.99800000	-----	.99800000	-----	-----	-----
R6-464	160	MAIN CHUTE NO. 1	.99310000	-----	.99310000	-----	-----	-----
R6-465	160	MAIN CHUTE NO. 2	.99310000	-----	.99310000	-----	-----	-----
R6-466	160	MAIN CHUTE NO. 3	.99310000	-----	.99310000	-----	-----	-----
R6-467	160	PILOT PARACHUTE	.99310000	-----	.99310000	-----	-----	-----
R6- 468	160	PILOT PARACHUTE	.99310000	-----	.99310000	-----	-----	-----
R6-469	160	PILOT PARACHUTE	.99310000	-----	.99310000	-----	-----	-----
R6-470	160	REEF CUTTER NO. 1	.99580000	-----	.99580000	-----	-----	-----

Table 3-4. (Continued)

ENVIRONMENTAL CONTROL SYSTEM - EARTH LANDING -LAUNCH ESCAPE - CREW

SOAR III NAME	SUBPHASE	COMPONENT	PARK REL.	Δ RELX10^{-4}	D.I.REL.	K_1	P_1(MTBF)	$P_3(K_2)$
R6-471	160	REEF CUTTER NO. 2	.99580000	-----	.99580000	-----	-----	-----
R6-472	160	REEF CUTTER NO. 3	.99580000	-----	.99580000	-----	-----	-----
R6-473	160	MANUAL MAIN CHUTE RELEASE SYSTEM	.99900000	-----	.99900000	-----	-----	-----
MO-401	6	MAN	1.0	NO CHANGE				
M-402	12-141	MAN	1.0	NO CHANGE				
M-403	12-159	MAN	1.0	NO CHANGE				
M-404	78-120	MAN	1.0	NO CHANGE				
M-405	78-120	MAN	1.0	NO CHANGE				
M-406	78-120	MAN	1.0	NO CHANGE				
MF6-412	9-162	MAN	1.0	NO CHANGE				
MF6-413	9-162	MAN	1.0	NO CHANGE				
MF6-414	9-145	MAN	1.0	NO CHANGE				
ML7-415	75	MAN	1.0	NO CHANGE				
ML7-416	75	MAN	1.0	NO CHANGE				
ML7-417	75-121	MAN	1.0	NO CHANGE				
ML7-418	75-121	MAN	1.0	NO CHANGE				
ML7-419	76	MAN	1.0	NO CHANGE				
ML7-420	102	MAN	1.0	NO CHANGE				
ML7-422	107	MAN	1.0	NO CHANGE				
MF7-423	75-121	MAN	1.0	NO CHANGE				
MF7-424	75-121	MAN	1.0	NO CHANGE				
MF7-425	77-103	MAN	1.0	NO CHANGE				
MF7-426	77-108	MAN	1.0	NO CHANGE				
MF7-427	102	MAN	1.0	NO CHANGE				
MF7-428	107	MAN	1.0	NO CHANGE				
MO-439	76-110	MAN	1.0	NO CHANGE				
MO-447	156	MAN	1.0	NO CHANGE				
MO-448	156-160	MAN	1.0	NO CHANGE				
MO-449	162	MAN	1.0	NO CHANGE				

[redacted]

Table 3-5. Relevant Flight Test Failure Data

	FIRST BURNING					SECOND BURNING			
	S	NT	F	R		S	NT	F	R
IGNITION	11	2	0	1.000	ABLE STAR	8	4	1	0.889
STEADY STATE	10	2	1	0.909		8	5	0	1.000
CUTOFF	9	4	0	1.000		8	5	0	1.000
				0.909					0.889

	FIRST BURNING					SECOND BURNING			
	S	NT	F	R		S	NT	F	R
IGNITION	108	13	2	0.982	AGENA	28	6	5	0.849
STEADY STATE	100	15	8	0.926		28	11	0	1.000
CUTOFF	100	21	2	0.980		27	11	1	0.964
				0.901					0.818

	FIRST BURNING					SECOND BURNING			
	S	NT	F	R		S	NT	F	R
IGNITION	36	0	0	1.000	TITAN I G,J, & M Series	29	3	4	0.879
STEADY STATE	33	0	3	0.917		26	6	4	0.867
CUTOFF	32	3	1	0.970		27	9	0	1.000
				0.889					0.762

CODE:

S - SUCCESS
NT - NO TEST
F - FAILURE
R - RELIABILITY

[redacted]

Table 3-6. Reasons for Failures

VEHICLE LAUNCH DATE	IGNITION	STEADY STATE	SHUTDOWN	SUBSYSTEM	REMARKS
ABLE STAR SECOND BURNING ONLY					
22 June 1960	S	S	S		Momentary flame-out during second ignition.
21 February 1961	F	NT	NT	Electrical	Decade counter malfunction.
AGENA SECOND BURNING ONLY					
23 August 1961	F	NT	NT	Propulsion	Oxidizer manifold switch failed.
26 January 1962	S	S	F	Guidance	Incorrect velocity meter calibration.
21 February 1962	F	NT	NT	Propulsion	Tank relief valve failed to reseat.
18 July 1962	F	NT	NT	Electrical	Overload prevented second ignition.
12 December 1962	F	NT	NT	Guidance	Velocity meter malfunction.
15 June 1963	F	NT	NT	Propulsion	Ullage rockets for 2nd burn fired at 1st burn.
TITAN I SECOND STAGE ONLY					
G5	F	NT	NT	Propulsion	Slow start--possible broken line.
J7	S	F	NT	Propulsion	Lox pump cavitated at cutoff minus 0.35 seconds.
J9	F	NT	NT	Propulsion	Gas generator valves did not open.
J10	F	NT	NT	Propulsion/ Electrical	Ignition signal locked out
J12	S	F	NT	Propulsion	Turbo pump failed.
J22	S	F	S	Propulsion	Possible restriction of LOX flow caused stage two to burn 6 sec longer than planned.
M1	S	F	NT	Flight Controls	Hydraulic pressure lost, missile tumbled.
M6	F	NT	NT	Electrical	No ignition due to relay problem.

CODE:

S - Success

NT - No Test

F - Failure

R - Reliability

[redacted]

Table 3-7. Agena Attitude Control Failures

Vehicle Launch Date	Time of Failure (Orbit #)	Time of Failure (Orbit x 90 minutes)	Failure Reason	Remarks
7 Nov 59	1	90	Electrical	Inverter failed, ACS lost.
20 Nov 59	0	--	Guidance	Horizon scanner/accelerometer integrator gas depleted.
24 May 60	1	90	Propulsion	Propellant venting torques required excess use of control gas.
13 Sep 60	16	1440	Valves	Valve froze--gas depleted.
20 Dec 60	1	90	Electrical	Valve control circuit failed--gas depleted.
8 Apr 61	10	900	Valves	Valve froze--control gas depleted.
17 Sep 61	33	2970	Electrical	Inverter failed--no power for ACS operation.
5 Nov 61	6	540	Valve	Valve held open--gas depleted.
7 Mar 62	10	900	Flight Controls	Flight control electronics failed--gas depleted.
28 Aug 62	45	4050	Horizon Sensor	Sensor failed--roll control lost.
29 Sep 62	1	90	Horizon Sensor	Head motor failed--loss of ACS.
7 Jan 63	4	360	Electrical	Power supply for Horizon Sensor failed.
12 Jul 63	15	1350	Propulsion	Propellant venting torques required excess use of control gas.
	143	12870		
Average	$\frac{143}{13} = 11$	$\frac{12870}{13} = 990$		

Failure Reason	Number of Failures	Orbit of Failure
ACS per se	4	16, 1, 10, 6
Flight Control or Guidance	5	10, 45, 1, 4, 0
Electrical	2	33, 1
Propulsion	2	1, 15

[redacted]

Table 3-8. Summary Table

SOURCE	EARTH PARKING ORBIT	DIRECT INJECTION	% IMPROVEMENT
(1) DAC Reliability Estimate (4.5 hour EPO)	0.742108	0.775464	4.3
(2) GE/SOAR III/Cindy I Reliability (77 minutes in EPO)	0.02245*	0.02322*	3.32
(3) Revised GE Reliability (2H 48M 50.6S EPO)	0.02153*	0.02322*	7.28
(4) Summation, MSFC Unreliability (4.5 hour EPO)	0.15422	0.13694	11.21
(5) Summation of MSFC Criticality (4.5 hour EPO)	0.04829	0.04598	4.81

TRW STL FLIGHT ANALYSIS MISSILE SYSTEM RESULTS	SECOND BURN	FIRST BURN
(6) Missile System A	0.889	0.909
(7) Missile System B	0.818	0.901
(8) Missile System C	0.762	—

* Individual Component Reliability Product and is not indicative of mission success.

3.4 SUMMARY OF IN-FLIGHT RELIABILITIES

It is apparent from Table 3-8 that reliability is increased by utilizing the direct injection type of mission. In addition, if more realistic reliabilities (e.g., the use of a reliability of less than 1.0 for S-IVB reignition) had been used in many subsystems, the increase in reliability shown in Table 3-8 would have been more significant.

3.4.1 Reaction Control System of the S-IVB

The histogram (Figure 3-1) of the failure times of the Agena attitude control system is not compatible with the hypothesis of a single Chance Failure Law which possesses the mean time-to-failure which was calculated in Section 3-3 (Table 3-7) for the attitude control system. Consequently, the actual failure times were used to calculate the probability of failure for an earth parking orbit of 170 minutes. This led to a failure probability of 5 percent as the estimate for the reaction control system of the S-IVB for earth parking orbit.

Similarly, the failure probability of the reaction control system of the S-IVB was estimated as 1 percent for the DI mission, since it was assumed that approximately 30 minutes would be required for the 180 degree turn-around maneuver (transposition) subsequent to S-IVB shutdown.

The above failure probabilities apply to the entire reaction control system (RCS) function (and hence would include failures due to the associated electric power, guidance sensors, propulsion, etc.) and are not simply confined to the RCS itself.

3.4.2 S-IVB Reignition

The S-IVB reignition reliability was estimated as 87 percent. This estimate was obtained by combining the flight test failures and successes for the hypergolic restarts and the ignitions in space of the cryogenic engines studied.

Figure 3-1. Histogram of Time of Failures in the Agena ACS System

3.4.3 Powered Stage Reliabilities

Based upon analysis of flight test data, the following are estimates of the reliabilities associated with the powered stages for the earth parking orbit injection mission:

	Reliability
S-IC	0.90
S-II	0.90
S-IVB 1st Ignition	0.92
S-IVB 1st Burn (Steady State) and Shutdown	0.975
S-IVB 2nd Ignition	0.87
S-IVB 2nd Burn (Steady State) and Shutdown	0.975

If a reliability of 0.87 is used for S-IVB reignition throughout Table 3-8, the resulting percentage increase in reliabilities of the DI mission over the EPOI is as follows:

Source	EPO Reliability With Reignition	Percent Increase
(1)	0.645634	16.74
(2)	0.01953	15.89

3.4.4 Relative In-Flight Reliability Model

The relative in-flight reliability (flight success probability) model which has been formulated is a simple series model and is as follows:

$$R_{EPO} = R_{DI} \cdot R_{reig} \cdot \frac{R_{S\text{-}IVB(0 \text{ and } t)}}{R_{S\text{-}IVB(t)}} \cdot R_{SP(0)}$$

where

R_{EPO} = Reliability of Saturn V/Apollo mission employing earth parking orbit injection

R_{DI} = Reliability of a Saturn V/Apollo mission employing direct injection

R_{reig} = Reliability of S-IVB reignition

$R_{S\text{-}IVB(0 \text{ and } t)}$ = Reliability of the S-IVB in earth parking orbit and in transposition

$R_{S\text{-}IVB(t)}$ = Reliability of the S-IVB in transposition

$R_{SP(0)}$ = Reliability of the Apollo spacecraft in earth parking orbit.

Replacing the quantities $R_{S\text{-}IVB(0 \text{ and } t)}$ and $R_{S\text{-}IVB(t)}$ by the estimated reliabilities of the S-IVB RCS function, which are 0.95 and 0.99, respectively, and replacing R_{reig} by its estimate, 0.87, then

$$R_{EPO} = R_{DI} \cdot 0.87 \cdot \frac{0.95}{0.99} R_{SP(0)}$$

Hence,

$$R_{EPO} = 0.835 \, R_{DI} \cdot R_{SP(0)}$$

and thus

$$R_{DI} = 1.197 \frac{R_{EPO}}{R_{SP(0)}}$$

Included in the reliability of the S-IVB RCS function are the reliabilities of not only the RCS itself but also the associated guidance and navigation sensors, the power supply, etc. There are, of course, some other S-IVB hardware whose reliabilities have not been included in the above numerical relationship, e.g., the vent valve operation during parking orbit.

3.4.5 Unsuccessful Flight and Crew Safety Probabilities

In support of the STL effort, General Electric Apollo Support Department, Daytona Beach, utilized the four reliability input sources (viz., GE, DAC, MSFC, and STL) to produce mission success/crew safety comparisons. Reference 5 describes the GE assumptions, analysis, and results; and presents the percentage changes (earth parking orbit injection versus direct injection) in the probability of unsuccessful flight (mission) and in the probability of crew loss.

The results of this mission success comparison indicate that an average of 1.2 percent fewer unsuccessful missions could be expected with the direct injection, based on the DAC, MSFC and GE/ASD data; and that an average of 3.3 percent fewer unsuccessful missions could be expected based on the historical flight data. Since the absolute level of mission success probability was not specified, it is not possible to make a direct comparison of these results with the results obtained in Section 3.4.4.

As a result of the increase in reliability through completion of S-IVB burn accomplished via direct injection, the probability of an abort is lessened during this period, while the probability of abort for the remainder of the mission is expected to remain approximately the same. Due to the difficulty of performing a successful abort after the completion of S-IVB burn, the DI type mission would, according to the GE/ASD analysis, appear to degrade the crew safety factor (see Reference 5). This degradation, expressed in terms of the average percentage increase in the probability of crew loss to be expected with direct injection, was estimated at about 4 percent based on the GE, DAC and MSFC data and about 12 percent based on the historical flight data. However, a closer analysis of the problem shows that the reason for the apparent degradation is that the less difficult aborts are less likely to occur, because of higher reliability through completion of S-IVB burn. At the same time, the probability of successful translunar injection is increased, increasing the probability of a successfully counted-down vehicle experiencing an abort after translunar injection. Since these aborts are more difficult, the probability of crew loss (given a successful countdown) is increased; but the probability of mission success (given a successful countdown) is also increased by approximately the same amount.

A more meaningful measure of crew safety would be the expected number of crew losses per successful mission. Although estimates were not made on this basis, it appears that any differences (between the two injection methods) in this measure would be insignificant.

The advantage of the parking orbit injection mode is in the number of expected successful countdowns possible per year, while the advantage of direct injection is in the number of successful translunar injections per successful countdown. Thus, while more launches are possible with parking orbit injection in a given year, a higher percentage of these can be expected to result in abort before achieving translunar injection. This implies that more boost vehicles would be required to insure a successful mission.

3.5 AREAS FOR CONTINUED STUDY

a) Advantages of a planned direct injection mission with an EPO injection mission as an alternative or backup. This type of planning would provide higher reliability (direct injection) while maintaining the capability and flexibility that is provided by an EPO injection mission.

b) Expand the sub-phase events to provide abort paths during sub-phase events rather than the present computational method of waiting for completion of a particular sub-phase event. For example, under present GE programming there is no abort path during S-IVB burn time.

c) As a result of b) it would be necessary to explore and identify in greater detail all malfunction detection methods and systems that are available to both air crew and ground operational support system (GOSS) personnel.

d) All reliabilities used in this report were based on an air crew and GOSS equipment reliability of 1.0. A more realistic approach would be to assign a crew reliability number based on a human engineering analysis and a GOSS reliability based on GOSS hardware analysis. An analysis of GOSS hardware would also help to define on-time launch probability in greater detail.

4. MISSION SUCCESS AND CREW SAFETY COMPARISONS

4.1 COMPARISON OF MISSION SUCCESS PROBABILITIES

The launch probabilities of Section 2.4 and the relative in-flight success probabilities (estimated from flight reliability histories) for the S-IVB reignition and S-IVB reaction control system function have been combined in Table 4-1 to show the comparative probabilities of mission success during a specified firing period for DI and EPOI trajectories. That is, for both trajectories, the definition employed is as follows:

$$\text{Mission success probability} = \text{Launch probability} \times \text{In-flight success probability}$$

The comparison of mission success probabilities was made for the 1.5-hour launch window of direct injection and for the 2.5 and 4.5-hour launch windows of earth parking orbit injection, both with and without the use of built-in holds. Specifically, the results of Table 4-1 were obtained by multiplying the ρ_3 values (i.e., the launch probabilities for the 3-day firing period) in Table 2-8 by the corresponding values for the relative in-flight success probabilities, which were based on the estimate of 0.87 S-IVB reignition reliability and the estimates of 0.95 and 0.99 reliability of the S-IVB reaction control system function for EPOI and DI, respectively. Other in-flight reliability differences between DI and EPOI (e.g., the reliability of the spacecraft during the 2 hours, 48 minutes and 50.6 seconds in earth parking orbit) have not been included in Table 4-1, since flight reliability histories were not explicitly used for obtaining the relevant estimates.

Table 4-1 shows that, if no built-in hold is used, EPOI has a 40 to 73 percent higher probability of mission success during a specified month than DI (assuming that a firing period exists for direct injection during the month). However, if the indicated built-in hold is used, then DI has a 13 percent higher probability of mission success during a specified month.

Table 4-1. Probability of Mission Success During Specified Firing Period

Mission Plan	Direct Injection (1.5-hour launch window)			Earth Parking Orbit Injection (2.5-hour launch window)			Earth Parking Orbit Injection (4.5-hour launch window)		
Built-In Hold Situation	Launch Probability (ρ_3)**	Flight Success Probability***	Mission Success Probability	Launch Probability (ρ_3)**	Flight Success Probability***	Mission Success Probability	Launch Probability (ρ_3)**	Flight Success Probability***	Mission Success Probability
No Built-In Hold	0.25	1.197 R_{EPO}	0.30 R_{EPO}	0.42	R_{EPO}	0.42 R_{EPO}	0.52	R_{EPO}	0.52 R_{EPO}
135-minute Built-In Hold Close to T-0*	0.49	1.197 R_{EPO}	0.59 R_{EPO}	0.52	R_{EPO}	0.52 R_{EPO}	0.52	R_{EPO}	0.52 R_{EPO}

*The Built-In Hold is 135 minutes in length and is inserted at that point in the countdown subsequent to which there is only one hold to go, on the average.

**Launch Probability (ρ_3) is the probability that liftoff will occur during a launch window in a 3-day firing period.

***REPO = Reliability (i.e., flight success probability) of the earth parking orbit (EPO) mission (2 hours, 48 minutes, 50.6 seconds in EPO).

The above comparison has been made assuming that the entire 3-day firing period is available for the DI mission in the month under consideration. Those months in which no firing period exists for the DI mission have, of course, a zero mission success probability. (By contrast, a firing period does exist every month for the EPOI mission.) Assuming that direct injection opportunities will exist during seven months per year (on the average) during the time period under consideration, the following conclusions can be drawn:

a) With direct injection, using a 1.5-hour launch window and the indicated built-in hold, the maximum expected number of successful countdowns is 3.4.

b) With earth parking orbit injection, using a 2.5-hour launch window and the indicated built-in hold (or using a 4.5-hour launch window), the maximum expected number of successful countdowns is 6.2.

The consequences of failure to meet a launch window within a firing period do not involve the loss of the vehicle, but only postponement of launch to a subsequent firing period; in contrast, an in-flight failure does involve the loss of the vehicle. These consequences are certainly not equivalent. For example, if the probability of mission success, given a successful countdown, is assumed to be 0.7 for the EPOI then the maximum expected number of successful missions per year becomes 2.9 for DI and 4.4 for EPOI. Accordingly, the expected number of vehicles lost (successfully counted down but launched on unsuccessful missions) would be 0.5 and 1.8 for DI and EPOI respectively.

Thus, the advantage of the parking orbit injection mode is in the number of expected successful countdowns possible per year, while the advantage of direct injection is in the number of successful translunar injections per successful countdown. While more launches are possible with parking orbit injection in a given year, a higher percentage of these can be expected to result in abort before achieving translunar injection. This means that more boost vehicles would be required to insure a successful mission.

4.2 UNSUCCESSFUL FLIGHT AND CREW SAFETY PROBABILITIES

In support of the STL effort, General Electric Apollo Support Department, Daytona Beach, utilized the four reliability input sources (viz., GE, DAC, MSFC, and STL) to produce mission success/crew safety comparisons. Reference 5 describes the GE assumptions, analysis, and results, and presents the percentage changes (EPOI versus DI) in the probability of unsuccessful mission (flight) and in the probability of crew loss.

The results of this mission success comparison indicate that an average of 1.2 percent fewer unsuccessful missions (flights) could be expected with direct injection, based on the DAC, MSFC, and GE/ASD data; and that an average of 3.3 percent fewer unsuccessful missions could be expected based on the historical flight data. Since the absolute level of mission success probability was not specified, it is not possible to make a direct comparison of these results with the results obtained in Section 3.4.4.

As a result of the increase in reliability through completion of S-IVB burn accomplished via direct injection, the probability of an abort is lessened during this period, while the probability of abort for the remainder of the mission is expected to remain approximately the same. Due to the difficulty of performing a successful abort after the completion of S-IVB burn, the DI mission would, according to the initial GE/ASD analysis, appear to degrade the crew safety factor (see Reference 5). This degradation, expressed in terms of the average percentage increase in the probability of crew loss to be expected with direct injection, was estimated at about 4 percent based on the GE and MSFC data and about 12 percent based on the historical flight data. However, a closer analysis of the problem showed that the reason for the apparent degradation is that the less difficult aborts are less likely to occur, because of higher reliability through completion of S-IVB burn. At the same time, the probability of successful translunar injection is increased, increasing the probability of a successfully counted-down vehicle experiencing an

abort after translunar injection. Since these aborts are more difficult, the probability of crew loss (given a successful countdown) is increased; but the probability of mission success (given a successful countdown) is also increased by approximately the same amount.

A more meaningful measure of crew safety is the expected number of crew losses per successful mission. An analysis of crew losses per successful mission was conducted by GE/ASD for further comparison of the two injection methods. The results of this analysis (Appendix D of Reference 5) indicate that the use of direct injection would result in a decrease in crew losses per successful mission as compared to earth parking orbit injection. This decrease is estimated at about 3.6 percent on GE and MSFC data, and about 9.5 percent based on historical flight data.

5. MAJOR RESULTS

This section summarizes the major results of the study on the probability of launch and flight success for direct injection and earth parking orbit injection missions of the Saturn V/Apollo vehicle.

5.1 LAUNCH PROBABILITY PARAMETERS

The average number of holds per successful countdown of the Saturn V/Apollo vehicle is estimated to be 5.5, with limits ranging from 5.0 to 6.7. The number of holds per successful countdown is expected to follow a Poisson probability distribution.

The average time lost per hold (including any time lost due to recycling to an earlier point in the countdown) is estimated to be 20 minutes. The time lost per hold is expected to follow a negative exponential probability distribution.

The probability of a non-scrub (if sea states are not considered) is estimated to be 0.43, with limits varying from 0.33 to 0.53. If sea states are considered, the above estimate and limits are to be multiplied by 0.71; hence, the best estimate for the probability of a non-scrub becomes 0.31, which indicates the importance of sea states in the successful meeting of a launch window.

5.2 LAUNCH PROBABILITY COMPARISON

The estimated on-time launch probability of the Saturn V/Apollo, based on historical data, was 0.42 for the earth parking orbit injection mode (2.5 hour launch window) and 0.25 for the direct injection mode (1.5 hour launch window). This estimate is for a 3-day firing period and includes the estimated effects of weather and sea state. By using a 135-minute scheduled hold late in the countdown, these estimates become 0.52 and 0.49, respectively. It was assumed that the hypothetical scheduled hold would not cause additional countdown holds due to failures induced by the potentially longer countdown.

With the above estimates, the expected number of successful countdowns per year becomes 5.0 for the parking orbit injection mode and 1.8 for direct injection, assuming no scheduled hold in either case and assuming that an attempt is made to launch each available launch opportunity. With a scheduled hold, these expected numbers become 6.2 and 3.4. Because of the greater launch windown length, the earth parking orbit injection mode (4.5-hr window) is expected to derive no significant gain from the use of a scheduled hold; however, the scheduled hold does improve the launch probability in the 2.5-hour window EPOI Mission.

5.3 MATHEMATICAL MODEL AND METHODS FOR CALCULATION OF LAUNCH PROBABILITIES

The mathematical (probabilistic) model for calculating launch probabilities has been given for any number, length and placement of built-in holds in the countdown, for any value of the average number of holds per successful countdown ($\overline{h}$) and the average time lost per hold (τ), and for any launch window length and firing period.

The major features of the mathematical model are as follows: the number of holds per successful countdown follows a Poisson probability distribution; the time lost per hold follows a negative expontential distribution; and the probability of not scrubbing the countdown, conditional upon beginning the countdown, is constant and independent from day to day during the firing period.

The launch probability results have been given in parametric form, with $\overline{h}$ ranging from 1 to 10 in increments of 1.0 and with a continuous launch window length varying from 0 to 400 minutes. Launch probabilities have been given for several built-in hold schemes. A built-in hold of 135 minutes inserted at that point in the countdown where there is one hold to go, on the average, appears to be the most realistic. The point of insertion of this hold in the countdown would correspond to about T-5 minutes.

Computer programs for the generation of launch probabilities and idle times associated with built-in holds have been described.

5.4 FLIGHT SUCCESS PROBABILITY COMPARISON

5.4.1 Relative In-Flight Success Probability

The relative increase in the in-flight success probability which can be accomplished by a direct injection mission vis-a-vis an earth parking orbit injection mission is estimated to be 20 percent. This increase is considered to be significant, and is based on a consideration of only the S-IVB reignition reliability and the reliability of the S-IVB reaction control system function.

The reignition reliability of the S-IVB is estimated to be 0.87. (S-IVB reignition is required for the EPOI mission, but is not required for the DI mission.) The reliability of the S-IVB reaction control system function (including the associated guidance and navigation sensors, propulsion and power supply) is estimated to be 0.95 for earth parking orbit injection (2 hr, 48 min, 50.6 sec, in parking orbit) and 0.99 for direct injection.

5.4.2 In-Flight Reliability Comparisons

In-flight reliability comparisons obtained by using the various reliability planning numbers of MSFC, DAC, and GE/ASD/DB are given in Table 3-8. All of these show a higher in-flight reliability for direct injection than for earth parking orbit injection. The difference ranges from a low of 3.3 percent to a high of 11.2 percent. In view of the short duration (77 minutes) parking orbit used in the GE/SOAR 111/Cindy I reliability figure, the value of 3.3 percent could realistically be ignored. The range would then extend from 4.3 to 11.2 percent with an average increase of 6.9 percent.

5.4.3 GE/Apollo Support Department's Unsuccessful Mission (Flight) and Crew Safety Probability Estimates

Data supplied to GE/ASD/DB (including the DAC and MSFC data listed in Table 3-8) were utilized in the GE computer program to obtain further comparisons of the two missions. The resulting input from

GE/ASD/DB to TRW/STL/FD (Reference 5) showed results that fell into an even more narrow range than the results in Paragraph 5.4.2, the difference being less than 0.5 percentage points between the GE, DAC and MSFC data sources. The exception was the historical reliability data, which was based on actual flight results, and indicated a greater difference between the two injection modes. Unfortunately, all of the GE results were presented in terms of the percentage change in unsuccessful missions, and therefore cannot be compared to the results obtained in 5.4.2 above.

The initial crew safety comparison made by GE/ASD using percentage change in crew loss probability (given a successful countdown) showed a significant difference between the two injection modes. A more meaningful measure of crew safety was found to be the expected number of crew losses per successful mission, since in the direct injection mode fewer successful countdowns would be necessary per successful mission. Numerical estimates of this parameter, also made by GE/ASD, showed that the expected number of crew losses per successful mission is from 3.6 to 9.5 percent lower (based on GE and MSFC data and historical flight data respectively) for direct injection.

6. CONCLUSIONS

The following conclusions are drawn from this portion of the study:

a) Flight sequence changes required for direct injection are limited to deletion of the S-IVB shutdown and restart, elimination of the earth parking orbit coast phase, and rescheduling of the crew safety checks, orbit checks, and communications coverage. The systems checks and navigation performed during parking orbit are, at present, primarily required because of the earth parking orbit coast phase.

b) The subsystems identified by GE/ASD as potentially contributing the greatest in-flight reliability increase as a result of using the direct injection mode are, in descending order:

CM (command module) guidance and navigation

S-IVB propulsion

IU (instrumentation unit) guidance and navigation

CM communications

IU environmental control

IU communications

S-IVB communications

S-IVB electrical

c) Four sets of reliability data and two reliability models were used to estimate the relative in-flight reliability of the two injection modes. The first model was formulated to assess only the difference in the in-flight reliability of the two modes. This model produced an average estimate of 7 percent higher reliability for direct injection, using planning data from DAC, MSFC and GE/ASD. This same model gave an estimate of about 20 percent higher reliability for direct injection using historical flight data. The latter estimate included only the estimated change in reliability for the S-IVB attitude control system and reignition, and did not account for the unreliabilities of the other subsystems listed.

The second model utilized to estimate the relative in-flight reliability was the GE/ASD SOAR III/Cindy I computer reliability model. This model was exercised with the same data as was used in the first mode, but the results were

presented in terms of the percentage decrease in the number of unsuccessful missions. This model produced an average of 1.2 percent fewer unsuccessful missions for direct injection with the DAC, MSFC and GE/ASD planning data, and about 3.3 percent fewer unsuccessful missions for direct injection using the historical flight data.

All estimates, made with both models, showed an increase in the probability of mission success (given a successful countdown) for the direct injection mode.

d) The estimated on-time launch probability of the Saturn V/Apollo, based on historical data, was 0.42 for the earth parking orbit injection mode (2.5 hour launch window) and 0.25 for the direct injection mode (1.5 hour launch window). This is for a 3-day firing period and includes the estimated effects of weather and sea state. By using a 135-minute scheduled hold late in the countdown, these estimates become 0.52 and 0.49, respectively. It was assumed that the hypothetical scheduled hold would not cause additional countdown holds due to failures induced by the potentially longer countdown.

With the above estimates, the expected number of successful countdowns per year becomes 5.0 for the parking orbit injection mode and 1.8 for direct injection, assuming no scheduled hold in either case and assuming that a launch attempt is made at each available launch opportunity. With a scheduled hold, these expected numbers become 6.2 and 3.4. Because of the greater launch window length, the 4.5 hr window earth parking orbit injection mode is expected to derive no significant gain from the use of a scheduled hold.

e) Defining mission success probability as the product of the on-time launch probability and the probability of a successful mission given a successful countdown, estimates of comparative mission success probability were made for the two injection modes. These estimates indicated that for a given launch opportunity, direct injection using a scheduled countdown hold had a higher mission success probability than earth parking orbit injection. However, due to the greater number of launch opportunities per year with parking orbit injection, the mission success probability of the parking orbit mode is higher for any given year.

f) The crew safety studies were based on the GE/ASD SOAR III/Cindy I computer reliability model and the appropriate abort trajectory data. These studies indicated that the expected number of crew losses per successful mission is significantly lower for direct injection. The difference was estimated to be about 3.6 percent using GE and MSFC data and about 9.5 percent using historical flight data.

7. RECOMMENDATIONS

The following recommendations are made:

a) That launch probability studies be continued on the Saturn V/Apollo vehicle and that they include the following: the maintenance of up-to-date estimates of launch probability and its ingredient parameters; the definition of countdown turnaround (recycle) time in the event of scrubs; the determination of the optimum and realistic placement and length of built-in holds compatible with operational constraints; and the generation of improvements in the countdown and in the associated launch probability.

b) That the effect of sea states and weather, and the persistence (autocorrelation) thereof, on the launch probability of the Saturn V/Apollo vehicle be further studied and that the analysis of sea states and weather be incorporated in the operational planning.

c) That the relative probabilities of flight (mission) success of the direct injection and earth parking orbit injection trajectories be interpreted in terms of the percentage changes in the probability of a successful mission. It is furthermore recommended that the change in the probabilities of flight (mission) success be interpreted by reference to the absolute values of flight success reliability.

d) That the scope of the analysis of existing in-flight reliability and failure data (as performed in the estimation of the reliabilities of S-IVB reignition and the S-IVB reaction control system function) be extended to include the analyses necessary to yield reliability estimates of the other pertinent differences between the earth parking orbit injection and direct injection trajectories, in particular, the estimate of the reliability of the spacecraft during earth parking orbit.

e) That the approach and scope of the analysis also be extended to include both the in-flight success probability and the crew safety probability of the entire Saturn V/Apollo mission. That is, these analyses should be conducted by the use of historical reliability data generated from the launches of many booster and space vehicles, and should be similar to those which have been performed on the launch probability parameters, the on-time launch probability itself, S-IVB reignition reliability and S-IVB reaction control system reliability.

REFERENCES

PART I

1. Communique' from NASA/MSC to STL on June 28, 1964 (C).

2. F. Lewis, R. Wolpert, "Direct Injection Launch Window Displays for the Years 1968, 1969, 1970," STL Memo 9883.5-10, July 17, 1964.

PART II

1. "A Study of Launch Probabilities for Space Mission of Atlas/Agena Vehicles (U)," Final Report, Volumes 1 and 2, Space Technology Laboratories/FD 63-252; January 1963. (C)

2. "Atlas/Centaur Launch Probability Study (U)," Volumes 1 and 2, Space Technology Laboratories/FD 63-365; June 1963. (C)

3. "A Study of Launch Probabilities for Titan II—Gemini and Atlas/Agena Redezvous Missions (U)," Space Technology Laboratories/FD 64-406; March 1964. (C)

4. "The Built-In-Hold and its Application in the Gemini Rendezvous Mission," Space Technology Laboratories/FD Technical Note; September 1964.

5. "Reliability Analysis of Apollo Post Liftoff Direct Injection Study," Final Report, GE/ASD/DB; 23 October 1964.

APPENDIX A

LAUNCH PROBABILITY COMPUTER PROGRAMS

The following is a description of the FORTRAN computer programs used to compute and plot the various relevant launch probabilities (both with and without the use of built-in-holds) for the Saturn V/Apollo and Gemini missions. A rule-of-thumb approximation to the launch probability when a built-in hold is used is also given.

A.1 PLSUM—P_L PROBABILITY

This program computes the conditional probability (P_L) of launch versus the dimensionless ratio K ($K \equiv W/\tau \equiv$ launch window divided by the average time lost per hold) for <u>any</u> $\bar{h}$, where $\bar{h}$ is the average number of holds per successful countdown. (The probability P_L is conditional upon the countdown not being scrubbed for technical reasons prior to T-0.) The output is a plotted graph for the values of K = 0(0.50)20. The input is a delta x, delta y and $\bar{h}$, where delta x is the number of plotter increments per unit value of the abscissa and delta y is the number of plotter increments per unit value of the ordinate.

A.2 PLCON—CONVOLUTION OF TWO P_L'S

This program computes the numerical integral for the convolution of two $\bar{h}$'s versus K. The convolution is a function of $\bar{h}_1$, $\bar{h}_2$ and ℓ, where $\bar{h}_1$ is the average number of holds subsequent to (or after) the built-in hold (BIH) and $\bar{h}_2$ is the average number of holds prior to (or before) the BIH and ℓ is the length of the BIH. It should be noted that for no BIH, i.e., $\ell = 0$, the convolution of $\bar{h}_1$ with $\bar{h}_2$ is simply the probability curve P_L for $\bar{h} = \bar{h}_1 + \bar{h}_2$. This can be used as a check on the program, which was done with excellent agreement. The convolution integral is described as follows:

This program also computes the average idle time $(\overline{I.T.})$ during the BIH, as follows

$$\overline{I.T.} = \sum_{i=1}^{J} (\Delta P_{2i}) \left[\ell - \frac{\tau}{8} - \frac{\tau}{4} (i - 1) \right] + P_2(0) \cdot \ell$$

where

$$J = \frac{\ell}{\Delta K}$$

$$\Delta P_{2i} = P_{L_{\overline{h}_2}} (i\Delta K) - P_{L_{\overline{h}_2}} \left[(i - 1) \Delta K \right]$$

$\tau \equiv$ Average time lost per hold

$\ell \equiv$ Length of BIH

and

$$P_2(0) = P_{L_{\overline{h}_2}} (0)$$

The ΔK used is 0.25.

The output is $P_{L(con)}$ on paper tape and/or $P_{L(con)}$ plot. The average idle time is typed out. The input is $\overline{h}_1$, $\overline{h}_2$, and the BIH length divided by τ.

A.3 PLCONCON—CONVOLUTION OF TWO OR MORE P_L CURVES

This program computes the conditional probability P_L for more than one BIH. The input is the convolution integral $P_{L(con)}$ from the PLCON program or the output from the PLCONCON program itself (since more than 2 BIH's may be used), along with $\overline{h}_i$ and a BIH. In this case $\overline{h}_i$ is defined as the average number of holds between the next BIH and the last BIH which means that if the PLCON program is run as an input to PLCONCON, then the $\overline{h}_1$ defined in A.2 above is the average number of holds between the first BIH and the second BIH. This program also computes the average idle time during a BIH. The output is on punched paper tape and/or a plot.

$$P_{L_{(con)}} = P_{L_{\overline{h}_1}}(W) \cdot P_{L_{\overline{h}_2}}(\ell) + \int_{\ell}^{\ell+W} P_{L_{\overline{h}_1}}(\ell + W - K)\, P_{L_{\overline{h}_2}}(K)\, dk$$

where

$K \equiv W/\tau$

$W \equiv$ Launch window length

$\tau \equiv$ Average time lost per hold

$\ell \equiv$ Length of BIH

and

$P_{L_{\overline{h}_2}} \equiv$ Derivative of $P_{L_{\overline{h}_2}}(K)$

The numerical integration is computed as follows

$$P_{L_{(con)}} = P_{L_{\overline{h}_1}}(W) \cdot P_{L_{\overline{h}_2}}(\ell) + \sum_{i=1}^{N} (\overline{P}_{1i}) \cdot (\Delta P_{2i})$$

where

$$N = \frac{W}{\Delta K}$$

$$\overline{P}_{1i} = \left\{ \frac{P_{L_{\overline{h}_1}}(W - i\Delta K) + P_{L_{\overline{h}_1}}\left[W - (i-1)\,\Delta K\right]}{2} \right\}$$

and

$$\Delta P_{2i} = P_{L_{\overline{h}_2}}(\ell + i\Delta K) - P_{L_{\overline{h}_2}}\left[\ell + (i-1)\,\Delta K\right]$$

A.4 TWO COUNTDOWNS—CONVOLUTION OF TWO VEHICLES

This program computes the convolution of two $P_{L(con)}$ curves for two different vehicles. Also computed is an "upper limit" probability curve. The upper limit curve assumes the two countdowns are independent and thus

$$P_{L_{(con)}} = P_{L_1}(i) \cdot P_{L_2}(i) \text{ for } i = 1, \cdots, N \text{ and } P_{L_1}$$
$$\text{upper limit}$$

is the probability for the first vehicle, and P_{L_2} is the probability for the second vehicle. Since in real life the countdown of the two vehicles (viz., Saturn V and Apollo) are neither completely independent nor dependent (e.g., Saturn V/Apollo, Atlas-Agena, Titan-Gemini, Thor-Delta, etc.), it is believed that the average of the convolution probability curve (which we have used to estimate launch probabilities) and the upper limit curve can serve as a good approximation to the true probability. The input is P_{L_1} and P_{L_2}, and the output is a plot of the convolution and the upper limit probabilities.

A.5 PLOTTER PROGRAMS USED

The following are the plotter programs which were used:

PENUP—raises plotter pen
PENDOWN—lowers plotter pen
OPLOT—origins the plot
SPLOT—scales and origins the plotter
PLOT—plots the ordinate versus the abscissa

A.6 RULE OF THUMB APPROXIMATION FOR CONVOLUTION

For an approximation to the convolution of two $\overline{h}$ curves, one can add the length of the built-in hold to the window length and read the $\overline{h}_2$ curve for the average number of holds prior to the built-in hold to get the probability of launch.

There are some qualifications on using this method, and they are listed as follows:

a) The built-in hold should be sufficiently near T-0 (i.e., $\overline{h}_1$ should be small).

b) We have found that the built-in hold should be less than $3W/2\tau$ and that W should be greater than, or equal to 3τ, where W is the window length and τ is the average time lost per hold.

An absolute upper limit can be placed on the convolution. The upper limit is the probability curve for $\overline{h}_1$, where $\overline{h}_1$ is the average number of holds subsequent to the built-in hold.

A.7 COMPUTER AND PLOTTER DESCRIPTION

The computer used for the checkout and running of these FORTRAN programs was a TRW-230 with a Calcomp 565 plotter at the Florida Division of TRW Space Technology Laboratories. It is realized that on most computer systems, the punch tape and read tape statements would have to be changed to mag tape read-write. If there are any questions about the programs, please contact C. L. Smith, TRW Space Technology Laboratories, Florida Division, 7001 N. Atlantic Ave., Cape Kennedy, Florida. The telephone number is 783-7811, extension 250.